

Sheffield Hallam University

Model studies of metal-slag reactions in reaction generated foams.

ACHESON, R.

Available from the Sheffield Hallam University Research Archive (SHURA) at:

<http://shura.shu.ac.uk/19198/>

A Sheffield Hallam University thesis

This thesis is protected by copyright which belongs to the author.

The content must not be changed in any way or sold commercially in any format or medium without the formal permission of the author.

When referring to this work, full bibliographic details including the author, title, awarding institution and date of the thesis must be given.

Please visit <http://shura.shu.ac.uk/19198/> and <http://shura.shu.ac.uk/information.html> for further details about copyright and re-use permissions.

100 518 601 4

TELEPEN



01941

Sheffield City Polytechnic Library

REFERENCE ONLY

ProQuest Number: 10694078

All rights reserved

INFORMATION TO ALL USERS

The quality of this reproduction is dependent upon the quality of the copy submitted.

In the unlikely event that the author did not send a complete manuscript and there are missing pages, these will be noted. Also, if material had to be removed, a note will indicate the deletion.



ProQuest 10694078

Published by ProQuest LLC (2017). Copyright of the Dissertation is held by the Author.

All rights reserved.

This work is protected against unauthorized copying under Title 17, United States Code
Microform Edition © ProQuest LLC.

ProQuest LLC.
789 East Eisenhower Parkway
P.O. Box 1346
Ann Arbor, MI 48106 – 1346

W13

Model Studies of Metal-Slag Reactions

in Reaction Generated Foams

by

R. Acheson

Part One

SHEFFIELD POLYTECHNIC
LIBRARY
669Q
AC
THESIS

04888.01

PREFACE

This dissertation is submitted for the degree of Doctor of Philosophy of the Council for National Academic Awards. The research described was carried out during the period from January 1972 to December 1974 in the Department of Metallurgy, Sheffield Polytechnic. No part of this dissertation has been submitted for a degree at any other university or college.

During the period of this work the author attended post graduate lecture courses on the following topics:

- (i) Process metallurgy,
- (ii) Computing and numerical analysis,
- (iii) Oxygen steelmaking,
- (iv) Iron making.

A conference was also attended, entitled,

Physical Chemistry of Process Metallurgy - The Richardson Conference
(Imperial College, London, July, 1973.)

The author wishes to express his thanks to his supervisors, Dr. A. W. D. Hills, Dr. R. Smith and Dr. B. C. Blakey, for many valuable discussions.

The author would also like to express his gratitude to all those members of the departmental technical staff and research colleagues who contributed in various ways during the course of this work. Especial thanks go to P. Fisher, J. Green, J. Jordan, D. O. Latimer and P. Roebuck. The author is indebted to Mr. E. W. Chandler for his considerable patience and skill in typing this thesis.

The provision of a Research Studentship by the Science Research Council is gratefully acknowledged.

R. Acheson

SYNOPSIS

A room temperature model has been developed which simulates certain aspects of the slag-metal-gas reactions that occur in I.D. steelmaking. In the model the molten iron was represented by a pool of sodium amalgam, the slag by a mixture of water and glycerol and the oxygen by a hydrogen chloride-nitrogen jet. Droplets of amalgam ejected from the bath by the impinging gas jet, reacted with the hydrogen chloride dissolved in the model slag to produce bubbles, thus forming a dynamic foam.

To gain more information about the fundamental refining processes in the model, the behaviour of single droplets of amalgam in acid media has been studied. When the sodium content of individual droplets was high, the rate of reaction was controlled by the discharge of hydrogen ions at the reaction interface, with rate dependence on the hydrogen ion concentration in the aqueous phase. This is analogous to decarburisation rate control by transport of oxygen ions in the slag phase.

Under hydrogen ion discharge control, the refining rate in the model converter initially increased but eventually attained an approximately steady value. The level of this rate plateau was shown to be strongly influenced by the rate of transfer of hydrogen chloride from the jet gases to the slag phase. Similarly in oxygen steelmaking the decarburisation rate plateau has been shown to be determined mainly by the oxygen blowing rate.

The model converter has been used to qualitatively investigate the effect of lance height, jet momentum and mass flow rate of gaseous reactant into the reaction vessel on the mean plateau refining rate. The results obtained compare favourably with analogous variables in steelmaking practice. In addition the effect on the refining rate of pressurising the reaction vessel has also been investigated. An improvement in refining rate was achieved, partly due to improved slag-metal drop contact and partly to increased hydrogen chloride flow rate. It is not believed that such a

significant improvement would be achieved for steelmaking conditions although there might be some advantage derived from improved control over slopping at high oxygen flow rates.

When the sodium content of single amalgam droplets fell below a critical level, determined by the acid concentration in the aqueous phase, the rate of reaction became controlled by sodium transport to the reaction interface. This is analogous to decarburisation rate control by carbon transport within iron droplets. In both the model converter and in steelmaking this gives rise to a progressively decreasing refining rate.

CONTENTS

List of symbols and subscripts

		Page
<u>CHAPTER ONE</u>	INTRODUCTION	1
<u>CHAPTER TWO</u>	LITERATURE REVIEW	
2.1	The L.D. Steelmaking Process	3
2.1.1.	Introduction	3
2.1.2	Oxygen supply	4
2.1.3	Slag formation	7
2.1.4	Refining characteristics	9
2.1.5	Foams and emulsions in steelmaking	12
2.1.6	Contribution of foams and emulsions to refining	13
2.1.7	Formation and stabilisation	17
2.1.8	The final stage of decarburisation	20
2.2	Model Studies of L.D. Steelmaking	21
2.2.1	The jet impingement zone	21
2.2.2	The splashing mode	23
2.2.3	Bath circulation	25
2.2.4	Mass transfer from a gas jet to a liquid	26
2.3	Single Droplets	29
2.3.1	Hydrodynamic behaviour of falling droplets	29
2.3.2	Mass transfer models	31
2.3.3	Surface phenomena	32
2.3.4	Previous experimental work on the refining of single droplets	33
	2.3.4(a) Iron alloy droplets	33
	2.3.4(b) Model studies	37
2.4	Previous work on the decomposition of sodium amalgam in aqueous solutions	39

<u>CHAPTER THREE</u>	PRELIMINARY WORK	43
3.1	Choice of model system	43
3.2	Preliminary experiments	45
3.2.1	The reaction between sodium amalgam and water	45
3.2.2	The reaction of sodium amalgam with acid solutions	47
3.3	The implications of the preliminary experiments	49
<u>CHAPTER FOUR</u>	SINGLE DROPLET STUDIES	50
4.1	Introduction	50
4.2	Theoretical considerations	51
4.2.1	Continuous phase control	52
4.2.2	Dispersed phase control	53
4.2.3	Sodium ion transport	54
4.2.4	Chemical kinetic control and hydrogen overpotential	55
4.3	Apparatus and Experimental Procedure	59
4.3.1	The mass transfer column	59
4.3.2	Droplet formation	59
4.3.3	Droplet collection	60
4.3.4	Gas collection	62
4.3.5	Preparation of aqueous solutions	63
4.3.6	Preparation of sodium amalgams	63
4.3.7	Treatment of used amalgams	64
4.3.8	Analysis of sodium amalgams	65
4.3.9	Experimental procedure - mass transfer experiments	65
4.3.10	Photographic techniques	68
	4.3.10(a) Droplet velocity determination	68
	4.3.10(b) High speed cine photography	69
	4.3.10(c) Still photography	69

4.4	Results	72
4.4.1	Visual observations	72
4.4.2	Velocity measurements	76
4.4.3	Mass transfer experiments	80
4.5	Discussion	84
4.5.1	The refining of high sodium content droplets in salt free solutions	84
4.5.2	The effect of sodium chloride additions to the aqueous phase	90
4.5.3	The refining of droplets with reduced sodium contents	92
4.5.4	Comparison with metal-slag systems	95
<u>CHAPTER FIVE</u> MODEL CONVERTER STUDIES		97
5.1	Introduction	97
5.2	Experimental Apparatus and Procedure	98
5.2.1	The converter and sundry equipment	98
	5.2.1(a) Gas supply	98
	5.2.1(b) The converter vessel	100
	5.2.1(c) The exhaust gas system	101
5.2.2	Sampling and analysis of gas mixtures	102
	5.2.2(a) Sample collection	102
	5.2.2(b) The chromatograph	103
	5.2.2(c) Calibration	104
5.2.3	Experimental procedure	105
5.2.4	Slag sampling techniques	107
5.2.5	Slag temperature measurement	108
5.2.6	Measurement of droplet splashing rates	109
5.3	Results of model converter experiments	111
5.3.1	General refining characteristics	111

5.3.2	The effect of varying the composition and momentum of the jet	114
5.3.3	The influence of lance height	116
5.3.4	The effect of sodium chloride additions to the aqueous phase	118
5.3.5	Refining at elevated pressures	120
5.3.6	Experiments at constant mass flow rates	122
5.3.7	Refining at low sodium concentrations	123
5.4	Discussion	125
5.4.1	Refining under hydrogen ion discharge control	125
	5.4.1(a) Qualitative Assessment of the Model Converter	125
	5.4.1(b) Mathematical Interpretation	127
	5.4.1(c) The Use of the Model to Simulate the Effects of Steelmaking control variables	138
5.4.2	Application to basic oxygen steelmaking	146
5.4.3	Refining at low solute concentration in the bath	154
<u>CHAPTER SIX</u>	<u>CONCLUSIONS</u>	157
References		159

Figures, tables and photographs

SYMBOLS

A	Area
C_i	Molar concentration of "i"
F_M	The ratio of sodium removal rate to the rate of HCl transfer to the model slag during the stage II refining period.
f_D	Drag coefficient
g	Acceleration due to gravity
h	Height of lance tip above surface of metal bath
k	Reaction rate constant for hydrogen ion discharge
K	A transport parameter
\dot{M}	Jet momentum
\dot{m}	Molar reaction rate
	'' denotes per unit area, ''' denotes per unit volume
n_o	Depth of penetration of gas jet into a liquid bath.
\bar{n}_{Cr}	Depth of jet penetration at onset of splashing mode.
P	Partial pressure
r	Radius
S	Foam structure group.
t	time
t_o	Incubation period
u	Velocity
V	Volume
\dot{V}	Volumetric flow rate
W	Molecular weight
∞	Mass transfer coefficient
β_i	Volume of gas produced when one mole of 'i' reacts
ϵ	Mean fraction of foam height through which bubbles must rise at their own velocity of rise.
ϕ	Angle at which droplets leave jet impingement crater.

- γ Fraction of amalgam droplet surface in contact with a particular phase
- ρ Density
- ρ_i^* Mass fraction of 'i'
- σ Surface tension
- σ_i Interfacial energy
- τ Life time of droplets in foam.
- μ Viscosity
- \dot{v} Number of metal droplets produced per unit time.

SUBSCRIPTS

Aq	Pertaining to the aqueous phase.
Av	An average value.
B	Within the bulk of a phase
b	Pertaining to the metal bath.
bub.	Pertaining to bubbles
C	Carbon
CaO	Lime
Cl ⁻	Chloride ions
CO	Carbon monoxide
con	Pertaining to the continuous phase.
crit	Critical composition for change in rate controlling mechanism
d	Pertaining to droplets
eq	Pertaining to equilibrium conditions
F	Foam
Fe	Iron
FeO	Ferrous oxide
G	Pertaining to a gas phase
H ⁺	Hydrogen ions
Hg	Mercury
H ₂	Hydrogen gas
HCl	Hydrogen chloride
H ₂ O	Water
i	At an interface
I	Initial composition
J	Pertaining to the jet
L	Pertaining to a liquid phase
LA	Within the lance
M	Pertaining to the model system.

Na Sodium
Na⁺ Sodium ions
NaCl Sodium chloride
O₂ Oxygen
[O] Oxygen in solution in iron.
0 At zero time
R Surface of metal phase available for reaction.
S Pertaining to the slag phase.
St Pertaining to steelmaking
T Total surface of metal phase.
v Pertaining to the converter vessel.
II Pertaining to the stage II refining period.

Since the initial plant trials in Austria during the early 1950's, oxygen steelmaking has been extensively adopted in most industrialised countries, mainly at the expense of the open hearth process. It is estimated that at the present time, oxygen refining processes account for over half of the World steel production. During the last decade, development has mainly been concentrated on the L.D. process, as opposed to the Kaldo, Rotor, O.L.P., etc., although in recent years there has been renewed interest in using tonnage oxygen in bottom blown converters.

A primary reason for the enthusiastic adoption of the L.D. process has been its ability to operate at extremely high refining rates, although this has been associated with control problems. These high rates which make the process so attractive from a production view point have never been completely explained or the mechanisms involved fully understood. It is generally believed however that the formation of slag-metal-gas emulsions are a key technical factor in the commercial success of the process. By providing a high interfacial area for mass transfer, these dispersions of droplets and bubbles in slag are thought to be the vehicle for the extremely high refining rates observed. The development of a better understanding of the mechanisms involved would prove valuable in establishing better steelmaking control and in designing future processes.

Study of the actual foams and emulsions encountered in commercial L.D. steelmaking operations has been inhibited by the inherent practical difficulties associated with making measurements in complex high temperature systems and also by the vigorous nature of the processes taking place within the converter vessel. Room temperature models, in general, do not suffer from these limitations. The development of a suitable room temperature system, which would simulate certain of the more essential aspects of the gas-slag-metal interactions operative in the L.D. process, was therefore thought to be desirable.

The work carried out during the course of this investigation fell into essentially four sections, which are described in the four principal chapters of this thesis. The relevant literature is reviewed in chapter two. In chapter three the preliminary experimental work involved in the development of the model converter system, based on the reaction of a sodium amalgam with an acidified aqueous solution, is briefly described. These simple experiments served to confirm the viability of the model system chosen and prompted the more extensive studies described in chapter five. The results of the preliminary experiments also indicated the need for research into the fundamental reaction mechanisms involved in the model process. This stimulated the single droplet studies described in chapter four.

2.1 THE L.D. STEELMAKING PROCESS

2.1.1 Introduction

The objective of the L.D. process is the conversion of molten blast furnace metal into steel. This involves the partial oxidation of carbon, silicon, phosphorus and manganese with an accompanying reduction in the sulphur level. Blast furnace hot metal for L.D. steel making ideally contains about 4 wt % C, 0.7 - 0.8 wt % Si, 0.7 - 0.8 wt % Mn, 0.03 wt % max.S and 0.15 wt % max.P.¹ In practice however, compositions vary widely depending upon the source of the iron ore. In some cases, special modifications have been made to the process to cope with particular compositional problems, e.g., the L.D.-A.C. process, which was specifically developed to cope with blast furnace metal with a high phosphorus content.

The essential feature of the L.D. process is the impingement of a jet of gaseous oxygen onto a bath of molten blast furnace metal, which may include cold scrap comprising up to 30% of the charge. Vessels with capacities of up to 300 t are commonly in use today and are of the characteristic pear shape, with an opening at the top for charging and slag removal. The taphole is situated on the front face just below this opening. Hot metal, scrap, lime and flux are charged directly to the vessel. At the end of the refining period, which generally takes about 15 - 20 minutes, the furnace is tilted to allow temperature measurement and the removal of samples for analysis. If the results are satisfactory the heat is ready for tapping, if not, then a second or third reblow each of a few minutes duration is applied. The steel is decoxidised and recarburised, if required, in the ladle.

The amount of literature concerning the L.D. process is considerable. It is beyond the scope of the present work to attempt a complete review so that only relevant features with respect to the present work

are outlined. More general reviews have been published by Lange ² and by Walker and Anderson. ³

2.1.2 Oxygen Supply

Oxygen is introduced into the vessel through a water cooled copper nozzle and the jet directed onto the metal bath. Much of the available knowledge on the structure of jets and their interaction with liquids has been derived from model studies. These are discussed in section (2.2). A review of the available literature concerning the structure and behaviour of oxygen steelmaking jets has been published by Chatterjee. ⁷

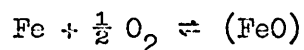
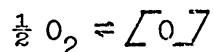
In L.D. steelmaking the oxygen jet leaves the nozzle at supersonic velocity. To achieve such a jet, the gas is blown through a convergent-divergent nozzle, the gas reaching sonic velocity in the throat and becoming supersonic in the diverging section. Much of the initial information on the structure of jets produced in this way was derived from work on jet propulsion. In steel making the situation is complicated by the fact that the relatively cold, jet gases are discharging into a very hot atmosphere, the reverse being true for jet propulsion. An extensive study of the structure and behaviour of super sonic jets as applied to basic oxygen furnaces has been made by Smith. ⁵ The converging-diverging nozzle is designed for a particular flow rate and operation outside this will cause shock waves. ^{4,5} The effect of these shock waves on the processes occurring inside the vessel is not clear, but they may influence the entrainment behaviour of the jet and possibly the interaction of the jet with the liquid bath.

A gas jet impinging on a liquid surface produces a depression surrounded by a raised lip, from which small waves move radially outwards. If the momentum is increased sufficiently, splashing occurs and droplets of the liquid are thrown out into the gas or slag phase above

the bath ⁸. The blowing practice employed in L.D. steelmaking is such that conditions are well within the range for considerable splashing to occur ^{78, 81}.

Flinn has shown that the oxygen jet can penetrate deep into the metal bath and may even contact the refractories at the bottom of the vessel giving rise to severe erosion ⁶. Various attempts have been made to predict the depth of penetration of the jet into the bath. These have been reviewed by Chatterjee ⁷⁸. Despite the large volume of literature, the true penetration during the course of an actual blow is not known. Meyer points out that as much as 30% of the metal charged may be dispersed as droplets in the slag, effectively increasing the lance height above the bath by an unknown amount. However, since decarburisation can occur within the bath, the metal may contain gas bubbles which tend to raise the level. These factors oppose each other and vary throughout the blow ¹¹.

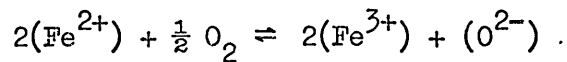
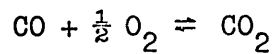
In the zone of impingement, oxygen goes into solution in the hot metal charge and iron oxides may be formed ⁸. Thermodynamic considerations indicate that the oxidation of silicon, carbon and manganese should occur preferentially ¹². However, due to the great excess of iron in the charge, iron oxides will undoubtedly form at the point of impingement and will be transferred to the slag ⁸.



The actual distribution of oxygen between the slag and the metal is not known since it is a complex function of a number of variables, including lance height and oxygen flow rate.

Once the blow is in progress the jet will be discharging into an atmosphere of carbon monoxide and the lance tip may even be submerged

in a layer of foam⁹. The constituents of the foam may become entrained into the jet to be oxidised still further.



Yakovlev has suggested that a considerable proportion of the free oxygen may be consumed in this way before the jet, now composed of a mixture of CO, CO₂, O₂, slag and metal droplets, impinges onto the bath¹³. Analysis of the waste gases leaving the vessel certainly indicate a high degree of oxygen utilisation, since they rarely contain more than 2% O₂¹⁴. Increased scrap melting rates may be induced by encouraging entrainment and combustion of CO to CO₂ in the jet by slightly increasing the lance height¹⁵.

Flinn, using experimental L.D. furnaces with capacities up to 2t, has shown that the oxygen jet is reflected at the metal surface, inducing circulation patterns, within the bulk bath⁶. The reflected portion of the jet provides sufficient shear forces at the liquid surface to produce radial motion outwards at the gas-metal interface, with the liquid returning downwards via the vessel walls and back along the furnace bottom, before rising centrally along the axis of the vessel to the point of impingement.

It is desirable to determine the optimum blowing conditions for a particular plant in order to produce the maximum metallic yield, whilst creating regular refining conditions so that the end point can be more easily predicted. The most serious loss to yield comes from "sparking", when metal is directly ejected from the vessel by the gas jet¹⁵. This appears to be associated with high jet momentums and lance heights which are too low, especially in the early part of the blow while the slag cover is inadequate⁹. Later in the blow a second type of ejection can occur which is associated with the formation of a foaming slag. If the

blow is too soft, then there will be inadequate turbulence in the metal bath and the iron oxide concentration in the slag may become excessive. In extreme conditions decarburisation becomes erratic and at times very violent^{6, 64}. This phenomenon, known as "slopping", when slag is ejected from the furnace, lowers the metallic yield as a result of entrained iron droplets and curtails the production rate because of the time required to clean up the vessel lip ring. Skull formation on the hood and lance may also become a problem¹⁶. Soft blowing at the beginning of the refining period does however encourage early slag formation, which is conducive to sulphur and phosphorus removal. A harder blow in the later stages favours decarburisation¹⁵.

In recent years there has been a trend towards the use of multi-hole nozzles. These are claimed to produce more uniform decarburisation rates with reduced foam formation and hence less slopping¹⁵. Experiments have been carried out with nozzles containing up to 12 holes, but in general the best results appear to be obtained with a 5 hole nozzle¹⁷. It has been found that the optimum lance height for different lance types, in a given furnace, all give the same impact area at the bath surface⁵. At their optimum lance height, the jet penetration achieved with multiple hole nozzles is equal to or greater than that of a single hole nozzle.

2.1.3 Slag Formation

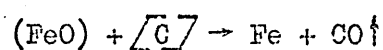
The slags encountered in oxygen steelmaking processes are a complex mixture of oxides containing up to 10 components together with small quantities of sulphides and fluxes such as Ca F_2 . No single component is present in sufficient quantity to be considered the solvent, however certain simplifying assumptions can be made. The principal oxides present are CaO , SiO_2 and FeO and it has been noted that the total concentration of these components remains reasonably constant at about 80 wt.% throughout the blow¹⁸. It has been argued that the use of a pseudoternary

$\text{CaO} - \text{SiO}_2 - \text{FeO}$ system (Figure 1) gives a good approximation of the true position of the liquidus limits of typical steelmaking slags. With the L.D. - A.C process the P_2O_5 content of the slag is too high to be ignored and the $\text{CaO} - \text{SiO}_2 - \text{P}_2\text{O}_5 - \text{FeO}$ quaternary system must be considered ¹⁶.

In the first few minutes of the blow, silicon, manganese and iron are oxidised producing a slag rich in SiO_2 , MnO and FeO ¹⁸. The early formation of a high silica content slag produces rapid fluxing of the lime. The slag layer adjacent to a lime particle becomes saturated in dicalcium silicate (C_2S), the presence of which is thought to inhibit further dissolution. Fluorspar is frequently added to aid the lime solution process. The natural reserves of fluorspar in this country are however diminishing rapidly and this factor, together with growing fears concerning the health hazards associated with its use, has prompted investigations to find alternative fluxes. Materials such as manganese oxide, bauxite and borates have been tried as alternatives to fluorspar, but with mixed success ²⁵.

As lime is taken into solution, the composition of the slag moves towards the CaO corner of the ternary system (Figure 1). The slag composition may enter the ($\text{C}_2\text{S} + \text{liquid}$) phase field during the second third of the blow, resulting in the precipitation of C_2S crystals in the melt ¹⁸. Heats in which this occurs are found to be prone to slopping. This is related to the increased tendency for foam formation, as a result of the marked increase in slag viscosity associated with the precipitation of solid C_2S crystals ¹⁹.

During the initial stages of the blow, the iron oxide content of the slag is high. This gradually decreases as lime is fluxed into the slag and as the decarburisation rate increases ⁴.



In the later stages of the blow the iron oxide content again rises as the decarburisation rate falls¹⁸. Analysis of the $\text{Fe}^{2+} / \text{Fe}^{3+}$ ratio in slag samples suggests that the oxygen potential of the slag may remain relatively constant during the middle portion of the blow²¹. The final iron oxide content of the slag is a complex function of the lancing conditions i.e. the jet momentum, oxygen flow rate, lance height, etc.²².

Bardenheuer has noted that the slag temperature rises rapidly during the early stages of the blow and can be as much as 300°C hotter than the bulk bath^{18, 24}. The temperature of the metal bath increases steadily throughout the blow so that at tapping the differential is less than 50°C ²³.

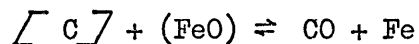
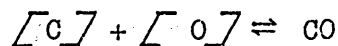
2.1.4 Refining Characteristics

Thermodynamic data for the reactions occurring is well documented and the predicted order of removal of elements in terms of their equilibrium oxygen potentials has been calculated²⁶. The theoretical order of oxidation of impurities should be silicon, carbon, manganese. In order for phosphorus to be oxidised, the activity of P_2O_5 must be lowered by using a basic slag. Figure 2 shows the change in the composition of the metal bath during the course of the blow and it will be noted that the oxidation of the different impurities appears to be occurring simultaneously¹¹. The kinetics of the overall process still appear to depend upon the removal of carbon and it is the description of the kinetics of decarburisation where controversy exists.

As predicted by thermodynamic considerations, most of the silicon is removed early in the blow. Initially the manganese content also drops rapidly as a result of oxidation, but later a slight reversion occurs followed by a second fall near the end of the blow. The increase during

the middle of the blow is thought to be associated with either the melting of scrap⁹ or possibly the direct reduction of manganese from the slag as a result of temperature changes and variations in slag composition which affect the activity of MnO^{3,23}. The early production of a basic slag with a high iron oxide content ensures favourable conditions for the oxidation of phosphorus²⁸. Despite the highly basic slag produced, the relatively high oxygen concentrations attained in the metal bath inhibit sulphur transfer. Only about half of the sulphur initially present in the charge can be removed during the course of the blow, indicating the necessity for careful control over the materials charged to the furnace²⁹.

The principal refining reaction is of course the removal of carbon.



The equilibrium relationship between the carbon and oxygen contents in the metal is well established^{30, 31}. The oxygen content of the bath increases in the early stages of the blow, reaching values well in excess of that in equilibrium with the carbon present²⁸. As the carbon concentration decreases, the oxygen content in the metal approaches its equilibrium value, becoming close at less than 0.1 wt.%C. Fujii has suggested that at tapping the L.D. process may be nearer to equilibrium than the open hearth with respect to the carbon-oxygen reaction. In some instances, values of the (wt % [C] x wt % [O]) product below the equilibrium line for CO at one atmosphere have been quoted, but the significance of this is not clear^{32, 33}.

The variation in decarburisation rate throughout a typical blow is illustrated in Figure 3. This may be idealised as shown in Figure 4 effectively dividing the blow into three periods.

The rate of decarburisation initially increases until a steady

value is eventually attained, although quite abrupt fluctuations about the mean rate can occur during this period. The initial increase in decarburisation rate appears to be critically dependent upon slag formation, since the plateau rate is attained more rapidly if a preformed slag is retained from the previous heat ¹¹. The plateau decarburisation rate is generally believed to be controlled by the rate of introduction of oxygen into the system ³⁴. The carbon concentration in the bath gradually decreases until eventually the transport of this species in the metal phase becomes rate controlling and hence the decarburisation rate begins to decrease. Carbon transport appears to become most important at compositions ranging from 1.2 to 0.2 wt.%C ⁴¹.

One of the main problems encountered in developing control techniques is that the decarburisation path can vary considerably from cast to cast despite using apparently identical conditions ¹¹. This behaviour has been noted with heats in which scrap has been deliberately excluded ¹⁵ and even when blowing onto simple iron-carbon alloy melts ³⁵. Meyer concluded that the process must be metastable and that minor differences in chemistry or blowing performance could lead to major differences in refining path.

The rate of decarburisation during the middle portion of the blow is primarily controlled by the rate of introduction of oxygen into the system. Ichinoe has shown experimentally that by increasing the oxygen blowing rate the plateau decarburisation rate increases and the overall blowing time is shortened ³⁶. The decarburisation efficiency of oxygen during this period is very high (80 - 100%). In practice the maximum rate of delivery of oxygen is restricted to that which avoids unreasonable amounts of material being ejected from the converter. This is reflected in the fact that the blowing time is practically independent of the converter capacity ¹⁶. Richardson has suggested that major reconsider-

ation of vessel design will be required if refining rates are to be further increased ³⁴.

Much controversy surrounds the explanation of the high refining rates encountered and in particular the decarburisation mechanism in the L.D. process. Early theories were based upon the concept that refining was principally taking place in a localised high temperature region at the point of impingement of the gas jet on the bath. Okhotski, carrying out experiments in a transparent crucible, has confirmed the existence of a primary reaction zone where the jet contacts the metal and also noted that gas evolution can occur from a secondary zone inside the metal bath, around the impact crater ³⁷. Various workers have claimed to have determined the temperature of the "hot spot" in actual steelmaking furnaces. Values range from 2000 to 2600 °C, i.e. 500 - 900°C in excess of the average bath temperature ^{4, 38, 39}. Mathematical models involving the direct oxidation of C, Si, Fe, Mn and P by the oxygen gas at the point of impingement have been developed and reasonable success is claimed ⁴⁰.

The concept of decarburisation taking place entirely in such a localised area as the jet impingement zone is difficult to reconcile with the very high oxidation rates observed. Slag samples, taken from L.D. furnaces, were shown to contain droplets of metallic iron and this led to the theory that in fact the majority of refining was taking place in a slag-metal emulsion and not in the metal bath as had been supposed.

2.1.5 Foams and Emulsions in L.D. Steelmaking

Systems consisting of small liquid droplets or gas bubbles, dispersed in a liquid medium, may be called an emulsion when the distances separating the neighbouring droplets or bubbles are large enough to allow the independent movement of the said drops or bubbles. When the

volume of the liquid medium in a gas-liquid emulsion is small, as compared with the total volume of gas bubbles, the medium will be present only in the form of thin films separating the adjacent bubbles. These cannot move freely and the system is called a foam ⁵¹.

It has long been known in open hearth steel making that a good deal of metal could be dispersed as droplets in the slag and that these droplets contributed to the decarburisation rate and the transfer of oxygen to the bulk bath ^{34, 42}. Foaming slags in open hearth practice were considered a hinderance since they inhibited heat transfer and oxygen transfer to the bath by increasing the diffusion distance, as well as interfering with the operation of the fuel burner ^{43, 44, 45}.

The existence of metal droplets in the slag in L.D. steelmaking has also been known for some time. Operators also realised that there was a relationship between the production of a controlled, foaming slag and the creation of favourable refining conditions, especially with respect to phosphorus removal ^{46, 47, 48}. It is only recently, however, that foams and emulsions in oxygen steel making have been studied in detail and their full importance to the process has begun to be understood.

2.1.6 Contribution of foams and emulsions to refining

Evidence that most of the refining in the L.D. process was taking place in a slag-metal emulsion, and not in the jet impingement zone, was obtained independently by Trentini and co-workers in France ^{16,49,50,51} and by Meyer and co-workers in the U.S.A. ^{11, 21}. Meyer's investigations were carried out on a 230t. L.D. furnace, whilst Trentini's were on an L.D. - A.C. plant.

During the course of a blow, the vessel was found to contain an appreciable volume of slag-metal-gas emulsion. Tap hole ejections were collected and the samples analysed. It was found that at times 30% or more of the total metallic charge could be dispersed in the slag. The majority of droplets collected were in the size range of 1 - 2 m.m. diameter. The interfacial area available for the refining reactions consequently was very large, at times reaching 50,000 m² in a 230 t. capacity converter ²¹.

The results from the chemical analysis of droplets confirmed that they were in a much more advanced state of refinement than the bulk bath. The absence of any droplets containing very low carbon contents added weight to the theory that oxygen transfer in the slag and hence the oxygen blowing rate, was rate controlling ³⁴. It was thought that carbon diffusion did not become rate controlling until the carbon concentration dropped to about 0.35 wt. % C. Meyer suggested that at the height of refining most of the decarburisation was occurring within the slag-metal emulsion and that over the entire blowing period as much as two thirds of the total carbon present was removed in this way, rather than from the bulk bath. Trentini noted that the conditions within the emulsion were especially favourable for dephosphorisation.

The residence time of droplets in the emulsion has been estimated to be about 3 minutes by Meyer ²¹ and 2 - 2.5 minutes by Price ⁹. Residence times may however vary significantly throughout the blow depending upon the volume and fluidity of the slag.

The mechanism proposed by Meyer for the decarburisation process, involved the unsteady state transfer of oxygen from the slag to droplets, which were completely surrounded by slag. Since the metal droplets could exist surrounded by slag for some period of time without contacting a CO gas bubble, a high degree of supersaturation could be

achieved with respect to the carbon-oxygen reaction. CO may be discharged by a number of mechanisms ¹¹:

- (a) By coming into contact with CO bubbles rising through the slag.
- (b) Heterogeneous nucleation at the slag-metal interface especially in the presence of solid particles in the slag.
- (c) Homogeneous nucleation - the observed carbon and oxygen concentrations were sufficiently high to suggest the possibility of this mode. CO bubbles formed in this way would grow at an explosive rate, leading to the destruction of the droplet and creating a still finer dispersion.

Meyer envisaged that the refining of droplets involved a cyclic oxidation and discharge process, each cycle taking as little as 10 seconds. In the first cycle, silicon would be oxidised and might retard the subsequent oxidation cycle.

Hazeldean has studied the decarburisation of single droplets in oxidising slags and suggests that the nucleation of CO bubbles may not be as difficult as once thought. It was shown that gas could be evolved continuously from the surface of a reacting droplet, although this may have been assisted by the close proximity of the crucible wall ^{128, 129}.

The techniques used by Meyer and Trentini have been criticised, since it is not known how representative the emulsion samples were of the conditions inside the furnace. The results do show that foams and emulsions can form inside the steelmaking vessel and do create a large surface area for reaction, although what proportion of the overall refining processes occurs within them is uncertain.

Wester has shown that a carbon boil can occur within the metal bath in the later stages of the blow ⁵⁶. Under normal blowing conditions this commenced after about 75% of the initial carbon present had been

removed. Refining in the first part of the blow was thought to occur principally in the slag-metal foam.

Price has attempted to remove samples directly from the vessel during the course of the blow using a weighted sample mould attached to a length of chain. Slag-metal emulsion solidified on the chain while a metal sample was simultaneously obtained from the mould. He estimated that during the course of the blow, only about one third of the carbon initially present was removed in the emulsion, and that the maximum proportion of the total metallic charge which could be emulsified at any time, was only about 15%. Unfortunately, Price was unable to take samples earlier than half way through the blow. Also, doubts have been expressed about the reliability of this technique for assessing the degree of emulsification, since it is possible that the number of dispersed droplets may be consistently underestimated ³.

Questions have been raised concerning the necessity for a slag-metal emulsion at all. In experiments in which either the amount of slag was minimised ⁵⁵ or in which a "dry slag" was produced, it has been shown that decarburisation is unaffected by the absence of an emulsion ^{52, 53, 63}. Decarburisation as a result of the direct interaction between ejected metal droplets and the gases above the bath may be important here. (See section 2.3.4(a)). Unfortunately these conditions are not conducive to good dephosphorisation ⁵². There is also evidence that the presence of a foaming slag may inhibit fume formation ⁵⁵.

Okano, after development of a mathematical model from practical considerations, has estimated that 75% of the carbon present is removed in the jet impact zone, 20% in the emulsion and the remainder by the nucleation of bubbles in the bath. His estimate of the oxygen-metal interfacial area appears to be much greater than the slag-metal interfacial area, which is difficult to reconcile with emulsion formation ⁵⁴.

The multiphase bubble dispersions encountered in LD steelmaking consist of gas bubbles, droplets of metal, minute solid oxide particles (e.g. precipitates of C_2S) and larger particles (e.g. lime) suspended in the liquid slag. The foam is dynamic in nature, in that its stability is dependent upon the continued evolution of CO from dispersed droplets and to a lesser extent from the bulk bath. If gas evolution ceases or is reduced significantly, then the foam collapses⁵¹.

Metal droplets are ejected from the bulk metal bath into the slag phase by a combination of:

- (i) The action of the impinging oxygen jet.
- (ii) The action of CO bubbles rising out of the bath into the slag.
- (iii) The resultant turbulence on the surface of the metal bath where surface waves impinge on one another²¹.

Of these primary modes of droplet formation, (i) is undoubtedly the most important.

Secondary emulsification may occur by the ejection of metal particles from droplets already in the foam, as a result of the nucleation of CO bubbles within the droplet^{119, 128, 129}.

The CO evolved from a droplet may help to stabilise its presence within the slag phase. Hazeldean has shown that the presence of gas bubbles around and within a reacting droplet can cause it to be buoyed up^{128, 129}. There is evidence that this can occur in steelmaking foams and hence will prolong the length of time the droplets are retained in the slag phase^{16, 51, 52}.

Although the slag-metal-gas emulsions encountered in L.D. steelmaking are essentially dynamic in character, accounts are given in the

literature of mechanisms, on the basis of which, some degree of stabilisation appears feasible. Possible mechanisms for the stabilisation of foams and emulsions in iron and steelmaking have been discussed by Kozakevitch ^{51, 57}.

High viscosity of the continuous phase is perhaps the most obvious factor stabilising both foams and emulsions. The presence of large, complex anions in the melt increase viscosity significantly. In typical basic oxygen furnace slags, the anions are small and move easily. It therefore appears improbable that this will contribute significantly to emulsion stabilisation, except possibly in the very early stages of the blow, whilst the slag temperature is low and silicon is being oxidised.

The apparent viscosity of a slag may however be increased significantly by the presence of a suspension of fine solid particles. Small quantities of suspended matter may stick to the surface of droplets or bubbles, preventing coalescence and inhibiting their separation from the system. The precipitation of dicalcium silicate in the L.D. process and the silicophosphate phase $\text{[(2CaO} \cdot \text{SiO}_2\text{)(3CaO} \cdot \text{P}_2\text{O}_5\text{)]}$ solid solution in the L.D.-A.C. process are known to be associated with excessive foam formation and slopping ^{16, 21, 51}.

On account of their large surface areas and the high interfacial energies associated with slag-metal-gas systems, the foams and emulsions encountered in steelmaking tend to be unstable. The adsorption of surface active solutes at the interface may assist stabilisation by lowering the interfacial energy. An extensive review of interfacial phenomena in metal and metal oxide systems has been presented by Kozakevitch ⁵⁹.

SiO_2 , TiO_2 , Fe_2O_3 and especially P_2O_5 have all been shown to lower the surface tension of steelmaking slags. Cooper and Kitchener have experimentally assessed the stability of foams in the SiO_2 -CaO- P_2O_5 system ⁵⁸.

Simple CaO-SiO₂ melts never gave a stable foam, but the decay time was sufficiently slow to suggest that a dynamic foam could be sustained. The addition of P₂O₅ brought about a marked increase in foam stability in melts containing greater than 50 mole % SiO₂. It was suggested that the high concentration of these surface active oxides at the interface could, in acid slags, result in the formation of a monomolecular film of anions, which would be more complex than those in the bulk melt. This film would have a much higher viscosity than the bulk slag and would consequently inhibit bubble coalescence and bursting. In basic slags of the compositions encountered in L.D. steelmaking, such complex groups will not form. Cooper and Kitchener noted that in slags containing less than 50 mole % SiO₂, P₂O₅ additions had little or no effect on foaming. Adsorption phenomena are thus unlikely to be important except in the very early stages of the blow, before significant amounts of lime have been taken into solution ¹⁶.

Little practical work has been carried out on the study of the adsorption of silicate and phosphate groups at metal interfaces, although mechanisms have been suggested by which droplet stabilisation may occur ⁶⁰. Again these mechanisms only appear feasible in acid melts.

The surface tension of iron, and iron alloys is lowered significantly by oxygen and sulphur in particular ⁵⁹. It has been suggested that spontaneous emulsification may occur when transfer of a surface active agent such as sulphur or oxygen is occurring. A concentration gradient of surface active elements along the interface can result in an interfacial energy gradient which may set up interfacial turbulence. This could create low pressure regions in the interfacial zone which may lead to spontaneous emulsification ^{59, 61}.

In the later stages of the refining process, the rate of decarburisation begins to drop below the plateau value and becomes dependent upon the carbon concentration in the metal. This can occur at compositions varying between 1.2 and 0.2 wt % carbon⁴¹, depending to some extent upon the oxygen blowing rate⁶². As the carbon content of the bulk phase approaches that of the emulsified metal, the emulsion begins to collapse, since not enough CO is being generated to sustain it. The decarburisation rate in these latter stages is believed to be dependent upon carbon transport within droplets in what is left of the emulsion, and within the bulk metal phase²¹.

During this period, the rate of decarburisation is no longer dependent upon the rate of oxygen supply through the lance, except in so far as the action of the oxygen jet supplies momentum to the bath for continued turbulence. In the production of very low carbon steels, therefore, lower blowing rates than those commonly used for refining can be employed¹⁵.

Szekely and Todd have attempted to relate the diffusion paths for carbon and oxygen through the emulsion to the composition at which the rate becomes dependent upon carbon concentration⁴¹. During the period of steady decarburisation, they showed that the diffusion path for oxygen was much longer than that for carbon. The composition at which carbon diffusion became important was shown to be variable, depending upon the geometric structure of the foam. In their model however, they considered a slag-metal-gas emulsion in which metal was the continuous phase. In L.D. steelmaking emulsions, the slag is generally believed to be the continuous phase, although the presence of an inverted emulsion in the metal bath has been suggested⁹.

The inherent practical difficulties associated with the study of the mechanisms operative within the L.D. vessel, has prompted a number of workers to develop room temperature models in order to simulate certain of the processes occurring. In some cases a model has been used to study a particular aspect of the process, e.g. the interaction between a gas jet and a liquid bath, interaction between a gas jet and a foam, slopping or splashing. In other cases, attempts have been made to study a more complete model of the process by involving a chemical reaction between the gas jet and the bath which produces a gaseous product.

2.2.1 The Jet Impingement zone

A gas jet impinging onto a bath of liquid produces a depression in the surface. Rosler and Stewart⁷⁹ have defined three modes of interaction between a vertical jet and the liquid:

(i) With a low jet momentum and/or a large lance height, a shallow depression is produced which has cylindrical symmetry about the vertical axis of the jet.

(ii) With increased jet momentum and/or reduced lance height, the depression becomes deeper and is frequently surrounded by a raised lip. At some critical depth droplets begin to be torn from the lip of the crater. This is known as the splash mode.

(iii) With further increase in velocity or reduction in nozzle height, much deeper penetration into the bath takes place, accompanied by an apparent reduction in the amount of outwardly directed splash. The impact crater becomes unstable, oscillating non-symmetrically about the vertical axis of the nozzle and possibly dispersing bubbles of gas into

the liquid phase. This is known as the penetration mode ⁸⁰.

The geometry of the depression produced by the impinging gas jet may be influenced by the jet momentum, the lance height, the nozzle diameter and the physical properties of both the liquid and the gas phases. Numerous investigators ^{65 - 77} have attempted to develop a relationship between these parameters, often with the aid of room temperature models. This aspect of jet-liquid interaction has been reviewed by Chatterjee ⁷⁸ and it is not proposed to elaborate further on this. Chatterjee ⁸¹ has suggested that the most widely applicable solution for the depth of depression formed is that developed by Wakelin ^{72, 73}.

$$\frac{n_o}{h} \left\{ 1 + \frac{n_o}{h} \right\}^2 = \frac{115}{\pi} \cdot \frac{\dot{M}}{Lgh^3} \quad - 2.1$$

Meyer ¹¹ has expressed doubt about the usefulness of relationships of the type shown above in practical steelmaking operations, since the true lance height is rarely known and often varies throughout the blow. The formation of a slag-metal emulsion effectively increases the lance height, whilst the presence of gas bubbles within the bath reduces the lance height. In addition, the position of the bulk slag-metal interface, for a given charge weight, will vary throughout a campaign depending on the state of wear of the refractory lining.

Few studies have been made of the conditions governing the onset of the penetration mode. Rosler and Stewart ⁷⁹ have investigated the effect of varying the surface tension of the liquid phase on the jet penetration characteristics. By studying the impingement of an air jet onto various water-ethanol solutions they were able to establish the regimes for stable, oscillating and splashing surface indentations, as a function of jet velocity and surface tension. Molloy ⁸⁰ has suggested that the oscillations and rotation of the depression associated with the penetration mode arise from instabilities inherent in the gas flow system.

He showed that a jet could oscillate if directed into a blind cavity in a solid block. Using a slice model he established the conditions under which the penetration and splash modes occurred, for an air jet impinging onto water. Extrapolation of these findings to commercial steelmaking operations⁹ suggest that the jetting conditions are well within the regime for the penetration mode. This is in agreement with Flinn's⁶ suggestion that the optimum refining conditions are produced when the oxygen jet penetrates to at least 50% of the depth of the metal bath.

The effect on jet penetration of covering the bath with a layer of liquid of lower density, to simulate the slag layer in steelmaking, has not been fully investigated. Maatsch⁶⁵, studying the interaction of an oxygen jet with aqueous zinc chloride solution, noted that the presence of a thin layer of oil on the bath increased the depth of penetration at low jet momentums. The increase was less marked at higher jet momentums or when using a thicker oil layer. Turkdogans experiments with a layer of oil on water showed that a dome formed in the lower liquid, below the jet impingement zone, when only the upper liquid was penetrated. Increasing the jet momentum, so that the jet penetrated through the upper layer, led to the emulsification of the water in oil.

2.2.2 The Splashing Mode

Investigations using room temperature models have shown that splashing commences at a definite critical depth of depression for each system and hence at a critical impact pressure^{66, 68}. Early attempts to correlate the physical properties of the phases in the system with the critical depth of depression for the onset of splashing are somewhat limited. Banks and Chandrasekhara suggested that the density of the liquid and the

gas were important ⁶⁶. Rosler and Stewart ⁷⁹ and Turkdogan ⁶⁸ observed a relationship between the surface tension and the critical depth of depression. Mathieu noted that the onset of splashing was influenced by the viscosity of the liquid and to a lesser extent by the lance height ⁷⁶.

With the aid of dimensionless analysis and the results of model studies, using various liquids and gases, Chatterjee ^{78, 81} was able to establish a relationship between the viscosity, density and surface tension of the liquid and the critical depth of depression:

$$\left\{ \frac{g \rho_L}{\sigma} \right\}^{\frac{1}{2}} \bar{n}_{cr} = 0.53 \log_{10} N_M + 11.33 \quad -2.2$$

For, $10^{-4} < N_M < 10^3$

where,

$$N_M = \left\{ \frac{g \mu_L}{\rho \sigma^3} \right\} \quad -2.3$$

Chatterjee estimated that for liquid steel the critical depth of depression would be approximately 2 cm. The blowing conditions normally encountered in steelmaking produce a depression in the metal bath considerably deeper than this and hence extensive disruption of the slag and metal layers is inevitable.

Quantitative studies of the volume and size distribution of the liquid droplets ejected by the impinging gas jet are rather limited.

A number of workers have measured the total volume of liquid ejected from a model converter by an impinging gas jet. Chedaile and Horvais ⁸³ found that the volume of liquid ejected from the vessel increased, with increasing jet momentum, up to a maximum value. Any further increase in momentum beyond this caused the volume of liquid ejected to be reduced. Sheridan ^{84, 85, 86} using a similar technique showed that a three hole lance produced less ejections from the model than a single hole lance. The main disadvantage of this technique is that it does not give any indication of the total volume of droplets splashed within the vessel.

Chatterjee^{78, 81} used a series of trays situated at the surface of the liquid in order to collect the droplets ejected from the impingement zone. Experiments with water indicated that on increasing the jet momentum or decreasing the lance height caused the amount of splashing to rise to a maximum value. Beyond this, further changes caused a decrease in the volume of liquid splashed. The maximum in the volumetric splashing rate appeared to be associated with the onset of the penetration mode.

The presence of a layer of foam on the bath has been shown to have a marked effect on splashing behaviour. KunLi⁸⁷ studied the splash patterns produced by jets, from inclined nozzles, impinging onto a bath of water covered by a layer of foam. The presence of the foam layer reduced the number of droplets leaving the bath, although their size tended to be larger and their distribution more random.

2.2.3 Bath Circulation

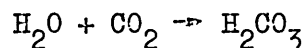
The transfer of momentum from the impinging gas jet induces motion within the metal bath. A number of workers have studied the flow patterns developed in models by introducing coloured dyes or colloidal particles into the liquid bath^{72, 73, 78, 88, 89, 90}. The pattern generally developed in the bath involves outward flow from the impact crater, down the side wall of the vessel, returning across the bottom and back upwards to the impingement zone. Flinn⁶ has shown that this mode of circulation is probably produced in commercial steel making baths. Maatsch and Sheridan however, have shown that when jetting onto a liquid in which the jet gases are highly soluble, a flow pattern in the reverse direction may be established^{89, 91}.

Kluth and Maatsch⁹² have studied the interaction of a gas jet

with a foam and have shown that the circulation pattern developed is critically dependent upon the lance height. When the lance tip was below the surface of the foam, the jet acted as a pump drawing the foam downwards along the jet axis. When the lance tip was above the level of the foam, the flow pattern was reversed.

2.2.4 Mass Transfer from a Gas Jet to a liquid

A number of workers have attempted to model the transfer of oxygen from the gas jet to the liquid iron bath in the L.D. process. The most widely used model system involves the transfer of CO₂ to either water or an aqueous solution of sodium hydroxide.



Wakelin^{72,73} has experimentally determined the mass transfer coefficient of CO₂ from a gas jet to a bath of water and obtained good agreement with a quasi-steady state diffusion model. A marked dependence of transfer rate on the liquid surface velocity was noted.

Dubrawka⁹⁹, studying CO₂ transfer from a jet to a bath of sodium hydroxide solution, noted that an optimum lance height existed for CO₂ absorption. The rate of CO₂ absorption increased by about 40% when nitrogen was simultaneously bubbled through the bath. The presence of a layer of foam on the surface of the bath was found to increase the reaction rate still further. This effect has also been noted by Bird⁹⁷.

The onset of vigorous splashing has been associated with an increase in the rate of CO₂ transfer to the bath^{96, 98}. Chatterjee^{78, 81} has

collected droplets ejected from a bath of water by an impinging CO₂ jet and has noted that their CO₂ content can be three to six times greater than that in the bulk bath.

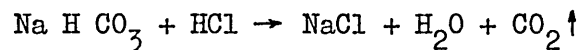
Demin¹⁰⁰ has used the transfer of ammonia to a bath of water, containing phenol phthalein indicator to assess the efficiency of mixing produced by an impinging ammonia-air jet. Increased mixing efficiency was shown to be associated with increased jet penetration and also by the use of an inclined nozzle.

Heat transfer analogies have been used to simulate mass transfer from a gas jet to a liquid bath. Sheridan and co-workers^{85, 86} have used a model involving the cooling of a water bath from 70°C to 40°C by an impinging air jet. Huang-Kim-Ho⁹³ has used a heat transfer analogy to simulate mass transfer when oxygen lancing an open hearth furnace. In this case an air jet, heated to 140-150°C, was introduced into a bath of aqueous potassium iodide solution, covered by a layer of oil to simulate the slag.

Chatterjee and Wakelin have examined the transfer of oxygen from an oxygen jet to a pool of molten silver, under conditions such that splashing did not occur. They were able to determine the mass transfer coefficient for the process and showed that the majority of oxygen transfer was occurring in the vicinity of the impact crater^{73, 78, 101}.

A number of workers have attempted to produce a more complete model of the L.D. process by involving a reaction between the jet gases and a solute in the liquid bath which produced a second gas. Van Langen⁹⁵ was one of the first to do this by impinging a jet of hydrogen chloride onto an aqueous solution of sodium bicarbonate, on which a paraffin layer floated to simulate the slag. The hydrogen chloride from the jet gases dissolved in the aqueous phase

and reacted with the carbonate in solution to produce carbon dioxide .



Similar systems have been used by Andonev ⁹⁴ and Shimotsuma ⁹⁰.

In an attempt to simulate sulphur and phosphorus transfer from the metal to the slag, Andonev dissolved potassium iodide and iodate in the aqueous solution. In the presence of hydrochloric acid, iodine was formed which was transferred to the paraffin slag.



For similar reasons, Shimotsuma in his model attempted to monitor the transfer of methyl orange from the paraffin slag to the aqueous phase.

Whilst the above models involve a reaction between the gas jet and the bath there is no reaction between the bath and the slag, since the paraffin layer is effectively inert. This is a fairly serious criticism in view of the importance placed upon the formation of foams and emulsions in current theories of the mechanism of L.D. refining.

Extensive reviews of the literature concerning the behaviour of single droplets have already been made by Crimes¹⁰² and Aeron¹⁰³ and hence only relevant features, with respect to the present work, will be outlined.

2.3.1 Hydrodynamic behaviour of falling droplets

A drop of one liquid falling through another behaves as a rigid sphere and obeys Stokes Law only when the Reynolds number is much less than unity. For steel in slag this corresponds to a diameter of less than 0.5 mm. As the diameter increases, internal circulation starts to occur within the drop, caused by the viscous forces operating at the surface with the continuous phase¹⁰⁵. Internal circulation tends to produce an increase in velocity beyond that predicted by Stokes Law. As the size increases further, the drop begins to deform to an oblate spheroid and the velocity eventually reaches a maximum value. The peak velocity is generally associated with increased droplet distortion and the onset of oscillations, both of which tend to reduce the velocity. Ultimately a size is reached at which the oscillations are so pronounced that the surface tension forces are no longer sufficient to prevent the break up of the droplet.

The generalised curve for the terminal velocity of droplets, falling through a liquid phase, as a function of droplet size is illustrated in Figure 5.

A number of workers have attempted to produce theoretical and empirical corrections to Stokes Law, allowing for various modes of

circulation within the drop. These only tend to be useful at low Reynolds numbers. In metallurgical processes, the droplets of interest have diameters between 1 and 5 mm with Reynolds numbers between 100 and 1000¹⁰⁴. These have both a wake from which vortices are torn off and well developed internal circulation patterns.

The most successful relationship between the terminal velocity of a free falling droplet and its size is that attributed to Hu and Kintner¹⁰⁷. They determined the terminal velocities of droplets of ten organic liquids, falling through a stationary water phase, covering the Reynold number range 10 to 2200. A correlation was obtained, for nine of the ten systems, in the form of a single curve (Figure 6) relating the drag coefficient (C_D), the Weber number (N_{we}), the Reynolds number (N_{Re}) and a physical property group (P) defined as:

$$P = \frac{4N_{Re}^4}{3C_D N_{we}^3} = \frac{\rho_c^2 \sigma_i^3}{g \mu_{con}^4 (\rho_d - \rho_{con})} \quad -2.4$$

A number of workers^{102, 108, 109} have also found reasonable agreement between the experimentally determined values of terminal velocity, for a number of other systems, and those predicted by the Hu and Kintner relationship, provided the continuous phase was not very viscous. Johnson and Braida¹⁸³ using continuous phases other than water, found that it was necessary to correct the correlation of Hu and Kintner for the difference in viscosity between water and the continuous phase. Thus the function $C_D N_{we} P^{0.15}$ (Figure 6) was amended to:

$$\frac{C_D N_{we} P^{0.15}}{\left\{ \frac{\mu_{con}}{\mu_{H_2O}} \right\}^{0.14}}$$

2.3.2 Mass transfer models

Although chemical control in metallurgical systems has been observed^{110, 111} it is generally accepted that at high temperatures, where most chemical reaction rates are rapid, mass transport control predominates. The factors which are likely to influence mass transport to and from droplets are the diffusion coefficients of the transferring species in the two phases, the size and rate of movement of the droplets, the degree of internal circulation and the amount of turbulence within both the droplet and the continuous phase. In addition, when the product of reaction is a gaseous phase, as for example in the decarburisation reaction, the nucleation of gas bubbles may have a significant influence on the kinetics of the process.

Mass transfer within a stagnant sphere has been considered by a number of workers^{112, 113}. Kronig and Brink¹¹⁴ and also Calderbank and Korchinski¹⁰⁹ have modified the rigid sphere diffusion treatment to allow for the effect of simple circulation patterns on the transport processes. Handlos and Baron¹⁰⁶ have considered the case of internally circulating droplets, which oscillate through small amplitudes, whilst Rose and Kintner¹¹⁵ have produced a model for more violently oscillating drops.

Mass transfer in the continuous phase has been extensively treated. Numerous solutions have been proposed for the case of mass transfer to and from stagnant spheres^{102, 103}. The Higbie penetration model¹¹⁶ has been applied to the case of circulating droplets.

The various mass transfer models available for single droplets have largely been developed by chemical engineers for application with aqueous and inorganic systems. In general the surface tension and density of the droplets in such systems are small, compared with those for liquid metals.

Richardson and co-workers^{102, 103, 104, 182} have studied the mass transport processes associated with the reaction of amalgam droplets with aqueous phases and the reaction of molten lead-zinc alloys with molten salts. The dispersed phase mass transfer coefficients determined for these systems proved to be about half those predicted by the Handlos and Baron model. Better agreement was obtained with larger droplets using the Rose and Kintner model. The continuous phase mass transfer coefficients were found to lie between the values predicted using the Higbie surface renewal model¹¹⁶ and those for a stagnant sphere. It would appear that for metals, possibly on account of their high surface tension, the circulation patterns developed within droplets are not as vigorous as for the aqueous-organic systems for which the Handlos and Baron and Higbie models are successful. It is therefore not possible to accurately predict the mass transfer coefficients in slag-metal systems.

2.3.3 Surface Phenomena

Interfacial turbulence can arise when a reaction taking place at an interface involves the transfer of a surface active agent. It arises when the eddies in the gas or liquid phase which bring reactants to the interface also bring about strong local changes in surface tension. Thus while the reaction is proceeding, the surface tension varies from one part to another over the interface and movement of the interface may consequently occur. Aeron has shown that during the oxidation of indium amalgam droplets by ferric nitrate solutions, interfacial turbulence can significantly increase the rates of mass transfer both in the dispersed and continuous phases.

Oxygen and sulphur both significantly lower the surface tension of iron and iron alloys⁵⁹. It is possible that in reactions in which these

elements are transferred, eddies in the metal or gas phases may bring about sufficiently large local changes in surface tension for interfacial turbulence to be set up ¹¹¹.

Surface active agents when adsorbed at an interface can decrease the mass transfer rates of other species. This occurs either by interference with the circulation patterns in the droplet or by reducing the effective interfacial area, by blocking transfer sites ¹⁰².

2.3.4. Previous experimental work on the refining of single droplets

2.3.4(a) Iron alloy droplets

A number of studies have been made of the reaction between iron-carbon alloys and oxidising gases. Whilst this work was largely prompted by the initial interest shown in spray steelmaking processes, the direct interaction of metal droplets with the jet and furnace atmosphere in L.D. steelmaking may be important, especially with the increasing trend towards operation with a dry slag practice.

A number of workers have studied the decarburisation of iron carbon droplets levitated in a stream of oxidising gas ¹¹⁷⁻¹²¹. It has been shown that the carbon-oxygen reaction can take place via two possible mechanisms. The first mechanism which was operative at higher carbon concentrations involved a surface reaction between carbon and oxygen and gave rise to little or no disruption of the droplet. The second mechanism involved a subsurface reaction, with carbon monoxide bubbles being nucleated inside the drop. Small metallic particles were frequently ejected from the droplet when this mode of decarburisation was operative. It was generally agreed by all workers that the former mechanism was controlled by counter current diffusion of the oxidant and product gases

in the boundary layer.

Distin ¹¹⁹ observed that the transition from surface to sub-surface nucleation could occur at various compositions, down to 0.3 wt % C, depending directly upon the rate of decarburisation while the first mechanism was operative. It was suggested that the transition occurred when the rate of carbon transport to the surface became insufficient to maintain the surface reaction ¹¹⁸. The carbon concentration at the interface would consequently drop to zero allowing oxygen to be absorbed onto the surface of the droplet, eventually forming a film of iron oxide ¹¹⁹. The bulk oxygen concentration in the droplet could then rise to a concentration which was sufficiently high to allow internal nucleation of CO. Distin observed that once the boil commenced the rate of decarburisation continued to be independent of carbon concentration until some lower carbon content was attained. This was believed to be due to the increased surface area for reaction and the increased turbulence, associated with the internal nucleation of carbon monoxide.

Richardson ¹¹¹ has suggested that the rate of carbon transport within the droplet at the transition between the two rate controlling mechanisms may be higher than Distin initially thought. It was suggested that slow chemical reaction at the interface, when the carbon content had fallen to a relatively low value, prevented oxygen being converted to carbon monoxide immediately on arrival, thus allowing the oxygen concentration to build up in the droplet.

Studies of the reaction of iron-carbon droplets during free fall through an oxidising gas have shown that the subsurface nucleation of CO commences at much higher carbon concentrations than with levitated drops ¹²²⁻¹²⁵. See and Warner ¹²⁵ suggested that internal nucleation began at about 3 to 4 wt % C, whilst Baker ¹²³ reported some degree of carbon boil at all compositions up to 4.5 wt.%C. This was attributed to the higher

degree of induced stirring produced by the levitation coil compared with that encountered during free fall. As with levitated drops the carbon boil was associated with the ejection of metal particles. The boil intensified as the carbon concentration decreased and destruction of the drop by explosion generally occurred at about 0.5 wt.% C. Roddis¹²⁴ suggested that transport in the gaseous phase only occurred at carbon contents greater than 4 wt.% C and at temperatures approaching 1600°C with pure oxygen. Attempts have been made to develop a simple counter current diffusion model^{118, 122, 123, 126, 127} for decarburisation when control lies in the gaseous phase. The rate controlling step once the boil has commenced is not clear. Baker and Ward¹²³ have suggested that joint transport of carbon and oxygen may be controlling.

The analysis of droplets, after levitation or free fall in a gaseous oxidant, have shown that the partial pressure of carbon monoxide in equilibrium with the carbon and oxygen in solution was well below that theoretically required for homogeneous nucleation to occur¹³⁹. The presence of a surface film of iron oxide is not thought to assist nucleation¹³⁸ and indeed the nucleation of carbon monoxide has been observed in nickel droplets containing carbon, when oxidation took place under conditions such that no metallic oxide formed¹¹¹. Nucleation may be assisted by the presence of surface active agents in solution in the droplet¹³⁷ or possibly vortices created at the droplet surface¹³⁶.

Hazeldean and co-workers^{128, 129} have made a qualitative study of the reaction between iron-carbon alloy droplets and an oxidising slag. An X-ray technique was employed to observe the evolution of carbon monoxide from droplets in molten $\text{CaO-SiO}_2\text{-Al}_2\text{O}_3$ slags containing various amounts of iron oxide. Two modes of carbon monoxide evolution were again noted. At higher carbon concentrations gas evolution involved a surface reaction, the bubbles apparently forming a complete halo around the drop.

At lower carbon contents internal nucleation of CO took place. A droplet containing initially about 4 wt.%C could be decarburised to less than 0.05 wt.%C in 2 - 3 minutes. The presence of sulphur or phosphorus in the metal generally reduced the rate of gas evolution, possibly due to their surface active nature, which would cause them to block possible sites for the decarburisation reaction. When silicon was present an induction period was observed during which gas evolution was slow or did not occur.

Gas bubbles rising through the slag phase produced a dynamic foam, the volume of which was very sensitive to the rate of gas evolution. The addition of P_2O_5 to the slag aided the stabilisation of the foam, possibly due to the reduction in surface tension.

Fragmentation of reacting droplets was frequently observed after the internal nucleation of CO had commenced. The coalescence of reacting droplets appeared to be difficult and, when it did occur, was associated with the explosive evolution of CO. Smaller droplets were frequently carried up into the foam, by adhering bubbles, where they were retained in the cell walls. Such droplets appeared to react more vigorously in the foam, possibly due to the presence of CO_2 , produced as a result of the reduction of iron oxides by CO.

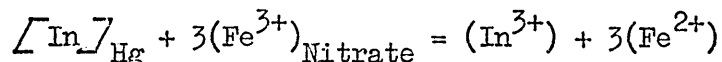
The reaction of molten iron droplets with typical blast furnace slags has been examined by a number of workers. Kozakevitch has used an X-ray technique to observe the changes in interfacial tension associated with the transfer of sulphur¹⁴⁰. The desulphurisation of iron-carbon alloys has been examined by Bargeron¹³⁰ and by Chon¹³¹. Ishii¹³² has studied the transfer of both silica and sulphur to $CaO-SiO_2-Al_2O_3$ slags.

2.3.4(b) Model Studies

Room temperature models, involving amalgam-aqueous systems, have been developed by Crimes^{102, 133} and Aeron¹⁰³ in order to simulate the mass transfer processes involved in the refining of single droplets.

Crimes¹⁰² studied the extraction of indium and zinc from amalgam drops during free fall through aqueous ferric nitrate solutions. He employed a layer of inactive carbon tetrachloride, below the ferric nitrate solution, in order to stop the reaction after allowing the amalgam drops to fall through a given height. Unfortunately the droplets carried a film of ferric nitrate solution down into the carbon tetrachloride layer, thus allowing the exchange reaction to continue. Crimes attempted to correct for this, but the results obtained have been seriously criticised.

Aeron¹⁰³ overcame the above difficulties by using a column made up of two sections. Mass transfer was allowed to take place during free fall in the upper section whilst in the lower section, separated from the upper by a constriction, the droplets were collected and the reaction allowed to go to completion. After removal and analysis of the solution in the lower section of the column, the extent of reaction during free fall could be determined. Aeron studied extraction processes involving the reactions:



The continuous and dispersed phase mass transfer coefficients were determined for the above systems.

Aeron has also developed a model involving the extraction of zinc from

lead-zinc alloy droplets by lead chloride in a molten salt solution at 450°C.



A similar system has been employed by Olander¹³⁵. Katz has studied the extraction of samarium from Bi - Mg - Sm drops by reaction with MgCl₂ in MgCl₂ - KCl - NaCl eutectic at 500°C¹³⁴.

As mentioned earlier in section 2.3.2 the mass transfer coefficients obtained for the above model systems were significantly different from the values predicted by the various theoretical models available. The difference is thought to arise from the high interfacial energy between the continuous and dispersed phases in the above model systems. It is thought that the circulation patterns developed within such droplets are not as vigorous as for aqueous-organic systems where the interfacial energy is lower and for which the theoretical models such as those developed by Handlos and Baron¹⁰⁶ and Higbie¹¹⁶ are successful.

IN AQUEOUS SOLUTIONS

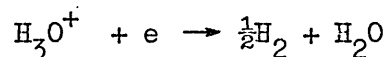
The first systematic study of the action of sodium amalgams on aqueous solutions was carried out by Fernekes¹⁴⁸. Samples of 0.07 wt.% Na amalgam were immersed in an excess of aqueous solutions of various inorganic and organic compounds and the course of the reaction followed by the volume of hydrogen gas liberated. In general, solutions of sodium salts tended to produce a slower rate of reaction than distilled water, whilst a faster reaction was obtained with acids and acid salts. Baker and Parker¹⁶¹, using a similar technique, noted that the rate of reaction of sodium amalgam with distilled water could be significantly altered by the presence of trace impurities.

Klein¹⁵¹ has studied the decomposition of 0.5 wt.% Na amalgams in aqueous hydrochloric acid and sodium hydroxide solutions containing various amounts of sodium chloride. The quantity of amalgam used was large compared with the amount being decomposed, so that during an experiment the concentration of sodium in the amalgam could be considered to remain constant. He was unable to obtain reproducible results in alkaline solutions, but in dilute acid solutions he met with more success and showed that the velocity of reaction could be considered to be made up of two terms, one corresponding to the velocity in distilled water and the other proportional to the concentration of the acid.

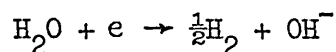
A number of workers^{150, 151, 152, 155, 156, 157} have studied the decomposition of a pool of amalgam in acid media, under conditions such that the amount of acid present was well in excess of that required to neutralise all the sodium present in the sample. Under these conditions the concentration of the acid could be considered to remain constant. Results showed that except at very low sodium concentrations in the amalgam, the rate of reaction was independent of the composition of the

amalgam but directly proportional to the acid concentration. The rate of reaction was observed to be proportional to the surface area for reaction but stirring had little effect provided the reaction area remained constant. Dunning, Kilpatrick and Fletcher did however note that the rate of reaction could become dependent upon amalgam composition with very weak acids (e.g. O-chlorophenol) or in very dilute solutions of the stronger acids (e.g. $10^{-4}N$ HCl) ^{155, 156}.

The dependence of the rate of sodium removal on the concentration of the acid reflects the fact that in acid media the reaction involves the discharge of the hydroxonium ion, which clearly must have an important bearing on the kinetics of the overall process.

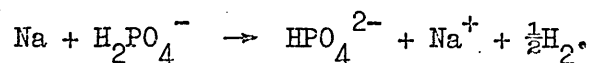


In neutral and alkaline solutions, the concentration of hydroxonium ions is low and hence the proton donor is probably a water molecule.



The experimental studies of the decomposition of alkali metal amalgams in neutral and alkaline solutions are rather limited and a great deal of discrepancy exists between the results of the various workers.

Bronsted and Kane ¹⁴⁹ examined the decomposition of dilute amalgams, containing 0.004 wt. % Na, in water and buffer solutions in the pH range 7 to 9. In a number of experiments with aqueous phosphate, glycoll and phenol buffers of constant hydrogen ion concentration, the velocity of reaction showed a linear increase with increasing buffer concentration. They attributed this to a direct reaction between the sodium and the acid component in the buffer solution, e.g.

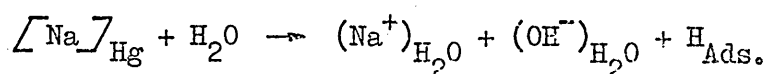


It was observed that the rate of reaction in a given solution was directly proportional to the square root of the concentration of sodium in the amalgam. This type of behaviour has been confirmed by other workers ^{155,156}.

Hammet and Lorch ¹⁵³ and Frumkin ¹⁵⁴ have showed that the rate of hydrogen evolution on a sodium amalgam surface is essentially the same as on a mercury surface polarised electrically to a potential equal to that established by the sodium-sodium ion equilibrium. The rate dependence on the amalgam concentration raised to the power 0.5 then follows directly from the Tafel equation using polarisation data for mercury surfaces at low current densities. This approach also predicts that the reaction velocity should vary inversely as the same fractional power of sodium ion activity. Bronsted and Kane ¹⁴⁹ did not carry out any quantitative work but did report that the addition of sodium chloride to neutral and alkaline solutions decreased the reaction velocity.

In the previous experimental work mentioned, it was normal practice to use a glass reaction vessel. Frumkin ^{158, 160} noted that the decomposition rates in alkaline solutions when carried out in a polystyrene cell were markedly lower than those carried out in a glass vessel. The relationship observed by Bronsted and Kane and the conclusions drawn from it are therefore only applicable in alkaline solutions where the reaction is aided by catalytic effects.

The mechanism of hydrogen evolution at mercury and amalgam cathodes in alkaline solutions has been examined by Bockris and Watson ¹⁵⁹. Mercury, in an alkaline solution, was polarised with a definite current density until the rate of decomposition of the amalgam formed became equal to the rate of metal cation discharge, and hence the amalgam potential reached its limiting negative value. The current density measured under such conditions is a measure of the hydrogen evolution rate. It was concluded that the slowest step in amalgam decomposition under these conditions was the chemical interaction of sodium with water.



Frumkin ¹⁵⁸ has carried out a similar electro chemical study of amalgam decomposition using polystyrene cells. He concluded that hydrogen evolution from alkaline solutions on mercury, at pH less than 10 was due to hydrogen ion discharge and at pH greater than 10 to a chemical interaction between sodium and water molecules. The rate of direct water molecule discharge was small compared with the other two mechanisms. Experiments in the pH range 2 to 10 showed that the rate of hydrogen gas evolution was directly proportional to the hydroxonium ion concentration.

The decomposition of sodium amalgam in aqueous media has been used as a model for slag-metal reactions by Shanahan ⁸². A model involving the reaction of 0.2 wt.% Na amalgam with $\frac{N}{10}$ sulphuric acid solution was employed to assess the efficiency of mixing produced by various agitation techniques.

It was noted in the previous chapter that a number of workers have already attempted to develop room temperature models of the L.D. process 90,94,9 All of these models involved a reaction between the gas jet and a solute in the bath, rather than a reaction between the slag phase and the bath. This is a serious criticism in view of the work of Meyer and Trentini 11, 16, 21, 49, 50, 51 who have shown that a slag foam exists within the converter during much of the blow and that a significant proportion of the metal in the converter is suspended as droplets in the foam. It appears that reactions between the droplets and the foam play an important role in the overall refining process. If this is so, it is essential that these reactions are replicated in any room temperature model that is used to study the basic oxygen steelmaking process.

Of the various reactions that occur between the metal and the slag, it is the oxidation of carbon that has the greatest influence on the formation of the slag foam since it is this reaction that produces the carbon monoxide gas in the foam. Hence, an essential requirement for any model of the process is that it should reproduce the production of gas during a reaction between the metal and the slag. The choice of suitable model systems is however very limited. The reaction between sodium, dissolved in mercury, and an acidified aqueous phase provides a room temperature system which does meet the above requirements,



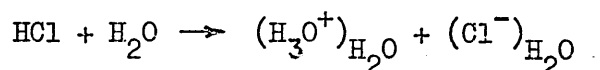
It is this system that has been used as a basis for the model developed in this work.

Mercury provides a suitable solvent for sodium, whilst also being effectively inert and immiscible with the aqueous phase. Just as slag floats on steel, the aqueous phase will float on mercury, although the phase density ratio is somewhat larger in the model than in steelmaking.

The important physical properties of mercury and water are compared with those of a typical L.D. slag and iron in Table 1. Additions of sodium do however tend to lower both the density and the surface tension of mercury ¹⁴¹. The maximum solubility of sodium in mercury at room temperature is 0.65 wt.%(Figure 7).

The viscosity of water can be increased significantly by additions of glycerol, a factor made use of by a number of workers studying model systems involving an aqueous phase ^{78, 102, 103, 109}. The viscosity ratio for the slag and metal in steelmaking is about 10:1. A 60 vol.% glycerol-water mixture gives a similar ratio for the phases in the model system. Figures 8 (a), (b), (c) and (d) show the variation of viscosity, density, surface tension and interfacial tension with mercury, for various glycerol-water mixtures. The interfacial tension between mercury and water-glycerol solution is relatively high, just as it is for slag-metal interfaces. This has been shown to be an important consideration when modelling slag-metal systems ¹⁰⁴. Glycerol is chemically inert, with respect to the components in the present model system, it is completely miscible with water and is not surface active in aqueous solutions ¹⁴².

In the initial experiments a nitrogen jet was employed to simply agitate the bath. In later experiments however, a nitrogen-hydrogen chloride gas mixture was used in order to simulate mass transfer from the jet to the model slag.



Whilst the model may appear acceptable on a qualitative basis, ideally one should also consider it in terms of similarity criteria. The problems involved in establishing precise dimensional similarity in a process such as L.D. steelmaking have been discussed by Holden and Hogg ¹⁴³. Unfortunately, the necessary conditions for complete similarity are so

complex as to be virtually impossible to achieve. The results of any model study will therefore be somewhat limited. Modelling of this kind does however provide qualitative information concerning the process and may suggest alternative quantitative approaches to the actual steelmaking problem.

3.2 Preliminary Experiments

3.2.1 The reaction between sodium amalgam and water

For the initial experiments, small quantities of amalgam were produced by dissolving sodium metal in mercury under a layer of liquid paraffin to prevent oxidation. Prior to use, the excess paraffin was removed with a pipette and the amalgam surface washed with petroleum ether. This too was removed with a pipette.

The reaction between sodium amalgam and distilled water proved to be very slow. 25 ml samples of amalgam, containing initially 0.6 wt.% Na, were allowed to react with approximately 50 ml. of distilled water in a 100 ml. beaker. Without agitation, the removal of sodium took several weeks to go to completion.

The hydrogen evolved by the reaction between sodium and water appeared to accumulate on the surface of the amalgam as a raft of bubbles at the centre of the bath. These tended to leave the raft in a steady stream from one or two localised areas. It was interesting to note that hydrogen bubbles appeared to be capable of nucleating and growing at the interface between the amalgam and the beaker. Once a bubble reached some critical size it appeared to rise up the interface between the amalgam and the beaker, cross the amalgam meniscus and join the raft on the surface.

This type of behaviour is probably further evidence in favour of Frumkin's suggestion^{158, 160} that a glass surface may catalyse the reaction between sodium amalgam and water. Since mercury does not wet glass, a thin film of water can probably exist between the surface of the beaker and the amalgam. The solubility of hydrogen in mercury is very low and hence bubbles can form at the interface, the reaction being catalysed by the glass surface.

Allowing a nitrogen jet to impinge onto the pool of amalgam produced considerable turbulence and splashing, but did not significantly increase the sodium removal rate. Figure 9 illustrates the extent of sodium removal achieved under these conditions. This was determined by allowing the jet to impinge onto the pool for a known period of time, after which a sample of the aqueous phase was removed and titrated against standardised hydrochloric acid solution to determine the amount of sodium hydroxide formed and hence the amount of sodium removed from the bath. It is interesting to note that the rate of sodium removal appears to be constant. Increasing the jet momentum increased the rate of sodium removal, presumably by creating a greater interfacial area for reaction. No attempt was made to determine the blowing rate in these early experiments.

The rate of reaction of sodium amalgam with water is clearly inadequate to sustain a dynamic foam and hence an alternative system was sought. By using an acidified aqueous phase, and hence increasing the hydroxonium ion concentration in solution, a marked increase in the rate of hydrogen evolution and general violence of the reaction was achieved.

The course of the reaction between a 25 ml sample of amalgam, initially containing about 0.6 wt.% Na, and an acidified aqueous solution was followed by monitoring the volume of hydrogen evolved, using the simple apparatus shown in Figure 10 (a). Aqueous solution of known acid concentration and of just sufficient volume to neutralise all the sodium present was introduced into the reaction vessel and the volume of gas evolved measured using a gas burette.

Typical results are illustrated in Figures 11 and 12.

Figure 11 shows that by increasing the concentration of the acid in the aqueous phase, the rate of gas evolution also increases. Additions of glycerol to the aqueous phase appear to reduce the rate of gas evolution. The rates of reaction produced by strong and weak acids are compared in Figure 12. At similar concentrations, strong acids such as hydrochloric produce a faster rate of reaction than weaker acids such as ethanoic and phosphoric. Clearly these results suggest that the concentration of free hydroxonium ions plays an important role in determining the kinetics of the process.

The effect of jetting onto a pool of amalgam covered by a layer of acidified aqueous solution was qualitatively investigated using the simple apparatus shown in Figure 10 (b). 50 ml of amalgam, containing initially about 0.6 wt.% Na, were covered by a similar volume of water-glycerol solution in a 250 ml. beaker. A nitrogen jet was allowed to impinge onto the bath, causing considerable splashing from the amalgam pool. Concentrated acid was introduced into the aqueous phase, from a reservoir, at a uniform rate.

During the course of the reaction the "slag" layer was transformed into a foam, the volume of which could be up to five times that of the

original aqueous phase present. The foam volume attained depended upon the viscosity of the aqueous phase and the rate of introduction of acid. Considerable numbers of amalgam droplets were observed falling through the foam layer, generally leaving streamers of hydrogen bubbles behind them. These droplets could take several seconds to traverse the height of the foam layer and many were left adhering to the walls of the beaker and the lance after termination of the experiment. During the early stages of the blow, large numbers of amalgam droplets could be ejected directly into the gas phase above the bath, without unduly disturbing the slag layer. This behaviour was generally observed when the aqueous phase was very viscous, but ceased once a reactive foam had developed. This is somewhat similar to the phenomenon known as sparking which occurs during the early stages of the blow in the L.D. process ¹⁵.

Three distinct stages could be identified in the refining process. As acid was introduced into the bath the foam steadily expanded until it reached a relatively constant volume, remaining at this throughout most of the blow. As sodium removal approached completion the foam gradually collapsed. Similar results were produced with both hydrochloric and acetic acid.

Preliminary attempts to follow the course of the reaction were made using a gas chromatograph. Samples of the gas leaving the reaction vessel were removed periodically, injected into the chromatograph and the hydrogen peak area determined. Typical results are illustrated in Figure 13. The rate of sodium removal appeared to reach a constant value, determined by the rate of introduction of the acid.

Experiments were performed with a pH electrode inserted into the aqueous phase. By controlling the acid flow rate from the reservoir, the acidity of the aqueous phase, especially with the weaker acids, could be maintained within a fairly narrow range.

These simple experiments served to show that the model system, at least on a qualitative basis, showed certain similarities with the slag-metal-gas interactions operative in the L.D. steelmaking process.

Various refinements of the basic reaction system were considered at this stage. In particular the use of a gas jet incorporating one of the water soluble acid gases, for example hydrogen chloride, appeared especially attractive in that it permitted a simulation of mass transfer from the jet gases to the bath. By mixing it with a suitable inert gas, independent control of the chemical and physical effects of the jet appeared feasible.

The model system finally evolved as a result of these preliminary experiments thus involved the impingement of a nitrogen-hydrogen chloride gas jet onto a bath of sodium amalgam, covered by a "slag" layer composed of a water-glycerol mixture.

It also became apparent at this time that a better appreciation of the fundamental reaction mechanisms involved in the refining of single droplets would be required in order to understand the processes occurring in the multiple droplet system created in the model.

4.1. Introduction

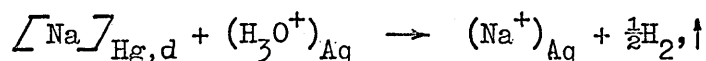
The behaviour of single, reacting droplets of sodium amalgam in acidified aqueous solutions was investigated in order to provide more information concerning the fundamental refining processes occurring in the model.

Amalgam-aqueous phase reaction systems have been extensively used in model studies of mass transport processes. Both Crimes and Aeron^{102, 103} have developed techniques for the study of reacting amalgam drops during free fall down a column containing an aqueous phase. Unfortunately the method used by Crimes has been subject to much criticism whilst Aeron's is not applicable to a reaction system in which a gas is evolved.

The technique evolved for the present work involved the formation of sodium amalgam droplets, of controlled size, at a capillary orifice. These were allowed to fall down a column of acidified water-glycerol solution. The volume of hydrogen gas produced could be measured and used to determine the amount of sodium removed during free fall through some predetermined height. Reaction was terminated when the droplets entered a layer of inert fluid in the lower part of the column. Carbon tetrachloride was generally used for this purpose since it is both immiscible with and of higher density than the aqueous phase employed. Any acid carried down in the wake of the droplet, or reaction products formed after entry into the inert fluid, were collected in a trap.

In addition to the mass transfer experiments, advanced photographic techniques have been employed in order to study the appearance of reacting droplets during free fall.

The reaction between a droplet of sodium amalgam and an acid solution,



involves a number of steps. These include:

- (i) The transport of reactants to the amalgam-aqueous phase interface.
- (ii) Chemical reaction at the interface.
- (iii) Transport of sodium ions away from the droplet.
- (iv) The nucleation of hydrogen bubbles and their escape from the droplet surface.

Any of these steps could control the rate of the overall process.

The conversion of adsorbed hydrogen atoms on the amalgam surface to bubbles of molecular hydrogen involves a nucleation and growth process. The formation of bubbles is opposed by forces resulting from the hydrostatic pressure of the liquid and the surface energy of the new interface. It is unlikely that these factors will be important in the present system however, since the turbulent conditions that exist at the back of a droplet during free fall will provide favourable conditions for the formation of bubbles. The bubbles at the reaction interface may influence the mass transport processes in other ways. Their presence will reduce the area of amalgam surface in contact with the acid solution and may modify the hydrodynamic behaviour of the falling droplet.

If we assume that the reaction at the interface is fast and that there are no bubble nucleation difficulties, then the process is likely to be transport controlled. Crimes and Olander^{102, 135} have presented a theoretical treatment for mass transfer in systems similar to the one under investigation. If the equilibrium constant for the reaction is large then the concentration of one or other of the reactants will

be zero at the interface and hence it is possible to develop rate equations for the conditions when the controlling species is in the continuous phase or in the dispersed phase. These two modes of control cannot operate simultaneously but may operate consecutively during the fall of a droplet through the aqueous phase.

4.2.1 Continuous phase control

The molar rate of transport of hydroxonium ions to the reaction interface is given by:

$$\dot{m}_{H^+} = \gamma_s A_d [\alpha_{H^+}]_{Aq} \left\{ [C_{H^+}]_{Aq B} - [C_{H^+}]_{Aq i} \right\} \quad -4.1$$

Under full continuous phase control the interfacial concentration of hydroxonium ions would be zero, in which case,

$$\dot{m}_{H^+} = \dot{m}_{Na} = \gamma_s A_d [\alpha_{H^+}]_{Aq} [C_{H^+}]_{Aq B} \quad -4.2$$

A mass balance on the droplet yields,

$$\dot{m}_{Na} = -V_d \frac{d[C_{Na}]_d}{dt} = -\frac{V_d \rho_{Hg}}{W_{Na}} \frac{d[\rho_{Na}^*]_d}{dt}, \quad -4.3$$

where W_{Na} is the atomic weight of sodium which is equal to 23 g/mol.

Eliminating \dot{m}_{Na} from equations 4.2 and 4.3

$$\frac{d[\rho_{Na}^*]_d}{dt} = \frac{-23 \cdot \gamma_s \cdot A_d [\alpha_{H^+}]_{Aq} [C_{H^+}]_{Aq B}}{V_d \rho_{Hg}} \quad -4.4$$

Since the volume of the aqueous phase is very much larger than that of a droplet, the acid concentration effectively remains constant and hence, in a given solution, the rate of sodium removal will remain constant while continuous phase control is operative.

Integrating between the boundary conditions,

$$\text{at } t = 0, \quad [\rho_{\text{Na}}^*]_d = [\rho_{\text{Na}}^*]_{d,I}$$

$$\text{and } t = t, \quad [\rho_{\text{Na}}^*]_d = [\rho_{\text{Na}}^*]_{d,B}$$

we obtain,

$$[\rho_{\text{Na}}^*]_{d,I} - [\rho_{\text{Na}}^*]_{d,B} = \frac{69. \gamma_s [\alpha_{\text{H}^+}]_{\text{Aq}} [\text{C}_{\text{H}^+}]_{\text{AqB}} t}{r_d \rho_{\text{Hg}}} \quad -4.5$$

The mobility of the hydrogen ion is however very high in aqueous solutions and hence continuous phase control involving this species is unlikely to be important.

4.2.2 Dispersed phase control

The molar rate of transport of sodium atoms to the reaction interface is given by:

$$\dot{m}_{\text{Na}} = \gamma_s A_d [\alpha_{\text{Na}}]_d \left\{ [\text{C}_{\text{Na}}]_{d,B} - [\text{C}_{\text{Na}}]_{di} \right\} \quad -4.6$$

Under full dispersed phase control the interfacial concentration of sodium will be zero, in which case,

$$\dot{m}_{\text{Na}} = \gamma_s A_d [\alpha_{\text{Na}}]_d [\text{C}_{\text{Na}}]_{d,B} \quad -4.7$$

$$= \frac{\gamma_s A_d [\alpha_{\text{Na}}]_d \rho_{\text{Hg}} [\rho_{\text{Na}}^*]_{d,B}}{r_d} \quad -4.8$$

23

By eliminating \dot{m}_{Na} from equations 4.3 and 4.8 we obtain,

$$\frac{d [\rho_{\text{Na}}^*]_d}{dt} = - \frac{3 \gamma_s [\alpha_{\text{Na}}]_d [\rho_{\text{Na}}^*]_{dB}}{r_d} \quad 4.9$$

The rate of sodium removal is thus dependent upon the bulk concentration of sodium in the droplet and since this will decrease as the droplet falls down the column, so too will the rate of sodium removal also decrease. Integrating between the boundary conditions,

$$\text{at } t = 0, \quad [r_{\text{Na}^-}^*]_d = [r_{\text{Na}^-}^*]_{d,I}$$

$$\text{and } t = t, \quad [r_{\text{Na}^-}^*]_d = [r_{\text{Na}^-}^*]_{d,B}$$

we obtain,

$$[r_{\text{Na}^-}^*]_{d,B} = [r_{\text{Na}^-}^*]_{d,I} \exp \left\{ - \frac{3 \gamma_s [\alpha_{\text{Na}^-}]_d t}{r_d} \right\} \quad 4.10$$

4.2.3 Sodium ion transport

The rate of transport of sodium ions away from the interface is given by,

$$\dot{m}_{\text{Na}^+} = \gamma_s A_d [\alpha_{\text{Na}^+}]_{\text{Aq}} \left\{ [C_{\text{Na}^+}]_{\text{Aq},i} - [C_{\text{Na}^+}]_{\text{Aq},B} \right\} \quad 4.11$$

which will be equal to the rate of sodium transport to the reaction interface \dot{m}_{Na} . The Sodium ion concentration gradient between the interfacial and bulk aqueous solution will therefore vary depending upon the value of \dot{m}_{Na} . Since the volume of the aqueous phase is much larger than that of a droplet the bulk sodium ion concentration effectively remains constant. Equation 4.11 may therefore be used to evaluate

$[C_{\text{Na}^+}]_{\text{Aq},i}$ for various values of \dot{m}_{Na} .

In order for the process of sodium removal from an amalgam drop to be mass transport controlled, the reaction at the surface of the drop must be relatively fast. Unfortunately no information appears to be available concerning the rate of this particular reaction at a mercury surface. There are however similarities between the mechanism involved in the evolution of hydrogen, as a result of the reaction between sodium amalgam and an acid, and the discharge of hydrogen at a cathode in an electrolytic cell. A considerable amount of research has been carried out on this latter process, with especial emphasis on the phenomenon known as hydrogen overpotential. It is beyond the scope of the present work to attempt a complete review so that only the relevant points will be summarised.

The potential (E) of an electrode, through which current flows, differs from the equilibrium potential (E_0), established when no current passes through the electrode. The difference between them is known as the overvoltage (η).

$$\eta = E - E_0 \quad 4.12$$

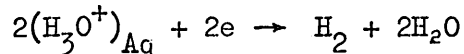
The over voltage may be attributed to a number of causes ¹⁷⁰.

The earliest known cases of activation over potential were those associated with the discharge of hydrogen and oxygen at a cathode, since the values of η involved are especially large. Significant over potentials are however associated with most electrode reactions. The magnitude of the hydrogen overvoltage varies considerably depending upon the cathode material, e.g. at a current density of 1 ma/cm^2 it ranges from 1.04v on mercury down to 0v on platinum ¹⁶⁷. In general, overpotential decreases with increasing temperature ¹⁷⁸. Its magnitude also varies with current density (i) according to the Tafel relationship,

$$\eta = a - b \log i \quad 4.13$$

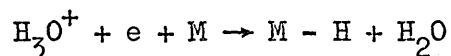
a and b are constants, their value being determined by the rate controlling mechanism operative at the cathode surface.

The evolution of hydrogen at a cathode in an acidified aqueous electrolyte can be represented by the equation:



This reaction can be considered to involve three stages ¹⁶²:

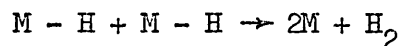
(i) The solvated proton approaches the cathode material (M), through the electrical double layer in the electrolyte, and is discharged onto a free site on the electrode surface to form an adsorbed hydrogen atom.



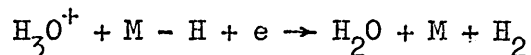
This is known as "the discharge reaction" ¹⁶³.

This process may be succeeded by one of two alternative methods by which the adsorbed hydrogen atoms may be removed from the cathode surface.

(ii) Adsorbed hydrogen atoms may combine by "the chemical desorption mechanism" ¹⁶⁴.



(iii) Alternatively the removal of an adsorbed hydrogen atom may be associated with the simultaneous arrival and discharge of another solvated proton.



This is known as "the electrodic desorption reaction" ¹⁶⁵

Thus, in the electrolytic evolution of hydrogen at a cathode surface, in an acidified aqueous electrolyte, the discharge reaction always occurs initially. It may continue to occur followed by either the chemical or the electrodic desorption process, with which it then occurs simultaneously in order to maintain the concentration of adsorbed hydrogen atoms on the surface.

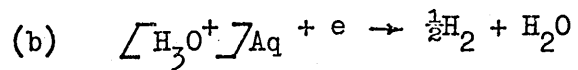
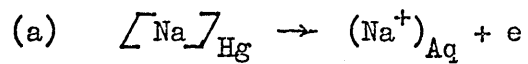
A considerable amount of experimental work has been carried out with the intention of determining the rate determining step operative on particular electrode surfaces^{168, 169}. Reviews are available of both the experimental techniques employed and the methods of interpretation of the results obtained^{166, 171, 173}. In the case of mercury it is generally agreed that the rate determining step is the slow discharge reaction^{166, 168, 172, 173, 174}. This implies that the formation of hydrogen atoms on the mercury surface occurs with difficulty, which is in agreement with the observed hydrogen adsorption behaviour of this metal¹⁷⁶. Metals with a comparatively high heat of hydrogen adsorption (e.g. Pt, Mo, W, Cu, Ni, Fe) all exhibit low over potentials, while those such as Hg, Cd, Pb and Tl, with low values, are associated with large hydrogen over voltages. Those hydrogen atoms formed at a mercury cathode will be rapidly removed by desorption processes and hence the surface concentration of hydrogen atoms will be low. The degree of hydrogen atom coverage of a polarised mercury cathode has been estimated to be less than 0.05%¹⁶⁸.

The rate of the discharge reaction can be directly related to the activity of hydrogen ions at the electrode surface ($\int a_{H^+}_s$) and the potential difference between the electrode surface (ϕ) and the centre of the charged hydrogen ion (ψ)¹⁶⁸.

$$i = \int a_{H^+}_s f(\phi - \psi) \quad 4.14$$

In practice it is found that the over potential on a mercury cathode falls progressively as the acid concentration is increased above 0.1 N^{168, 175, 177}. The relationship is however complex and is not fully understood. Below 0.1 N the overpotential is independent of the hydrogen ion concentration.

The evolution of hydrogen on an amalgam surface, as a result of the reaction between sodium and an acidified aqueous phase, can be considered to involve two processes:



Reaction (b) will involve a discharge stage and a desorption stage similar to those taking place on a mercury cathode in an electrolytic cell. It is again possible that the rate of the discharge reaction may determine the speed of the overall process. In this case, the rate of decomposition would be determined by the rate of discharge of hydrogen ions on to the amalgam surface, at a potential determined by the activity of the sodium in the amalgam and the concentration of sodium ions in solution.

A schematic diagram of the equipment used for the mass transfer experiments is shown in Figure 14 with a photograph of the actual apparatus on Plate 1.

4.3.1 The mass transfer column

The reaction column was fabricated from 6 mm thick perspex sheet. Its overall length was 70 cm and it was of square cross section, with internal dimensions of 4 cms. A square section column was employed since the flat walls would permit photography of falling droplets, without the problems of image distortion, which would have been encountered with a round tube. The column could be adjusted for vertical alignment by means of two pairs of support screws.

The ends of the column were covered by perspex plates, each held in place by eight bolts. Rubber seals ensured that the column was gas tight. The droplet collection device was supported on the top of a 16 mm i.d., pyrex glass tube which passed through the bottom plate and was held in position by a rubber bung. The bung acted as a seal whilst still permitting the position of the inner column to be adjusted to give various heights of fall for the reacting droplets. The upper plate supported the capillary tip, at which the droplets were formed, and gas inlet and outlet ports. These gas ports were used to flush out the column with high purity argon prior to an experiment, in order to prevent oxidation of the amalgam.

4.3.2 Droplet formation

Sodium amalgam was held in a constant head reservoir until required. To avoid oxidation, this was flushed with high purity argon prior to the

introduction of the amalgam. From the reservoir, the amalgam flowed into a 35 cm long, horizontal, precision bore (0.25 mm i.d.), pyrex capillary. This was connected to a capillary tip at which the amalgam was allowed to flow out and form into droplets. The horizontal capillary provided the main resistance to the flow of amalgam and thus determined the rate of droplet formation. The tip consisted of a short length of glass capillary which had been drawn down in a flame. The end had been ground flat and flame polished. Both the size of the bore and the area of the flat surface at the end of the tip were found to influence the size of droplets produced. It was also noted that the droplet frequency and also, to a lesser extent, the droplet size were dependent upon the overall head of mercury. An amalgam reservoir with a relatively high cross sectional area was thus employed in order to minimise the change in liquid head during the course of an experiment.

Droplets were released from approximately 2 cm above the surface of the aqueous phase. Crimes¹⁰² has shown that under these conditions a droplet will attain its terminal velocity in the liquid phase within 2 cm of entering the liquid and hence any anomalous effects during this period will be minimised.

Droplet sizes were determined by collecting and weighing a known number. This was generally carried out as a check after every experiment since it was found that the size of droplets being produced could be significantly altered if the tip became contaminated with water or grease, etc.

4.3.3 Droplet collection

A reacting droplet of amalgam, falling from the acidified aqueous phase into the carbon tetrachloride layer, carried a small volume of

acid with it into the lower liquid. This allowed the reaction to continue for some time. It was thus necessary to introduce a trap to collect the hydrogen evolved once the droplet had entered the carbon tetrachloride.

A diagram of the droplet collection apparatus is shown in Figure 15 and a photograph of a droplet entering it on Plate 2. Falling droplets were captured in the glass funnel, which had previously been vertically aligned with the capillary tip using a plumb bob. The length of time spent by a droplet in the funnel was short compared with the overall time in contact with the acid and hence it was assumed that anomalies due to wall effects were negligible. The falling droplets were deflected by a glass bead and entered the carbon tetrachloride phase where they were collected in a small cup. Hydrogen and the entrapped film of aqueous solution tended to rise from the cup and were again deflected by the bead. The upper section of the inner column had been calibrated to enable the volume of trapped hydrogen to be estimated.

The trapped hydrogen, acidified aqueous solution and amalgam drops effectively increased the volume of material within the inner column. This would have caused carbon tetrachloride to be forced back up the funnel. In order to maintain a constant reaction height, it was necessary to continuously drain liquid out of the inner column by the tap provided. By collecting and weighing this liquid, a measure of the total volume of fluid introduced into the column could be obtained. Since the entrapped aqueous phase rarely formed a complete circumferential film around the funnel, its volume had to be determined from a knowledge of the volumes of hydrogen and amalgam drops collected and the total volume change of the contents of the inner column. The end of the drain tube was filled with water since carbon tetrachloride tended to dissolve the grease from the drain tap leading to seepage from the column. Errors in weighing, introduced by the general volatility of carbon tetrachloride were also eliminated.

Experience has shown that a stable interface, between the acidified solution in the main column and the carbon tetrachloride within the inner column, could be maintained throughout the experiment. It was noted that the acid - CCl_4 interface could project below the end of the funnel and adhere to the top of the glass bead, which thus provided a stable datum point. The shape of this short column of liquid provided a means of monitoring the rate at which fluid had to be drained from the inner column.

Whilst it has been implied that carbon tetrachloride is inert, it should be noted that this is not strictly true. There is in fact a slow reaction with sodium ^{amalgam} but this does not significantly alter the volume of the fluid within the inner column.



Reaction with sodium metal is explosive !

4.3.4 Gas collection

The volume of hydrogen evolved by a droplet during its fall through the aqueous phase provided a simple, direct measure of the extent to which sodium removal had occurred. The gas volume was measured using a gas burette which had been connected to the top of the mass transfer column by a length of P.V.C. tubing. During the course of an experiment the position of the burette was adjusted to maintain the pressure in the top of the column at one atmosphere.

This arrangement for gas collection also provided a simple means of checking the column for leaks. A small excess gas pressure could be applied to the inside of the sealed column. Any change in the water level in the gas burette was then indicative of a gas leak.

4.3.5 Preparation of aqueous solutions.

All aqueous solutions were made up from Analar grade reagents with distilled water in graduated flasks. The determination of hydrochloric acid concentrations was carried out by titration against sodium hydroxide solutions of known strength, using phenol phthalein as indicator.

4.3.6 Preparation of sodium amalgam

For the preliminary experiments, sodium amalgams were prepared by direct dissolution of sodium metal in triple distilled mercury. This was initially carried out under a layer of paraffin or later in a glove box flushed out with high purity argon, in order to prevent oxidation of sodium. The dissolution of sodium in mercury is strongly exothermic and is often very violent. Initiating the dissolution reaction was also found to be difficult, due to the presence of surface oxidation products on the sodium, and especially so in amalgams approaching saturation, when the sodium could become coated in layers of intermetallic compounds. This method of preparation was clearly inadequate for the regular production of large volumes of amalgam.

Sodium amalgams in quantities in excess of 500 cm^3 , were produced by electrolysis of sodium hydroxide solution. The cell used was 17 cm square and 17 cm deep and was fabricated from 6 mm thick perspex sheet. The electrolyte was Analar sodium hydroxide solution, containing approximately 150 g/l - the cell holding about 2 litres of this. A platinum anode was employed. Electrical contact with the mercury cathode was achieved via a stainless steel strip passing through an Araldite plug in the side wall of the cell and across the floor of the cell.

The cell was operated at a direct current of about 5 amps from a Farnell stabilised power supply (Type TSV 70 Mk 2). Sodium was discharged at the mercury cathode whilst oxygen was liberated at the anode. The formation of crystals of sodium-mercury intermetallic compound on the surface of the amalgam indicated when saturation had been achieved. The amalgam could be drained from the cell through a hole in the side wall, below the floor level of the cell. The base of the cell was slightly tilted towards the drain hole. A short length of 1 mm i.d., glass capillary was cemented into the taphole, with a piece of polythene tubing connected to this. The capillary helped to prevent excessive amounts of Na Hg_4 from leaving the cell. Small amounts of NaHg_4 were, in practice, carried out of the cell with the liquid amalgam, but these served to maintain the amalgam in a saturated condition, since inevitably some sodium was oxidised during handling.

The amalgam from the cell was collected under alcohol, in a plastic bottle, for storage until required.

4.3.7 Treatment of used amalgams

After use, any sodium remaining in the amalgam was neutralised by contact with dilute hydrochloric acid solution. The mercury was then washed, first with distilled water and then with ethanol. Excess alcohol was allowed to evaporate. The mercury was filtered through a perforated filter paper and the resulting stream of metal allowed to fall down a nitric acid tower containing 5 v% HNO_3 solution. The mercury flowing from the swan-neck capillary at the base of the tower was collected under distilled water, washed and then returned to the electrolytic cell for re-use.

4.3.8 Analysis of sodium amalgams

An amalgam sample of about 10 g was required. In the case of the single droplet studies this was obtained as droplets from the capillary tip and with the model converter studies as a direct sample from the metal bath, removed with the aid of a 5 ml. pipette. The sample was placed in a beaker with a few drops of phenol phthalein solution and 25 ml. of $\frac{N}{10}$ hydrochloric acid solution were introduced from a pipette. The beaker was then agitated until all the sodium was neutralised. This condition was indicated when hydrogen ceased to be evolved and a tendency for the sample to break up into small moderately stable drops on agitation. The remaining hydrochloric acid was neutralised by titration against $\frac{N}{10}$ sodium hydroxide solution. The amount of sodium initially present could then be calculated. The sample of mercury was washed with distilled water and then with ethanol. After allowing to dry, the sample was weighed and hence the composition of the amalgam determined.

It is estimated that this method of analysis is accurate to 1.0%. This constitutes a maximum error of ± 0.005 wt % in an amalgam containing 0.5 wt % Na.

4.3.9 Experimental Procedure - Mass transfer experiments

The assembled apparatus for the mass transfer experiments is shown in Figures 14 and 15 and Plate 1.

The relative positions of the base plate and the inner column were first adjusted to give the required height of fall for the droplets, whilst ensuring that the column and plate remained perpendicular. The inner column could then be partially filled with carbon tetrachloride and any air in the drain tube expelled. Distilled water was introduced

into the end of the drain tube, through the glass tap, using a plastic bottle. After topping up with carbon tetrachloride, the droplet collection assembly could be inserted into the top of the inner column, taking care to prevent entrapment of air below the funnel. With the rubber seal in place, the bottom assembly could be bolted to the main column.

Using a glass funnel, the aqueous phase was introduced through the top of the main column and allowed to run down the side wall, to avoid splashing into the droplet collection funnel. The top plate, with its rubber seal, could then be bolted in position and the capillary tip fastened in position. By means of the two pairs of support screws, the capillary tip and the collecting funnel were vertically aligned, using a plumbline.

In order to prevent oxidation of the amalgam, the system had to be flushed with high purity argon, usually at a rate of $300 - 400 \text{ cm}^3$ per minute for a period of one hour. The amalgam reservoir also had to be flushed with argon for a similar period of time. After introduction of amalgam into the reservoir, the plastic tube between it and the capillary generally required squeezing in order to expel any trapped gas.

Just prior to commencing the run, a little fluid was drained from the inner column, so that the acid-carbon tetrachloride interface just touched the glass bead below the droplet collection funnel. The taps on the gas inlet and outlet ports could then be closed and the level of fluid in the gas burette noted.

Droplets of the required size were allowed to fall down the column at a rate of about 30 per minute. The duration of a run varied from about 2 to 5 minutes. Throughout the run, water had to be drained continuously from the inner column, in order to maintain the acid-carbon tetrachloride interface at a constant position, and collected in a previously weighed

bottle. Also, the gas burette was slowly raised in order to maintain the gas pressure inside the column at one atmosphere.

An experiment was terminated, when a suitable number of droplets had passed down the column, by interrupting the flow of amalgam from the reservoir. The distance from the liquid surface to the top of the glass bead was then measured using a cathetometer and the volume of hydrogen collected in the gas burette and trapped under the droplet collection funnel were determined. The amount of water drained from the inner column during the course of a run was obtained by weighing the collection bottle. At this stage it was usual to carry out a check on the size of the droplets being produced at the tip and also to collect two samples of amalgam for analysis.

The mass transfer column could then be drained and the bottom plate together with the inner column removed, thus allowing the funnel and collecting cup to be lifted clear. After neutralisation with dilute hydrochloric acid the amalgam collected was washed with both distilled water and ethanol, allowed to dry and finally weighed. The rest of the apparatus could then be dismantled, washed and allowed to dry, prior to the next experiment.

The change in composition of a known number of droplets of a certain size, which had fallen a given distance through the aqueous phase, was calculated from the volume of hydrogen liberated. Small corrections were made for the volume of aqueous phase carried down into the carbon tetrachloride by the droplets and also for the partial pressure of water vapour in the evolved hydrogen.

4.3.10 Photographic Techniques

4.3.10(a) Droplet velocity determination

The terminal velocity attained by a falling droplet was required in order to calculate the time for which it was in contact with the acid solution and hence determine the rate at which mass transfer was occurring. In all the experiments, droplets were released from about 2 cm above the surface of the acid phase, so that on entry to it they were travelling at approximately their terminal velocity. Crimes¹⁰² has shown that under these conditions the terminal velocity is achieved very rapidly.

Droplet velocities were experimentally determined using conventional cine photography. A Bolex H 16 camera was employed with either Kodak Tri X or Ilford Mark V film at a speed of 32 frames per second. In order to confirm their accuracy the filming speeds of the camera were recalibrated by Sheffield Photographic Company just prior to these experiments.

The mass transfer column was set up in the same way as for the mass transfer experiments, but with the inner column adjusted to give the maximum height of fall possible (i.e. about 60 cm). During filming, droplets were allowed to fall continuously down the column, at a rate of about 30 per minute. Oblique illumination using a single light source was employed.

Three datum lines were marked on the front of the column dividing it into two 25 cm sections, thus giving a total useful height of 50 cm. This permitted the velocities in the upper and lower halves of the column to be compared, whilst still obtaining an overall velocity for the total column. The top reference line was about 5 cm below the surface of the aqueous phase, thus eliminating the effects of any period required to

attain terminal velocity. Particular care was taken to horizontally align the camera lens with the central datum mark so that parallax errors in the upper and lower sections would be equal.

The films obtained were examined at low magnifications using a transmission light microscope, fitted with an improvised film holder, and the velocities obtained by counting the number of frames it took a droplet to traverse the distance between reference marks. The point at which a droplet passed a given mark could be estimated to an accuracy of half a frame, thus giving a maximum possible error of one frame, for fall between a given pair of marks. This constitutes a maximum error of about 3% for the overall velocity and 6% for the velocity over half of the column height. A slight correction had to be made to the results in order to allow for parallax effects due to the datum lines being some 2.3 cm in front of the line of fall of the droplets.

4.3.10(b) High speed cine photography

This was employed in order to study the motion of droplets and their accompanying wake. A Beckman and Whitely "Magnifax" high speed camera was used with Ilford Mk.V film at a speed of 3200 frames per second. This equipment was kindly loaned by the Department of Chemical Engineering and Fuel Technology at the University of Sheffield.

4.3.10(c) Still Photography

General photographs of droplets during free fall, showing a large proportion of the length of the column, were taken using a Zenith B 35 mm camera with an F2 Helios lens and using Ilford FP4 film. Illumination was provided by a Sunpak DC 7 electronic flash unit, which had a

nominal flash duration of $1/1000$ th of a second.

In order to gain more information concerning the surface topography, attempts were made to obtain close-up photographs of single reacting droplets. For these experiments a Nikon F camera with bellows attachment was employed and photographs were taken on Kodak Panatomic X or Tri X. Various commercial electronic flash units with nominal flash durations down to $1/50,000$ th of a second were experimented with, but all were found to be incapable of "freezing" the motion of droplets. Satisfactory results were eventually obtained with a Courtenay Micro-1020 micro flash unit. This had a nominal flash duration of two micro seconds with a maximum output of 50 joules at 10 kV. This too was kindly loaned by the Department of Chemical Engineering and Fuel Technology at the University of Sheffield.

The flash unit head was placed in contact with the side wall of the mass transfer column. Sheets of white card, placed parallel to the opposite wall and across the front of column, acted as additional light reflectors. The camera lens passed through a circular hole cut in the card obscuring the front of the column, at a point approximately 30 cm below the surface of the aqueous phase. A sheet of matte black paper, hung about two feet behind the column, provided a dark background. The flash synchronisation device on the camera was coupled to the flash unit's power supply by an extension lead. A shutter speed of $\frac{1}{8}$ th of a second at an aperture of f22 was employed.

In order to produce individual droplets, the drop formation apparatus had to be modified slightly. The plastic tube and three way tap between the constant head reservoir and the horizontal capillary were removed and replaced by a short length of rubber tubing and a screw clip. This permitted small volumes of amalgam to be introduced into the rubber tubing and then trapped between the clip and the capillary. By squeezing

the rubber tube, amalgam could be forced along the capillary and individual drops formed at the tip.

The total height of column within the field of view of the camera was only about 2 cm. To allow for human reflexes, it was necessary to press the cable release while the droplet was passing a point still some distance above the camera. This distance varied between 4 and 9 cm above the centre of the camera lens, depending upon the velocity of the droplets and the reflexes of the photographer.

The aqueous phase used in all the single droplet studies consisted of a 60v % glycerol-water solution, since this medium was employed as the "slag" phase in all the model experiments. To this solution was added various amounts of HCl, up to 3 moles per litre, and sodium chloride, up to 2.0 moles per litre. The initial sodium content of the amalgam was also varied during the course of the work, the maximum concentration employed being 0.6 wt %

4.4.1 Visual Observations

A droplet size of 2.4 mm diameter was employed for most of the mass transfer experiments and attempts were made to maintain the droplet size at this value for the photographic studies. Unfortunately the technique used to form individual droplets was not as reproducible as that employed to produce a controlled stream of droplets for the mass transfer experiments, and hence some size variation will be apparent in the subsequent photographs.

The initial photographs were taken with a Zenith B camera with an f2 Helios lens and Sumpak DC7 electronic flash unit. Plate 3 shows a droplet of amalgam, of approximately 2 mm diameter and containing initially about 0.5 wt % Na, during free fall through 1.1 N Hydrochloric acid, glycerol-water solution. This photograph illustrates the general visual appearance of all the reacting droplets observed. The stream of hydrogen bubbles evolved as a result of the reaction between sodium and the acid is visible, but no information can be gained concerning the distribution of gas on the surface of the droplet.

It was noted that bubble formation did not appear to commence

immediately the droplet entered the aqueous phase. For the system illustrated on Plate 3, there appears to be a period, equivalent to a distance of fall of about 4 cm, during which reaction is either slow or does not occur. The length of this "incubation period" was found to be very sensitive to the composition of the aqueous phase. Further observations on this feature will be described in the next section.

The trail of bubbles produced by a reacting droplet tended to be somewhat irregular. This behaviour is illustrated more clearly on Plate 4. The regions of high bubble density tended to rise rapidly, contracting into spherical formations as they did so, before ultimately breaking up into clusters of small individual bubbles, which rose more slowly to the top of the column.

Two high speed cine films were taken of droplets falling through the same 1.1 N HCl solution. The irregularities in the stream of bubbles produced by the reacting droplet appeared to be due to periodic variations in the size of the wake formed behind the droplet. Gas appeared to be evolved at a steady rate from the droplet surface, allowing the volume of bubbles in the wake to increase progressively until some critical size was reached, when a group of bubbles could break away. This consequently left a much diminished volume of gas in the wake region, which would proceed to steadily grow again.

The droplets, during their fall through the aqueous phase, took the shape of an oblate spheroid, with their major axis perpendicular to the direction of fall. The larger droplets appeared to be oscillating slightly and rotating about an axis parallel to the direction of fall. In some cases the wake appeared to be non-symmetrical about the vertical axis of the drop and rotation about this axis caused the bubble stream leaving the wake to assume a helical pattern.

The high speed cine films obtained were of only moderate quality, exhibiting both excessive contrast and limited definition. This is an inherent problem with the technique, caused by the necessity to use high intensity lighting with high A.S.A. films. This line of research was consequently not pursued any further. In order to obtain more information concerning the surface topography of reacting droplets, it was necessary to develop the photographic techniques described in the previous section, involving the use of a micro-flash unit with a Nikon F camera and bellows unit.

The appearance of reacting amalgam droplets, containing initially about 0.55 wt % Na, in 0.5N, 1.1 N, 1.5 N and 2.1 N hydrochloric acid solutions are illustrated on Plates 5, 6, 7 and 8 respectively. It will be noted that on each of the photographs there appear three roughly circular discs lying along the horizontal axis of the droplets. The central dark area is a reflection of the camera lens, while the lighter areas on the left and right hand sides of the droplet are respectively, the reflections of the micro flash unit and a white card used as a light reflector.

In 0.5 N solution (Plate 5) the hydrogen gas bubbles are confined to a relatively small area at the back of the droplet, leaving the front surface clear. The slightly irregular shape of this droplet suggests that it was oscillating. This is a little surprising in view of the fact that its diameter is well below that corresponding to the maximum terminal velocity for the system, (Figure 16), which is generally associated with the onset of oscillation. By increasing the acid concentration to 1.1 N a larger proportion of the droplet surface became covered by bubbles (Plate 6). The front of the drop still appears to be free from bubbles, although some can be seen adhering to the droplet surface at the point at which flow separation occurs. The wake has a slightly

stepped appearance suggesting that the droplet may have been rotating. In 1.5 N solution there is evidence of bubble formation on the front surface of the droplet (Plate 7), whilst in 2.1 N solution a large proportion of the droplet surface is apparently covered by bubbles (Plate 8). The bubbles on the front surface are very small and appear to increase in size as they are swept to the back of the drop. Whilst the droplets in 2.1 N solution still took the form of an oblate spheroid there was no evidence to suggest that they might be oscillating. It is possible that the bubbles at the interface assist in stabilising the shape of the droplet and may inhibit the development of circulation patterns within it.

On a purely qualitative basis the above results suggest that on increasing the acid concentration in the aqueous phase the rate of gas evolution increases, which is associated with an increase in the apparent surface coverage of the droplet by bubbles. There is also a slight trend for the size of bubbles being evolved to increase with increasing acid concentration. Despite the close proximity of bubbles in the wake region, coalescence did not appear to be occurring to any significant extent.

The amount of sodium chloride formed by a reacting droplet was relatively small and hence the change in concentration of the aqueous phase was negligible. In the model converter process however, the sodium chloride content of the aqueous phase increases progressively throughout an experiment and the limit of solubility may eventually be exceeded.

Photographs were taken of droplets during free fall through 1.0 N HCl solution containing 1.0 mole of sodium chloride per litre (Plate 9) and also 1.5N HCl solution containing 2.0 moles of NaCl per litre (Plate 10), which is a saturated solution at this acid concentration. These may be compared with Plates 6 and 7 respectively, where the aqueous phase did not contain any sodium chloride. The apparent surface coverage by

hydrogen bubbles remained approximately the same in both cases. The size of the bubbles being produced however, decreased significantly in those solutions containing sodium chloride and also the transition zone between the bubble free and bubble covered regions became more clearly defined.

The effect of varying the initial composition of the amalgam was examined in 1.1 N and 2.0 N HCl solutions. Plates 6, 11 and 12 are photographs of droplets containing initially 0.55, 0.34 and 0.06 wt % Na respectively, in 1.1 N HCl solution. The droplets shown on Plates 6 and 11 are very similar in appearance, but Plate 12 shows a marked change in behaviour. At low sodium concentrations the droplet has become entirely covered by relatively large bubbles, yet the overall rate of gas evolution appears to have decreased, since it is possible to see through the wake.

A similar change in appearance was noted in 2.0 N HCl solution. Plate 8 shows a droplet which initially contained 0.55 wt % Na, while Plate 13 shows a droplet which initially contained 0.18 wt % Na. In both cases a high proportion of the droplet surface is covered by bubbles, but at low sodium contents the bubbles on the front surface of droplet are significantly larger than at higher sodium contents.

4.4.2 Velocity measurements

A knowledge of the terminal velocity attained by reacting droplets, during free fall through the aqueous phase, was necessary in order to calculate the mass transfer rates and hence the rate coefficients for the process, from the experimentally determined extraction data. Various correlations have been presented which relate the terminal velocity of a liquid droplet falling through another liquid to the size of the droplet

and the physical properties of the system. The most successful of these is that attributed to Hu and Kintner¹⁰⁷ which was outlined in Section 2.3.1. Johnson and Braida have modified this relationship, by introducing a correction factor for use with systems where the viscosity of the continuous phase is greater than that of water¹⁸³. Crimes¹⁰² and also Calderbank and Korchinski¹⁰⁹ have however determined the terminal velocity of mercury droplets during free fall through water-glycerol solutions and found good agreement with the Hu and Kintner relationship, provided the viscosity of the aqueous phase was not very high.

It is reasonable to expect that the Hu and Kintner relationship should give a satisfactory prediction of the terminal velocity attained by sodium amalgam droplets during free fall through 60 v% glycerol-water solution. Values of the necessary physical properties of the phases concerned were obtained from Figure 8 and Table 1. By use of the graphs shown on Figure 6 the terminal velocity, as a function of the droplet size, was obtained for the system under investigation (Figure 16).

A droplet size equivalent to a sphere with a diameter of 2.4 mm was used in the majority of the mass transfer experiments. The Reynolds number for this system is about 100. From Figure 16 the terminal velocity of a 2.4 mm diameter droplet should be 62.5 cm/sec. The velocity measured by Crimes for the same system was 57 cm/sec¹⁰². Introduction of the Johnson and Braida correction factor for the viscosity of the continuous phase yielded a much lower prediction of the terminal velocity expected (42 cm/sec.).

The terminal velocity attained by sodium amalgam droplets during free fall through acidified water-glycerol solutions was measured using conventional cine photography. Droplets containing initially about 0.55 wt % Na were again considered in the first series of experiments.

The effect on the terminal velocity of varying the hydrochloric acid content of the aqueous phase is illustrated in Figure 17. These results are also presented in Table 3. The terminal velocity attained initially decreases quite markedly with increasing acid concentration, but appears to reach a constant value in solutions greater than about 2.0 N. Clearly this behaviour can be related to the change in visual appearance described in the previous section. It was noted that as the acid concentration increased, the apparent surface coverage by bubbles also increased. The presence of bubbles adhering to the surface would increase the general buoyancy forces on the droplet and also modify the fluid flow patterns both inside and around the droplet. The terminal velocity would appear to only reach a constant value when the apparent fractional surface coverage by bubbles approaches unity.

From Table 3 it will be noted that the velocity in the upper half of the column is generally less than that in the lower half. The difference is small and is close to the limit of accuracy of the measurement technique, but the consistency of the results suggest that it is a real phenomenon. This may possibly be attributed to slight changes in the rate of gas evolution during passage down the column or due to interaction with bubbles rising up the column. Since there were always more bubbles in the upper section than in the lower, at any given time, they would tend to impede a falling droplet more in the upper section. The difference in velocity between the upper and lower sections of the column is however small and hence a mean value has been employed in order to calculate the mass transfer rates.

In addition to velocity measurements an estimate of the incubation period could be obtained from the cine films. This was defined as the time interval between the droplet entering the aqueous phase and the appearance of bubbles in the wake region. The estimation of the position of this latter point was difficult since the filming speed was inadequate

to totally "freeze" the motion of the droplet. The results obtained are presented in Figure 18, which shows that the incubation period decreases progressively as the acid concentration in the aqueous phase is increased. The incubation period could not be estimated in solutions which were greater than 1.5 N, due to the high concentration of bubbles in the top few centimetres of the column. The incubation period did not appear to be significantly altered by the presence of bubbles already in the column.

In the previous section it was noted that the presence of significant amounts of sodium chloride in solution could alter the visual appearance of reacting droplets. The terminal velocity was determined in 1.0, 1.5 and 2.1 N solutions containing various amounts of sodium chloride up to the solubility limit for that particular solution. The results obtained are presented in Table 5 and graphically in Figure 19. In all cases there is a tendency for the terminal velocity to decrease with increasing sodium chloride concentration.

Estimation of the incubation period in solutions containing significant amounts of sodium chloride was difficult. The hydrogen bubbles evolved were very small and hence rose slowly, causing the solution in the upper half of the column to become almost opaque. The limited results obtained however suggest that the incubation period increased with increasing salt content (Figure 20).

It was noted in the previous section that when the sodium content of the amalgam droplets fell to a relatively low level the apparent surface coverage by bubbles increased and also the size of the bubbles themselves increased. Table 4 shows that this behaviour is also associated with a decrease in the terminal velocity attained. The velocities in the upper and lower sections of the column are again similar. The addition of 0.5 moles per litre of sodium chloride to the aqueous phase

did not appear to significantly alter the terminal velocity attained.

More exaggerated changes in velocity were observed with very small droplets. These initially fell down the column evolving gas in a similar manner to larger droplets. Eventually, after a certain amount of sodium had been removed, they began to decelerate. This was associated with a decrease in the rate of gas evolution and a tendency for the bubbles to adhere longer to the droplet surface. Eventually a droplet would be left adhering to one or two bubbles which grew slowly in size. If the droplet was sufficiently small, when this situation was reached it could begin to rise back up the column. This behaviour is illustrated on Plate 14. On reaching the surface, the bubbles burst allowing the droplet to fall freely again. If the droplet still contained some sodium another bubble could form and the process was repeated again.

4.4.3 Mass transfer experiments

The reaction between droplets of sodium amalgam and 60v% glycerol-water solution, containing up to 3.0 moles per litre of HCl and up to 2.0 moles per litre of NaCl was examined. Amalgams containing up to 0.6 wt % Na were employed. Droplets were allowed to fall through a pre-determined height, varying from 15 to 60 cm, down a column containing the acidified aqueous phase. The volume of hydrogen gas liberated was used to determine the amount of sodium removed and the time the droplets spent in contact with the acid phase was related to the distance of free fall by the velocity data presented in the previous section. A droplet size equivalent to a sphere with a diameter of 2.4 mm was employed in most of the experiments.

The relationship between the rate of sodium removal from a droplet

and the hydrochloric acid concentration in the continuous phase was investigated in the initial experiments. Aqueous solutions containing 0.50, 1.00, 1.47, 2.01 and 2.73 moles of HCl per litre were employed and the initial composition of the amalgam was maintained at about 0.55 wt % Na. The actual initial composition of the amalgam used for each set of experiments is given in Table 6. By standardising the experimental technique and by using the same batch of amalgam, the initial composition could be maintained within a fairly narrow range for a common set of experiments. The larger compositional variations between different sets of experiments are associated with the use of fresh batches of amalgam from the cell.

The extent of sodium removal for various contact times in each of the above solutions is illustrated in Figures 21, 22(a), 23(a), 24(a) and 25(a). Individual results are presented in Table 16. The point at which the line intercepts the x-axis has been assumed to be the same as the incubation period noted in the previous section. In a particular solution the rate of sodium removal appears to be constant and hence independent of the instantaneous composition of the droplets. The rate of sodium removal in each solution has been determined and the results are presented in Table 6 and illustrated graphically in Figure 26(a). It will be noted that the rate of sodium removal increases with increasing acid concentration in the aqueous phase. At low acid concentrations the relationship between these two variables is approximately linear, but begins to deviate from this in solutions greater than about 1.0 N. The line drawn in Figure 26(a) has been extrapolated through the origin, even though the rate of sodium removal will not be zero in a neutral solution. The concentration of hydroxonium ions would however be low and reaction would probably occur by direct interaction with water molecules.

The dependence of the rate of sodium removal on the acid concentration in the aqueous phase is still valid at slightly lower amalgam

compositions than those considered in the above series of experiments. Figure 22(a) illustrates the results obtained with amalgams initially containing 0.56 and 0.27 wt % Na in 1.00 N solution, whilst Figure 25(a) shows the effect of using amalgams initially containing 0.58 and 0.43 wt % Na in 2.73 N solution. With both pairs of results, deviation from a common straight line is only observed when a significant amount of sodium has been removed.

The effect on the sodium removal rate produced by the addition of sodium chloride to the aqueous phase has been most extensively studied in 1.47 N HCl solutions, although additional experiments have also been carried out in 0.91 N (Figure 22(b)), 2.01 N (Figures 24(b) and 24(c)) and 2.73 N solutions (Figure 25(b)). The initial composition of the amalgam used was again maintained at about 0.55 wt % Na in all these experiments.

The extent of sodium removal achieved for various contact times in 1.47 N solutions, containing 0, 0.5, 1.0 and 1.75 moles of sodium chloride per litre is illustrated in Figures 23(a) to 23(d). The observed rates of sodium removal are presented in Table 7 and are illustrated graphically in Figure 27 as a function of the sodium chloride concentration in the aqueous phase. It will be noted that the rate of sodium removal decreases as the sodium chloride content of the continuous phase is increased. Similar behaviour was observed in 2.01 N and 2.73 N solutions to which salt additions had been made. The effect of an excess of insoluble sodium chloride, held in suspension, has not been examined, although this situation did arise in the model converter.

Despite the effect of sodium chloride additions, the rate of sodium removal was still to some extent dependent upon the concentration of hydroxonium ions in solution. This is illustrated by Figure 26(b), where the rate of sodium removal observed in a number of solutions with various

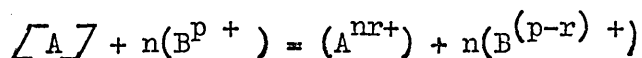
acid concentrations, all containing 0.5 moles of NaCl per litre, is compared with those obtained in salt free solutions.

It was noted earlier that the rate of sodium removal from a droplet was independent of the composition of the amalgam over a significant range of sodium contents. If however the initial sodium concentration in the droplet was reduced to a sufficiently low level, then a change in behaviour was observed. For Figure 28(a) the continuous phase contained 2.01 moles of HCl per litre and the amalgam initially contained 0.185 wt % Na. The rate of sodium removal is no longer constant and is significantly lower than that observed earlier, when the initial sodium content of the amalgam was higher (Figure 24(a)).

The composition at which the change in refining behaviour is observed has been determined in 2.01 and 2.73 N HCl solutions, using amalgam initially containing 0.27 and 0.32 wt % Na respectively (Figures 28(b) and 29). The change in behaviour appears to occur at 0.21 wt % Na in 2.01 N solution and 0.23 wt % Na in 2.73 N solution. The refining characteristics at low sodium contents have been examined in 2.01 N solution containing 0.5 and 1.0 mole of NaCl per litre (Figures 28(c) and 28(d)). Due to the relatively low rates of sodium removal produced, the reproducibility of the initial amalgam composition imposed limitations on the accuracy of the results in the above experiments. Also, in obtaining the above graphs it was necessary to use a mean value for the droplet velocity. The change in refining behaviour appears to be associated with the marked change in the visual appearance of the droplet and the decrease in terminal velocity noted in the previous sections. It is to be expected therefore, that the velocity may be varying continuously throughout the concentration range over which these changes in behaviour occur. Considerable errors may therefore exist in these particular results.

4.5.1 The refining of high sodium content droplets in salt free solutions

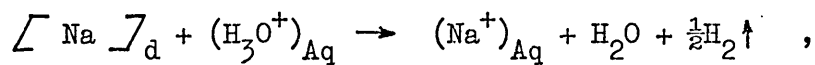
It has already been noted (Section 2.3.4(b)) that a number of workers have successfully developed suitable model systems in order to simulate the transfer of solute elements from liquid metal droplets to a slag phase. These in general have involved an exchange reaction of the type:



where $\lceil \quad \rceil$ and (\quad) represent species dissolved in the dispersed and continuous phases respectively. Such an exchange process between two immiscible liquids involves the transport of reactants to the interface and the transport of products away from it and also chemical reaction at the interface. The overall rate of exchange may therefore be determined by either transport processes, reaction kinetics or a combination of both.

It is generally believed¹⁰² that provided the reactant species are relatively simple, charge transfer reactions of the type shown above are inherently fast and hence their rate is likely to be determined by transport processes. In addition, if the equilibrium constant for the reaction is large it follows that the concentration of either one or other of the reactants must be zero at the interface, provided that equilibrium exists there. The overall rate for the process is then determined by either transport in the continuous phase or by transport in the dispersed phase, but not both simultaneously^(102, 135). By using experimental systems which satisfy the above condition it becomes possible to determine the resistance to mass transfer in each phase¹⁰³.

The reaction involved in the present model study of slag-metal droplet interactions also involves an apparently simple charge transfer mechanism.



and hence one might also expect this reaction to be fast. This model does however differ significantly from other systems previously studied in that one of the products of reaction is a gas. The equilibrium constant for the reaction, expressed in molar activities and taking pure metal as the standard state for sodium, is 10^{46} ¹⁸¹. In addition, the mobility of the hydrogen ion in aqueous solutions is sufficiently high to assume that the interfacial concentration of this species is equal to that in the bulk solution. One would therefore expect that the interfacial concentration of sodium in the amalgam would be zero. The rate of sodium extraction would then be governed by transport processes within the drop which can be related to the bulk concentration of sodium in the amalgam by the equation derived in section 4.2.2,

$$\frac{d\left[\text{Na} \right]_d}{dt} = - \frac{3 \gamma_s}{r_d} \left[\alpha_{\text{Na}} \right]_d \left[\text{Na} \right]_{d,B} \quad - 4.9$$

Aeron ¹⁰³ has determined the mass transfer coefficient within amalgam droplets to be approximately 4×10^{-4} m/s and this may be used to evaluate equation 4.9 (Figure 30).

The experimental results obtained did not however confirm the above theory. The rate of sodium removal from a droplet, when the sodium concentration was relatively high, appeared to be solely dependent upon the acid concentration in the aqueous phase. This tends to confirm the findings of earlier workers ^{155, 156} although the experimental conditions used were significantly different.

On a qualitative basis the experimental results might be explained in terms of transport control in the continuous phase. The transport of hydrogen ions in the aqueous phase would then control the process, in which case the rate of sodium removal would be given by equation 4.4, derived in section 4.2.1.

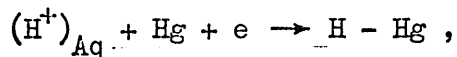
$$\frac{d[\text{Na}^*]_d}{dt} = - \frac{23 \cdot \gamma_s \cdot A_d [\alpha_{\text{H}^+}]_{\text{Aq}} [C_{\text{H}^+}]_{\text{Aq B}}}{v_d r_{\text{Hg}}} - 4.4$$

In view of the high ionic mobility of hydrogen ions in aqueous solutions this mode of control would probably be unlikely. Aeron¹⁰³ has determined the mass transfer coefficient for Pb^{2+} ions to be 0.8×10^{-4} m/s in water-glycerol solution similar to that employed here. The ionic mobility of the hydrogen ion is about an order of magnitude greater than that for the Pb^{2+} ion and hence a reasonable estimate of the mass transfer coefficient for this species would be 8×10^{-4} m/s¹⁴⁶. The theoretical rate of sodium removal may then be obtained as a function of the acid concentration in the aqueous phase by substituting appropriate values into equation 4.4, assuming for the present that γ_s is equal to one (Figure 31). It will be noted that the experimentally observed rates are well below those predicted by the hydrogen ion transport theory. Certainly at low acid concentrations the difference cannot be accounted for simply on the basis of the apparent surface coverage by bubbles. Comparison with Figure 30 would also suggest that the range of sodium concentrations over which the rate of reaction depended on the sodium content of the amalgam would be more extensive than was suggested by experimental results. The difference between the theoretical and experimental lines on Figure 31 may actually be greater than shown, since it has been suggested that Aeron's estimates of the dispersed phase and continuous phase mass transfer coefficients may be up to 25% and 17% low respectively¹⁸².

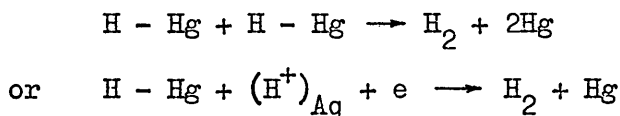
The results indicated on Figure 31 would therefore tend to suggest that some other aspect of the reaction mechanism involving the hydrogen ion must be important.

It has already been noted (section 4.2.4) that the over potential for the evolution of hydrogen at a mercury cathode in an aqueous electrolyte is quite considerable. This has been attributed to the slow nature

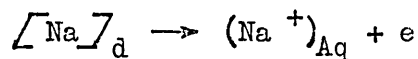
of the discharge reaction,



arising from the inability of a mercury surface to sustain high concentrations of adsorbed hydrogen atoms. The subsequent desorption reactions to form hydrogen molecules are believed to proceed with relative ease.



The evolution of hydrogen at the surface of a sodium amalgam droplet in an acidified aqueous solution must involve a similar mechanism. Hydrogen ions will be discharged at cathodic sites on the droplet surface, in this case the electrons for the process being provided by the oxidation of sodium at anodic sites.



Just as with over potential, the rate of the overall process is likely to be controlled by the rate of the discharge reaction.

The discharge process is effectively a first order reaction with rate dependence on the concentration of hydrogen ions (or more strictly the hydrogen ion activity) in the aqueous phase. This conclusion is also implied in equation 4.14 for the over potential phenomenon¹⁶⁸. On a qualitative basis these suggestions would appear to be in line with present experimental observations. Since the volume of the continuous phase is large, compared with that of a droplet, then the hydroxonium ion concentration will remain effectively constant throughout an experiment and hence the rate of sodium removal remains constant at some value determined by the acid concentration. The molar rate of sodium removal is thus given by:

$$\dot{m}_{Na} = \gamma_s A_d k [C_{H^+}]_{Aq.B}, \quad 4.15$$

where k is the rate constant for the discharge reaction.

By combining equations 4.15 and 4.3, \dot{m}_{Na} may be eliminated to give:

$$\frac{d [r_{Na}^*]_d}{dt} = \frac{69. \gamma_s k}{r_d r_{Hg}} [C_{H^+}]_{Aq,B} \quad 4.16$$

By plotting the experimentally observed rate of sodium removal against the hydrogen ion concentration a straight line should be produced, the gradient of which could then be used to determine the reaction rate constant. Unfortunately the resulting line (Figure 26(a)) only appears to be linear at lower acid concentrations. This can be attributed to a progressive decrease in γ_s as the rate of hydrogen evolution increases and also to the increasing deviation from ideal behaviour of the hydrogen ions in solution. If we assume that γ_s approaches unity in solutions of low acid concentration ($< 1.0N$), then the gradient of this portion of the curve on Figure 26(a) yields a value of approximately 2.9×10^{-4} m/s for the reaction rate constant. This may be compared with the estimated value of the mass transfer coefficient for hydrogen ions of 8×10^{-4} m/s.

Photographs of reacting droplets have shown that the apparent surface coverage by bubbles increases as the rate of hydrogen evolution increases. This is associated with an increase in the buoyancy forces acting on a droplet and hence a reduction in its terminal velocity. The true surface coverage by hydrogen bubbles is difficult to ascertain since it is not known what portion of each individual bubble is actually in contact with the droplet surface. The close approximation of Figure 26(a) to linearity for solutions which are less than 1.0 N suggests that γ_s under these conditions is close to one. This is much greater than would be suggested simply by examination of Plates 5 and 6. The deviation of Figure 26(a) from linearity at higher acid concentrations represents 8% at 1.5 N, 15% at 2.0 N and 30% at 2.75 N. This must be attributed to both variations in γ_s and also the deviation from ideal behaviour of the

hydrogen ion in solution. In all cases however, the variation from linearity is much less than would be suggested by the apparent surface coverage by bubbles indicated on Plates 7 and 8.

The general appearance of the droplets shown on Plates 5, 6 and 7 has led to speculation concerning the distribution of the anodic and cathodic sites on the droplet surface. In solutions up to 1.5 N, the hydrogen bubbles appeared to concentrate at the rear of the droplet leaving the front surface apparently clear. Local values of the mass transfer coefficient are higher at the front of a droplet and therefore it is a more favourable site for the transport of sodium. This suggests that anodic sites might have been established at the front of the droplet where oxidation of sodium atoms was taking place. The liberated electrons would be conducted to cathodic sites away from the front of the droplet, where discharge of hydrogen ions could take place. The turbulent conditions that exist towards the rear of the drop would certainly provide favourable conditions for the nucleation of bubbles.

In 1.5 N solution (Plate 7) isolated bubbles are visible on the front surface of the droplet, while in 2.1 N solution considerable numbers of bubbles are apparent in the frontal region. These bubbles are much smaller than those at the rear of the drop, giving the front surface a somewhat unusual appearance (Plate 8). These observations would tend to suggest that the anodic and cathodic sites are distributed more randomly over the droplet surface than implied by the photographs of droplets in less concentrated acid solutions.

The reason for the incubation period, during which gas evolution was apparently inhibited, is not clear. It may possibly reflect some initial difficulty in nucleating bubbles arising from the slow accumulation of adsorbed hydrogen atoms on the amalgam surface.

Additions of sodium chloride to the aqueous phase have been shown to produce a marked decrease in the rate of sodium removal from a reacting droplet. Figure 26 illustrates the effect on the rate of sodium removal of introducing 0.5 moles/litre of NaCl to solutions of varying acid concentration. For Figure 27 various amounts of sodium chloride, up to 1.75 moles/litre, were added to a 1.47 N, HCl solution. This behaviour is accompanied by a marked decrease in the size of the gas bubbles evolved (Plate 10) and a slight reduction in the terminal velocity attained by the droplet during free fall (Figure 19).

The sodium ions formed as a result of the reaction between the amalgam and the acidified water glycerol solutions must be transported away from the anodic sites on the droplet surface. The rate of transport of sodium ions away from the interface is given by:

$$\dot{m}_{\text{Na}^+}'' = \left[\alpha_{\text{Na}^+} \right] \left\{ \left[C_{\text{Na}^+} \right]_{\text{Aq.i}} - \left[C_{\text{Na}^+} \right]_{\text{Aq.B}} \right\} \quad 4.17$$

The rate of discharge of hydrogen ions and hence the rate of removal of sodium from the amalgam is given by:

$$\dot{m}_{\text{Na}}'' = k \left[C_{\text{H}^+} \right]_{\text{Aq.B}}, \quad 4.18$$

where k is the rate constant for the discharge reaction, which was estimated to be $2.9 \cdot 10^{-4}$ m/s in the previous section.

$$\text{Since, } \dot{m}_{\text{Na}}'' = \dot{m}_{\text{Na}^+}'' \quad , \quad 4.19$$

we may equate expressions 4.17 and 4.18 to obtain an equation involving the interfacial concentration of sodium ions,

$$\left[C_{\text{Na}^+} \right]_{\text{Aq.i}} = \left[C_{\text{Na}^+} \right]_{\text{Aq.B}} + \frac{k \left[C_{\text{H}^+} \right]_{\text{Aq.B}}}{\left[\alpha_{\text{Na}^+} \right]_{\text{Aq}}} \quad 4.20$$

The conditions for sodium transport are more favourable at the front of a droplet and the rear surface will also tend to be more obscured by bubbles. If then we consider only the frontal region of the drop it is reasonable

to assume a local value for the mass transfer coefficient away from the surface of about $1.6 \times 10^{-4} \frac{10^3}{\text{m/s}}$. By substituting appropriate values into equation 4.20 it is possible to determine the interfacial concentration of sodium ions, for various bulk concentrations of sodium chloride, as a function of the acid concentration in the aqueous phase (Figure 32).

The maximum solubility of sodium chloride in 60 v % glycerol-water solution, at 25°C, is 2.95 moles per litre¹⁸⁰. By using the solubility product for this solution, the solubility of sodium chloride in solutions containing various amounts of HCl has been estimated and the results superimposed on Figure 32.

Examination of Figure 32 shows that in certain solutions the solubility product for sodium chloride is likely to be exceeded at the surface of the droplet, which would result in the formation of salt crystals. It is possible that the presence of these salt crystals might have an adverse effect on the kinetics of the surface reaction, although the thermodynamics of the reaction suggest that this would be unlikely. An interfacial layer of salt crystals might act as a physical barrier to the transfer of reactants, effectively reducing the surface area available for reaction, so that,

$$\gamma_S = 1 - (\gamma_{H_2} + \gamma_{NaCl}) \quad 4.21$$

In a solution containing 1.47 moles of HCl/litre, increasing the bulk sodium chloride concentration would increase the amount of insoluble salt formed at the interface, resulting in a progressive decrease in the value of γ_S . This would explain the observed decrease in the rate of sodium removal. Unfortunately, photographs of reacting droplets in salt solutions have failed to reveal the presence of any such crystallites. Their volume would be comparatively small however and the photographic techniques used might be inadequate to detect their presence.

It was noted that the addition of sodium chloride to the aqueous phase also brought about a marked reduction in the size of the bubbles produced. Sodium chloride is not thought to be surface active in aqueous solutions and hence this phenomenon is difficult to explain in terms of changes in the surface properties of the system. The presence of sodium chloride crystals at the surface of the droplet may increase the number of sites available for bubble nucleation resulting in the production of larger numbers of smaller bubbles. The observed decrease in bubble diameter may be associated with an increase in γ_{H_2} which would contribute to the general decrease in the rate of sodium removal.

It is interesting to note that on Figure 32 the interfacial concentration of sodium chloride for a droplet in 2.1 NHCl solution is in excess of the solubility limit even when the bulk concentration of NaCl is zero. The sudden appearance of large numbers of small bubbles on the front surface of the droplet on Plate 8 may possibly be associated with the formation of salt crystals which would assist bubble nucleation.

4.5.3 The refining of droplets with reduced sodium contents

Experimental results have indicated that provided the sodium content of the amalgam is relatively high the rate of sodium removal is independent of the composition of the amalgam. This is not true when the sodium content has fallen below some critical value, determined by the acid concentration in the aqueous phase. The type of behaviour observed at reduced sodium contents is illustrated by Figure 28(a), where the amalgam initially contained 0.19 wt % Na. This suggests that under these conditions the transport of sodium within the droplet may be controlling the overall refining rate, in which case the composition of a droplet after falling for some period of time "t" through the aqueous phase should be given by

equation 4.10. A slight correction must be introduced however, to account for the incubation period. This gives,

$$\left[r_{Na}^* \right]_{d,B} = \left[r_{Na}^* \right]_{d,I} \exp \left\{ - \frac{3 \gamma_s \left[\alpha_{Na} \right]_d (t-t_0)}{r_d} \right\}$$

4.22

Taking logarithms,

$$\log_{10} \left[r_{Na}^* \right]_{d,B} = \log_{10} \left[r_{Na}^* \right]_{d,I} - \frac{3 \gamma_s \left[\alpha_{Na} \right]_d (t-t_0)}{2.303 r_d}$$

4.23

This has the general form of a straight line relationship. The results shown on Figure 28(a) can be presented in this form (Figure 33) and a straight line is obtained, which indicates that sodium transport control is operative. The gradient of the line is given by:

$$\frac{3 \gamma_s \left[\alpha_{Na} \right]_d}{2.303 r_d} = 0.208$$

4.24

The value of $\left[\alpha_{Na} \right]_d$ is approximately $4 \times 10^{-4} \text{ m/s}^{103}$ and the equivalent radius of the droplets used was 1.2 mm. Substitution of these into equation 4.24 yields a value for γ_s of approximately 0.5 which means that 50% of the droplet surface was effectively being masked by hydrogen bubbles. The close approximation of Figure 33 to linearity suggests that γ_s must remain fairly constant, at this value, during the droplets passage down the column. This high degree of bubble coverage is reflected in the general appearance of reacting droplets with reduced sodium contents (Figures 12 and 13).

The behaviour of the bubbles on the surface of the reacting droplet appeared to be significantly different from that observed while hydrogen ion discharge was rate controlling. The maximum surface coverage by bubbles in 2.0 N solution at high sodium contents was estimated to be about 15%, while at reduced sodium concentrations in the droplet it reached about 50%. While hydrogen ion discharge control was operative the value

of γ_s appeared to increase with increasing rate of hydrogen evolution, yet with the onset of sodium transport control and reduced rates of gas evolution, the value of γ_s also appears to increase. At low sodium concentrations in the droplet the hydrogen bubbles apparently adhere to the surface of the droplet for a longer period, allowing them to grow to a larger size, which in turn produces a marked decrease in the terminal velocity attained by the droplet. The reason for this change in behaviour is not understood, but may possibly be associated with changes in the surface properties of the amalgam at reduced sodium contents.

Attempts have been made to experimentally determine the composition at which the rate controlling mechanism changed from hydrogen ion discharge to sodium transport. In 2.01 N acid solution the critical sodium content was about 0.21 wt %, whilst in 2.73 N solution it was about 0.23 wt %.

The rate of the hydrogen ion discharge reaction is given by equation 4.18 while the rate of sodium transport under conditions of full dispersed phase control is given by,

$$\dot{m}_{Na}'' = [\alpha_{Na}]_d [C_{Na}]_{d,B} \quad 4.25$$

By eliminating \dot{m}_{Na}'' from equations 4.18 and 4.25 an expression can be obtained giving the critical composition at which the change in controlling mechanism occurs.

$$[C_{Na}]_{CRIT} = \frac{k [C_{H^+}]_{Aq B}}{[\alpha_{Na}]_d} \quad 4.26$$

In practical terms,

$$[\rho_{Na}^*]_{CRIT} = \frac{k \cdot [C_{H^+}]_{Aq B} \cdot 23}{[\alpha_{Na}]_d \rho_{Hg}} \quad 4.27$$

By substituting appropriate values for the constants in equation 4.27, the critical sodium content has been evaluated as a function of the acid concentration in the aqueous phase (Figure 34). The experimentally

determined values of the critical droplet composition in 2.01 and 2.73 N solutions are also indicated on Figure 34. It will be noted that the experimentally determined values are higher than the theoretical prediction. This can probably be ascribed to the deviation from ideal behaviour of the hydrogen ion in concentrated acid solutions. More strictly the hydrogen ion activity should have been used, rather than acid concentration, but lack of information concerning water-glycerol solutions has prevented this. There may also be errors in the experimental values, arising from the use of a mean velocity, when in fact it may actually vary continuously through the composition range during which the mechanism change is taking place.

4.5.4 Comparison with metal-slag systems

It is interesting to compare the results of these model experiments with the refining of iron-carbon droplets in an oxidising slag and in particular with the work of Hazeldean and co-workers^{128, 129}.

Hazeldean noted that especially at low carbon concentrations the carbon monoxide bubbles, formed as a result of the oxidation of carbon, could remain attached to a droplet inhibiting its descent through the slag and in some cases causing it to be buoyed up. Similar behaviour has been noted in the model system when the sodium concentration in the droplet was low. There is also evidence that this may occur in L.D. steel making foams^{16, 51, 52}.

Hazeldean observed that the carbon monoxide gas frequently formed an apparently complete halo around a reacting droplet, although the definition of the x-ray photographs obtained was rather limited. It was suggested that a gaseous oxidation mechanism involving the CO/CO_2 system might be operative. The presence of a gas halo has also been observed

around droplets in the model system, yet there is no comparable gaseous redox system available.

At high carbon concentrations it is believed that the rate of decarburisation is controlled by the rate of oxygen transport in the slag, in which case the molar rate of carbon removal is given by.

$$\dot{m}_c = \gamma_{s,d}^A \left[\alpha_{FeO} \right]_s \left[C_{FeO} \right]_{s,B} \quad 4.28$$

In the model system, continuous phase mass transport control was not encountered, but rate dependence on the hydrogen ion concentration in the aqueous phase, which is the analogue of the oxygen concentration in the slag, was observed.

$$\dot{m}_{Na} = \gamma_{s,d}^A k \left[C_{H^+} \right]_{Aq,B} \quad 4.15$$

At low carbon concentrations in the droplet, transport of carbon can become rate controlling,

$$\dot{m}_c'' = \left[\alpha_c \right]_d \left[C_c \right]_{d,B} \quad 4.29$$

Similarly in the model, sodium transport control has been observed .

$$\dot{m}_{Na}'' = \left[\alpha_{Na} \right]_d \left[C_{Na} \right]_{d,B} \quad 4.25$$

The reaction mechanism does however differ in that with the iron-carbon system, CO bubble nucleation generally occurs within the droplet at low carbon concentrations. In addition, with the decarburisation reaction there is no analogous product of reaction to the sodium chloride produced by the model system.

The blast furnace metal and the slag phase in the L.D. steelmaking process were simulated in the model system by a pool of sodium amalgam covered by a layer of water-glycerol solution. The supersonic oxygen jet was represented by a subsonic gas jet composed of a mixture of nitrogen and hydrogen chloride. This was allowed to impinge onto the surface of the amalgam bath causing droplets to be sprayed out into the aqueous phase. In addition, the aqueous phase dissolved HCl from the jet gases causing it to become strongly acidic. The amalgam droplets reacted with the acid to produce hydrogen bubbles which resulted in the formation of a dynamic foam. By analysis of the waste gases leaving the converter, the rate of sodium removal could be monitored.

The model converter process has been used to study the effect of a number of recognised steel making variables and also to investigate the effect of certain modifications to normal steelmaking practice.

A diagram of the model converter and ancillary equipment is shown in Figure 35 and a general view of the apparatus can be seen on Plate 15.

The apparatus can be considered in three main sections:

- (a) The gas supply
- (b) The converter vessel
- (c) The exhaust gas system.

For reasons of safety, these were all sited beneath a fume extraction hood and surrounded by a polythene curtain, which extended down to within 20 cm of the floor.

5.2.1 (a) The Gas Supply

The gases used were supplied in cylinders by B.O.C. Oxygen free nitrogen, with a quoted minimum purity of 99.9%, and technical grade hydrogen chloride, with a quoted minimum purity of 99.0%, were employed. Hydrogen chloride is highly soluble in water (see Table 2) and on dissolving in the aqueous slag phase, dissociated to provide free hydroxonium ions for the reaction with sodium amalgam. The nitrogen gas acted as an inert diluent which made possible the use of comparatively high jet momentums without the necessity to use excessively high HCl flow rates. Its presence also allowed some degree of independent control over the chemical function of the jet, as a source of one of the reactant species, and its physical effects, in creating droplets and stirring the bath.

The flow rates of the gases were controlled by means of the needle valves on the cylinder regulators. For prolonged runs, or when using a high HCl flow rate, a heater was attached to the regulator on the HCl cylinder to prevent excessive cooling.

The gas flow rates were monitored by means of a pair of Series 1000 Rotameters. A number 7 Rotameter with a Koranite float was used in conjunction with the hydrogen chloride supply and a number 18 Rotameter, with an aluminium alloy float was used to measure the nitrogen flow rate. The quoted accuracies of 7 K and 18 A Rotameters are respectively $6\frac{1}{2}\%$ and 4% at their maximum flow rate. The temperature and pressure of the gas leaving each Rotameter was monitored.

The two gas streams were introduced into a common mixing vessel with a single outlet pipe made of polythene tubing, leading to the lance. Air could be bled into the mixing vessel through a tap. This was only necessary after terminating an experiment, in order to prevent the aqueous phase being drawn back up the lance, as a result of the continued dissolution of hydrogen chloride remaining in the system.

The lance simply consisted of a length of parallel bore, 4mm i.d. glass tubing. Its tip had been ground, so that it was both flat and perpendicular to the axis of the lance, and flame polished. The temperature and pressure of the gas mixture entering the lance were monitored. The jet momentum was calculated from the relationship:

$$\dot{M} = \frac{\rho_{G,LA} \dot{V}_{G,La}^2}{A_{LA}} \quad 5.1$$

The lance passed through a rubber seal in the top of the model converter and was held in position, perpendicular to the surface of the bath, by a clamp. The height of the lance tip above the amalgam surface could be varied and was measured using a cathetometer. In most experiments the lance tip was below the surface of the model slag and its height above the amalgam surface had to be determined from the position of a paint mark placed on the lance about 4 cm from its tip.

5.2.1(b) The converter vessel

The converter vessel (Plate 16) was made in two sections by vacuum forming sheets of 3 mm thick Perspex over machined aluminium formers. Figure 36 shows the cross sectional profile of the model which represents, to a 1:30 scale, a 90 tonne converter at Normanby Parks Works, Scunthorpe at some time in the middle of a typical campaign. A 10 cm high cylindrical offtake, with an internal diameter of 7 cm was bolted on to the top of the vessel. This section was fabricated from 6 mm thick perspex sheet. The lance, the exhaust gas pipes and the sampling probes all passed through and were supported by this upper section. The three sections of the converter vessel were bolted together by means of flanges, which were made from 6 mm thick perspex sheet and cemented in position. Rubber gaskets, sandwiched between the flanges ensured that the vessel was gas tight.

The vessel was designed to hold 500 cm^3 of amalgam in a pool with a maximum depth of 5.5 cm. In all experiments the "slag" phase consisted of 250 cm^3 of 60 v % glycerol-water solution. The choice of the slag volume used was somewhat arbitrary, but was influenced by the need to have an adequate volume in order to take a reasonable amount of sodium chloride into solution, whilst still being comparable with the slag-metal volume ratio encountered in typical L.D. steelmaking practice. 250 cm^3 of water-glycerol solution produced a "slag" layer 1.8 cm deep with an interfacial area of 125 cm^2 in contact with the amalgam pool.

During the course of an experiment the vessel, mounted on a stand, was totally immersed in a tank of water. This served three purposes. Firstly, in the event of any gas leakage from the vessel, hydrogen chloride would not escape into the atmosphere. Secondly, both the dissolution of hydrogen chloride in water and the reaction of sodium with an acid are exothermic and hence the water in the tank prevented the vessel becoming too hot. Finally, for photographic work, the flat front of the tank and

the water within it helped minimise distortional effects produced by the curvature of the vessel.

5.2.1(c) The exhaust gas system

The exhaust gases were composed of a mixture of nitrogen, hydrogen and hydrogen chloride. These left the reaction vessel by two independent systems (Figure 35). The main exhaust gas stream was washed free from hydrogen chloride, by bubbling it through a tank containing about 40 l of water, before introducing it into the laboratory fume extraction system.

Samples for hydrogen analysis were removed from a secondary exhaust gas system. A flow rate of about 10 l/min was maintained through this. The gas mixture was washed free from hydrogen chloride by bubbling it through a bottle containing 1.5 l of distilled water. Hydrogen and nitrogen are only sparingly soluble in water and hence the composition of the gas mixture was not significantly altered by this treatment. Any excess water entrained in the gas stream was collected in a trap. The gas mixture finally passed through a series of sample tubes which could be sealed by taps at both ends, thus allowing a sample to be trapped within them. Up to 15 sample tubes were attached to the system, but flow through a maximum of only 3 was permitted any instant. As one tube was sealed, with a sample inside it, a new one could be opened allowing the gas stream to flow through it. Samples were generally taken at intervals of 30 seconds. The gas mixture passing through the sample tube was introduced into the laboratory fume extraction system.

The effect on the refining process of varying the pressure in the reaction vessel was examined in a series of experiments. The pressure inside the vessel was increased by introducing a constriction into the

exhaust pipe, close to the model converter. The constriction simply took the form of a plastic plug, through which a small hole had been drilled. By varying the size of the hole in the plug, different pressures could be achieved inside the vessel.

5.2.2 Sampling and analysis of gas mixtures

By measuring the volumetric flow rate of nitrogen through the system and the hydrogen content of the waste gases, it was possible to determine the rate of sodium removal from the amalgam in the reaction vessel. The concentration of hydrogen in the waste gases was low, generally less than 5 v %, and hence analysis techniques involving gas chromatography were employed. The high diffusivity and the relatively high thermal conductivity of hydrogen make it ideally suited to this method of analysis.

5.2.2(a) Sample collection

The gas sample tubes were made from 20 cm long pieces of 12 mm i.d., pyrex, glass tubing with a tap sealed into either end. A small hole was cut through the wall of the tube about 5 cm from one end using a diamond cutting wheel. This allowed a hypodermic needle to be inserted into the tube, in order to remove samples for injection into the chromatograph. A piece of self sealing silicone rubber strip was placed over the hole and held in place by a double turn of stainless steel wire. Before assembly, the interface between the rubber strip and the glass surface was sprayed with Edwards silicone sealant, which after leaving to harden overnight produced a gas tight seal. The tubes were generally checked to ensure that they were gas-tight by connecting one end to a manometer and introducing gas into the other end, to produce a slight excess of pressure in the tube. Any change in the manometer reading indicated a leak. The rubber

seal was replaced and the taps cleaned and greased prior to every experiment.

After the withdrawal of a specimen for analysis it was necessary to replace the volume of gas removed from the tube by introducing an equivalent volume of a suitable liquid, in order to prevent a negative pressure being created. This was achieved by totally immersing the sample tube in a bath of hydrogen saturated water. The tube was held in a clamp, inclined at an angle of about 30° to the horizontal, with the end nearest the rubber seal uppermost. A small amount of air was generally trapped in the open end of the lower tap and before the tap could be opened this had to be flushed out using a syringe filled with water. The upper tap was left closed. The hypodermic needle of the gas syringe could then be inserted into the tube through the rubber seal and a sample withdrawn, whilst still maintaining a slight positive pressure inside the tube. Before introducing a sample into the chromatograph, the hypodermic needle was always washed in alcohol and dried to prevent water being introduced into the separation columns.

5.2.2(b) The chromatograph

A Fisons Mini I gas chromatograph was employed. The unit included two columns, one containing silica gel and the other containing a 5 A molecular sieve of 40 - 60 mesh. The latter was found to be more suitable for hydrogen analysis. Samples were introduced into the active column, through an injection port sealed by a siliconerubber serum cap, using a Hamilton gas tight syringe. The detector employed in the instrument consisted of a two thermistor katharometer. The optimum operating conditions were determined by trial and error and are summarised in Table 8.

Both columns periodically required reactivating in order to prevent the accumulation of moisture, which could seriously effect the accuracy of

the instrument. Reactivation was carried out after every third experiment by heating the columns in an oven at 525°C , whilst passing high purity argon through them at a pressure of 10 Kg f/cm^2 (15 lb f/in^2). The total heating time was 15 minutes after which they were allowed to cool, while still passing a stream of argon through them. This procedure was rigorously adhered to as slight variations could bring about significant changes in the calibration of the instrument.

Samples were introduced into the chromatograph using a 1 ml Hamilton gas-tight syringe. The sample volume employed was 0.5 ml and this could be reproduced to an accuracy of 0.5%

Attempts were made to continuously analyse the gases leaving the vessel with the aid of a katharometer, sited in the waste gas stream. Both hot wire and two thermistor type katharometers were improvised. This work was abandoned after difficulties were encountered in maintaining a constant flow rate and in stabilising the temperature of the gases flowing through the instrument.

5.2.2(c) Calibration

Figure 37(a) shows a typical analysis trace produced on the chart recorder after the injection of a gas sample into the chromatograph. The first peak is attributed to hydrogen whilst the second broader peak is due to nitrogen. The dotted line indicates the position of the oxygen peak. This was occasionally observed in the first sample taken after the commencement of an experiment, but its appearance on any other occasion indicated that the sample tube was leaking and that the result was consequently invalid.

The area enclosed by a peak is a measure of the quantity of that component in the specimen. The area under the hydrogen peak was

determined by approximating it to a triangle as shown in Figure 37(b). Normally four separate specimens were taken for analysis from each gas sample and the mean hydrogen peak area determined. Using a previously prepared calibration chart, the composition of the sample could then be determined. From a knowledge of the flow rate of nitrogen through the model converter and after applying a small correction for the vapour pressure of water in the sample, the rate of sodium removal from the amalgam could be determined.

Mixtures of hydrogen and nitrogen in various ratios were produced by mixing the gas streams from a pair of Quickfit FMO/S flowmeters using di-n-butyl phthalate as the manometer fluid. These were calibrated using an Alexander Type 809 gas meter, which had a quoted accuracy of $\pm 0.25\%$. The gas streams were mixed by passing them through a column containing coarse silica gel particles. The resulting gas mixture was introduced into a second vessel, with a silicone rubber plug in the wall, through which samples could be removed using a gas tight syringe. Gas mixtures containing up to 5 v % H_2 were produced in this way and used to calibrate the chromatograph.

As an additional check on the above method, a number of cylinders containing hydrogen-nitrogen mixtures of known composition were purchased from B.O.C. Special Gases Division. These contained 1.05, 3.10 and 5.00 % hydrogen. The results obtained with these mixtures agreed with those produced by the previously described method. These standard gas mixtures were also used to check the calibration of the chromatograph after every experiment. It was found that results could be reproduced to an accuracy of about $\pm 7\%$.

5.2.3 Experimental Procedure

A general view of the assembled apparatus is shown on Plate 15. The converter vessel was initially positioned in the perspex tank and horizontally aligned on its stand, using a spirit level.

The sodium amalgam used in the model converter experiments was produced by the method described in section 4.3.6. Using a measuring cylinder, 500 cm³ of amalgam were introduced into the reaction vessel, through a funnel, with its tip submerged below the surface of a pool of distilled water. This helped to minimise sodium oxidation. Most of the water layer was removed using a 25 ml and a 5 ml pipette, leaving a thin film covering the amalgam surface. More distilled water was introduced and then removed in the same way, to eliminate any sodium hydroxide formed during the transfer of amalgam to the vessel. A small quantity of water-glycerol solution, of the same composition as that used for the model slag, was carefully introduced into the vessel by pouring it down the inside wall. This too was removed, leaving a thin film over the amalgam surface to prevent sodium oxidation. This was repeated twice. 250 ml of the aqueous "slag" solution could then be introduced into the vessel.

Two samples each of about 10 g were removed from the amalgam bath at this stage, using a 5 ml pipette, and analysed for sodium using the method described in section 4.3.8.

The top section of the converter, together with its sealing gasket, could then be bolted in position and the lance inserted to the desired height above the amalgam surface with the aid of a cathetometer. The vertical alignment of the lance was always checked, to ensure that it was perpendicular to the liquid surface, before clamping it in position. Finally the outer tank was filled with water, totally immersing the model converter.

An experiment was commenced by introducing nitrogen and hydrogen chloride into the system at some predetermined flow rate. One operator was required to control the flow rate of the gases and also to monitor the temperature and pressure of the gas leaving the rotameters. A second person was required to monitor the temperature and pressure of the gas mixture entering the lance and also the pressure within the vessel. The volume of the foam in the

vessel was measured at regular intervals, using the graduated marks on the outer surface of the vessel, by a third person. Gas samples were taken at 30 second intervals by a fourth person. Most experiments were terminated after about six minutes, by interrupting the flow of hydrogen chloride. Nitrogen was allowed to flow through the system, at a reduced rate, for another minute in order to flush out any gaseous hydrogen chloride remaining.

While the contents of the reaction vessel were allowed to cool, attention was turned to the analysis of the gas samples taken, using the techniques described in the previous section.

Once the outer tank had been drained the vessel could be dismantled. Large numbers of small amalgam droplets were frequently found adhering to the walls of the vessel and the entrance to the exhaust gas system. These had to be washed free using a distilled water jet. The pool of amalgam in the vessel could then be removed and any remaining sodium neutralised by contact with dilute hydrochloric acid. Treatment of the used amalgam was the same as described in section 4.3.7.

5.2.4 Slag Sampling Techniques

In the initial experiments with the model converter, the acidity of the aqueous phase was monitored using a pH meter coupled to a glass electrode inside the vessel. There were however, certain limitations with this technique. No correction for the temperature variation within the vessel was possible at this time. There may have been errors in the results produced by the glass electrode arising from the hydrophilic nature of glycerol. The acid concentration in the aqueous phase increased rapidly, causing the pH to reach zero very soon after commencing the blow and hence preventing any information being obtained concerning the later stages of the blow.

Attempts were made to remove samples directly from the vessel during the course of the blow using a 25 ml pipette, inserted directly through an

open port in the top of the vessel. Samples of foam, containing about 5 ml of aqueous solution and entrapped droplets, were successfully collected in this way, with the aid of a pipette bulb. The hot acid gases escaping from the sampling port together with a fine spray of mercury droplets, made it a somewhat hazardous technique.

The most successful technique devised for sampling the foam is illustrated in Figure 38. A small positive pressure, equivalent to about 3 cm of mercury even under normal operating conditions, was produced inside the vessel. This was utilised to force samples of liquid out of the vessel via a 2 mm i.d. glass tube, inserted through the top of the vessel. The end of this tube was positioned just below the surface of the quiescent slag layer, at mid radius position. During the course of an experiment, liquid was continuously forced up the glass tube and the sample which collected in the reservoir was removed at one minute intervals using a pipette. The volume of the sample obtained was about 3 ml. The HCl concentration was determined by titration against sodium hydroxide solution, of known concentration, using phenol phthalein indicator. The main drawback with this method was that the sample obtained was not representative of the model slag at the instant of sampling, necessitating a slight adjustment of the position of the origin on the plotted results.

5.2.5 Slag temperature measurement

A thermometer inserted into the vessel soon became totally obscured by foam. The temperature of the foam was therefore continuously monitored with the aid of a Pyrotenax chromel-alumel thermocouple in a stainless steel sheath. This was connected to a Honeywell Elektronik 194 chart recorder. The thermocouple was inserted into the slag at mid radius position with the tip about 1 cm above the surface of the amalgam.

Slag samples and foam temperature measurements were generally taken

during the course of the same experiment. These were conducted separately from experiments in which gas sampling was being carried out.

5.2.6 Measurement of droplet splashing rate

The effect of varying the lance height and jet momentum on the rate of splashing from the amalgam bath was briefly investigated using the modified vessel shown on Plate 17. The alterations to the vessel are also illustrated in Figure 39.

A section was removed from the side and base of the vessel and an open compartment in the form of a truncated wedge, made from 2 mm thick Perspex sheet, was introduced through it and cemented in place. It was intended that amalgam droplets, ejected from the bath by the impinging jet, would be trapped in this compartment and by collecting them for a known period of time, the splashing rate could be measured. The lower end of this droplet trap was bolted to the top of a rectangular column, which had been fabricated from 6 mm thick Perspex sheet. By observing the free fall of droplets down the lower part of this column it was anticipated that an estimate of their size distribution could be obtained.

The assembled apparatus is illustrated on Plate 18. In these experiments the gas jet contained only nitrogen and hence there was very little reaction between the amalgam and the aqueous phase. There was consequently no need to immerse the vessel in water. Due to the presence of the droplet trap the capacity of the vessel was reduced to 480 ml. The droplet trap and column were filled with the water-glycerol solution and a further 250 ml added to give a layer 1.8 cm deep above the amalgam surface.

A Perspex lid fitted over the top of the trap to prevent droplets entering while the gas flow rate was being adjusted. This lid was fastened to a length of stainless steel wire which passed through a rubber seal in the top of the

vessel. Once a stable gas flow rate had been achieved the lid could be smoothly removed and droplets collected for a known period of time. Since the angle subtended by the wedge was known to be 15° , an estimate of the splashing rate over the total cross sectional area of the bath could be obtained.

An attempt was made to estimate the size of the droplets being collected by photographing them during free fall through the lower section of the column. A similar photographic technique to that described in section 4.3.10(c) was employed. The lip of the droplet trap had been filed to an acute angle in order to minimise droplet fragmentation on the edge, which would have modified the observed size distribution. Unfortunately it was not possible to develop this technique fully in the time available and only limited results have been obtained.

5.3.1 General refining characteristics

The progress of a typical experiment is illustrated by Plates 19(a) to 19(f). Plate 19(a) shows the model converter just before the start of a blow. The vessel contained 500 ml of approximately 0.6 wt % Na amalgam covered by 250 ml of 60 v% glycerol-water solution.

A blow was commenced by introducing a mixture of nitrogen and hydrogen chloride gas through the lance at some predetermined flow rate (Plate 19(b)). Hydrogen chloride from the jet gases dissolved in the model slag causing it to become strongly acidic. The amalgam reacted with this acidified water glycerol solution producing hydrogen bubbles which caused a foam to develop (Plate 19(c)). The foam volume reached a maximum value about 3 minutes after the start of the blow (Plate 19(d)) and then proceeded to slowly collapse. Plate 19(e) shows the level of the foam just prior to terminating the blow. This was generally carried out about six minutes after the start of the blow, by interrupting the flow of gas through the lance. Despite the fact that perhaps only half of the sodium initially present in the amalgam had been removed, the collapse of the foam was fairly rapid, taking only about 20 seconds for the volume to fall to that of the original slag present (Plate 19(f)). L.D. steel making foams also collapse rapidly after termination of blowing, reflecting their dynamic nature.

The jet gases themselves did not contribute directly to the expansion of the foam. Plate 20 illustrates a blow in which the jet gases contained only nitrogen. Although considerable turbulence is evident in the jet impingement zone, the slag phase has not expanded significantly.

The impinging jet gases not only provided acid for the refining reaction but also ejected large numbers of droplets from the metal bath. During the initial stages of the blow, before the development of the foam, relatively

large drops of amalgam, up to several millimetres in diameter, were frequently observed being ejected through the slag phase in the vicinity of the jet impingement zone. Even when the foam had developed, smaller droplets together with volumes of slag were continuously ejected high into the vessel, before falling back into the foam or running down the walls of the converter. The ejection of aqueous droplets into the gas space above the bath would undoubtedly assist the transfer of HCl to the slag phase ^{78, 81}. Amalgam droplets falling through the foam, close to the converter wall, were frequently observed. Reacting droplets were accompanied by a white trail of hydrogen bubbles (Plate 21). Apart from these droplets nothing was visible through the foam layer, since the hydrogen bubbles formed made it virtually opaque.

After terminating a blow, especially when the sodium content of the amalgam was low, large numbers of small droplets (< 0.5 mm dia.) tended to accumulate in the meniscus between the surface of the amalgam and the vessel wall. Some of these were attached to bubbles which eventually carried them to the surface where the bubble burst allowing the droplet to fall back through the slag. This could be repeated several times. Similar behaviour was observed in the single droplet studies (Plate 14) and comparisons may be made with observations in slag-metal systems ^{16, 51, 52, 128, 129}. Whether such behaviour could occur during the course of a blow in the model converter is not known. The turbulence produced by the gas jet may prevent the permanent attachment of amalgam droplets to particular bubbles.

The circulation patterns produced in the foam layer by the gas jet were especially well developed. The surface layers of the foam appeared to move outwards from the jet impingement zone, down the wall of the vessel and back across the surface of the metal bath towards the axis of the vessel. This is in the opposite direction to that observed by Kluth and Maatsch ⁹², although they studied the impingement of a gas jet onto stable foams of large bubbles at lance-bath distances generally greater than those employed here. It was not possible to ascertain whether any complementary circulation patterns were

induced in the amalgam bath. There was however a tendency to set up a standing wave at the surface of the amalgam bath, which rotated about the vertical axis of the vessel. This probably arose from instabilities in the jet since for most experiments the jetting conditions were within the penetration mode.

The duration of the blow was limited to about 6 minutes for most experiments. Not all of the sodium initially present could be removed in this time, except in those experiments when the amalgam contained deliberately reduced amounts of sodium. The blow was limited to this period in order to prevent excessive amounts of insoluble sodium chloride accumulating in the model slag.

Samples removed from the model slag showed that the acid concentration increased throughout the blow and hence the solubility limit for sodium chloride would steadily decrease. However, the temperature of the slag also increased throughout a blow which would tend to enhance sodium chloride solubility. In those experiments where the highest rates of sodium removal were encountered, insoluble sodium chloride crystals were observed after about four minutes from the start of the blow, in samples removed from the vessel and allowed to cool to room temperature. Terminating a blow after about 6 minutes and allowing the vessel contents to cool caused significant amounts of sodium chloride to precipitate, making the aqueous phase very viscous.

By carefully monitoring the flow of nitrogen through the model converter and by analysing the exhaust gases it was possible to relate the rate of hydrogen evolution to the rate of sodium removal from the bath. The majority of the experiments were carried out with amalgam initially containing about 0.6 wt % Na. A limited number were also carried out with amalgam initially containing about half this amount, in order to study the refining characteristics at low sodium concentrations. The refining behaviour for various experimental conditions is described in detail later but it is useful to mention here the general form of the sodium removal rate curves obtained.

With amalgams initially containing about 0.6 wt %, two distinct stages

were identified in the refining process. These may be compared with Stage I and II on the idealised decarburisation curve for the L.D. process shown in Figure 4. Initially the rate of sodium removal increased rapidly. Eventually, an approximately steady rate was achieved, the value of which was influenced by the operating conditions. Whether it is reasonable to consider this stage as a true rate plateau is open to debate. As with Stage II decarburisation in the L.D. process (Figure 3), there were quite abrupt changes in the rate of sodium removal, together with more general trends, all within the limits of accuracy of the analysis techniques used. It is useful however to consider it as a rate plateau and use the mean refining rate during this period as a criteria for comparing sets of data.

At reduced sodium concentrations a third refining stage was observed during which the rate of sodium removal progressively decreased. This is comparable with Stage III on the decarburisation rate curve (Figure 4).

5.3.2 The effect of varying the composition and momentum of the jet

It has been shown that the rate of sodium removal from a single droplet of amalgam is dependent upon the acid concentration in the aqueous phase, provided that the sodium content in the droplet is sufficiently high. It is reasonable to expect that the rate of sodium removal from the metal bath in the model converter would, to some extent, be dependent upon the acid concentration in the model slag and hence would be related to the rate of supply of hydrogen chloride to the system.

Experiments were carried out to determine the effect of varying the composition of the jet gases on the refining characteristics of the model, using amalgam initially containing about 0.6 wt % Na. Two series of experiments were performed, one using a jet momentum of 77 mN and the other a jet momentum of 102 mN. The height of the lance tip above the amalgam surface was set

at 2.5 mm for both series of experiments.

The above conditions were chosen in order to produce a jet within the deep penetration mode⁸⁰. The conditions employed on commercial L.D. steel making plants are believed to be such that the jet penetrates to a depth of between 50 and 80% of the overall depth of the metal bath^{6, 9}. Using equation 2.1 the depth of penetration into the amalgam bath by jets with momentums of 77 mN and 102 mN has been estimated to be 3.6 cm and 4.1 cm respectively. The overall depth of the amalgam pool was 5.5 cm. Chatterjee⁸¹ has estimated that the critical depth of penetration for the onset of splashing from a pool of mercury is 0.8 cm and clearly this will be exceeded in these experiments. The need to produce reasonable rates of gas evolution, in order to sustain a foam, and also practical and economic limitations on the apparatus were also taken into consideration when deciding the blowing conditions to be used.

The refining curves obtained by using various jet compositions, ranging from 7.2 to 14.6 v % HCl, while maintaining the jet momentum at 77 mN are illustrated in Figures 40 to 44. The refining curves produced when using a jet momentum of 102 mN with jet compositions ranging from 6.4 v % to 13.1 v % HCl are illustrated in Figures 45, 46, 47, 48, 54 and 74. The conditions used for each experiment are summarised on Table 9.

The refining curves obtained were of the general form described in the previous section. All showed an initially rapid increase in the rate of sodium removal followed by a second period during which the refining rate remained fairly constant. The Stage II refining period appeared to be achieved more rapidly and also at generally higher rates, as the rate of introduction of HCl into the system was increased. As suggested in the previous section, it is convenient to use the mean rate achieved during Stage II as a criteria for comparing results. In Figure 49(a) the mean Stage II refining rate is plotted against the jet composition for each series of experiments. The rate of sodium removal clearly increases with increasing HCl concentration in the jet gases.

Enhanced refining rates would also appear to be associated with higher jet momentums.

The foam volume, like the refining rate, also increased rapidly in the early stages of the blow, eventually reaching a maximum value at a time which coincides with the start of the Stage II refining period. This is best illustrated on Figure 45 where the results obtained with jet compositions of 6.4 and 13.1 v % HCl are presented together. The maximum foam volume attained appeared to be independent of the blowing conditions.

Samples have been removed from the model slag during the course of a blow and analysed to determine the acid concentration. Figure 50 illustrates the change in composition of the slag phase during the course of a blow using a jet momentum of 102 mN and jet compositions of 6.4 and 13.1 v % HCl. The acid concentration in the slag is clearly related to the hydrogen chloride content of the jet gases which probably accounts for the observed effects on the rate of sodium removal.

The temperature of the model slag was also influenced by the composition of the jet (Figure 51). This is probably associated with the increased rate of dissolution of HCl from the jet gases and increased rates of sodium removal from the amalgam, since both reactions are exothermic.

5.3.3 The influence of lance height

The rate at which droplets were torn from the amalgam bath by the impinging gas jet and returned to the bath outside the area of the central crater, was determined for various lance heights at jet momentums of 77 and 102 mN, using the apparatus and techniques described in section 5.2.6. The results obtained are illustrated in Figure 52, the splashing rate being defined as the volumetric rate at which droplets were returned to the bath over its total area outside the immediate vicinity of the impact crater. The volumetric rate

of droplet ejections increased steadily as the lance height was reduced below that required for the onset of splashing⁸¹ until some critical height was reached, below which the rate of ejections increased abruptly. Results became erratic as the lance tip was brought very close to the amalgam surface. At all lance heights, the splashing rates produced by a jet with a momentum of 102 mN were consistently greater than those produced by a 77 mN jet.

Attempts were also made to determine the size distribution of the droplets being ejected from the bath, by photographing them as they fell into the collection column. Plate 22 shows a typical photograph obtained. The majority of the droplets observed were very small, generally less than 1 mm in diameter. Occasionally, isolated droplets of up to several millimetres in diameter were observed, presumably arising from instabilities in the jet impact crater. Estimation of the size distribution of the droplets falling into the trap proved to be impossible, due to their generally small size and the very large numbers in which they were being created, especially at the smaller lance heights used.

The methods used to measure the splashing rate and to estimate the size distribution of the droplets formed were only of an exploratory nature and clearly the techniques used require further development. The results obtained do however serve to indicate the large number of droplets which can be formed by the impinging gas jet and hence the large interfacial area which can be created in the model slag-metal-gas emulsion.

The experiments conducted to evaluate the effect of varying the lance height on the refining characteristics of the model are summarised in Table 10.

The individual refining curves obtained for each lance height are presented in Figures 53 to 58. All these experiments were carried out with a gas mixture containing 12.1 v % HCl and at a jet momentum of 110 mN.

Figure 59 indicates that as the lance height is raised, the mean stage II refining rate decreases progressively, although possibly not as much as one

might have expected from the results of the splashing rate experiments. At a lance height of 44 mm, the rate of ejection of droplets from the bath is very low (Figure 52), yet the mean stage II refining rate is still 70% of the maximum mean refining rate observed in this series of experiments (Figure 59). This suggests that reaction at the interface between the bulk amalgam pool and the slag phase can contribute significantly to the overall refining rate.

It is interesting to note that at very elevated lance heights, the variation in refining rate observed during the stage II period could be quite significant (Figure 58). Similar erratic changes in gas evolution rate can also occur in L.D. steelmaking when an excessively soft blowing practice is being employed^{6, 64}. In steelmaking this is attributed to the excessive accumulation of iron oxide in the slag coupled with inadequate agitation of the bulk bath by the gas jet. Similarly in the model if stirring in the bulk amalgam bath is inadequate then the surface layers may become depleted in sodium causing the rate of sodium removal to fall and thus allowing the acid concentration in the slag to rise. Fresh amalgam being swept to the surface would then encounter the highly acid slag and the rate of gas evolution would increase markedly.

As the lance height was raised the rate of sodium removal from the amalgam fell progressively and hence less HCl was being consumed from the slag. One would therefore expect that the acid concentration in the slag would increase more rapidly with increasing lance height. This behaviour is confirmed by Figure 60 which shows the change in acid concentration in the aqueous phase throughout a blow, using lance heights of 2.5 mm and 20.5 mm. The temperature variation in the foam, for the same pair of experiments is shown in Figure 61.

5.3.4 The effect of sodium chloride additions to the aqueous phase

Single droplet experiments have shown that additions of sodium chloride to the aqueous phase can reduce the rate of sodium removal from a drop. In

the model converter, the sodium chloride content of the slag was initially zero, but increased progressively throughout an experiment. Towards the end of a typical 6 minute blow the solubility product for sodium chloride could even be exceeded, resulting in the precipitation of crystals within the aqueous phase.

Figure 62 compares the results of two experiments carried out under almost identical conditions. In one case however, the aqueous slag phase initially contained no salt whilst in the other it contained 2.0 moles/l of NaCl. The experimental conditions are summarised in Table 11 and the results for the "salt free" experiment are shown in Figure 48. The variation in temperature and HCl concentration in the slag phase are compared for a similar pair of experiments in Figures 63 and 64.

During the early stages of the blow, the relative rates of sodium removal for the two experiments were as anticipated. The results of the experiment using an aqueous solution initially containing no salt, were consistently higher than those with a slag solution containing 2 moles/l of NaCl. The stage II refining rate eventually attained in the experiment to which sodium chloride had been added to the slag was however, significantly greater than that observed with the "salt free" experiment. Such behaviour is difficult to explain simply on the basis of the results of the single droplet experiments alone.

During the course of a blow, droplets falling close to the wall of the vessel could be observed during their passage through the foam. With a slag initially containing no sodium chloride, droplets of about 1 mm in diameter took about 2 seconds to traverse the height of the foam. In the experiment in which the slag phase initially contained 2.0 moles/l of NaCl, the solubility product for sodium chloride was soon exceeded causing salt crystals to precipitate and hence making the slag rather viscous. In this case, 1 mm diameter droplets, close to the wall of the vessel, took about five seconds to traverse the height of the foam, suggesting that the residence time of droplets in the foam as a whole may have increased. Such an increase in the residence time

might explain the relative values of the mean stage II refining rate. It is interesting to note that the foam volume and hence the residence time for bubbles in the slag phase, did not appear to be influenced to the same extent by the premature precipitation of salt crystals (Figure 62(b)).

5.3.5 Refining at elevated pressures

A series of experiments were performed in order to test a theory that the refining rates in the model converter might be enhanced by increasing the pressure within the vessel. The basis for this theory will be discussed in section 5.4.1.

The conditions used in this series of experiments are summarised in Table 12 and the sodium removal rate curves for the experiments at elevated pressures are illustrated in Figures 65 to 68. The refining curves for the experiments conducted at a vessel pressure of one atmosphere are illustrated in Figures 41 to 43. The composition of the gas mixture used was 12.3 v % HCl, the jet momentum was 77 mN and the lance height was 2.5 mm. As before the initial composition of the amalgam used was approximately 0.6 wt % Na. The effect of increasing the excess vessel pressure up to a value of 0.75 atmospheres was studied.

Figures 69 and 70 indicate that an increase in the internal vessel pressure is associated with an increase in the mean stage II rate of sodium removal and a decrease in the maximum foam volume attained. Examination of Table 12 however, shows that as the pressure increased the volumetric flow rate of HCl and N₂, converted to S.T.P., also increased. This can be attributed to the increase in the density of the gas passing through the Rotameters. In order to maintain a constant Rotameter reading and hence a constant jet momentum, the mass flow rate of gas had to be effectively increased. It has been shown in section 5.3.2 that an increase in the rate of introduction of hydrogen chloride into

the vessel will in itself produce an increase in the rate of sodium removal, which must in part account for the enhanced rates associated with an increase in vessel pressure.

The results obtained by varying the jet composition at one atmosphere pressure, using a jet momentum of 77 mN and a lance height of 2.5 mm, are illustrated on Figure 49(a). These may be presented slightly differently by plotting the mean stage II rate for each experiment against the effective flow rate of hydrogen chloride at S.T.P. (Figure 49(b)). The graph may then be used to evaluate the relative contributions of pressure and HCl flow rate to the refining rates obtained using elevated pressures inside the vessel (Figure 71). This approach is not strictly correct since in the experiments conducted at one atmosphere pressure, the change in mass flow rate of HCl was achieved by varying the composition of the jet and hence presumably the concentration gradient between the bulk gas phase and the gas in contact with the aqueous phase. This approach does however give a useful indication of the contribution to the overall refining rate of pressurising the vessel.

Figure 71 indicates that the refining rate is indeed enhanced by pressurising the vessel. At the maximum excess vessel pressure employed in this series of experiments, 0.75 atmospheres, approximately 15% of the observed mean stage II refining rate is attributable to the pressure increase alone. Linear extrapolation of these results suggests that, at an excess vessel pressure of one atmosphere the contribution to the refining rate of pressurising the system would be about 20%, under these blowing conditions.

The composition and temperature of the model slag has been monitored throughout blows in which the vessel pressure has been increased. Figures 72 and 73 suggest that at elevated pressures, both the temperature and acid concentration in the model slag increase slightly more rapidly than at one atmosphere pressure.

5.3.6 Experiments at constant mass flow rate

In the previous section it was mentioned that the mass flow rate of gas through the lance had to be increased in order to maintain the jet momentum constant, when the internal pressure in the reaction vessel was increased. If however, the mass flow rate of gas into the vessel had been maintained at a constant value then the jet momentum would have fallen. Pairs of experiments have been performed using the same mass flow rate of jet gases but differing vessel pressures, in order to compare the refining rates produced under these conditions.

The experimental conditions used and the results obtained are summarised in Table 13. The sodium removal rate curves for each pair of experiments are compared in Figures 74 and 75. The variation in slag temperature and acid concentration during the blow, for a pair of experiments carried out under similar conditions to those used to obtain Figures 75(a) and 75(b), are illustrated in Figures 76 and 77.

It will be noted that in both pairs of experiments, the mean stage II refining rates achieved at constant mass flow rate are very similar. It has been shown in section 5.3.2 that the rate of sodium removal can be influenced by the jet momentum, whilst in section 5.3.5 it was shown that the refining rate could be enhanced by pressurising the reaction vessel. By maintaining a constant mass flow rate of gases through the lance, the pressure inside the vessel could only be increased at the expense of jet momentum. The effects of the two variables on the refining rate therefore essentially neutralise each other. The constancy of the mean stage II refining rate suggests that the contribution of each of these variables is very similar, at least over the rather limited range of experimental conditions studied here.

5.3.7 Refining at low sodium concentrations

In all of the previous experiments the initial composition of the amalgam used was approximately 0.6 wt % Na. A limited number of experiments have also been conducted using amalgam initially containing about half of this amount of sodium. These are summarised in Table 14.

The sodium removal rate curves produced in these experiments were significantly different from those obtained with high sodium content amalgams. Figures 78 and 79 illustrate the results of two experiments carried out under similar conditions to those used to produce Figure 48 (Table 9), with the exception that the initial composition of the amalgam used was approximately 0.3 wt % Na. The early stages of the blow were similar. The rate of sodium removal increased rapidly, eventually reaching a maximum at a similar value to the mean stage II refining rate in Figure 48. The rate of sodium removal then decreased steadily as the blow proceeded, despite the fact that a significant amount of sodium still remained in the amalgam. The change in acid concentration throughout the blow did not appear to be affected by the change in the initial sodium content of the amalgam (Figure 80). The slag temperature did however reach a maximum value, reflecting the decrease in the rate of sodium removal in the later stages of the blow. (Figure 81).

Single droplet studies showed that at low sodium concentrations the rate controlling process became that of sodium transport in the amalgam. The composition at which the controlling mechanism changed from hydrogen ion discharge was shown to be dependent upon the acid concentration in the aqueous phase. The change in the refining characteristics of the model converter are probably related to this change in rate controlling mechanism.

By determining the area under the curves in Figures 78 and 79 it is possible to obtain the rate of sodium removal as a function of the amalgam composition and hence estimate the composition at which the controlling mechanism changes in the model converter (Figure 84). This will of course be influenced by the

initial composition of the amalgam and the acid concentration in the aqueous phase. Super imposed on Figure 84 are the results of two experiments conducted with an elevated vessel pressure (Figures 82 and 83). There is clearly a great deal of variation in the results shown in Figure 84. The decrease in refining rate associated with the change in rate controlling mechanism appears to occur at lower sodium concentrations in those experiments where the initial sodium content of the amalgam was lowest, yet in theory one would expect the reverse behaviour.

Figures 85 and 86 compare the results obtained when using lance heights of 2.5 and 20.4 mm. It will be noted that the amalgam composition at which the refining rate decreases is greater for the experiment carried out with the larger lance height. The critical composition for the change in rate controlling mechanism for single droplets has been shown to increase with increasing acid concentration while the acid concentration in the model slag has been shown to increase more rapidly as the lance height is raised (Figure 60). These two factors probably explain the observed change in the critical composition as the lance height is raised.

The results obtained for this particular area of investigation are clearly very limited and more work is required. They do however serve to show that the change in refining mechanism observed with single droplets is reflected in the behaviour of the multiple droplet system and that the change occurs over a comparable composition range.

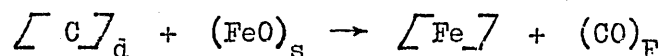
5.4.1 Refining Under Hydrogen Ion Discharge Control5.4.1 (a) Qualitative Assessment of the Model Converter

The model converter developed during the course of this work appears to simulate most of the important gas-slag-metal interactions observed in the L.D. steelmaking process. The impinging gas jet caused large numbers of droplets to be ejected from the metal bath into the model slag, while at the same time hydrogen chloride from the jet gases dissolved in the aqueous slag causing it to become highly acidic. The dual function of the oxygen jet in steelmaking, namely its physical contribution in creating droplets and hence a large surface area for reaction and its chemical effect in providing one of the reactant species, were consequently simulated in the model. In steelmaking however, the transfer of oxygen to the slag phase is not a simple dissolution process and hence there is no analogy in the model with the reaction between iron and oxygen in the jet impingement zone.

The amalgam droplets within the slag phase reacted with the acid in solution producing hydrogen bubbles which resulted in the formation of a foam.



This is analogous to the reaction of iron-carbon alloy droplets in an oxidising slag to form carbon monoxide bubbles.



There is however, no analogous product of reaction to the sodium chloride produced by the reaction in the model system. In the single droplet studies it was noted that the presence of sodium chloride in the aqueous

phase could influence the rate of reaction of amalgam droplets. Its accumulation in the model slag during the course of a blow and its consequent effect on refining rates might impose limitations on the usefulness of the model.

Just as in L.D. steelmaking, the foam produced in the model converter was dynamic in character⁵¹. If the blow was interrupted then it collapsed quite readily, reflecting the inability of water-glycerol solutions to sustain a stable foam¹⁴². The jet gases did not appear to contribute directly to the gas within the foam, as illustrated by Plate 20, but they did contribute indirectly by agitating the bath and providing one of the reactant species.

The sodium removal rate curves for the model system were of a similar form to the decarburisation rate curves encountered in L.D. steelmaking (Figures 3 and 4). The rate of sodium removal increased rapidly during the first few minutes of the blow while the foaming slag was being established, but eventually attained a rate plateau, although significant variations about the mean value were observed. As in oxygen steelmaking, the rate controlling mechanism appeared to change in the later stages of the blow when the composition of the metal bath fell below some critical value. The refining rate then proceeded to decrease as the blow continued.

In oxygen steelmaking the slag temperature increases rapidly in the early stages of the blow, eventually reaching a relatively steady value^{18, 24}. In the model however, the slag temperature appeared to increase steadily throughout a typical six minute blow. This behaviour probably explains the decrease in foam volume observed after the plateau refining rate had been achieved. During the first few minutes of the blow the temperature of the model slag steadily increased and the foam expanded as the rate of hydrogen evolution increased. Once the stage II rate plateau had been achieved the rate of gas evolution remained relatively constant. The temperature of the

slag however continued to rise, causing its viscosity to decrease and hence allowing the bubbles formed within it to escape more easily.

5.4.1. (b) Mathematical Interpretation

According to the theories of Meyer and Trentini, up to two thirds of the carbon initially present in the steelmaking bath can be removed via droplets dispersed in the slag-gas foam^{11,16}. Carbon removal from droplets within the foam is probably especially important in the first half of the blow, before the start of the carbon boil in the bulk bath⁵⁶. For most of the model experiments therefore the blowing conditions were chosen in order to maximise the contribution of refining processes occurring within the foam. Jet momentums ranging from 77 to 110 mN were employed and, except for one series of experiments, the lance height above the surface of the amalgam pool was 2.5 mm. The jet penetration under these conditions was estimated to be between 60 and 75% of the overall depth of the bath (see section 5.3.2), which is comparable with the depth of penetration believed to be attained by the oxygen jet into the pool of steel in an L.D. converter^{6,9}. The conditions employed were consequently well within the regime in which Chatterjee predicts that considerable splashing will occur from an amalgam bath^{78, 81}. This was also confirmed experimentally (Figure 52). Since hydrogen chloride only behaves as an acid in the presence of water, it was hoped that by using a relatively low lance height the entrainment of the aqueous slag phase into the jet would be minimised and hence any reaction occurring in the jet impact crater could be ignored.

The overall rate of sodium removal from the droplets dispersed in the foam is given by:

$$\dot{m}_{Na,F} = A_R \cdot \dot{m}_{Na,d} \quad 5.2$$

where A_R is the total surface area available for reaction between the amalgam droplets and the aqueous phase and $\dot{m}_{Na,d}$ is the mean rate of sodium

removal per unit area of droplet surface.

If droplets are being ejected from the metal bath, by the impinging gas jet, at a rate \dot{V} and the mean surface area of the individual droplets formed is \bar{A}_d , then the total surface area of droplets in the foam (A_T) is given by:

$$A_T = \dot{V} \cdot \bar{A}_d \cdot \bar{\tau}, \quad 5.3$$

where $\bar{\tau}$ is the mean residence time for droplets in the foam.

While an amalgam droplet is in the foam it will contact both the acidified water-glycerol solution and also bubbles of hydrogen. Only a fraction of its surface ($\gamma_{S,F}$) will therefore be in contact with the aqueous phase and hence the effective total area available for reaction will be:

$$A_R = \gamma_{S,F} \cdot \dot{V} \cdot \bar{A}_d \cdot \bar{\tau} \quad 5.4$$

It should be noted that $\gamma_{S,F}$ has a slightly different physical significance than the variable γ_S encountered in the previous chapter. In the single droplet work, γ_S is the fraction of the surface area of the drop that is not covered by gas produced by the reaction of that drop. For a droplet in the converter, $\gamma_{S,F}$ represents the fraction of the surface area of the drop not covered by gas from the reaction of all the drops in the foam.

The single droplet experiments showed that, provided the sodium content of a droplet was sufficiently high, the rate of sodium removal was controlled by the rate of discharge of hydroxonium ions at the amalgam surface and hence,

$$\dot{m}_{Na,d}'' = k [C_{H^+}]_{Aq,B} \quad 4.18$$

The overall rate of sodium removal from the droplets in the foam is therefore given by:

$$\dot{m}_{Na,F} = \gamma_{S,F} \cdot \dot{V} \cdot \bar{A}_d \cdot \bar{\tau} \cdot k [C_{H^+}]_{Aq,B} \quad 5.5$$

The hydrogen ions for the reaction with sodium were transferred from the gas jet to the model slag, as hydrogen chloride, at some rate \dot{m}_{HCl} . At the same time however, hydrogen ions were being consumed by the reaction with sodium at a rate $\dot{m}_{\text{Na,F}}$. The rate of accumulation of acid molecules in the slag will therefore be related to the difference between the rates of these two processes.

$$\frac{d \left[\text{C}_{\text{H}^+} \right]_{\text{Aq,B}}}{dt} = \frac{\dot{m}_{\text{HCl}} - \dot{m}_{\text{Na,F}}}{V_S} \quad 5.6$$

By substituting for $\dot{m}_{\text{Na,F}}$ using equation 5.5 we obtain,

$$\frac{d \left[\text{C}_{\text{H}^+} \right]_{\text{Aq,B}}}{dt} = \dot{m}_{\text{HCl}} - \left\{ \gamma_{\text{S,F}} \cdot \dot{V} \cdot \bar{A}_d \cdot T \cdot k \left[\text{C}_{\text{H}^+} \right]_{\text{Aq,B}} \right\} \quad 5.7$$

The acid concentration in the model slag should therefore be obtainable by integrating the above expression. Unfortunately \dot{m}_{HCl} is likely to vary throughout an experiment and will also be influenced by the concentration of hydrogen chloride in the bulk slag phase.

Mass transfer from a gas jet to a liquid has been studied by a number of workers and solutions are available for blowing conditions which produce a stable impact crater ^{73, 101}. With the present model system however, blowing conditions were chosen so that both the jet and the impingement crater in the amalgam bath would be unstable. In addition, the lance tip was generally submerged below the surface of the model slag. Large numbers of aqueous phase droplets were ejected into the gas space above the bath, which would undoubtedly assist the transfer of hydrogen chloride to the bulk slag layer. The information in the literature is therefore not applicable to the model system under consideration.

In order to simplify the problem it is reasonable to assume that the rate of transfer of hydrogen chloride from the jet gases to the aqueous slag phase involves a relationship of the form:

$$\dot{m}_{\text{HCl}} = K_J \left\{ \left[\text{C}_{\text{H}^+} \right]_{\text{eq,J}} - \left[\text{C}_{\text{H}^+} \right]_{\text{Aq,B}} \right\} \quad 5.8$$

K_J is a transport parameter incorporating both a mass transfer coefficient and the surface area available for the transfer process. $[C_{H^+}]_{eq,J}$ is the aqueous phase hydrogen ion concentration in equilibrium with the jet gas.

Using this approach one might expect that the observed refining behaviour would be that illustrated on Figure 87. As hydrogen chloride was transferred from the jet gases $[C_{H^+}]_{Aq,B}$ would increase and hence \dot{m}_{HCl} would tend to decrease as indicated by equation 5.8. The increasing hydroxonium ion concentration in the bulk slag would however encourage the removal of sodium from the amalgam droplets in the foam and hence $\dot{m}_{Na,F}$ would tend to increase as the blow proceeded. Eventually a limiting refining rate would be attained when $\dot{m}_{Na,F}$ reached equality with \dot{m}_{HCl} , after which the acid concentration in the aqueous phase would remain constant.

$$\frac{d [C_{H^+}]_{Aq,B}}{dt} = \frac{\dot{m}_{HCl} - \dot{m}_{Na,F}}{V_S} = 0 \quad 5.9$$

Equations 5.5 and 5.8 may therefore be combined to obtain an expression for the acid concentration in the bulk aqueous phase at the limiting refining rate.

$$[C_{H^+}]_{Aq,B,lim} = \left\{ \frac{1}{1 + \frac{\gamma_{S,F} \dot{V}_{A_d} \tau_k}{K_J}} \right\} [C_{H^+}]_{eq,J} \quad 5.10$$

A more general expression for the variation in the acid concentration during the course of a blow may be obtained by substituting for \dot{m}_{HCl} in equation 5.7, using equation 5.8, and then solving the resulting differential equation.

$$[C_{H^+}]_{Aq,B} = [C_{H^+}]_{eq,J} X \left\{ 1 - \exp\left(-\frac{K_J t}{V_S X}\right) \right\} \quad 5.11$$

where,

$$X = \frac{1}{1 + \frac{K_J}{\gamma_{S,F} \dot{V}_{A_d} \tau_k}} \quad 5.12$$

By substituting equations 5.10 and 5.11 into equation 5.5 expressions can be obtained for respectively the limiting refining rate and the variation in refining rate throughout an experiment.

$$\dot{m}_{Na,F,lim} = \left\{ \frac{1}{\frac{1}{K_J} + \frac{1}{\gamma_{S,F} \dot{V} \bar{A}_d \tau_k}} \right\} [C_{H^+}]_{eq,J} \quad 5.13$$

$$\dot{m}_{Na,F} = \gamma_{S,F} \dot{V} \bar{A}_d \tau_k [C_{H^+}]_{eq,J} \times \left\{ 1 - \exp\left(\frac{K_J t}{V_S X}\right) \right\} \quad 5.14$$

Unfortunately this approach, which considers perhaps the most obvious explanation for the rate plateau and the general refining characteristics of the model system is not substantiated by the experimental results. In practice although a rate plateau was achieved, the acid concentration in the slag phase appeared to increase continuously throughout the blow. This would imply that $\dot{m}_{Na,F}$ and \dot{m}_{HCl} did not reach equality. The reason for this behaviour is not fully understood and a full quantitative explanation is not possible. It is however useful to discuss some of the factors which will complicate the simple mathematical interpretation described above.

When equation 5.8 was considered earlier it was implied that \dot{m}_{HCl} would tend to decrease as $[C_{H^+}]_{Aq,B}$ increased. An estimate of the way in which \dot{m}_{HCl} actually varies throughout a blow can be obtained for those experiments where both the rate of sodium removal, $\dot{m}_{Na,F}$, and the change in acid concentration in the model slag were monitored, since at any instant during the course of the blow,

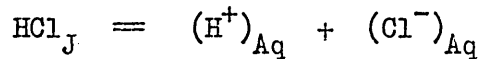
$$\dot{m}_{HCl} = \dot{m}_{Na,F} + V_S \frac{d [C_{H^+}]_{Aq,B}}{dt} \quad 5.15$$

The rate of change of acid concentration in the model slag,

$\frac{d [C_{H^+}]_{Aq,B}}{dt}$, may be obtained from a tangent to the slag composition curve.

Figure 88 shows the variation in \dot{m}_{HCl} during the course of an experiment obtained using the above method from the data presented in Figures 48 and 50. It will be noted that \dot{m}_{HCl} initially increases, reaches a maximum value at approximately the same time as the maximum foam volume is achieved and then proceeds to fall steadily throughout the remainder of the blow. The initial increase in \dot{m}_{HCl} is probably associated with the expansion of the foam in the early stages of the blow, manifesting itself in equation 5.8 as a progressive increase in K_J . As hydrogen chloride was transferred to the aqueous phase $\left[C_{\text{H}^+} \right]_{\text{Aq,B}}$ would increase and hence would tend to have an adverse effect on \dot{m}_{HCl} . In addition it is possible that $\left[C_{\text{H}^+} \right]_{\text{eq,J}}$ would tend to decrease during the course of an experiment, which would further reduce \dot{m}_{HCl} .

The transfer of hydrogen chloride from the gas jet to the model slag may be represented by the chemical equation,



The equilibrium constant for this reaction is:

$$K_{\text{eq}} = \frac{\left[C_{\text{H}^+} \right]_{\text{eq,J}} \cdot \left[C_{\text{Cl}^-} \right]_{\text{eq,J}}}{P_{\text{HCl},J}} \quad 5.16$$

Hence after rearranging,

$$\left[C_{\text{H}^+} \right]_{\text{eq,J}} = \frac{P_{\text{HCl},J} K_{\text{eq}}}{\left[C_{\text{Cl}^-} \right]_{\text{eq,J}}} \quad 5.17$$

The chloride ions in solution may be considered to arise from two sources, those associated with HCl molecules and those associated with the sodium chloride produced by the refining reaction. Hence,

$$\left[C_{\text{Cl}^-} \right]_{\text{eq,J}} = \left[C_{\text{H}^+} \right]_{\text{eq,J}} + \left[C_{\text{NaCl}} \right]_{\text{Aq,B}} \quad 5.18$$

The concentration of sodium chloride in the model slag increased continuously during the course of an experiment and hence one would

expect that $\left[C_{H^+} \right]_{eq,J}$ would tend to decrease. This trend would clearly have an adverse effect on \dot{m}_{HCl} as predicted by equation 5.8. In addition the temperature of the model slag always increased continuously throughout a blow and hence K_{eq} would tend to decrease which would also adversely influence $\left[C_{H^+} \right]_{eq,J}$ ¹⁸⁰.

By substituting for $\left[C_{Cl^-} \right]_{eq,J}$ in equation 5.17, using equation 5.18, and rearranging the resulting expression, a quadratic equation is obtained.

$$\left[C_{H^+} \right]_{eq,J}^2 + \left[C_{NaCl} \right]_{Aq,B} \left[C_{H^+} \right]_{eq,J} - P_{HCl,J} K_{eq} = 0 \quad 5.19$$

Taking the positive solution,

$$\left[C_{H^+} \right]_{eq,J} = -\frac{\left[C_{NaCl} \right]_{Aq,B}}{2} + \frac{1}{2} \sqrt{\left[C_{NaCl} \right]_{Aq,B}^2 + 4 P_{HCl,J} K_{eq}} \quad 5.20$$

However, the concentration of sodium chloride in the slag phase is equal to the concentration of sodium chloride initially present in the water-glycerol solution, which in all except one experiment was zero, plus the amount of sodium chloride created as a result of reaction with the amalgam. Assuming the slag-metal-gas emulsion to be the primary vehicle for sodium removal from the amalgam, then,

$$\left[C_{NaCl} \right]_{Aq,B} = \int_0^t \frac{\dot{m}_{Na,F}}{V_S} dt = \frac{Y_{S,F} \bar{A}_d \bar{V}^2 k}{V_S} \int_0^t \left[C_{H^+} \right]_{Aq,B} dt$$

By substituting for $[C_{NaCl}]_{Aq,B}$ in equation 5.20 and then eliminating

$[C_{H^+}]_{eq,J}$ from equation 5.8 an expression may be obtained for \dot{m}_{HCl} .

This in turn may be substituted into equation 5.7 to obtain the differential equation:

$$\begin{aligned}
 v_S \frac{d [C_{H^+}]_{Aq,B}}{dt} = \frac{K_J}{2} \left\{ - \frac{\gamma_{S,F} \dot{V} \bar{A}_d \tau_k}{v_S} \int_0^t [C_{H^+}]_{Aq,B} dt \right\} \\
 + \frac{K_J}{2} \sqrt{ \left\{ \frac{\gamma_{S,F} \dot{V} \bar{A}_d \tau_k}{v_S} \int_0^t [C_{H^+}]_{Aq,B} dt \right\}^2 + 4 P_{HCl,J} K_{eq} } \\
 - [C_{H^+}]_{Aq,B} \left\{ K_J + \gamma_{S,F} \dot{V} \bar{A}_d \tau_k \right\} \qquad 5.22
 \end{aligned}$$

This is clearly very complex and does not easily yield a solution.

A solution using numerical analysis is possible but a number of the parameters involved still requires determination and in any case the result would have little relevance to basic oxygen steelmaking.

It has been shown in the above discussion that the accumulation of sodium chloride in the reaction vessel has a significant effect on the rate of transfer of HCl to the model slag and hence upon the refining rates achieved in the model converter. The composition of the slag phase, both in terms of the HCl and NaCl contents, may also have a considerable influence on the rate of reaction of droplets within the foam - a factor which would further complicate the mathematical interpretation of the system. This is

probably best illustrated by comparison with certain aspects of the single droplet studies, described in the previous chapter.

In the model converter, droplets of various sizes come into contact with an aqueous solution of progressively increasing acid concentration. A similar situation has been described in Chapter Four where the reaction of droplets of the same size with solutions containing various amounts of HCl was investigated (see Figure 26). It was noted that, although in theory there should have been direct proportionality between the reaction rate and the acid concentration, in practice significant deviation from linearity was observed in solutions which were more than 1.5 N. This was attributed to:

- (i) Increasing surface coverage of the droplets by bubbles.
- (ii) The deviation from ideal behaviour of hydrogen ions in solution.
- (iii) Possible precipitation of NaCl crystals on the droplet surface.

These same factors are also likely to be important when considering the refining rate of droplets within the foam created in the model converter.

Both the life time of a droplet in the foam (τ) and the fraction of its surface in contact with the model slag ($\gamma_{S,F}$) are likely to be influenced by the volume of gas in the foam. As the foam expands in the first few minutes of the blow, then $\gamma_{S,F}$ will probably decrease while τ will increase. This trend might be reversed once the maximum foam volume has been achieved. The single droplet studies showed that γ_S was related to the acid concentration in the aqueous phase. It is possible that this might also apply in the model converter foam and hence $\gamma_{S,F}$ would tend to decrease steadily throughout the blow. The effect of $\gamma_{S,F}$ on the overall

refining rate in the model converter will be discussed in more detail later.

The single droplet studies also showed that addition of sodium chloride to the aqueous phase could adversely affect the refining rate. It was suggested that this might be associated with a decrease in the reaction rate constant or possibly a decrease in γ_S , arising from either the precipitation of salt crystals on the droplet surface or a change in the size of the hydrogen bubbles produced. In the model converter, the sodium chloride concentration in the aqueous phase increased continuously throughout a blow. A progressive decrease in either k or $\gamma_{S,F}$ would tend to adversely affect the refining rate of the droplets in the slag-metal-gas foam in the model converter, which would tend to offset the effects of the increasing hydrogen ion concentration. The refining rate plateau may therefore be associated with the attainment of a dynamic balance between the increasing acid and NaCl concentrations. Similarly with the single droplet results, the superimposition of the effects of a progressively increasing salt concentration on Figure 26 (a) would result in an increasing tendency towards the creation of a rate plateau. It is difficult to estimate the solubility of sodium chloride in the model slag due to the variation in both temperature and acid concentration, but it is possible that in the later stages of the blow the solubility limit may have been exceeded. The presence of these insoluble crystallites in the bulk solution would further inhibit the removal of sodium from the droplets in the foam.

The early stages of the experiment depicted in Figure 62, where the aqueous phase initially contained 2.0 moles of NaCl / litre, suggest that the salt present does indeed tend to depress the refining rate in the model converter. Once the stage II refining period was attained however, the reverse would appear to be true. As outlined in section 5.3.4, the presence of a significant excess of insoluble salt crystals undoubtedly increased the apparent viscosity of the model slag resulting in a marked increase in the residence time of droplets in the foam (τ) and hence in the total

surface area of amalgam droplets available for reaction. This has also resulted in a slight increase in the efficiency of utilisation of the HCl transferred from the jet gases, in removing sodium from the amalgam. This may be assessed by means of a factor F_M , which is defined as:

$$F_M = \left[\frac{\dot{m}_{Na,F}}{\dot{m}_{HCl}} \right]_{II,Av} = \left[\frac{\dot{m}_{Na,F}}{\dot{m}_{Na,F} + V_S \frac{d [C_{H^+}]_{Aq,B}}{dt}} \right]_{II,Av} \quad 5.23$$

In this case $\dot{m}_{Na,F}$ is the mean stage II refining rate and $\frac{d [C_{H^+}]_{Aq,B}}{dt}$ is the estimated mean rate of change of acid concentration in the model slag during the stage II period. For the experiment illustrated in Figure 62, where the model slag initially contained 2.0 moles of NaCl per litre, the value of F_M was 0.71, whereas for the equivalent experiment where no NaCl was initially present in the model slag, the value of F_M was slightly lower at 0.65.

In steelmaking, the precipitation of C_2S crystals is believed to be associated with a marked increase in the apparent slag viscosity, which can cause the foam to overflow from the converter mouth ^{16,18,19,21,51}. In the model however, the precipitation of salt crystals did not apparently inhibit the ability of bubbles to escape from the foam. This apparent anomaly can possibly be explained in terms of the relative surface properties of the precipitate - droplet and precipitate - bubble interfaces.

From the foregoing discussion it is apparent that a complete mathematical interpretation of the refining processes operative in the model converter is not possible. The factors influencing many of the variables involved, e.g. $\dot{\gamma}$, $\gamma_{S,F}$, τ , are not fully understood and indeed in some cases there would appear to be complex inter relationships between variables. In particular, the effects of the accumulation of NaCl in the model slag, for which there is no direct analogue in steelmaking, would appear to impose severe limitations on the usefulness of any mathematical

model for interpreting decarburisation kinetics in the L.D. process.

5.4.1 (c) The Use of the Model to Simulate the Effects of Steelmaking Control Variables

Although it has not been possible to quantify the refining kinetics in the model converter in terms of a mathematical formulation, there are still a number of fundamental characteristics which it has in common with the L.D. steelmaking process. In this context the model still provides a useful means of qualitatively assessing the effects of various steelmaking control variables on the refining rate. Just as with decarburisation in the L.D. process (Figures 3 and 4), the rate of sodium removal in the model converter is characterised by an initial rapid increase followed by a second period when the refining rate is approximately constant. The mean refining rate attained during the stage II period does appear to provide a criteria for comparing the effects of various alterations to the experimental conditions. In particular the model has been used to investigate the effect on the refining rate of variations in lance height, jet momentum and molar blowing rate of hydrogen chloride - all of which have analogous variables in steelmaking practice. In addition the model has been used to investigate a theory that enhanced refining rates may be produced when the pressure within the converter is increased.

Variation of the lance height provides perhaps the most widely used means of applying in blow control to the course of the steelmaking process. Both the lance height and the jet momentum have a marked effect on the rate at which droplets are ejected from the metal bath (\dot{V}) and hence on the surface area available for reaction in the foam ($\dot{V} \bar{A}_d \tau$). Figure 52 illustrates the results of some simple attempts to estimate the rate of droplet formation within the model converter. Various workers have noted that the splashing rate produced by a gas jet impinging onto a bath of a single liquid reaches a maximum value, associated with the onset of the

penetration mode, as the lance height was reduced below that at which splashing commenced 78, 81, 83. The presence of the slag layer in the present model system would appear to suppress this effect. The splashing rate produced when the lance tip was brought very close to the amalgam surface was in any case much greater than that at the onset of the penetration mode.

The total surface area of droplets in the foam could not be estimated with any degree of accuracy, due to the inability to measure the mean droplet size or the life time of droplets in the foam. The droplets falling into the collection trap within the vessel ranged in size from less than 0.5 mm diameter upto several millimetres in diameter, with a bias towards the smaller sizes. It is not known to what extent the larger droplets were fragmenting on the lip of the trap. Attempts were made to estimate the size distribution using photographic techniques, but these were unsuccessful. Droplets of about 1 mm in diameter, falling close to the vessel wall, took about 2 seconds to traverse the height of the foam. To what extent the close proximity of the vessel wall influenced this value is not known, but it does give an indication of the droplet residence times to be expected.

At jet momentums of 77 mN and 102 mN with a lance height of 2.5 mm, which were the blowing conditions most commonly used, the splashing rates were estimated to be about 250 and 500 ml per minute respectively (Figure 52). The total surface area of droplets in the foam for these blowing conditions, assuming various values for \bar{T} and \bar{A}_d , has been estimated in Table 15. The reaction area in the foam could clearly be very large compared with the bulk surface area of the bath.

The results of two series of experiments carried out to study the refining rates produced when using jet momentums of 77 and 102 mN are illustrated in Figure 49 (a). The plateau refining rates achieved using a jet momentum of 102 mN were consistently greater than those produced by a

77 mN jet, reflecting the greater surface area of droplets available for reaction with the higher momentum jet.

The value of F_M , as defined by equation 5.23, was obtained for three of the above experiments. These are indicated in Table 9. It will be noted that F_M attained a value of about 0.65 for those experiments using a jet momentum of 102 mN and about 0.50 with a 77 mN jet. This undoubtedly reflects the increased rate of droplet formation and hence the increased surface area available for reaction in the foam, associated with the higher momentum jet. However, considering that the splashing rate has been approximately doubled by increasing the jet momentum from 77 to 102 mN, the change in F_M is relatively small. The reason for this will become apparent later in this section.

Much larger variations in \dot{V} were produced in the series of experiments conducted at various lance heights (Table 10). By increasing the lance height, and hence reducing \dot{V} , the mean stage II refining rate was observed to decrease, although not as much as one might have expected. At a lance height of 44 mm, the rate of ejection of droplets from the bath was very low (Figure 52), yet the mean stage II refining rate was still 70% of the maximum rate observed (Figure 59). This suggests that reaction at the interface between the bulk amalgam bath and the model slag phase could contribute significantly to the overall refining rate under these conditions. The relatively high refining rate achieved when using a lance height of 44 mm (Figure 58) is probably in part due to the increased acid concentration in the model slag associated with refining at increased lance heights and also the improved contact with the model slag since there is relatively little gas held within the foam. It therefore does not represent the refining rate at the bulk slag-metal interface when large numbers of droplets are being created.

The rate equations derived earlier should strictly be rewritten to

include the surface area of the bulk bath. Equation 5.4 then becomes:

$$A_R = \gamma_{S,F} \dot{V} \bar{A}_d \tau + \gamma_{S,F,b} A_b \quad 5.24$$

Hence,

$$\dot{m}_{Na} = (\gamma_{S,F} \dot{V} \bar{A}_d \tau + \gamma_{S,F,b} A_b) k [C_{H^+}]_{Aq,B}, \quad 5.25$$

assuming that the same rate constant applies for both the surface of the bulk bath and droplets dispersed in the foam.

The interfacial area between the model slag and the quiescent metal bath was 0.012 m^2 . Surface turbulence produced by the impinging gas jet would tend to increase this slightly during the course of the blow. With a large lance height or a low jet momentum, the term $(\gamma_{S,F} \dot{V} \bar{A}_d \tau)$ would tend to be small and hence reaction at the surface of the metal bath would become important. With the fairly hard blowing conditions used for most of the experiments $(\gamma_{S,F} \dot{V} \bar{A}_d \tau)$ would be much larger than $(\gamma_{S,F,b} A_b)$ and hence the reaction taking place at the surface of the bulk amalgam bath can probably be ignored. The rapid collapse of the foam when blowing ceased and hence when droplets were no longer being created, is further evidence to substantiate this suggestion.

As the lance was raised or the jet momentum reduced, the available surface area for reaction would tend to decrease and hence the rate of sodium removal from the amalgam would be expected to decrease. However, the rate of transfer of HCl to the model slag (\dot{m}_{HCl}) remains unchanged, or may even increase since at greater lance heights the conditions for slag entrainment into the jet are more favourable. Since equation 5.6 still applies, one would therefore expect the acid concentration in the model slag to increase more rapidly at greater lance heights and in fact this is what is observed (Figure 60). This would tend to produce a faster rate of reaction at the surface of the amalgam in contact with the aqueous phase and hence would offset, at least to some extent, the effects of the reduced total surface area.

This tendency for the refining rate in the model to be self stabilising at some value determined mainly by the rate of transfer of gaseous reactant from the jet to the slag, reflects an inherent characteristic of the L.D. steelmaking process. Meyer has discussed this aspect of the process ¹¹. In particular he attempted to account for the variations in rate observed during the stage II decarburisation period in terms of a dynamic balance between the jetting conditions, the quantity of metal droplets in the foam and the state of oxidation of the slag.

When using comparatively large lance heights, the rate of sodium removal from the amalgam bath became rather erratic (Figure 58). Similar behaviour has been observed in steelmaking ^{6, 64}. As outlined in section 5.3.3 this probably arises from inadequate stirring of the bulk bath by the impinging gas jet, causing the surface layer to become denuded of sodium. This allows the concentration of acid in the slag to rise. When fresh metal is eventually swept to the surface, rapid evolution of gas occurs.

It has been shown that the refining rate in the model converter tends to be self stabilising at some value strongly influenced by the rate of transfer of HCl from the jet gases to the model slag. The effect of changes in \dot{m}_{HCl} has therefore been investigated since this is likely to have a far greater influence on the refining rates attained than either the jet momentum or lance heights.

By altering the composition of the gas jet, while maintaining all other blowing parameters constant, the flux of HCl molecules to the surface of the model slag and hence the rate of transfer, could be varied. The two series of experiments carried out are summarised in Table 9. As expected, it was found that by increasing the mass flow rate of hydrogen chloride to the reaction vessel the acid concentration in the slag phase increased more rapidly, producing an enhanced rate of sodium removal.

In basic oxygen steelmaking, the lance height, the jet momentum and the oxygen flow rate provide the main control variables. In the previous pages the attempts made to investigate the effects of the analogous variables in the model system have been discussed. The model converter has also been used to test the effect of certain modifications to conventional steel-making practice. In particular it has been suggested that an increase in the pressure within the converter might enhance the rate of sodium removal from the droplets in the foam.

It has already been noted that a droplet will contact both the aqueous phase and gas bubbles during its passage through the foam. Only a fraction, $\gamma_{S,F}$ of its surface will therefore be available for the reaction between hydrogen ions and sodium. If the foam was homogenous and there were no preferential paths for the droplet to move through it, then $\gamma_{S,F}$ would be equal to the volume fraction occupied by the aqueous phase in the foam.

$$\gamma_{S,F} = \frac{V_S}{V_F} = \left\{ 1 - \frac{V_G}{V_F} \right\} \quad 5.26$$

If we consider a single droplet falling through the foam in the model converter, then the rate at which sodium is being removed from it will to some extent be dependent upon the value of $\gamma_{S,F}$

$$\dot{m}_{Na} = \gamma_{S,F} A_d k [C_{H^+}]_{Aq,B} \quad 5.27$$

By increasing the external pressure on the foam, the gas within it would be compressed and $\gamma_{S,F}$ would increase. The rate of sodium removal from the drop would therefore be enhanced. An increase in the pressure within the vessel would tend to make bubble nucleation more difficult but this is unlikely to influence the rate of mass transfer in either the model system or in steelmaking foams.

A series of experiments were carried out in order to test the validity of the above theory. The results obtained are summarised in Table 12 and

Figures 69 and 70. Increasing the vessel pressure from 1.0 atmosphere to 1.75 atmospheres caused the maximum foam volume attained to decrease from 625 ml to 375 ml. This is slightly greater than one would have expected from simply compressing the gas present at one atmosphere. This may be attributed to the change in overall height of the foam, enabling bubbles to escape more easily, possible changes in the degree of induced stirring by the jet or simply inaccuracies in the method of measuring the foam volume. The corresponding change in $\gamma_{S,F}$, using equation 5.26, is from 0.40 at 1.0 atmospheres to 0.67 at 1.75 atmospheres, which constitutes an increase of almost 70%.

The rate of sodium removal from the amalgam was shown to increase with increasing vessel pressure. As explained in section 5.3.5 this was partly due to a change in the mass flow rate of HCl gas into the reaction vessel. The contribution due to the increase in $\gamma_{S,F}$ was estimated to be about 15% of the mean stage II refining rate at 1.75 atmospheres. This would appear to be a rather small increase when compared with the estimated change in $\gamma_{S,F}$. However, just as with the experiments conducted at various lance heights, this can probably be explained in terms of the tendency for the refining rate to be self stabilising at some value strongly influenced by the rate of transfer of HCl to the model slag. Provided \dot{m}_{HCl} remains constant, any attempt to increase the rate of sodium removal from the amalgam must result in the acid concentration in the model slag increasing less rapidly. The two effects will therefore tend to oppose each other resulting in a relatively minor change in the refining rate.

It is possible that an increase in the pressure within the model converter may also have an adverse effect on other variables influencing the refining rate. For example, a reduction in the height of the foam might tend to decrease the residence time of droplets within it. Decreasing the value of \mathcal{T} and hence the surface area available for reaction would therefore tend to counteract any increase produced in $\gamma_{S,F}$.

In addition to the effect on $\gamma_{S,F}$ there is a secondary benefit to be derived from pressurising the reaction vessel. In L.D. steelmaking the oxygen blowing rate, and hence the maximum decarburisation rate is restricted to that which avoids unreasonable amounts of material being ejected from the converter. By pressurising the vessel, the foam height would be diminished, allowing a higher oxygen blowing rate to be employed before slopping became excessive. In addition, a greater mass flow rate of oxygen could be achieved without increasing the jet momentum. When assessing this aspect of the model experiments it is more useful to consider the refining rate in terms of the rate of sodium removal per unit volume of foam. The results obtained have been treated in this way and are presented in Figure 89, clearly showing the beneficial effect of pressurising the reaction vessel.

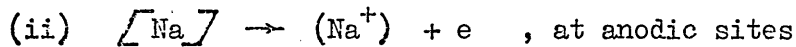
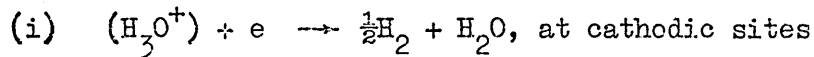
The experiments conducted at constant mass flow rate of gases served to illustrate the opposing effects of vessel pressure and jet momentum. While increasing the vessel pressure tended to increase $\gamma_{S,F}$, the reduced jet momentum necessary to maintain a constant mass flow rate caused \dot{V} to decrease. The two effects virtually neutralised each other and hence there was no net change in the refining rate.

It has been assumed in the previous discussion that equation 5.26 gave a reasonable estimate of $\gamma_{S,F}$. Hazledean has noted that iron droplets falling through a slag foam will adhere to the bubble cell walls^{128,129}. Similar behaviour has been observed with the model system. Amalgam droplets allowed to fall down a column of foam, produced by allowing a pool of amalgam to react with acidified water-glycerol solution at the bottom of the column, were also observed to follow the contours of the bubble cell walls. Single droplet studies have also showed that the coverage of the amalgam surface by hydrogen bubbles is related to the rate of sodium removal and hence the hydrogen ion concentration in the aqueous phase. Similarly in the foam produced in the model converter, the size and distribution of

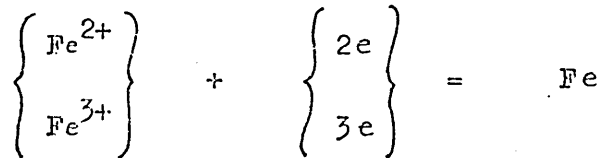
bubbles close to a droplet may be different from that some distance away, especially if bubbles are tending to coalesce in the bulk foam. Clearly it is possible that the foam may be heterogeneous and there may be preferential droplet paths through it. The accuracy of equation 5.26 as a measure of $\gamma_{S,F}$ is therefore in doubt.

5.4.2 Application to Basic Oxygen Steelmaking

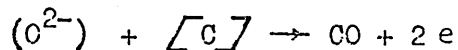
It has been suggested that the reaction between sodium and an acid at the surface of an amalgam droplet can occur in two stages,



The application of this idea to the reaction between molten iron-carbon droplets and molten slag suggests that at cathodic sites the reaction would be of the form:



The electrons for this reaction would be provided by the discharge of oxygen ions at anodic sites,



While the carbon content of the droplet remained relatively high this would lead to the nucleation and growth of carbon monoxide bubbles at the droplet surface (Section 2.3.4 (a)). As in the model, the presence of gas bubbles at the interface would effectively reduce the area available for the transport and reaction of the species involved.

The rate of decarburisation of the droplets dispersed in the foam created in an oxygen steelmaking vessel is given by:

$$\dot{m}_{C,F} = A_R \cdot \dot{m}_{C,d}'' \quad 5.28$$

As in the model system, the available surface area for reaction is given by,

$$A_R = \gamma_{S,F} \dot{V} \bar{A}_d \tau \quad 5.29$$

At high carbon concentrations it is believed that the rate of decarburisation is controlled by oxygen transport in the slag phase. Under steelmaking conditions the equilibrium constant for the decarburisation reaction is large²⁶ and hence the interfacial concentration of carbon can be assumed to be zero. In this case,

$$\dot{m}_{C,d}'' = [\alpha_{FeO}]_S [C_{FeO}]_{S,B} \quad 5.30$$

Hence,

$$\dot{m}_{C,F} = \gamma_{S,F} \dot{V} \bar{A}_d \tau [\alpha_{FeO}]_S [C_{FeO}]_{S,B} \quad 5.31$$

assuming for convenience that only ferrous ions are present in the slag.

For a simple iron-carbon melt, the gaseous oxygen introduced into the converter will be consumed in forming CO bubbles, iron oxides and by dissolving in the molten iron alloy.

$$2 \dot{m}_{O_2} = \dot{m}_{CO} + \dot{m}_{FeO} + \dot{m}[O]$$

While the carbon content of the bath is high it is reasonable to assume that the amount of oxygen going into solution is small³⁰ and therefore we can write:

$$\dot{m}_{FeO} = V_S \frac{d[C_{FeO}]_S}{dt} = 2 \dot{m}_{O_2} - \dot{m}_{CO} \quad 5.32$$

Virtually all of the oxygen blown into the converter is consumed by the reactions taking place and hence it is reasonable to assume that \dot{m}_{O_2} is a constant^{14, 36}. The rate of carbon monoxide evolution is equal to the rate of decarburisation and hence \dot{m}_{CO} may be replaced by expression 5.31.

$$V_S \frac{d[C_{FeO}]_S}{dt} = 2 \dot{m}_{O_2} - \gamma_{S,F} \dot{V} \bar{A}_d \tau [\alpha_{FeO}]_S [C_{FeO}]_{S,B} \quad 5.33$$

Assuming, $[C_{FeO}]_S = 0$ at $t = 0$

and $[C_{FeO}]_S = [C_{FeO}]_{S,B}$ at $t = t$,

expression 5.33 may be rearranged and integrated between these limits to give,

$$[C_{FeO}]_{S,B} = \frac{2 \dot{m}_{O_2}}{\gamma_{S,F} \dot{V} \bar{A}_d \tau [C_{FeO}]_S} \times \left\{ 1 - \exp \left(- \frac{\gamma_{S,F} \dot{V} \bar{A}_d \tau [C_{FeO}]_S t}{V_S} \right) \right\} \quad 5.34$$

By substituting this expression into equation 5.31 we obtain,

$$\dot{m}_{C,F} = 2 \dot{m}_{O_2} \left\{ 1 - \exp \left(- \frac{\gamma_{S,F} \dot{V} \bar{A}_d \tau [C_{FeO}]_S t}{V_S} \right) \right\} \quad 5.35$$

The rate of decarburisation of droplets dispersed in the foam is therefore determined by essentially two variables. \dot{m}_{O_2} is the rate of introduction of oxygen into the converter while the bracketed term in equation 5.35 describes the structure and reactivity of the slag-metal-gas emulsion formed. V_S is the volume of slag in the foam, $(\dot{V} \bar{A}_d \tau)$ is the surface area available for reaction, $\gamma_{S,F}$ is related to the volume ratio of gas and slag in the foam, $[C_{FeO}]_S$ is the mass transfer coefficient of the oxidising species in the slag phase and t is the time the foam has been in existence. In view of the relationship between the variables in this group it is reasonable to replace it by a single term S_{St} .

$$\dot{m}_{C,F} = S_{St} \cdot 2 \dot{m}_{O_2} \quad 5.36$$

$$\text{where, } S_{St} = \left\{ 1 - \exp \left(- \frac{\gamma_{S,F} \dot{V} \bar{A}_d \tau [C_{FeO}]_S t}{V_S} \right) \right\} \quad 5.37$$

The nature of the variables in the foam structure group, S_{St} , are such that it will have possible values ranging from 0 to 1. Unfortunately little is known concerning the magnitude of the variables in the foam structure

group for steelmaking conditions. An estimate of the value of S_{St} can be obtained using the data presented by Meyer²¹. In a 230 t capacity B.O.S. vessel, the total surface area of droplets in the foam was estimated to be about 50,000 m² and the total weight of slag present was about 32 tonnes. The value of $\left[\propto_{FeO} \right]_s$ is approximately 1.2 mm/s¹⁰² and assuming $\gamma_{S,F}$ was approximately 0.2 then,

$$S_{St} \simeq \left\{ 1 - \exp(-t) \right\}, \quad 5.38$$

where t is the time in seconds from the commencement of the blow. As the blow proceeds the value of S_{St} will rapidly approach unity. The slag-metal-gas emulsion does however take a finite time to develop to the conditions described by Meyer and hence in the initial stages of the blow the surface area available for reaction in the foam will be small. S_{St} will therefore increase slowly in the first few minutes of the blow, but will eventually attain a value of one. The decarburisation rate would therefore achieve a constant value determined by the oxygen blowing rate, at a constant iron oxide content in the slag. In practice this is what tends to happen^{21,34,36} although the situation is complicated by the consumption of oxygen by other refining reactions and also by the problems of slag formation.

Similarly with the model system, the mean stage II sodium removal rate has been shown to be influenced by \dot{m}_{HCl} , although other variables must be taken into consideration. It is interesting to note that had \dot{m}_{HCl} also been a constant then expression 5.7 could have been integrated and the resulting equation used to obtain the overall rate of sodium removal from the droplets in the foam,

$$\dot{m}_{Na,F} = \dot{m}_{HCl} \left\{ 1 - \exp \left(- \frac{\gamma_{S,F} \dot{V} \bar{A}_d \tau k t}{V_s} \right) \right\} \quad 5.39$$

This is very similar in structure to equation 5.35 obtained for steelmaking conditions. The bracketed term in the above expression would therefore have given a physical significance the term, F_M , introduced earlier and

hence would have provided a similarity criteria for comparison with steel-making conditions. Unfortunately \dot{m}_{HCl} proved to vary quite significantly during the course of an experiment and this approach cannot be used.

In the model system, equality between \dot{m}_{HCl} and $\dot{m}_{\text{Na,F}}$ was never achieved. The ratio of sodium removal rate to the rate of HCl transfer to the model slag during the stage II refining period, as defined by F_M , varied between about 0.5 and 0.7. It was shown that the operating conditions could be controlled to influence the values of \dot{V} , \mathcal{T} and $\gamma_{\text{S,F}}$. Changes in these could in turn alter the rate of sodium removal from the amalgam and hence the value of F_M . However, it was also shown that there was often a complex interaction between variables and that the refining rate tended to be self stabilising at some value determined mainly by the rate of transfer of HCl to the aqueous phase. Large changes in \dot{V} , \mathcal{T} and $\gamma_{\text{S,F}}$ were therefore required in order to produce even a moderate change in the refining behaviour.

If the value of the foam structure factor, S_{St} , calculated from Meyers data is typical of all basic oxygen steelmaking conditions then changes in the value of \dot{V} , \mathcal{T} and $\gamma_{\text{S,F}}$ are likely to produce even smaller changes in the refining characteristics than in the model system. Hence with steelmaking conditions of the type described by Meyer and Trentini, where the majority of decarburisation is taking place within the slag-metal-gas emulsion, the rate of supply of oxygen to the slag phase is the predominant factor controlling refining rates.

The effects of lance height variations on the refining characteristics of the L.D. process are well known. A hard blowing practice is believed to favour decarburisation while a soft blowing practice encourages slag formation and hence phosphorus removal¹⁵. Similarly with the model system, increasing the lance height produced a decrease in the rate of sodium removal from the amalgam. This was accompanied by an increase in the acidity of the

model slag which is analogous to the increase in the iron oxide content of the slag produced by a soft blowing practice in the L.D. process. The blowing conditions and the range of lance heights employed in oxygen steel-making operations are such that large numbers of droplets are ejected from the metal bath at all times throughout the blow⁸¹. The reduced decarburisation rate associated with soft blowing may be due more to the utilisation of the available oxygen for more favourable reactions under the conditions produced, rather than the reduced surface area for reaction in the foam.

It was shown, using the model converter system, that refining rates could be enhanced as a result of the increase in $\gamma_{S,F}$ produced by increasing the pressure within the reaction vessel. An increase in the mean stage II refining rate of about 15% was produced by increasing the vessel pressure from 1.0 to 1.75 atmospheres. In view of the value of the foam structure factor calculated from Meyers results, the analogous effect on the decarburisation rate in steelmaking is likely to be somewhat smaller. As outlined earlier, a secondary advantage might be derived from the improved control over slopping at high oxygen blowing rates. To some extent this could be achieved by improved slag composition control without the need to modify the ancillary equipment which vessel pressurisation would require.

Localised variations in the value of $\gamma_{S,F}$ within the steelmaking foam might provide an explanation for the changes in decarburisation rate observed during the stage II refining period. A sudden increase in the number of droplets in the foam as a result of the unstable action of the jet, a deliberate reduction in the lance height or a change in the viscosity of the slag phase, would tend to produce an increase in the rate of carbon monoxide evolution. This would immediately cause the volume fraction of gas held up in the foam to increase and hence $\gamma_{S,F}$ would tend to decrease. The iron oxide content of the slag would also tend to fall. These would effectively reduce the rate of supply of oxygen ions to the droplet surface and

the reaction rate would therefore decrease. The net effect would be to cause the decarburisation rate to oscillate about some mean value determined by the rate of supply of oxygen to the slag phase. The fluctuations in sodium removal rate in the model converter during the stage II refining period may also be explained in terms of an analogous mechanism. This again illustrates the inherent self stabilising character of the refining rate in reaction generated foams.

This approach to oxygen steelmaking is obviously somewhat simplified. Neither the contribution to decarburisation of reaction in the jet impingement zone or as a result of a carbon boil in the bath have been considered. Many operators claim to use a 'dry slag' practice where foam formation is minimised without any deleterious effect on the decarburisation rate. In this case decarburisation may be occurring via droplets ejected into the oxidising gaseous atmosphere above the bath. Some reactive slag formation must occur in order that the level of sulphur and phosphorus in the metal can be controlled.

In the model experiments the slag volume was maintained constant. In steelmaking the products of oxidation of iron, silicon, manganese and phosphorus all contribute to the volume of the slag, which increases throughout a blow. The addition of lime to produce a basic slag, with the concomitant problems of lime dissolution, introduces a further variable. For a simple iron-carbon melt with a CaO-FeO slag,

$$\rho_S \frac{dV_S}{dt} = W_{CaO} \cdot \dot{m}_{CaO} + W_{FeO} \cdot \dot{m}_{FeO} \quad 5.40$$

\dot{m}_{CaO} is the rate of dissolution of lime from the solid particles and ρ_S is the mass density of the slag.

Both τ and $\gamma_{S,F}$ are probably related to the volume of the foam created. Acheson and Hills have suggested possible solutions for both these variables 184.

$$\gamma_{S,F} = \frac{V_S}{V_F} = 1 - \epsilon \frac{\beta_c \Gamma \dot{m}_c \Gamma_F}{U_{\text{bub}} A_V} \quad 5.41$$

$$\tau = \frac{2U_o \sin \phi}{g \left\{ 1 - \frac{\rho_F}{\rho_{Fe}} \left(1 - \frac{3f_D U_o^2 \sin \phi}{8r_d g} \right) \right\}} \quad 5.42$$

Further expansion of equation 5.35 is clearly possible, but the resulting expressions are complex and probably of only limited use.

The experiments conducted at low sodium contents in the amalgam were little more than exploratory in nature. They do however suggest that as observed in the single droplet studies, there is a change in the rate controlling mechanism below some critical amalgam composition. This is probably associated with the change from hydrogen ion discharge control to sodium transport control in the amalgam. Clearly it is possible to draw analogies between this behaviour and the change in decarburisation rate in steelmaking associated with the change from oxygen transport control to carbon transport control.

The rate of sodium removal from droplets in the foam would again be given by:

$$\dot{m}_{Na,F} = A_R \cdot \dot{m}_{Na,d}'' \quad 5.2$$

If the rate of sodium removal from droplets in the foam is determined by the rate of sodium transport to the reaction interface, then,

$$\dot{m}_{Na,d}'' = [\alpha_{Na}]_d [C_{Na}]_{d,B} \quad 4.25$$

Hence, substituting for A_R from equation 5.4,

$$\dot{m}_{Na,F} = Y_{S,F} \dot{V} \bar{A}_d \tau [\alpha_{Na}]_d [C_{Na}]_{d,B} \quad 5.43$$

This approach can also be applied to steelmaking conditions. The decarburisation rate of iron droplets at high carbon concentrations, is believed to be controlled by oxygen transport in the slag phase. The interfacial carbon concentration in a droplet is sufficiently high to permit the formation of CO at the surface ¹¹⁷⁻¹²¹. As the bulk carbon concentration in the drop decreases, the interfacial concentration also decreases until it reaches zero. At this stage carbon transport becomes rate controlling and the oxygen content within the metal droplet rises, eventually causing CO

bubbles to be nucleated within the droplet. Richardson has suggested that there may be an intermediate stage where kinetic control may be operative ¹¹¹. The internal nucleation of CO bubbles leads to severe disruption of the droplet and prediction of the decarburisation rate under these conditions becomes difficult ¹¹⁹. It is possible however, to predict the bulk carbon concentration at which the interfacial composition becomes zero. For carbon transport control,

$$\dot{m}'_{C,d} = [\alpha_C]_d [C_C]_{d,B} \quad 4.29$$

Hence,

$$\dot{m}_{C,F} = \gamma_{S,F} \dot{V} \bar{A}_d \tau [\alpha_C]_d [C_C]_{d,B} \quad 5.44$$

Once internal nucleation of CO begins the effective surface area of the droplet will increase significantly and secondary emulsification may occur by the fragmentation of the drop. At the instant when the interfacial carbon concentration falls to zero the rate of carbon transport in the droplet will equal the rate of oxygen transport in the slag phase. Eliminating $\dot{m}_{C,F}$ from equations 5.36 and 5.44

$$[C_C]_{d,Crit} = \frac{2 \dot{m}_{O_2}}{\gamma_{S,F} \dot{V} \bar{A}_d \tau [\alpha_C]_d} S_{St} \quad 5.45$$

If refining is still predominantly occurring in the foam, then as before the foam structure group, S_{St} , will be approximately unity. Hence equation 5.45 may be simplified,

$$[C_C]_{d,Crit} = \frac{2 \dot{m}_{O_2}}{\gamma_{S,F} \dot{V} \bar{A}_d \tau [\alpha_C]_d} \quad 5.46$$

This is clearly a somewhat simplified approach to the problem since neither equation 5.43 for the model system or equation 5.44 for steelmaking conditions take into consideration the variation in solute concentration between droplets during their passage through the foam. The composition of droplets in the foam will also have fallen well below the critical value

some time before it is achieved in the bulk bath.

In steelmaking the transition to carbon transport control is associated with the collapse of the foam, since the rate of gas evolution is inadequate to sustain it. An advance model of the process would therefore have to take into consideration both decarburisation occurring in the jet impingement zone and as a result of the carbon boil in the bulk bath.

The nature of the variables in the denominator of equation 5.46 suggest that the metal composition at which the mechanism change occurs may be influenced by the structure of the foam. Similarities may possibly be drawn between this term and the geometric factor proposed by Szekeley to explain the variability of the bath composition at which the mechanism change takes place ⁴¹. The ability to predict the critical composition for the mechanism change would certainly be a useful control parameter. Clearly more work is required in this area of investigation.

A room temperature model has been developed which simulates certain aspects of the slag-metal-gas reactions that occur in reaction generated foams of the type encountered in L.D. steelmaking. In the model the molten iron was represented by a pool of sodium amalgam, the slag by a mixture of water and glycerol and the oxygen by a hydrogen chloride-nitrogen jet. Droplets of amalgam ejected from the bath by the impinging gas jet, reacted with the hydrogen chloride dissolved in the model slag to produce hydrogen bubbles, thus forming a dynamic foam.

The behaviour of single droplets of amalgam in acid media has also been studied in order to gain more information about the fundamental refining processes occurring in the model converter. With high sodium concentrations in the amalgam droplets, the refining rate was shown to be dependent upon the acid concentration in the aqueous phase, the process probably being controlled by the rate of discharge of hydrogen ions. The presence of hydrogen bubbles adhering to the droplet surface had an adverse effect on the refining rate achieved. Sodium chloride additions to the aqueous phase also tended to reduce the refining rate but the mechanism involved is not fully understood. With low sodium concentrations in the amalgam droplets, the refining rate became dependent upon the sodium concentration, implying that transport of this species to the reaction interface was controlling the rate of the overall process.

It has not been possible to develop a mathematical model for the refining processes occurring within the model converter. For steelmaking conditions it has been shown that the rate of decarburisation during the stage I and II periods is influenced by two factors, the structure of the foam and the rate of transfer of oxygen from the gas jet to the slag phase. When the surface area available for slag-metal reaction in the foam is very large, the decarburisation rate becomes self stabilising at some value strongly influenced by the rate of transfer of the reactant species from the jet gases to the slag phase.

The model converter has been used to qualitatively investigate the effect of lance height, jet momentum and mass flow rate of gaseous reactant into the reaction vessel on the mean stage II refining rate. The results obtained compare favourably with analogous variables in steelmaking practice. In addition the effect on the refining rate of pressurising the reaction vessel has also been investigated. An improvement in the refining rate was achieved, partly due to improved slag-metal drop contact and partly to increased hydrogen chloride flow rate. It is not believed that such a significant improvement would be achieved for steel making conditions although there might be some advantage derived from improved control over slopping at high oxygen flow rates.

When the sodium concentration in the amalgam fell below some critical level the refining rate in the model converter decreased producing a third refining stage comparable with refining under carbon transport control in the L.D. converter.

- 1 M. D. Ward J.I.S.I., 1970, 208, p 445
- 2 K. W. Lange Archiv fur das Eisenhüttenwesen, 1971, 42, (4),
p 233, B.I.S.I.T. 9410
- 3 R. D. Walker and D. Anderson Iron and Steel
Part I 1972, June, p 271
Part II 1972, August, p 403
Part III 1972, October, p 497
- 4 K. Kawakami J. of Metals, 1966, 18, p 836
- 5 G. C. Smith J. of Metals, 1966, 18, p 846
- 6 R. A. Flinn et al Trans. Met. Soc. A.I.M.E., 1967, 239, Nov., p 1776
- 7 A. Chatterjee Iron and Steel
Part I 1972, Dec., p 627
Part II 1973, Feb., p 38
- 8 V. B. Okhotskii Steel in the U.S.S.R., 1972, June, p 443
- 9 D. J. Price Ph.D. Thesis, Brunel Univ., Dec., 1973
- 11 H. W. Meyer J.I.S.I., 1969, June, p 781
- 12 F. D. Richardson and J. H. E. Jeffes J.I.S.I., 1948, 160, p 261
- 13 V. V. Yakovlev, et al Steel in the U.S.S.R., 1973, July, p 554
- 14 Y. F. Mikhnevich et al Steel in the U.S.S.R., 1971, Jan., p 28
- 15 H. W. Meyer et al from Heat and Mass Transfer in Process Met., ed
A. W. D. Hills, Inst. of Mining and Met., 1967,
p.173
- 16 B. Trentini, Trans. Met. Soc. A.I.M.E., 1968, 242, Dec., p 2377
- 17 B. V. Nikiforov et al Stalin English, 1970, March, p 189
- 18 F. Bardenheuer et al Blast Furnace and Steel Plant, 1970, June, p 401
- 19 V. I. Yavoiskii et al Stalin English, 1970, 8, August, p 597
- 20 H. von Ende et al Archiv fur das Eisenhüttenwesen, 1968, 39, p 177
B.I.S.I.T. 1592
- 21 H. W. Meyer et al J. of Metals, 1968, July, p 35
- 22 A. V. Marinin and V. A. Bolshakov Stalin English, 1968, Oct., p 826
- 23 S. Tsuda et al Trans.I.S.I.Jap., 1970, 10, p 112

- 24 F. Bardenheuer et al Stahl und Eisen, 1968, 88, p 613 B.I.S.I.T. 1632
- 25 J. Green Ph.D. Thesis, Sheffield Polytechnic, 1975
- 26 C. Bodsworth and H. B. Bell Phys. Chem. of I. & S. Manufacture, Longmans, 1972 2nd Edition.
- 27 S. G. Afanasev Stalin English, 1969, July, p 620
- 28 T. F. Pearson et al J.I.S.I., 1966, Oct., p 997
- 29 M. Yoshii & M. Ichinohe Tetsu to Hagane, 1970, 56(2), p 178 B.I.S.I.T. 8854
- 30 H. C. Vacher & E. H. Hamilton Trans. A.I.M.E., 95, p124
- 31 A. V. Bradshaw & F. D. Richardson I.S.I. Special Report No. 92, p 25
- 32 T. Fujii et al Trans. I.S.I.Jap., 1969, 2, p 437
- 33 G. R. Fitterer from Chem.Met.of I. & S. - Proc.Int. Conf. on Chem. Met., Univ. of Sheffield, 1972, p 184
- 34 F. D. Richardson Jernkont Ann, 1969, 153, p 359
- 35 K. Li et al, Trans. A.I.M.E., 1964, 230, p 71
- 36 M. Ichinoe et al Proc. I.C.S.T.I.S. - Trans. I.S.I. Jap., 1971,11, p 233
- 37 V. B. Okhotski Steel in the USSR., 1973, August, p 630
- 38 V. S. Kocho et al ibid, 1971, August, p 614
- 39 V. I. Yavoiski ibid, 1971, Oct., p 779
- 40 S. Asai & I. Muchi Trans. I.S.I.Jap., 1970, 10, p 250
- 41 J. Szekeley & M. R. Todd Trans. Met. Soc. A.I.M.E., 1967, 239, Oct., p 1664
- 42 Y. P. Nikitin et al Izv. VUZ Chern Met., 1966, (6), p 67, B.I.S.I.T. 10266
- 43 B. M. Larsen A.I.M.M.E. O.H. Conf. Proc., 1949, 32, p 231
- 44 D. E. Todd ibid, 1962, p 106
- 45 P. M. Bills B.I.S.R.A. Report No. SM/C/3/62
- 46 J. Pearson Iron and Coal, 1960, Dec., p 1407
- 47 R. A. Hacking ibid, 1960, Nov., p 1107
- 48 D. J. Jones et al J. of Metals, 1963, August, p 577
- 49 P. V. Riboud et al I.R.S.I.D., 1969, March, 64, p 1

- 50 P. V. Riboud et al C.D.S. Circ., 1970, 4, p 987
- 51 P. Kozakevitch J. of Metals, 1969, July, p 57
- 52 F. E. Rote & R. A. Flinn Met. Trans., 1972, June, 3, p 1373
- 53 B. C. Welbourn & R. Kulig B.I.S.R.A. Report, SM/A/BRP/53/71
- 54 S. Okano Proc. I.C.S.T.I.S. - Trans I. & S.I. Jap., 1971, 11, p 227
- 55 V. T. Lutsenko & P.V. Umrikhin, Steel in the U.S.S.R., 1972, Jan., p 31
- 56 J. A. Wester et al Silver Jubilee Symposium - Indian Inst. of Metals New Delhi, 1972, Feb.
- 57 P. Kozakevitch from Phys. Chem. of I. & S., ed. J. F. Elliot, 1956, p 89
- 58 C. F. Cooper & J. A. Kitchener J.I.S.I., 1959, Sept., p 48
- 59 P. Kozakevitch from Liquids: Structure, Properties & Solid Interactions, ed. T. J. Hughel, Elsevier Pub. Corp., 1965, p 243
- 60 R. C. Urquhart & W. G. Davenport J. of Metals, 1970, June, p 36
- 61 W. K. Lu & A. E. Hamielec Chem. Met. of I. & S. - Proc. of Int. Conf. on Chem. Met., Univ of Sheffield, 1972, p 110
- 62 E. A. Krichevstov et al Steel in the U.S.S.R., 1974, Jan., p 17
- 63 T. Kootz & A. Altgeld Thyssenforschung, 1970, 2, (4), p 121
- 64 G. C. Smith & D. A. Dukelow J. of Metals, 1964, April, p 357
- 65 J. Maatsch Technische Mitt Krupp Forschung, 1962, April, 20, P 1, B.I.S.I.T. 3064
- 66 R. B. Banks & D. V. Chandrasekhara J. Fluid Mech., 1963, 15, p 13
- 67 R. B. Banks & A. Bhavamai J. Fluid Mech., 1965, 23(2), p 229
- 68 E. T. Turkdogan Chem. Eng. Sci., 1961, 21, p 1133
- 69 V. I. Yavoiski et al Steel in the U.S.S.R., 1973, March, p 184
- 70 V. I. Yavoiski et al ibid, 1974, Jan., p 20

- 71 V. N. Golyatin et al Russ. Met., 1968, (4), p 11
- 72 W. G. Davenport et al from Heat & Mass Transfer in Process Met., ed. A. W. D. Hills, I.M.M., 1967, p 207
- 73 D. H. Wakelin Ph.D. Thesis, Univ. of London, 1966
- 75 R. D. Collins & H. Lubanska Brit. J. of Appl. Physics, 1954, 5, p 22
- 76 F. Mathieu Rev. Univ. des Mines, 1962, 18, p 482 B.I.S.I.T. 3639
- 77 E. Dennis ibid, 1963, 19, p 367 B.I.S.I.T. 3538
- 78 A. Chatterjee Ph.D. Thesis, Univ. of London, 1970
- 79 R. S. Rosler & G. H. Stewart J. Fluid Mech., 1968, 31(1), p 163
- 80 N. A. Molloy J.I.S.I., 1970, Oct., p 943
- 81 A Chatterjee & A. V. Bradshaw J.I.S.I., 1972, March, p 179
- 82 C.E.A. Shanahan from Phys. Chem. of I. & S. Making, ed. J. F. Elliot, 1956, p 165
- 83 J. Chedaille & M. Horvais CDS Circ. Inf. Tech., 1962, 19(2), p 361 B.I.S.I.T. 3057
- 84 A. D. Robertson & A. T. Sheridan J.I.S.I., 1970, July, p 625
- 85 P. Jervis et al United Steel Co. Report, No. F. & F. R. 5561/-/67
- 86 A. T. Sheridan ibid, No. F. & F.R. 5561/1/67
- 87 Kun Li J.I.S.I., 1960, Nov., p 275
- 88 O. K. Tokovoi et al Steel in the U.S.S.R., 1971, Jan., p 26
- 89 J. Maatsch Tech. Mitt Krupp Forsch. Ber., 1963, 21, May, p 1 B.I.S.I.T. 3696
- 90 T. Shimotsuma Nippon Kokan Tech Rep. - Overseas, 1967, Jan., p 13
- 91 A.T. Sheridan from Heat and Mass Transfer in Process Met., ed. A. W. D. Hills, I.M.M., 1967, p 242
- 92 K. H. Kluth & J. Maatsch Tech Mitt Krupp Forsch. Ber. 1964, 22(3), p 93 B.I.S.I.T. 4242
- 93 Huang-Kin-Ho & G. I. Demin Steel in the U.S.S.R., 1971, Jan., p 30
- 94 S. M. Andonev & I. A. Vainshtein Stalin English, 1967, Nov., p 913

- 95 J. M. van Langen J.I.S.I., 1960, Nov., p 262
- 96 R. H. Parker B.I.S.R.A. Report No. SM/A/24/69
- 97 B. Bird B.Sc. Project, Dept. of Met., Sheffield Poly., 1972
- 98 B. Cunliffe *ibid*, 1973
- 99 E. G. Dubrawka J. of Metals, 1961, June, p 448
- 100 G. I. Demin et al Izv. VUZ Cher Met., 1967, 7, p 173
B.I.S.I.T. 5975
- 101 A. Chatterjee et al Met. Trans., 1972, 3, Dec., p 3167
- 102 P. B. Crimes Ph.D. Thesis, U. of London, 1968
- 103 S. M. Aeron Ph.D. Thesis, U. of London, 1971
- 104 F. D. Richardson Met. Trans., 1971, 2, p 2747
- 105 M. J. Hadamard Comptes Rend, 1911, 152, p 1735
- 106 A. E. Handlos & T. Baron A.I.Ch.E.J., 1957, 3, p 127
- 107 S. Hu & R. C. Kintner *ibid*, 1955, 1, p 42
- 108 A. D. Pasternak & D. R. Olander *ibid*, 1968, 14, p 235
- 109 P. H. Calderbank & I. J. O.Korchinski Chem. Eng. Sci., 1956, 6, p 65
- 110 E. T. Turkdogan Trans. A.I.M.E., 1963, 227, p 1265
- 111 F. D. Richardson from Chem. Met of I. & S.- Proc. Int. Conf. Met. Chem. U. of Sheffield, 1972, p 82
- 112 A. B. Newman Trans. A.I.Ch.E., 1931, 27, p 203
- 113 T. Vermulean Ind. Eng.Chem., 1953, 45, p 1664
- 114 R. Kronig & J. C. Brink App. Sci. Res., 1950, A-2, p 142
- 115 P. M. Rose & R. C. Kintner A.I.Ch.E.J., 1966, 12(3), p 531
- 116 R. Higbie Trans.A.I.Ch.E., 1935, 31, p 365
- 117 L. A. Baker et al Trans. Met. Soc.A.I.M.E., 1964, 230, p 1228
- 118 L. A. Baker et al *ibid*, 1967, 239, p 857
- 119 P. A. Distin et al J.I.S.I., 1968, 206, p 821

- 104 -
- 120 D. G. C. Robertson & from Heterogeneous Kinetics at Elevated Temperatures,
A. E. Jenkins eds. G. R. Belton & W. L. Worrel 1970, New York,
Plenum Press, p 393
- 121 R. S. Kaplan &
W. O. Philbrook Trans.Met.Soc. A.I.M.E., 1969, 245, p 2195
- 122 R. G. Baker J.I.S.I., 1967, 205, p 637
- 123 L. A. Baker &
R. G. Ward J.I.S.I., 1967, 205, p 714
- 124 P. G. Roddis J.I.S.I., 1973, Jan., p 53
- 125 J. B. See & N. A. Warner J.I.S.I., 1973, Jan., p 44
- 126 A. E. Hamielec et al Can. Met. Quart., 7(1), p 27
- 127 L. A. Baker ibid, 7(4), p 217
- 128 M. W. Davies et al from The Richardson Conf., eds. J. H. E. Jeffes &
R. J. Tait, I.M.M., July 1973, p 95.
- 129 E. W. Mulholland et al J.I.S.I., 1973 Sept., p 632
- 130 W. N. Bargeron et al Trans. A.F.S., 1969, 77, p 303
- 131 M. Chon et al Trans. I.S.I. Jap., 1971, 11, p 500
- 132 K. Ishii et al ibid, 1971, 11, p 507
- 133 P. B. Crimes B.I.S.R.A. Report No. MG/A/72/64
- 134 H. M. Katz et al Trans.A.I.M.E., 1960, 218, p 770
- 135 D. R. Olander Nuclear Eng.Sci., 1968, 31, p 1
- 136 R. B. Dean J. App. Physics, 1944, 15, May, p 446
- 137 H. S. Levine Met.Trans., 1973, 4, March, p 777
- 138 R. S. Kaplan &
W. O. Philbrook Met.Trans., 1972, 3, Feb., p 483
- 139 A. V. Bradshaw Le Vide, 1968, No. 138, Nov., p 376
- 140 P. Kozakevitch et al Iron & Coal Trades Review, 1955, April, p 963
- 141 Yung Lee Ind.Eng.Chem. - Prod.Res.Dev., 1968, 7(1), Mar., p 66
- 142 J. J. Bikerman Foams: Theory & Industrial Applications, Reinhold
Pub. Corp., 1953, p 57
- 143 C. Holden &
A. Hogg J.I.S.I., 1960, Nov., p 318

- 144 W. F. Porter et al from Heat and Mass Transfer in Process Met., ed. A. W. D. Hills, I.M.M., 1966, p 79
- 145 C. D. Hodgman Handbook of Chem. and Physics, Chem. Rubber Co. Ltd., 1959
- 146 H. Remy Treatise on Inorg. Chem., Elsevier Pub. Co., 1956
- 147 K. Narita & T. Onoye Trans. I. & S.I.Jap., 1971, 11, p 401
- 148 G. Fernekes J. Phys.Chem., 1903, 7, p 611
- 149 J. N. Bronsted & N. L. R. Kane J. Am. Chem. Soc., 1931, 53, p 3624
- 150 W. Fraenkel et al Z. Anorg..Chem., 1928, 171, p 82
- 151 A. Klein Zeitschrift fur anorganische und allgemcine chemie 1924, 137, p 39
- 152 W. Fraenkel & H. Heinz ibid, 1924, 133, p 153
- 153 L. P. Hammet & A. E. Lorch J. Am.Chem. Soc., 1932, 54, p 2128
- 154 A. Frumkin Disc. of the Faraday Soc., 1947, 1, p 57
- 155 F. A. Fletcher & M. Kilpatrick J. Phys. Chem., 1938, 42, p 113
- 156 W. G. Dunning & M. Kilpatrick ibid, 1938, 42, p 215
- 157 Moriguchi & Mitsukuri J. Chem. Soc. Jap., 1931, 52, p 425
- 158 A. Frumkin Electrochimica Acta, 1970, 15, p 289
- 159 J. O'M. Bockris & R. G. H. Watson J. de Chemie Physique, 1952, 49, p 70
- 160 A Frumkin from Advances in Electrochem., Vol. I, ed. P. Delahey & C. Tobias, 1961, p 65
- 161 H. B. Baker & L. H. Parker J. Chem. Soc., 1913, 103, p 2060
- 162 J. O'M. Bockris & G. Kortum Textbook of Electrochemistry, Vol. II, Elsevier Pub. Co., 1951
- 163 E. Gruz & M. Volmer Z. Physik Cehm., 1930, 150A, p 203
- 164 J. Tafel ibid, 1905, 50A, p 641
- 165 N. I. Kobosew & N. Nekrassow Z. Elektrochem., 1930, 36, p 529
- 166 J. O'M. Bockris & A. K. N. Reddy Modern Electrochemistry, Vol. II, Macdonald, 1951

- 167 C. W. Wood & A. K. Holliday Physical Chemistry, Butterworths, 1964, p 284
- 168 A. N. Frumkin from Advances in Electrochemistry and Electrochemical Engineering, ed. P. Delahey & C. Tobias, Vol. I 1961, p 65
- 169 A. N. Frumkin ibid, Vol. 3, 1964, p 287
- 170 K. J. Vetter Electrochemical Kinetics, Academic Press, 1967
- 171 B. E. Conway Theory and Principles of Electrode Processes, Ronald Press, 1965
- 172 A. Frumkin Disc. of the Faraday Soc., 1947, 1, p 57
- 173 J. O'M. Bockris & E. C. Potter J. Electrochem. Soc., 1952, 99(4), p 169
- 174 J. O'M. Bockris & A. M. Azzam Trans. Faraday Soc., 1952, 48, p 145
- 175 J. O'M. Bockris & R. Parsons ibid, 1949, 45, p 916
- 176 B. E. Conway & J. O'M. Bockris J. Chem. Physics, 1957, 26,(3), p 532
- 177 A. J. de Bethune & G. E. Kimball J. Chem. Physics, 1945, 13,(2), p 53
- 178 B. Post & C. F. Hiskey J. Am. Chem. Soc., 1950, 72, p 4203
- 179 M. Hanson Constitution of Binary Alloys, McGraw Hill, 1958
- 180 W. F. Linke Solubilities, Vol. II, 4th ed., 1965, American Chem. Soc.
- 181 W. M. Latimer Oxidation Potentials, 2nd ed., Prentice Hall, 1952
- 182 S. M. Aeron et al Trans. Inst. Min. Met., 1974, 83, p 168
- 183 A. I. Johnson & L. Braida Can.J. Chem. Eng. 1957, 35, p 165
- 184 R. Acheson & A. W. D. Hills from Physical Chemistry of Process Metallurgy - The Richardson Conference, ed. J. H. E. Jeffes and R. J. Tait, Inst. of Mining & Met., 1973, p 153.

100 518 701 0

TELEPEN

C1941



Sheffield City Polytechnic Library

REFERENCE ONLY

6313

Model Studies of Metal-Slag Reactions

in Reaction Generated Foams

by

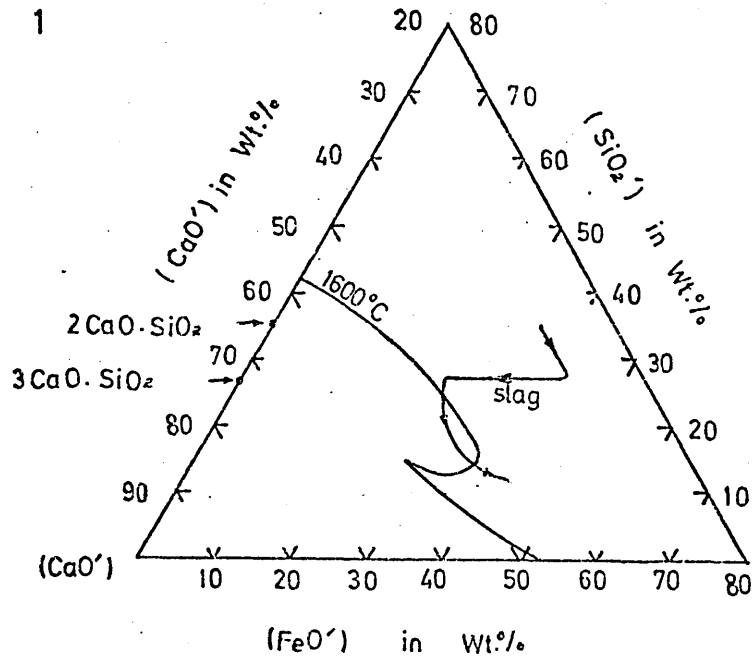
R. Acheson

Part Two

SHEFFIELD POLYTECHNIC
LIBRARY
669Q
AC
THESIS

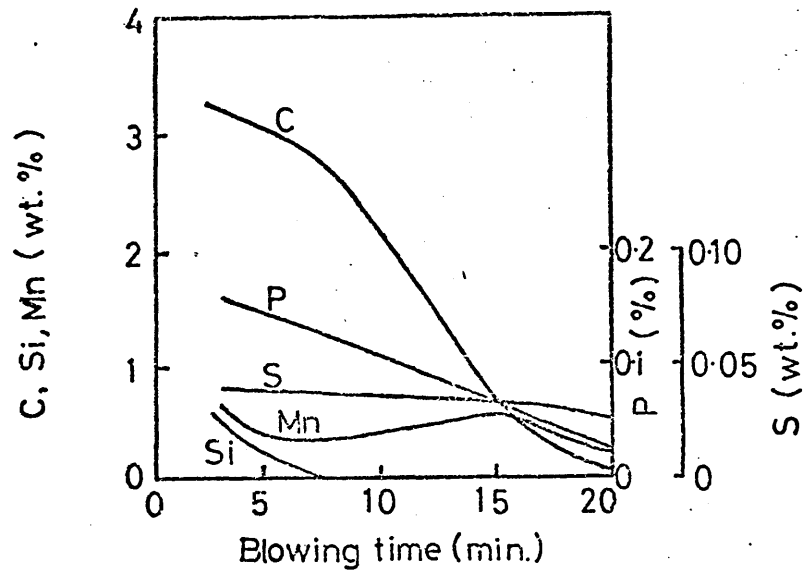
~~04000 01~~

Figure 1



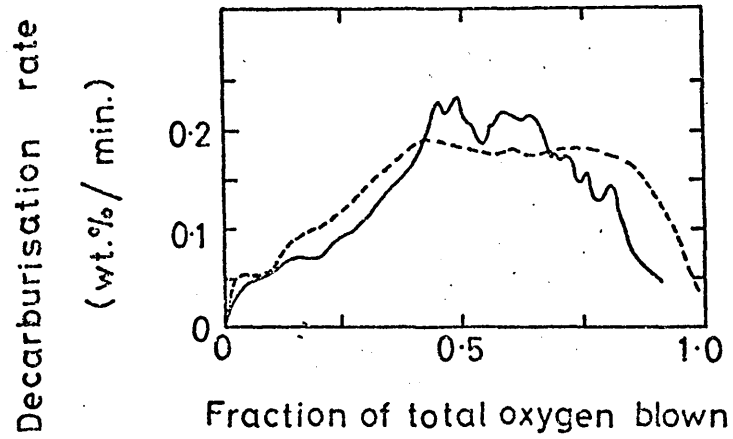
Variation in slag composition throughout a blow [18]

Figure 2



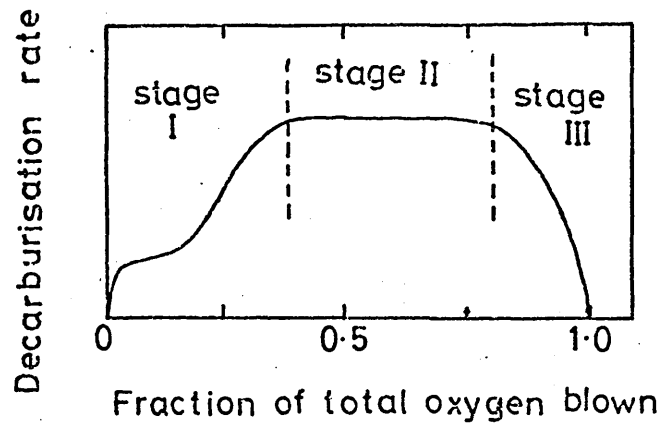
Changes in bath composition during blow. [3]

Figure 3



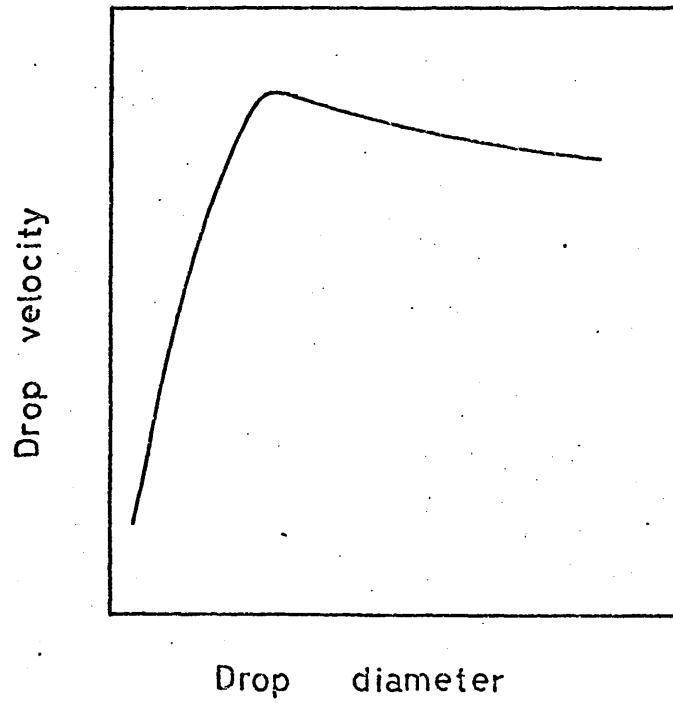
Typical decarburisation rate curves. [11]

Figure 4



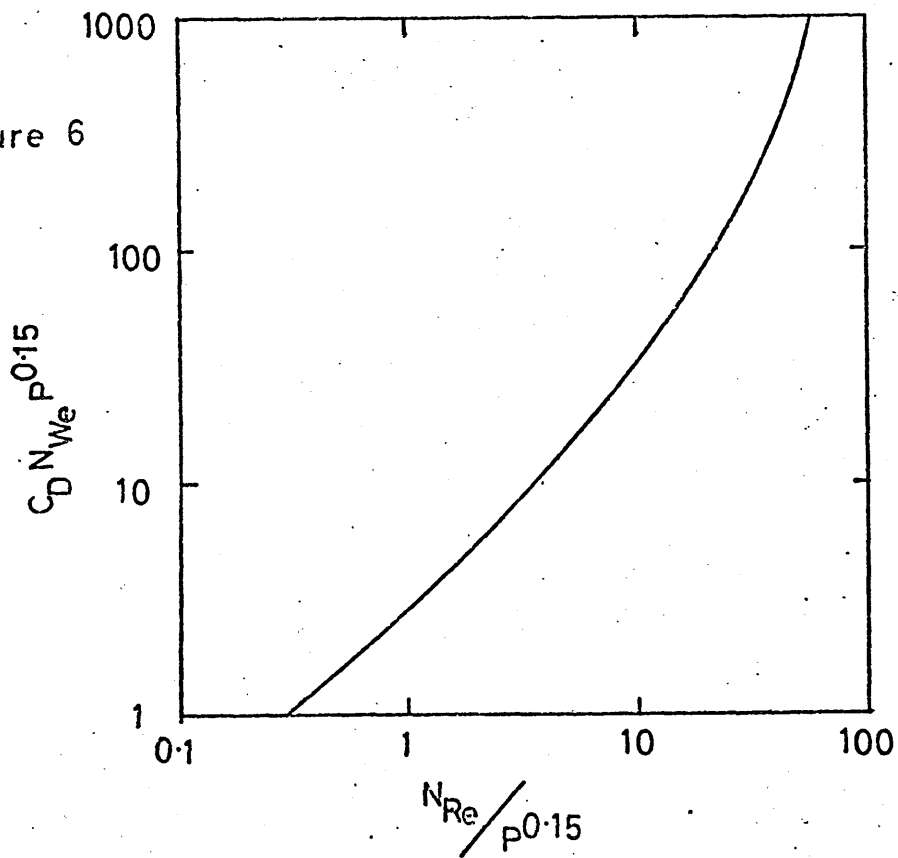
Idealised decarburisation rate curve. [3,11]

Figure 5



Relationship between terminal velocity and droplet diameter. [104]

Figure 6



Hu & Kintner correlation for drop velocity. [107]

Table 1
 Properties of liquid phases 144, 145, 147.

	Density (10^{+3} kg/m ³)	Surface Tension (10^{-3} N/m)	Viscosity (10^{-3} kg/ms)
At 1600°C:			
Iron	7.2	1200	. 5.0
Basic slag	3.0	500	50.0
At 20°C			
Mercury	13.55	465.0	1.55
Water	1.00	73.4	1.00
Glycerol	1.26	63.3	1,490

Table 2
 Properties of gases used 145, 146.

	Density at 0°C (kg/m ³)	Solubility in water (m ³ of gas per m ³ of water at 20°C & 1 atmcs. pressure)
Hydrogen	0.090	0.0182
Hydrogen chloride	1.639	450
Nitrogen	1.251	0.0164

Figure 7

The Hg-Na binary equilibrium diagram [179].

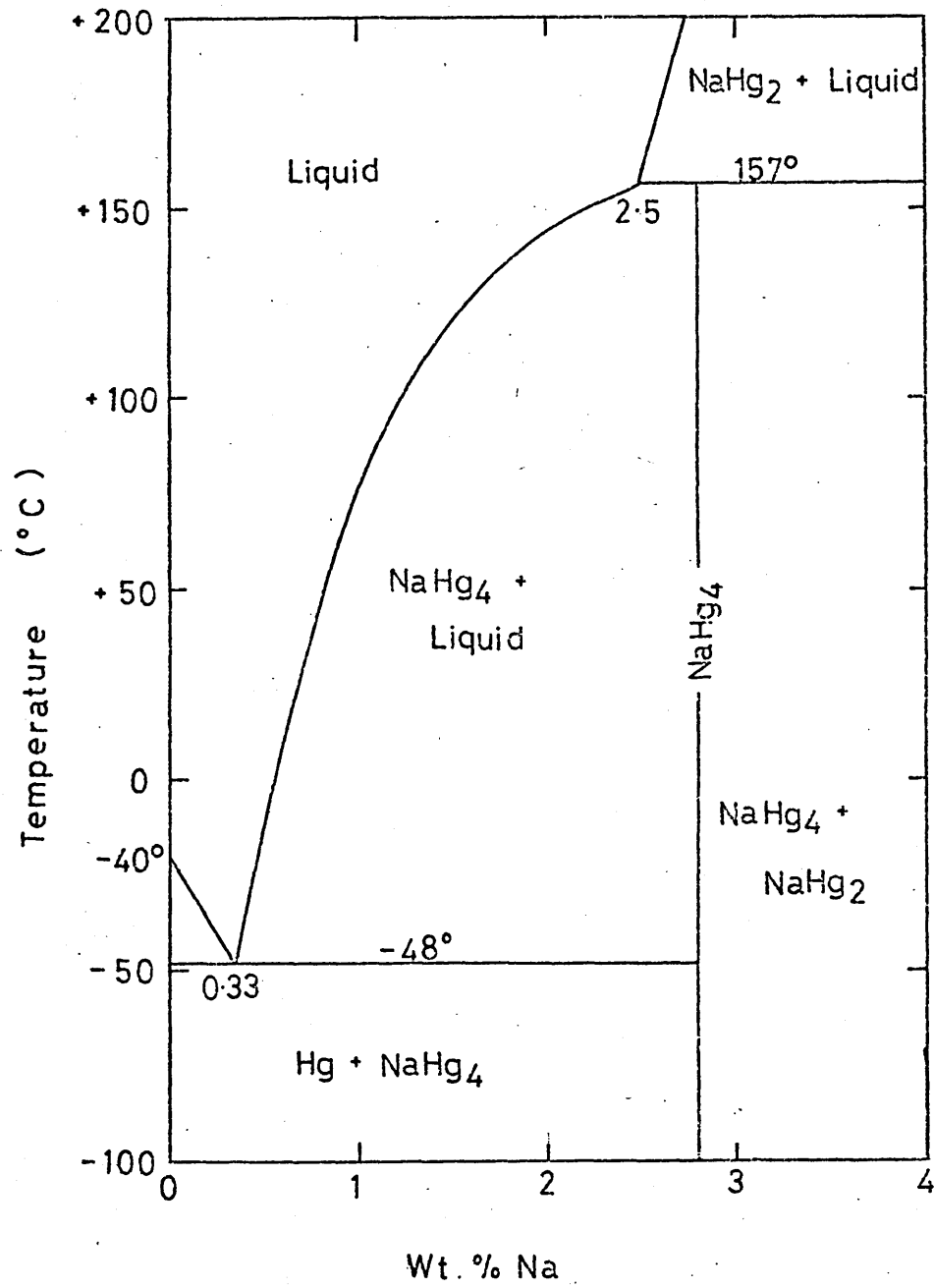
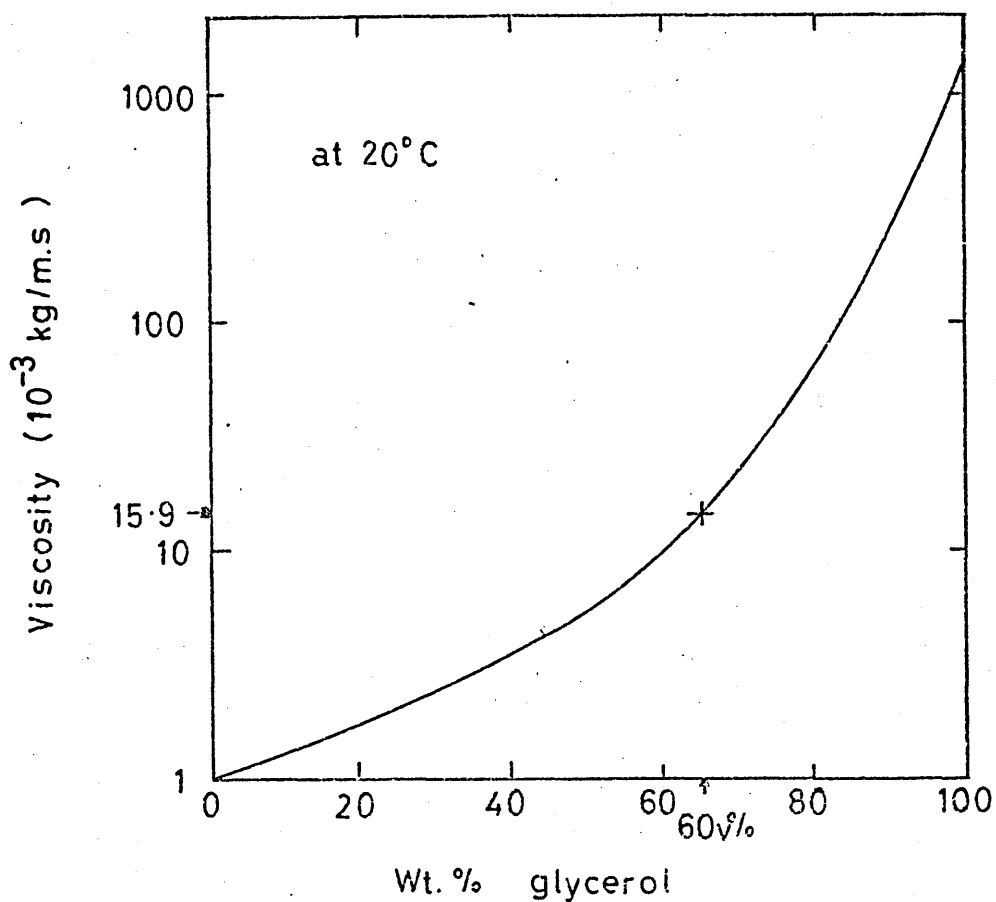


Figure 8

The physical properties of water-glycerol solutions .

(a) Viscosity [145].



(b) Density at 20°C [145,180]

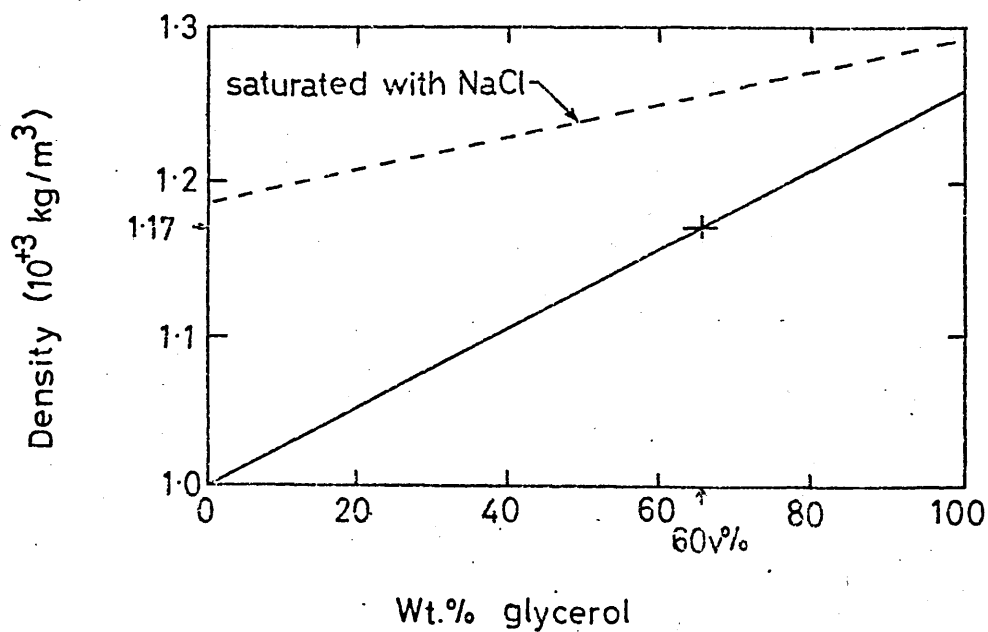
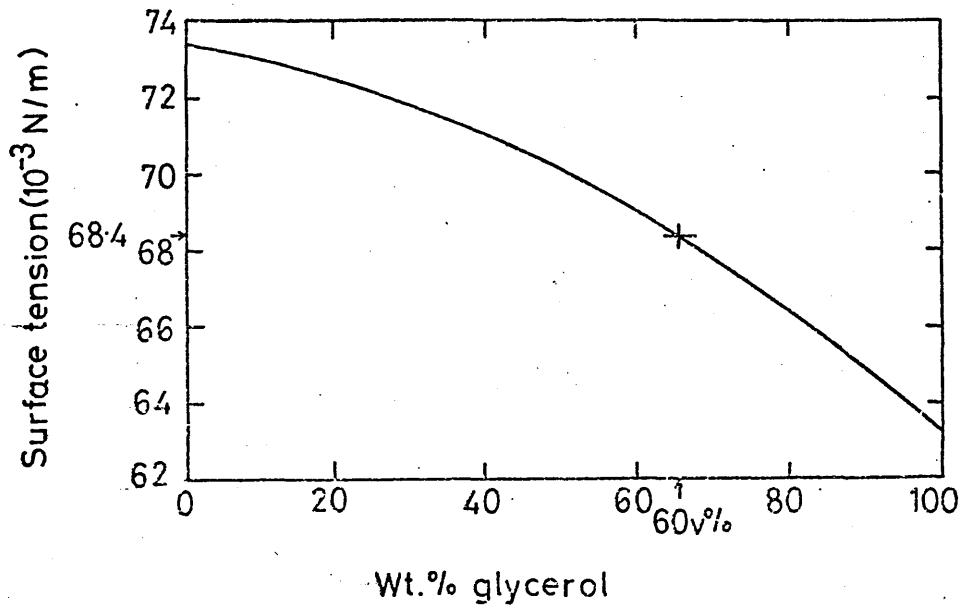


Figure 8.(cont.)

(c) Surface tension [145].



(d) Interfacial energy with mercury [109].

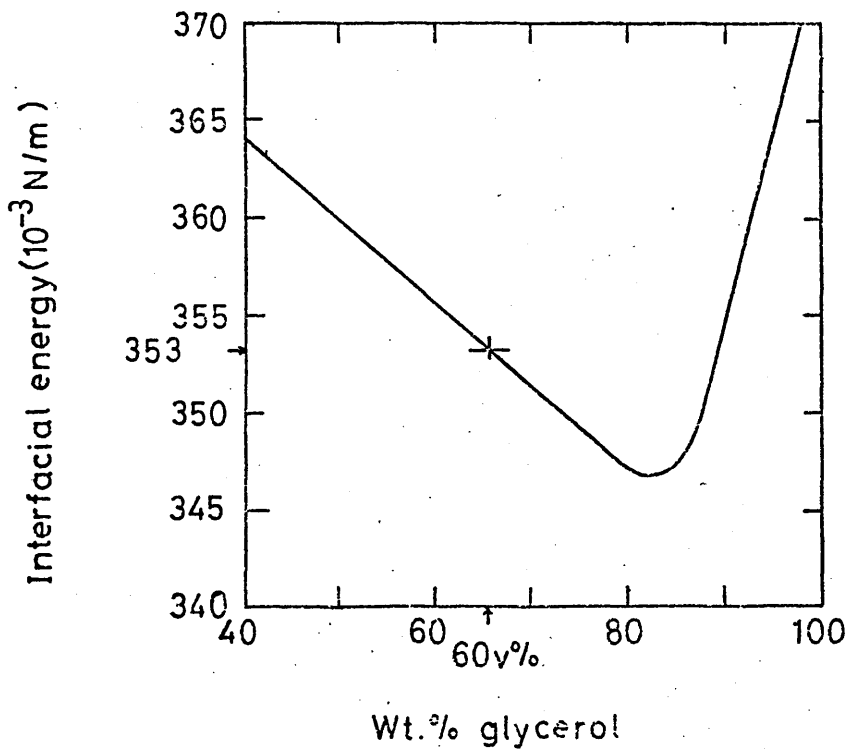
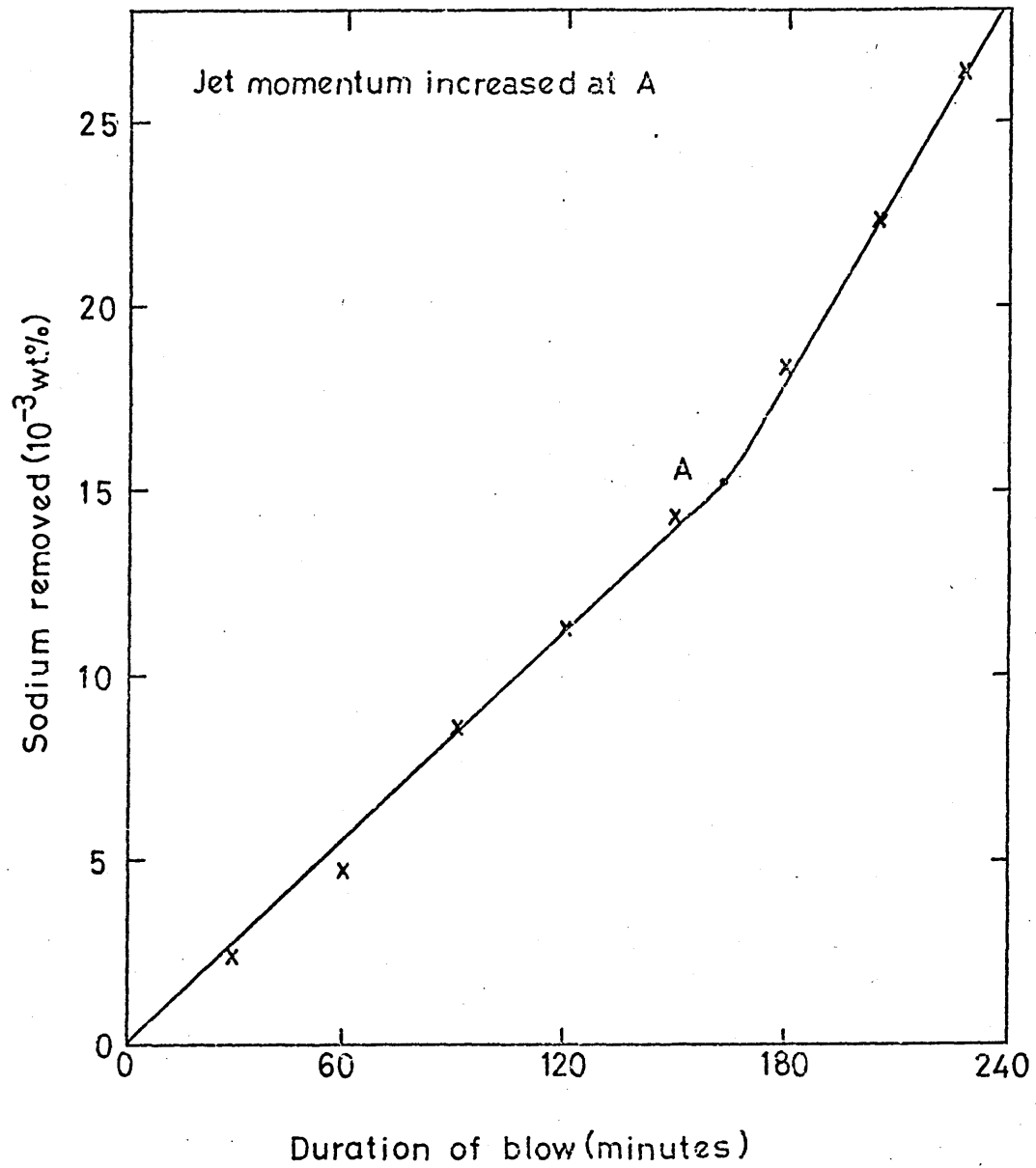


Figure 9

The reaction between sodium amalgam and water
when jetting with nitrogen.



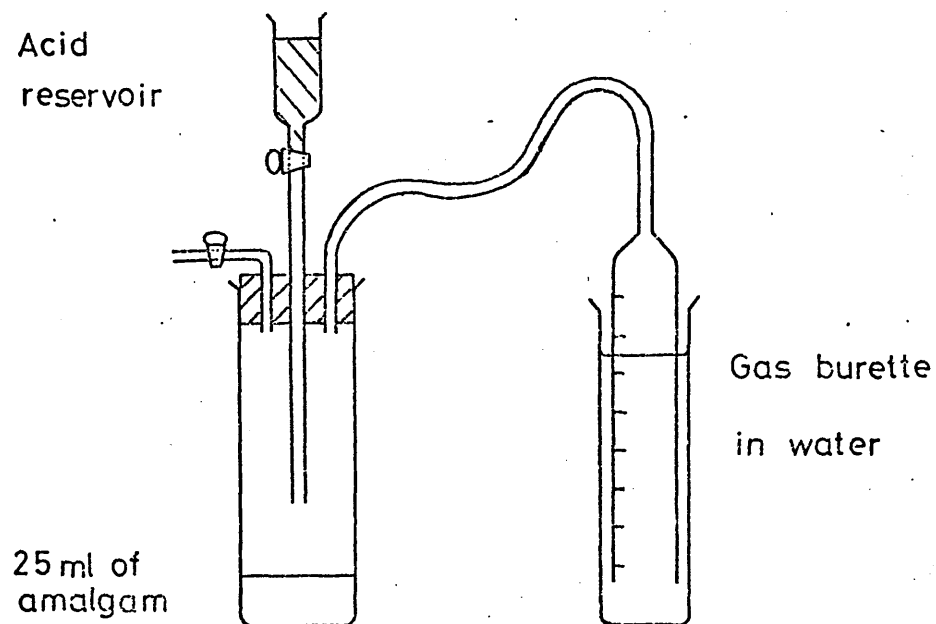
25 ml of water

25 ml of amalgam

$[C_{Na}]_{Hg,I} \equiv 0.6$ wt.%

Figure 10

(a) Apparatus for studying the reaction between a pool of amalgam and an acid.



(b) Apparatus for initial jetting experiments.

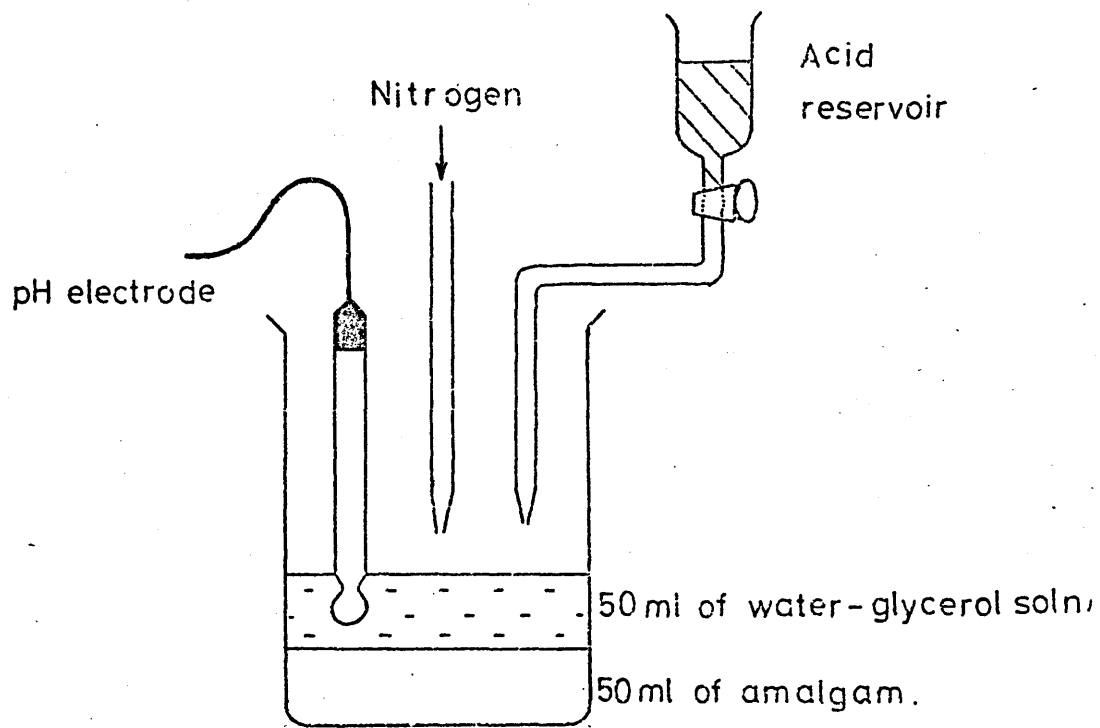


Fig. 11 The reaction between a pool of sodium amalgam and acetic acid solutions.

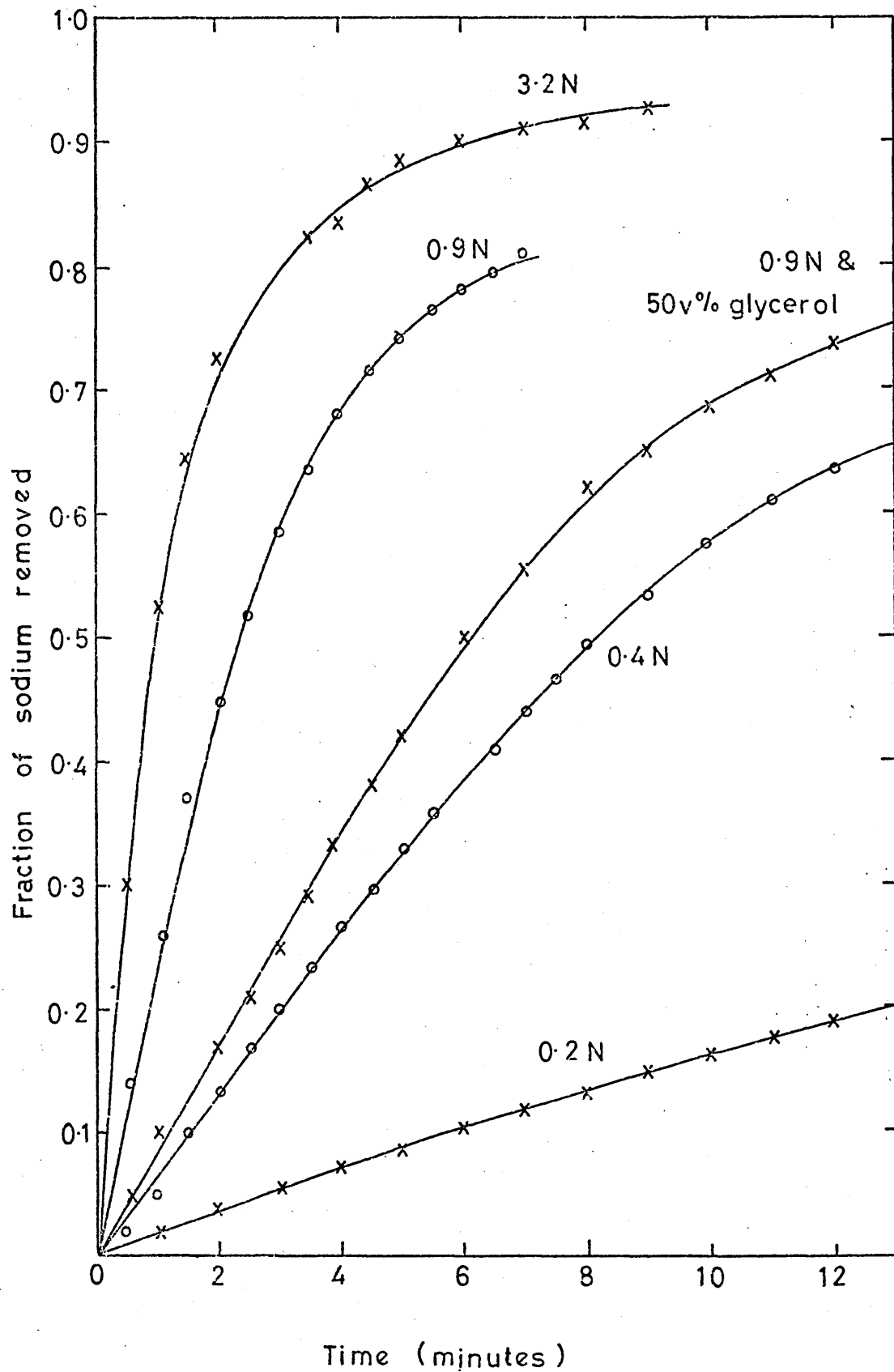


Fig.12 The reaction between a pool of sodium amalgam and various acids.

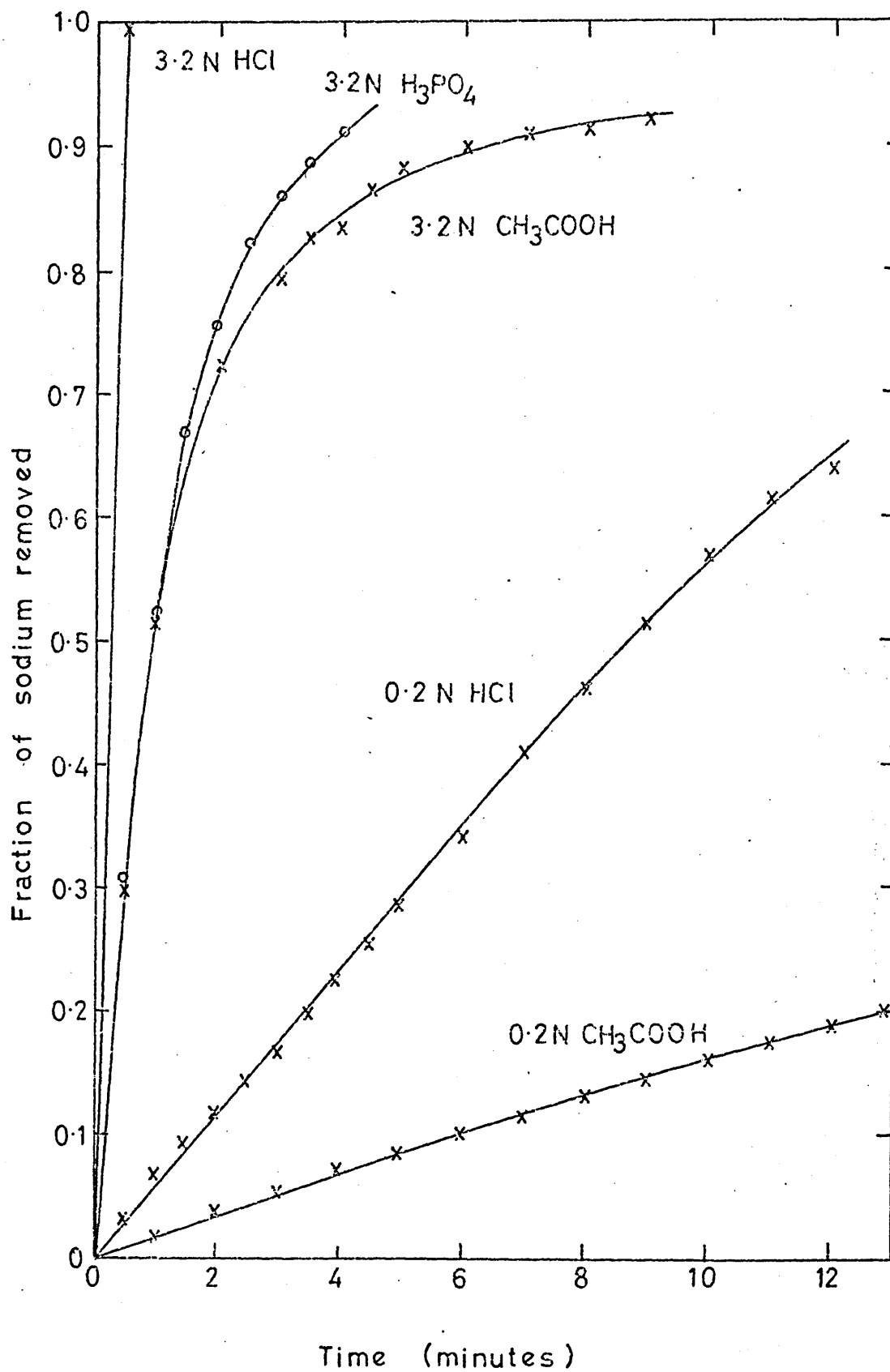
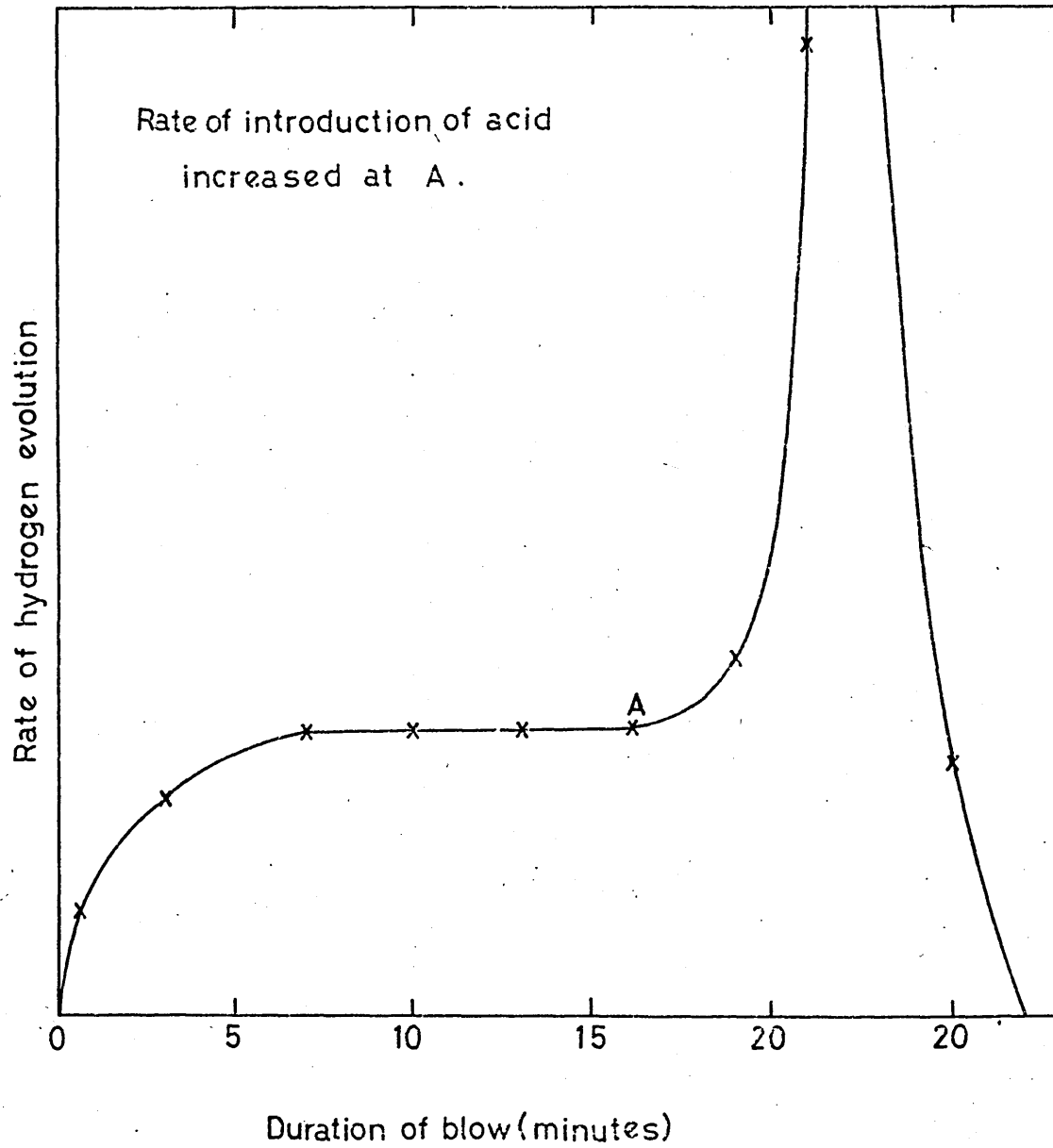


Figure 13

Jetting onto a pool of amalgam & water while
introducing 7.0N ethanoic acid.



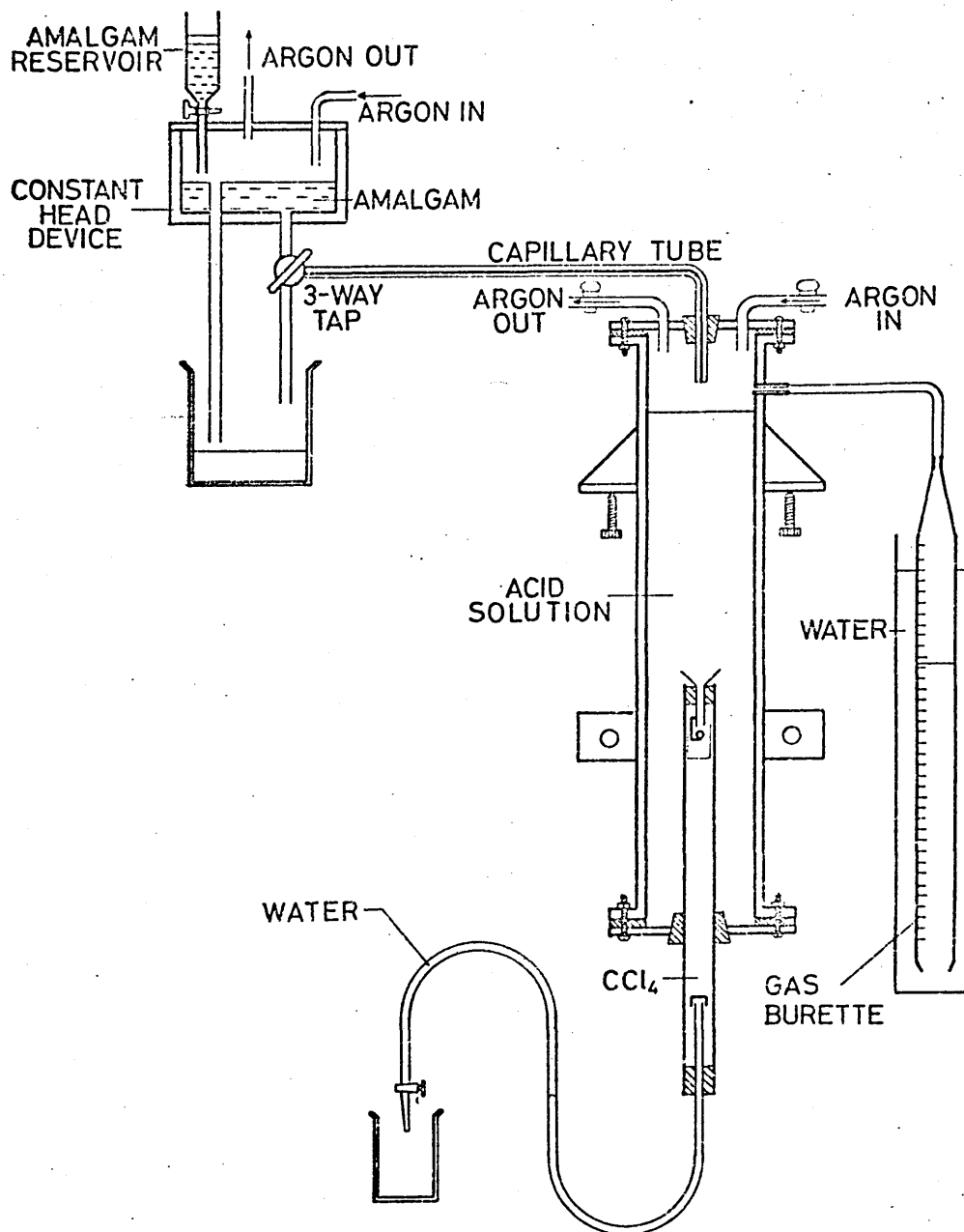
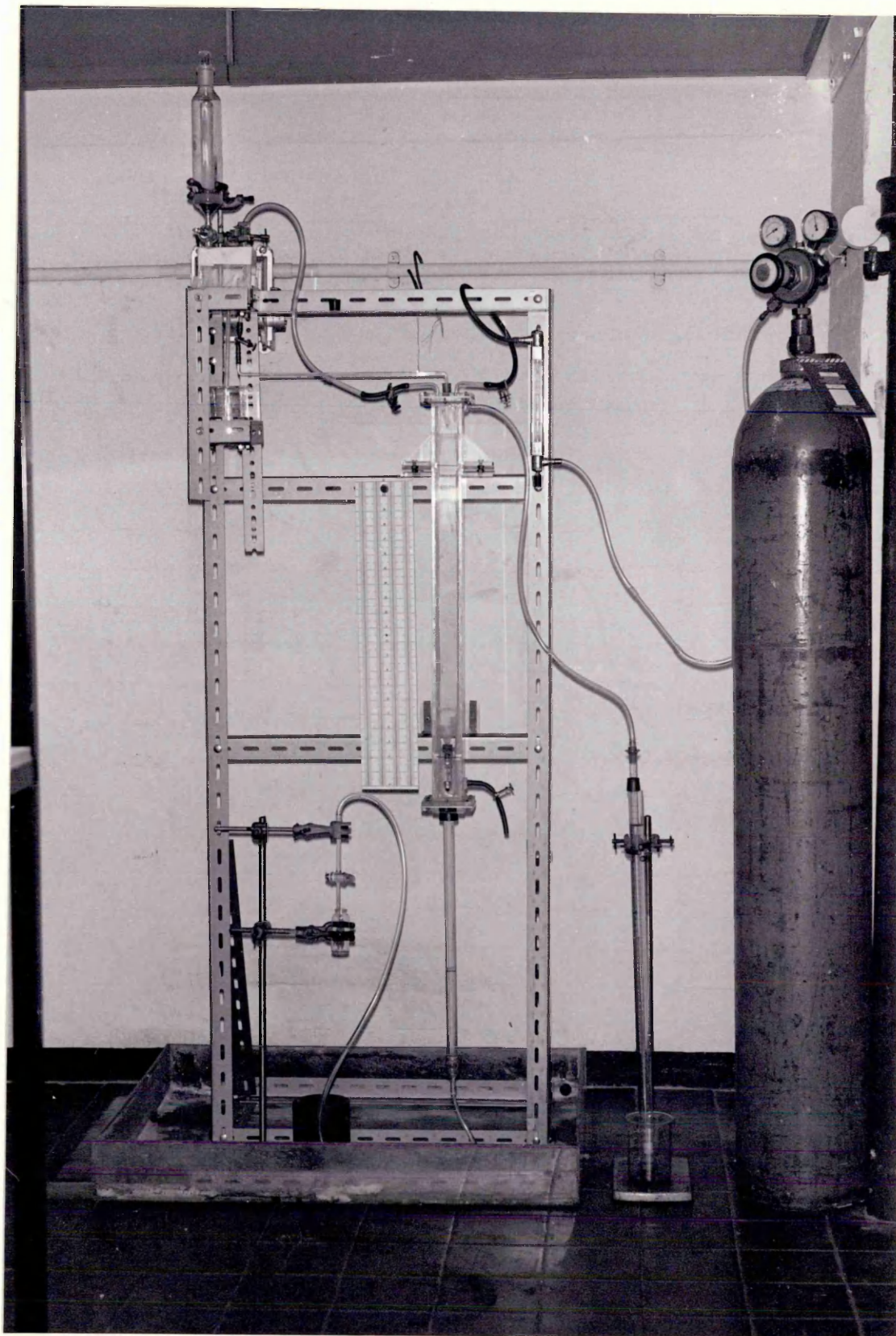


Figure 14 Apparatus for investigating the behaviour of single amalgam droplets.

PLATE 1

A general view of the apparatus used to investigate the behaviour of single amalgam droplets during free fall through acidified aqueous solutions.



Vertical section assembly

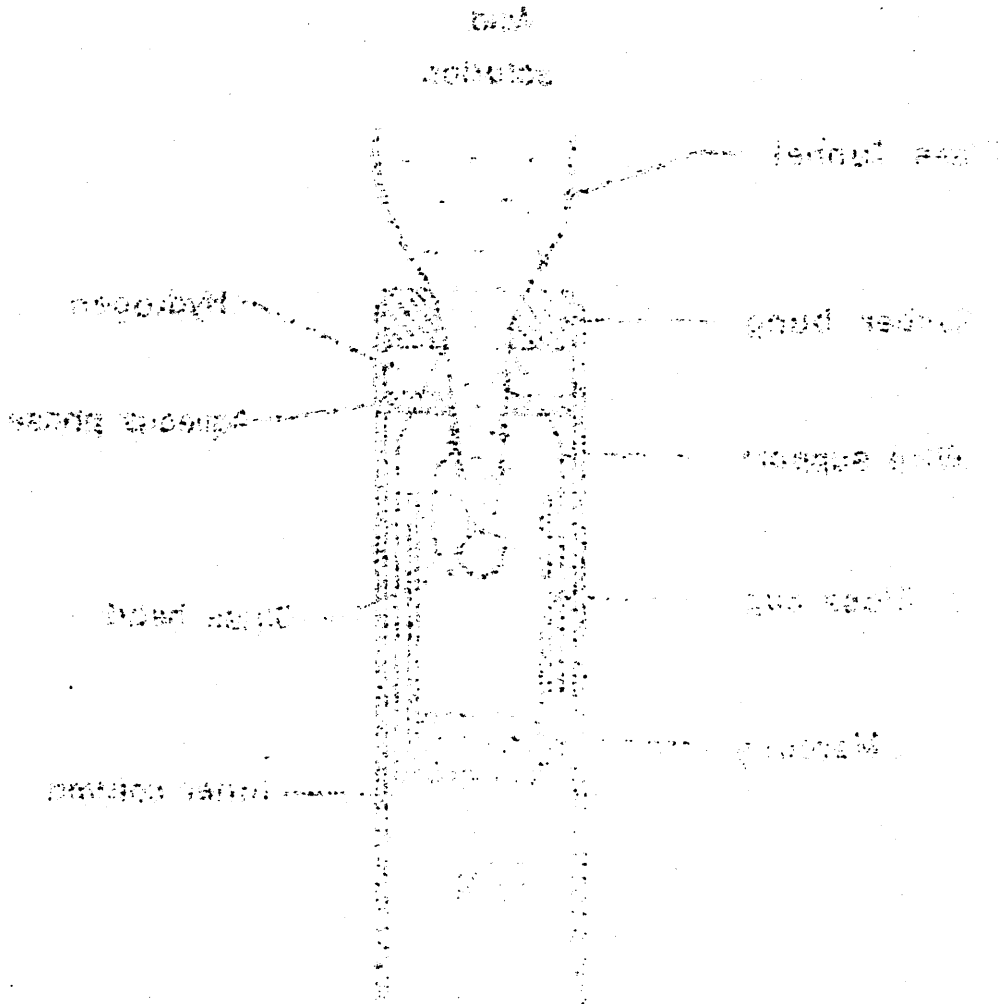


Figure 15

Droplet collection assembly.

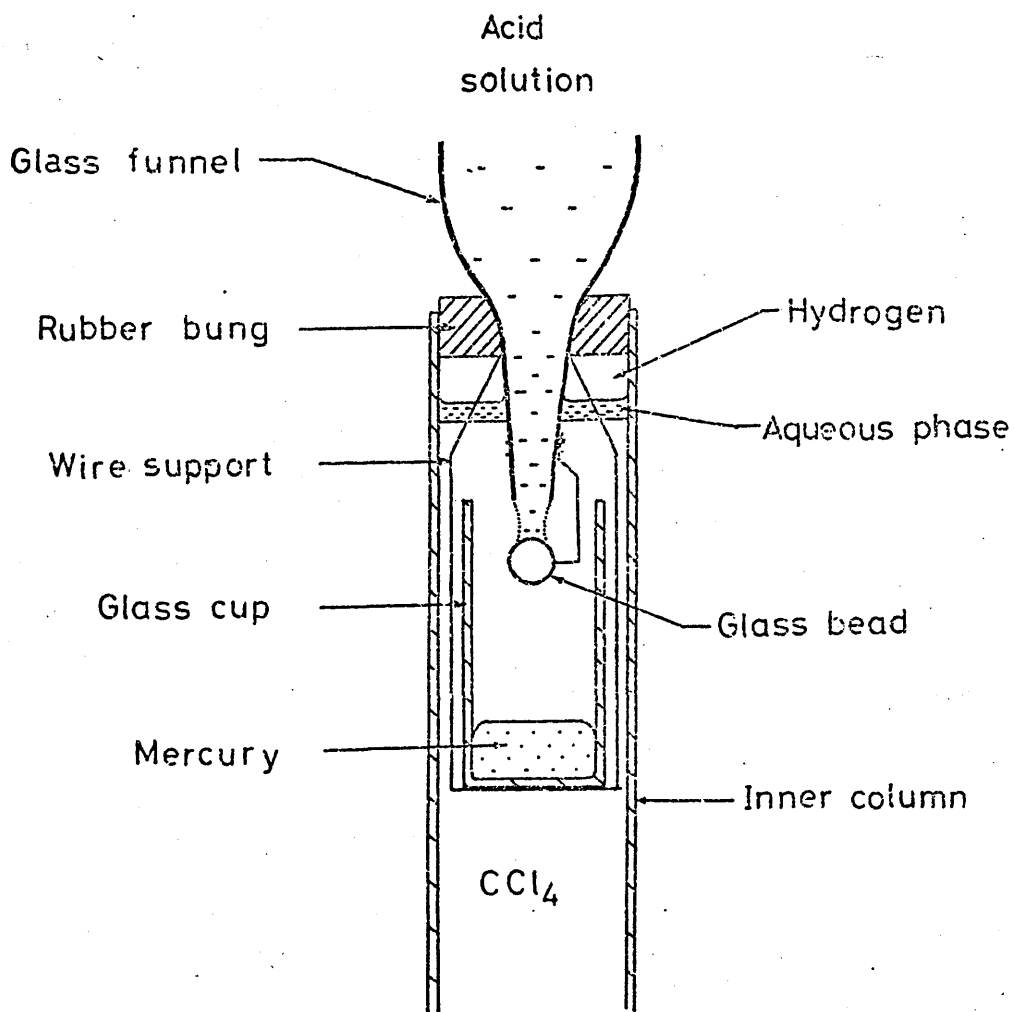


PLATE 2

A single amalgam droplet entering the droplet
collection assembly.

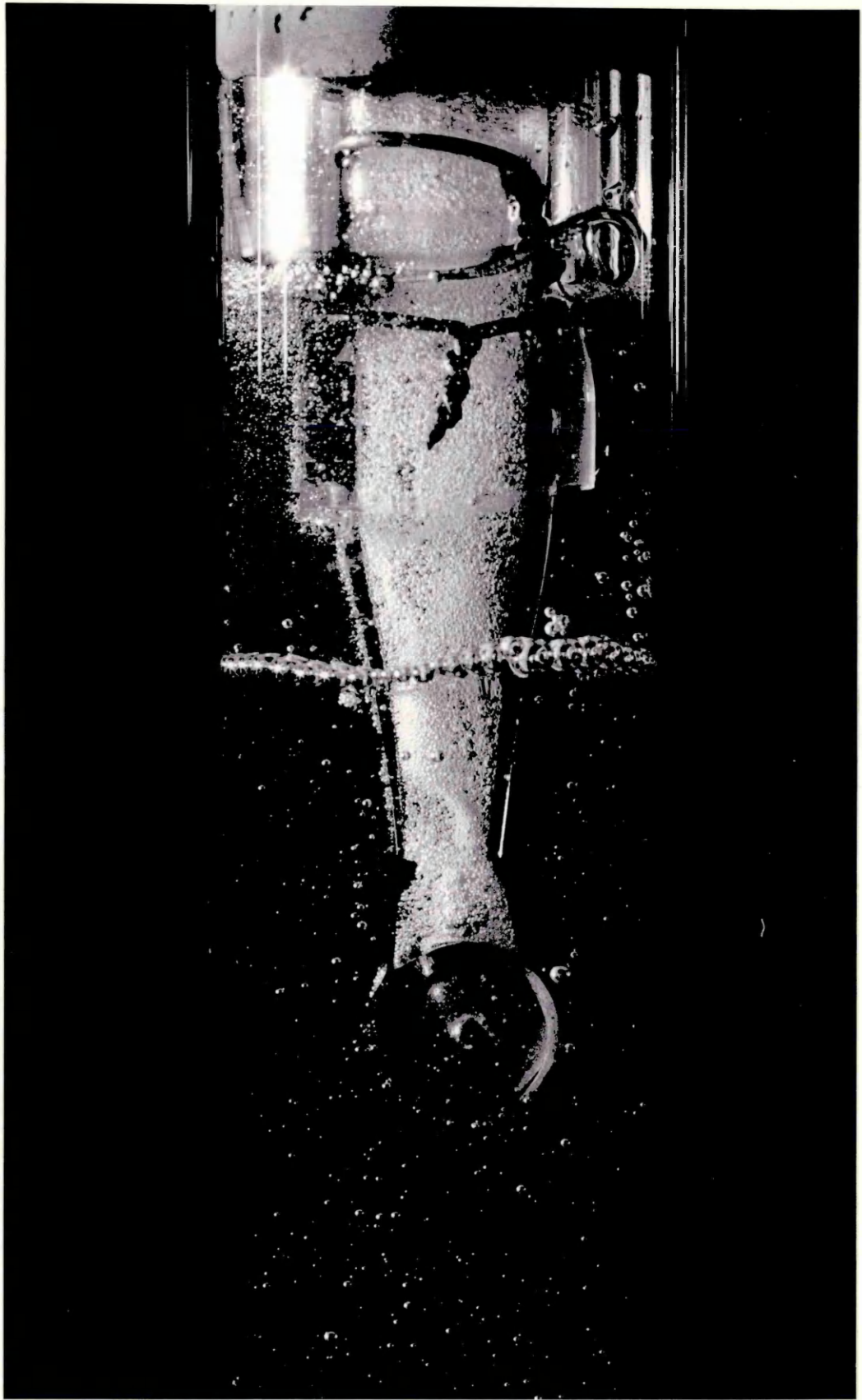


PLATE 4

A droplet of amalgam, of approximately 2 mm diameter and containing initially about 0.5 wt. % Na, during free fall through 1.1 N HCl water-glycerol solution. Note the irregularities in the stream of bubbles left by the reacting droplet.

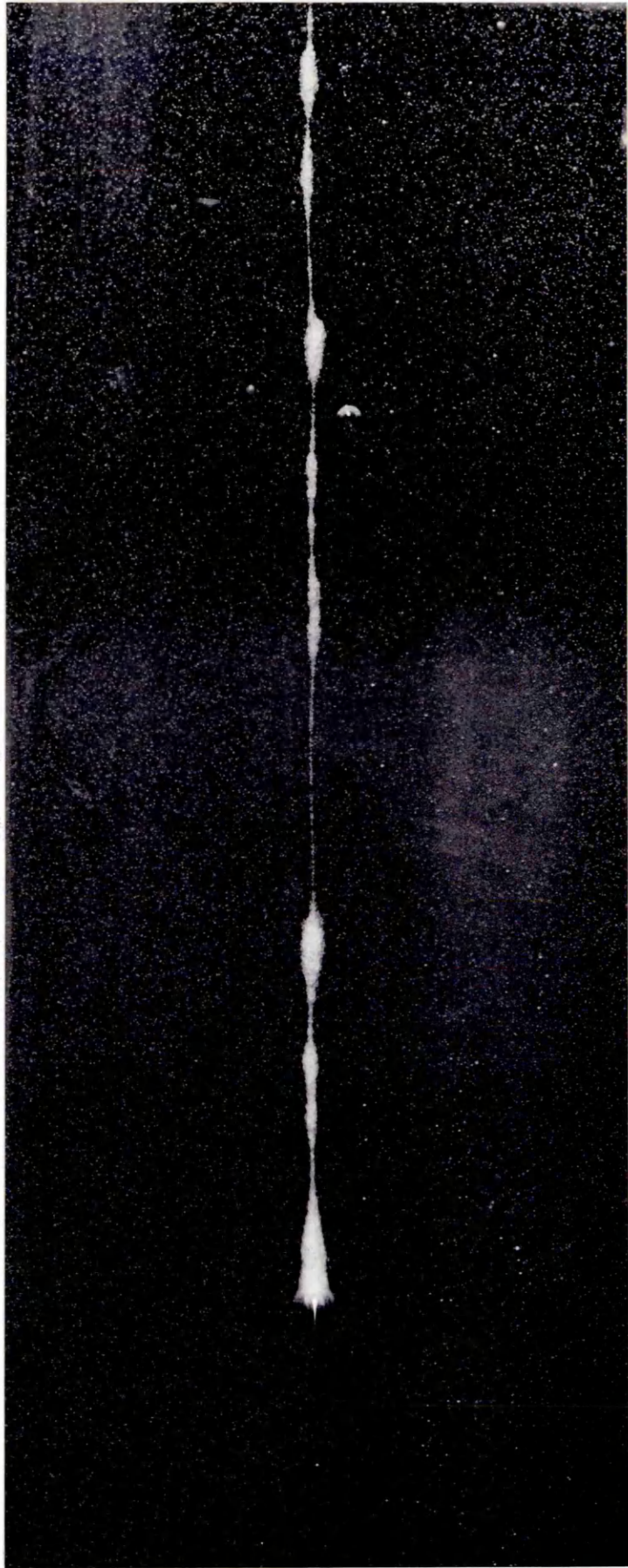


PLATE 3

A general view of the mass transfer column showing a droplet of amalgam, of approximately 2 mm diameter and containing about 0.5 wt. % Na, during free fall through 1.1N HCl, water-glycerol solution.

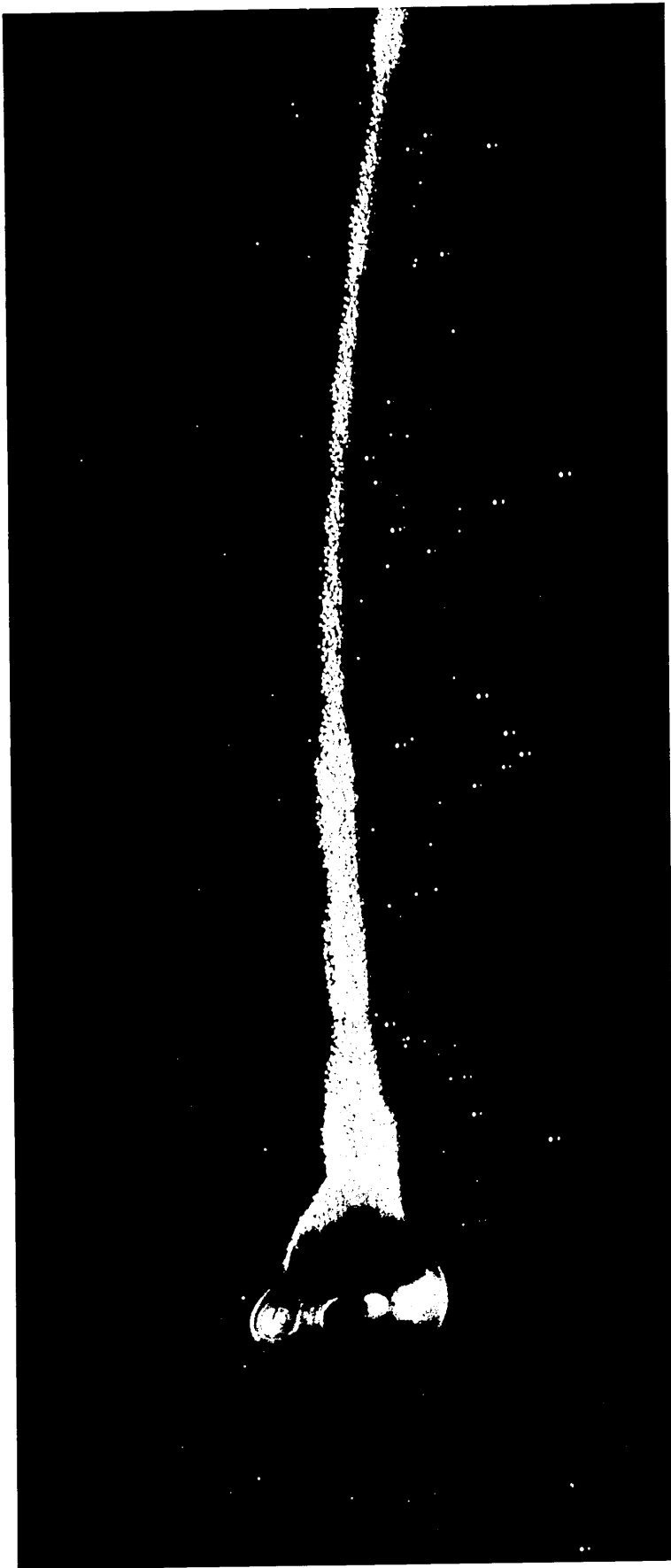


PLATE 5

An amalgam droplet, initially containing 0.55 wt. % Na, during free fall through 0.5 N HCl, water-glycerol solution.

15 x actual size

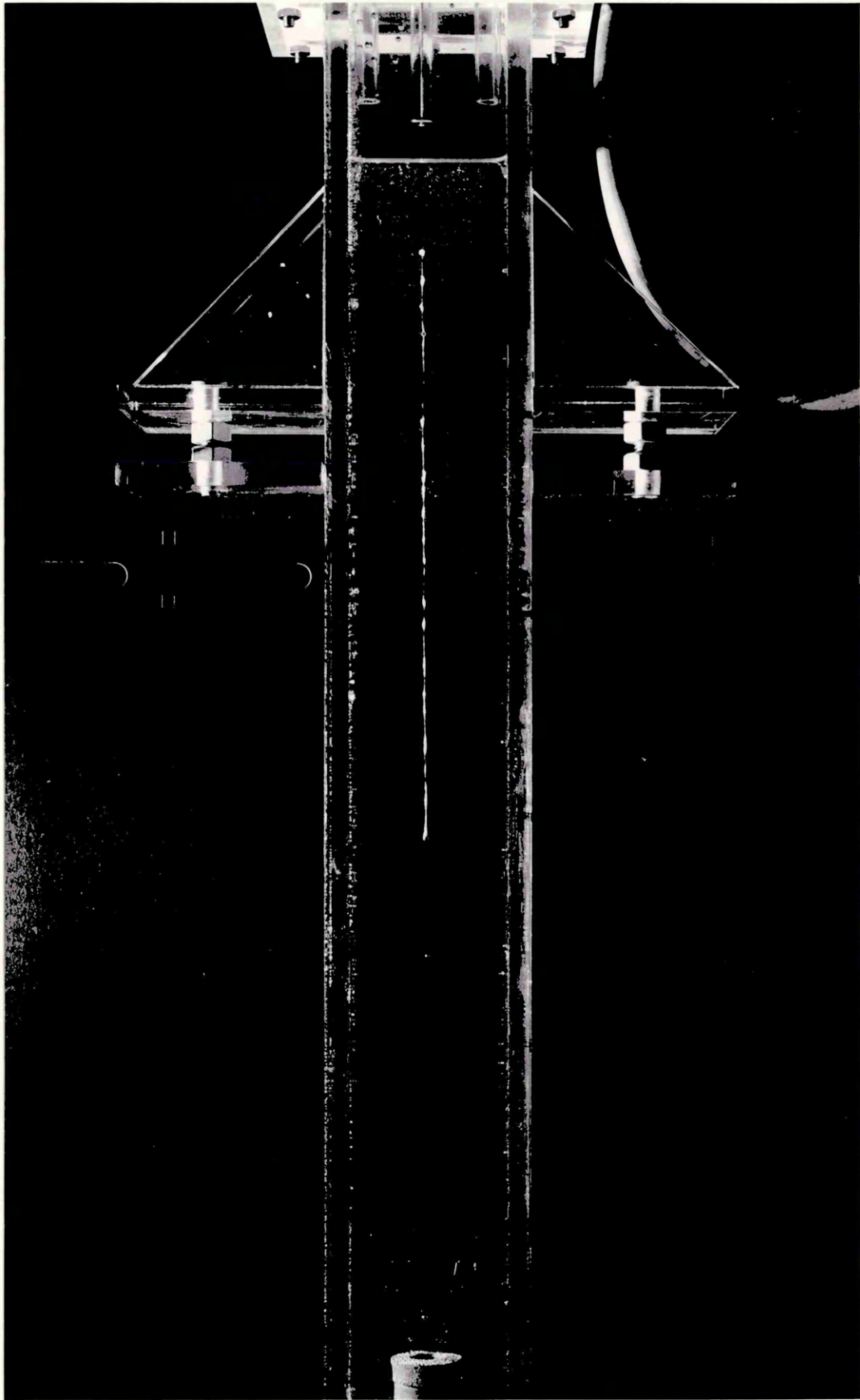


PLATE 6

An amalgam droplet, initially containing 0.55 wt.% Na,
during free fall through 1.1 N HCl, water-glycerol solution.

15 x actual size

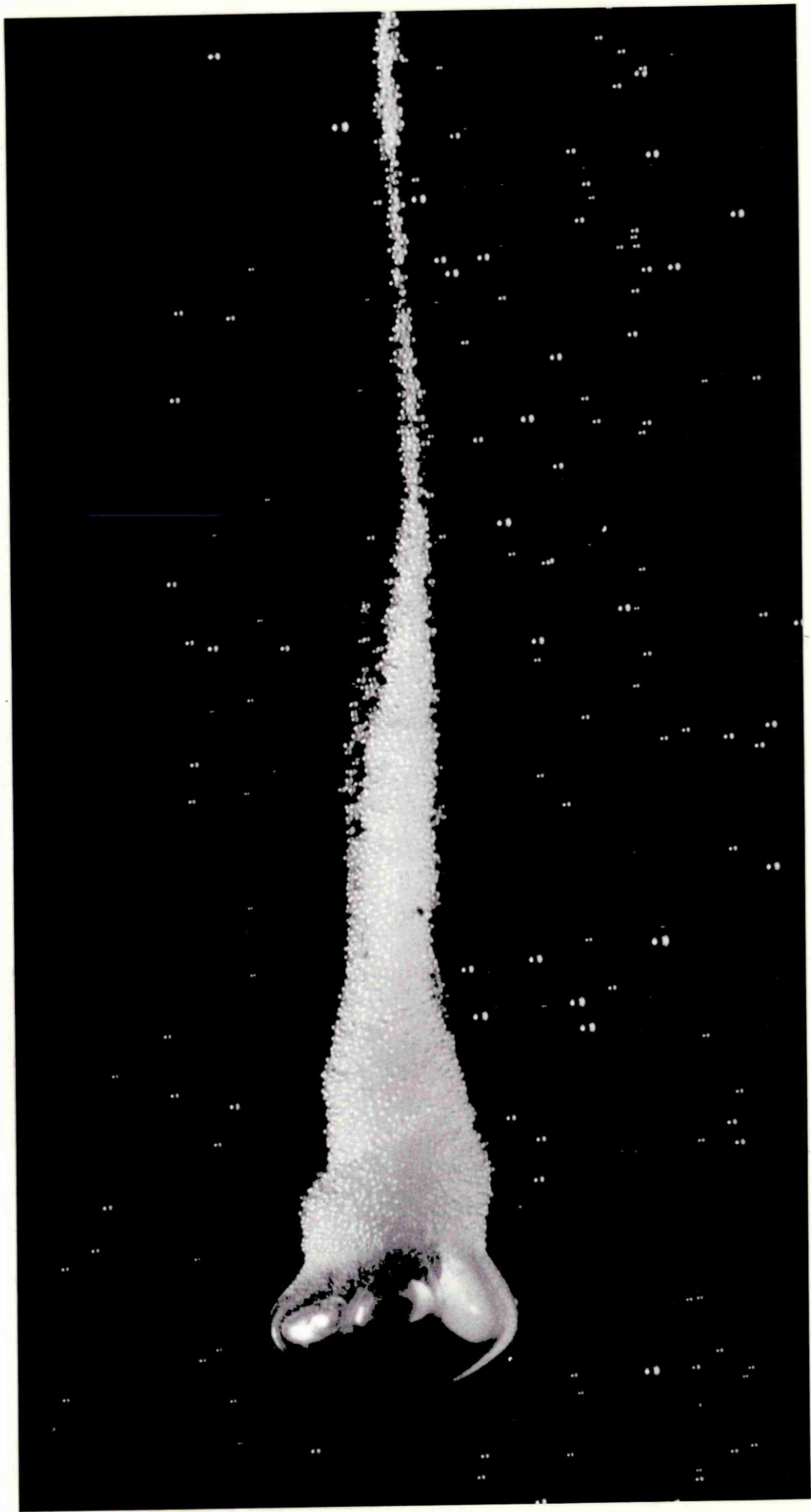


PLATE 7

An amalgam droplet, initially containing
0.55 wt. % Na, during free fall through 1.5 N HCl, water-
glycerol solution.

15 x actual size

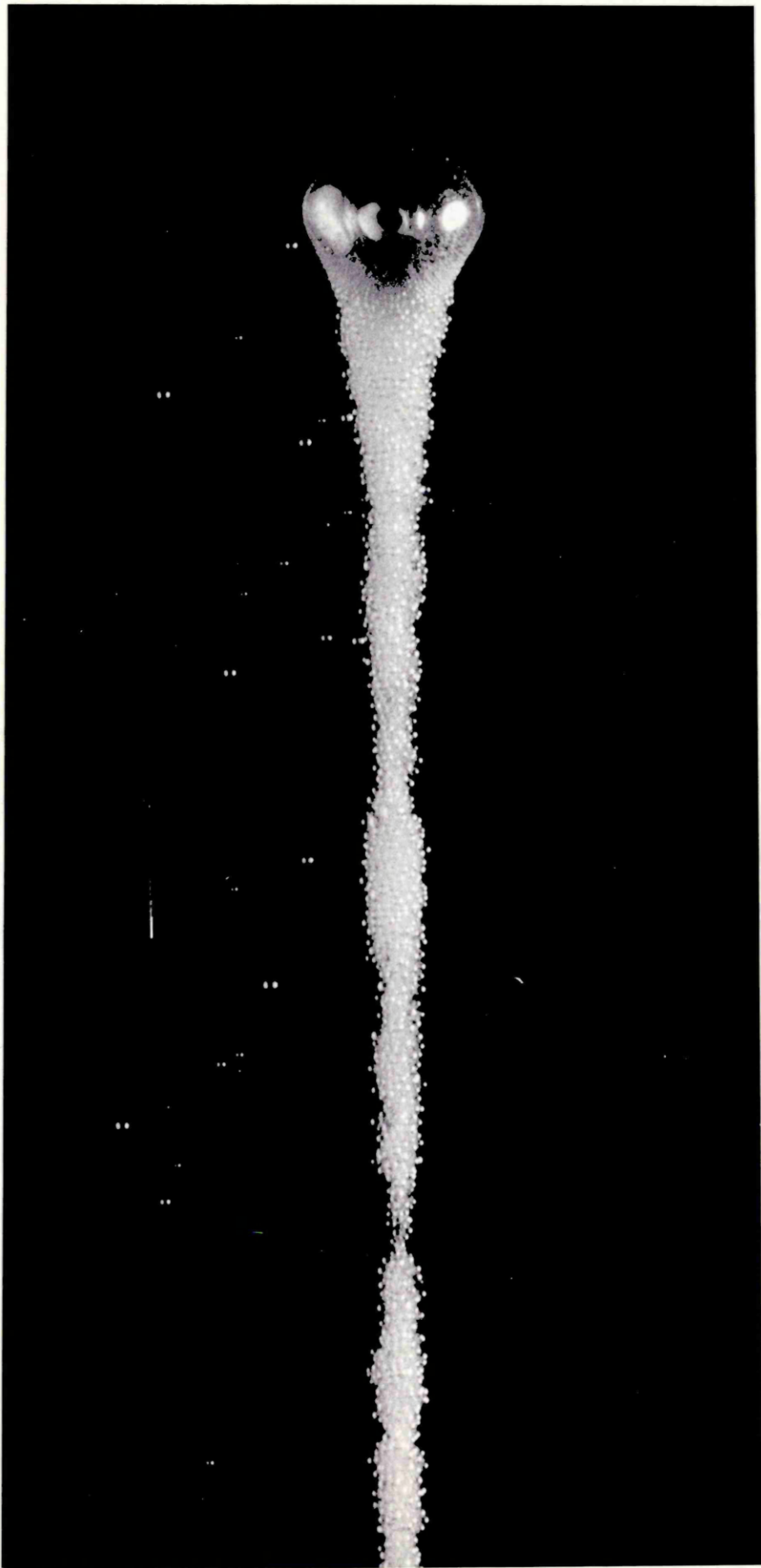
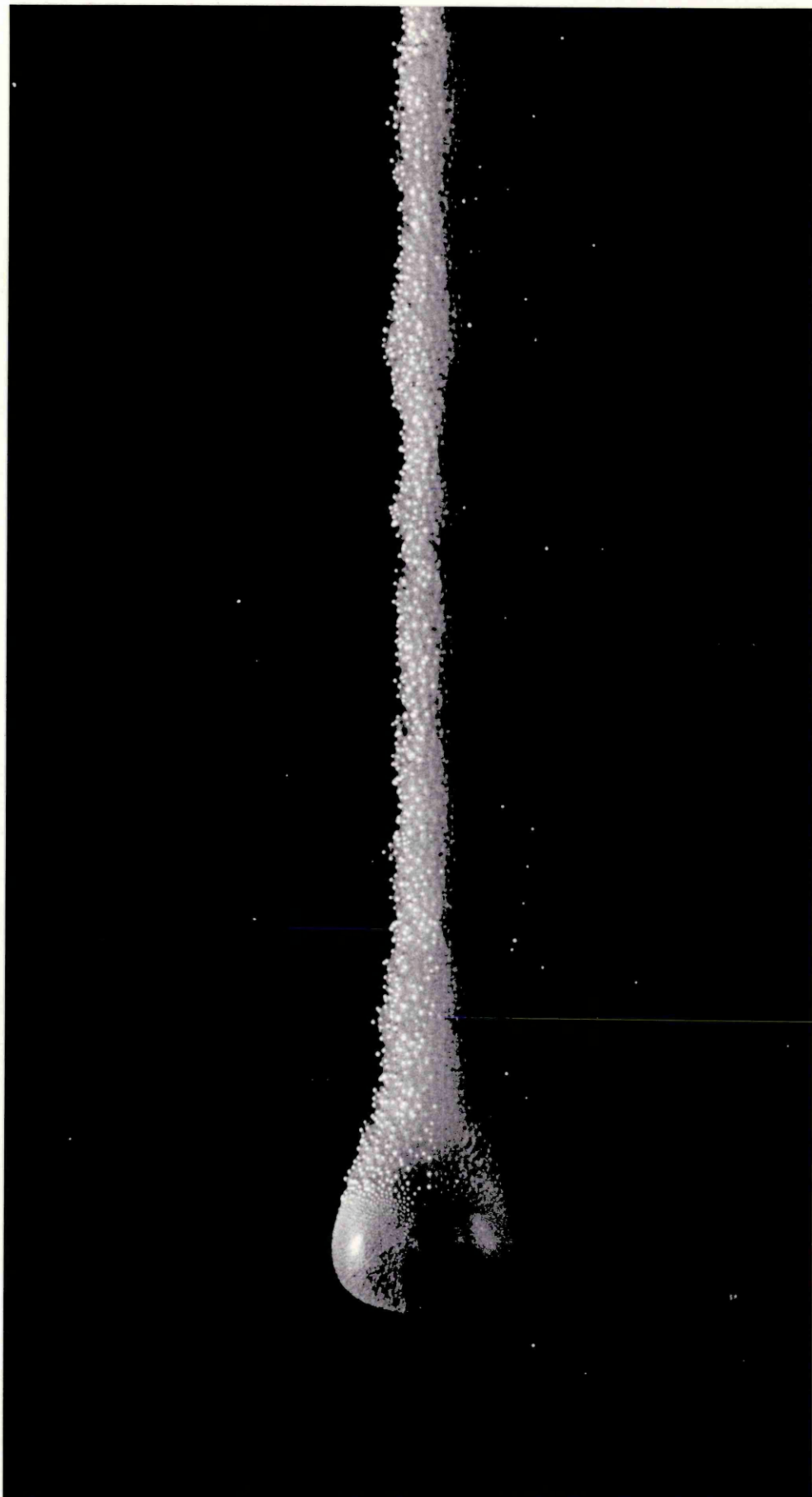


PLATE 8

An amalgam droplet, initially containing
0.55 wt. % Na, during free fall through 2.1 N HCl water-
glycerol solution.

15 x actual size



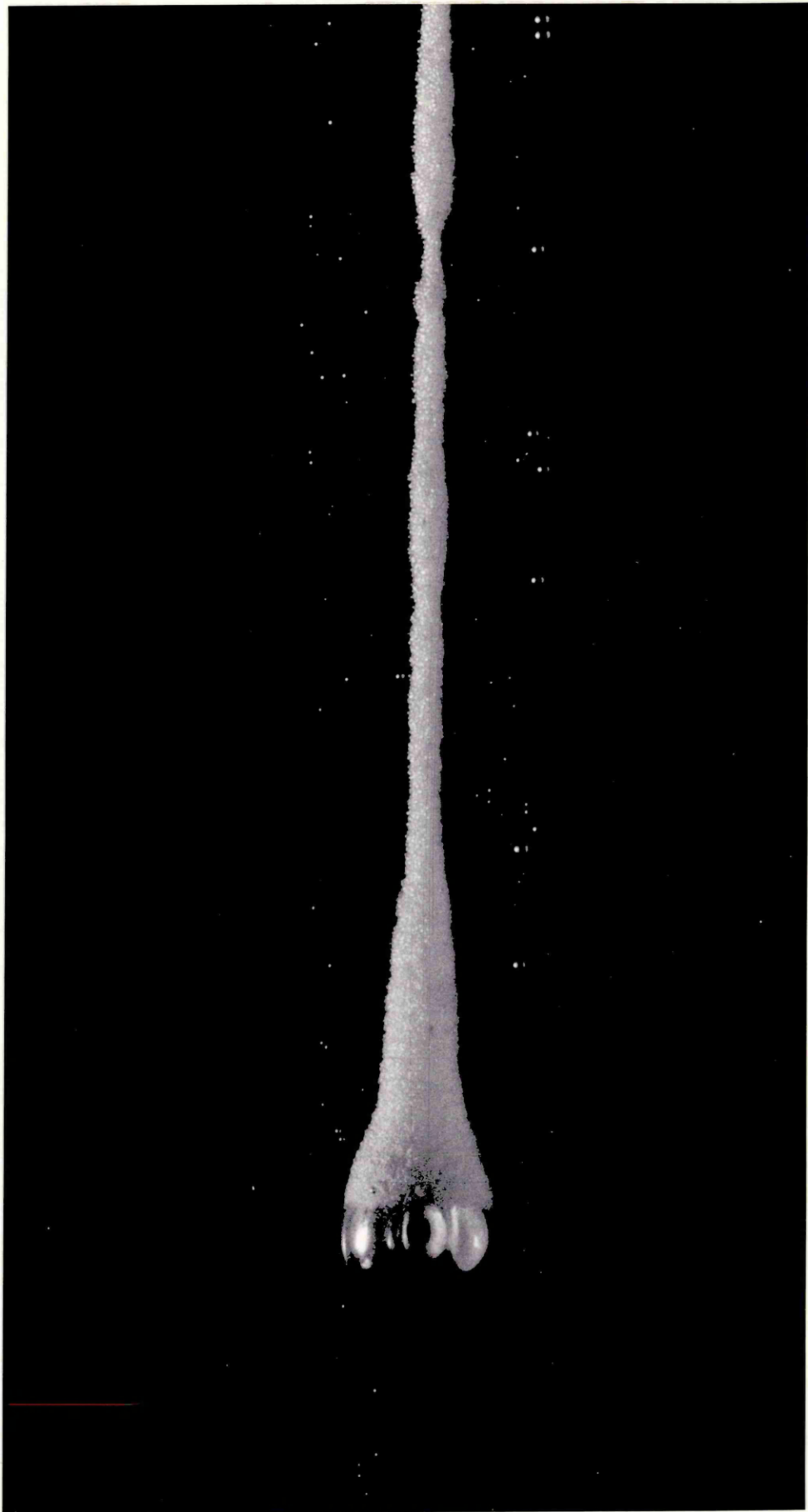


PLATE 9

An amalgam droplet, initially containing
0.55 wt. % Na, during free fall through 1.0 N HCl, water-
glycerol solution containing 1.0 mole of NaCl per litre.

15 x actual size

PLATE 10

An amalgam droplet, initially containing about 0.55 wt. % Na, during free fall through 1.5 N HCl, water-glycerol solution containing 2.0 moles of NaCl per litre.

15 x actual size

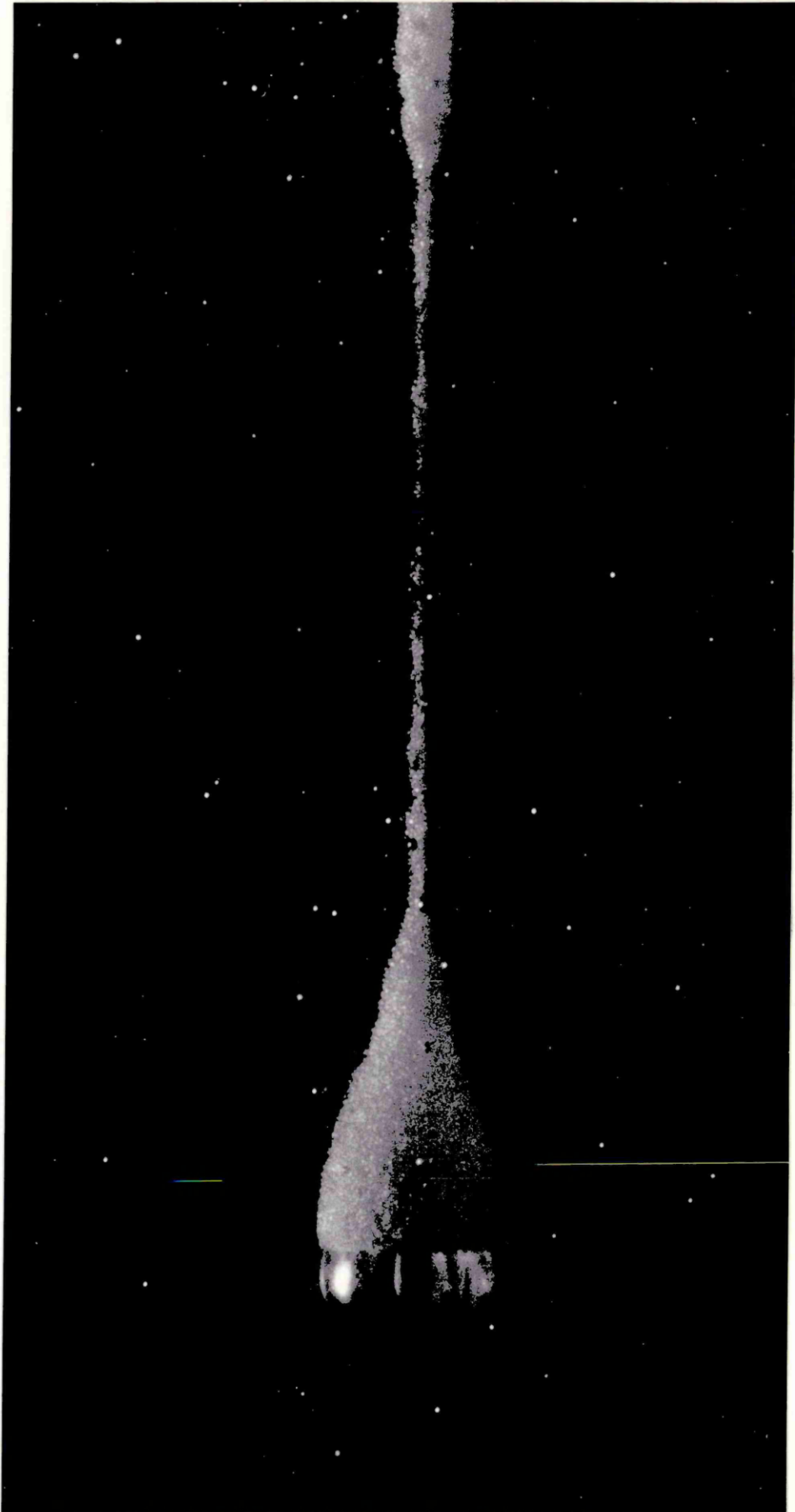


PLATE 11

An amalgam droplet, initially containing
0.34 wt. % Na, during free fall through 1.1 N HCl, water-
glycerol solution.

15 x actual size.

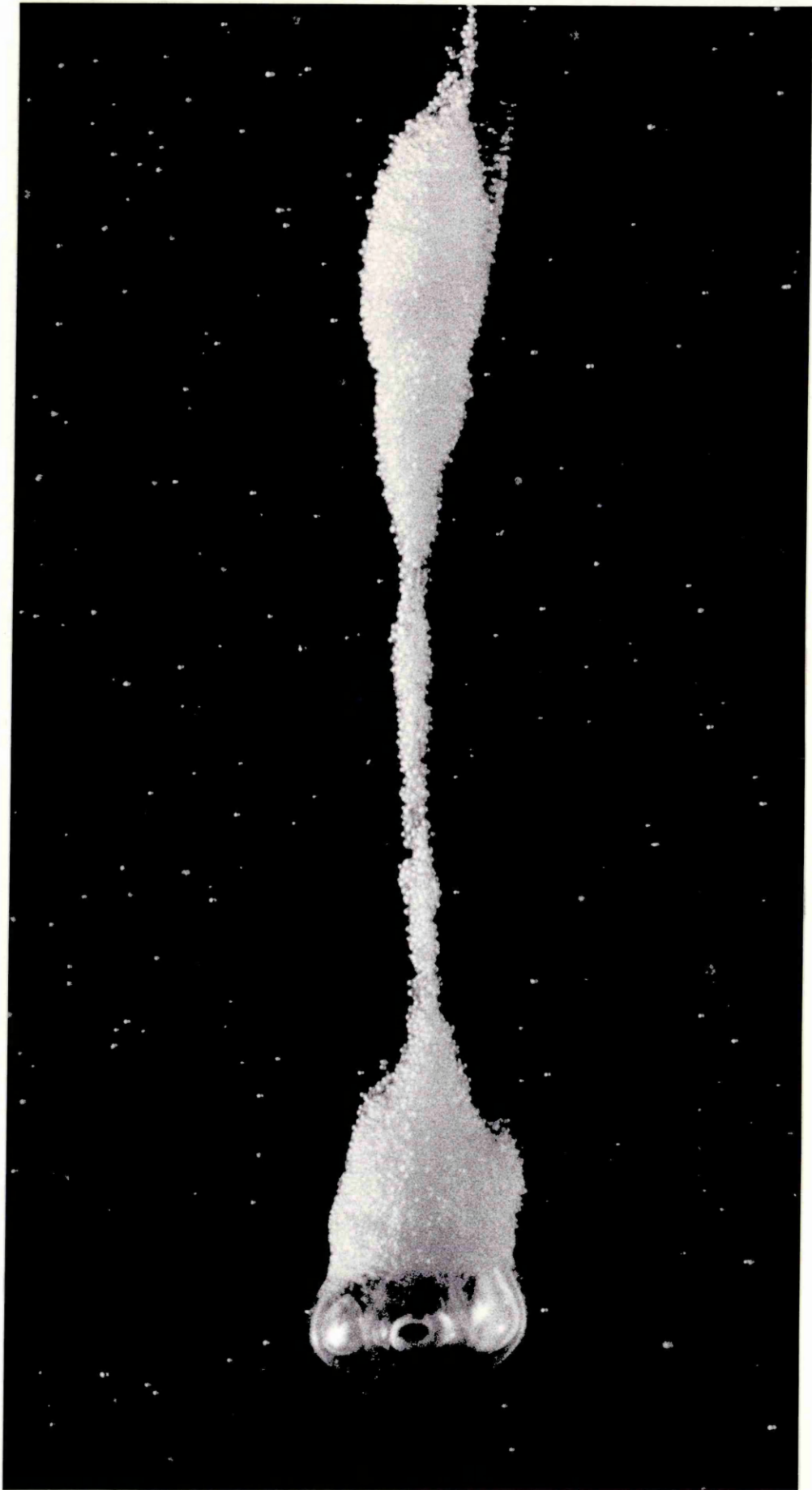


PLATE 12

An amalgam droplet, initially containing
0.06 wt. % Na, during free fall through 1:1 HCl, water-
glycerol solution.

15 x actual size

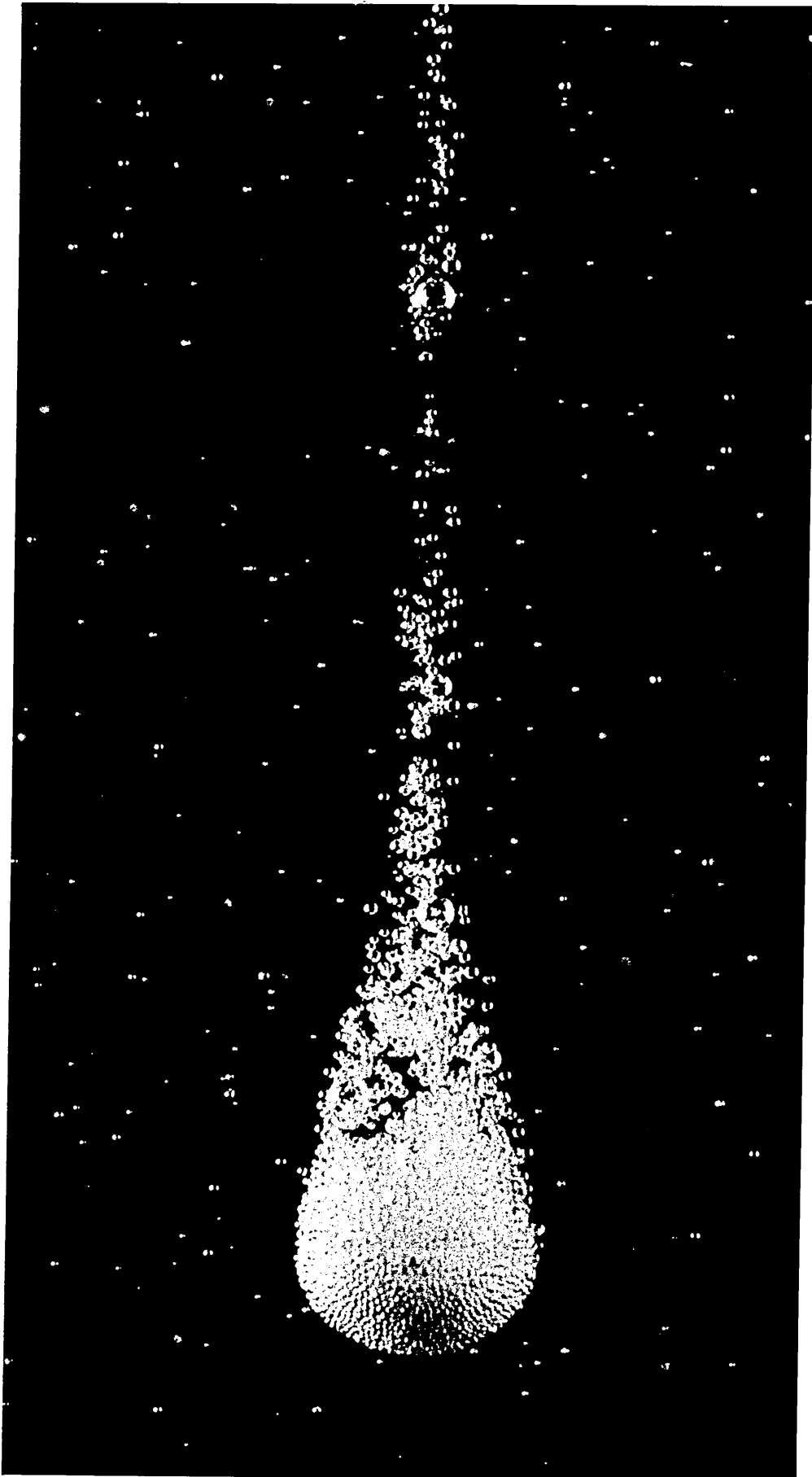
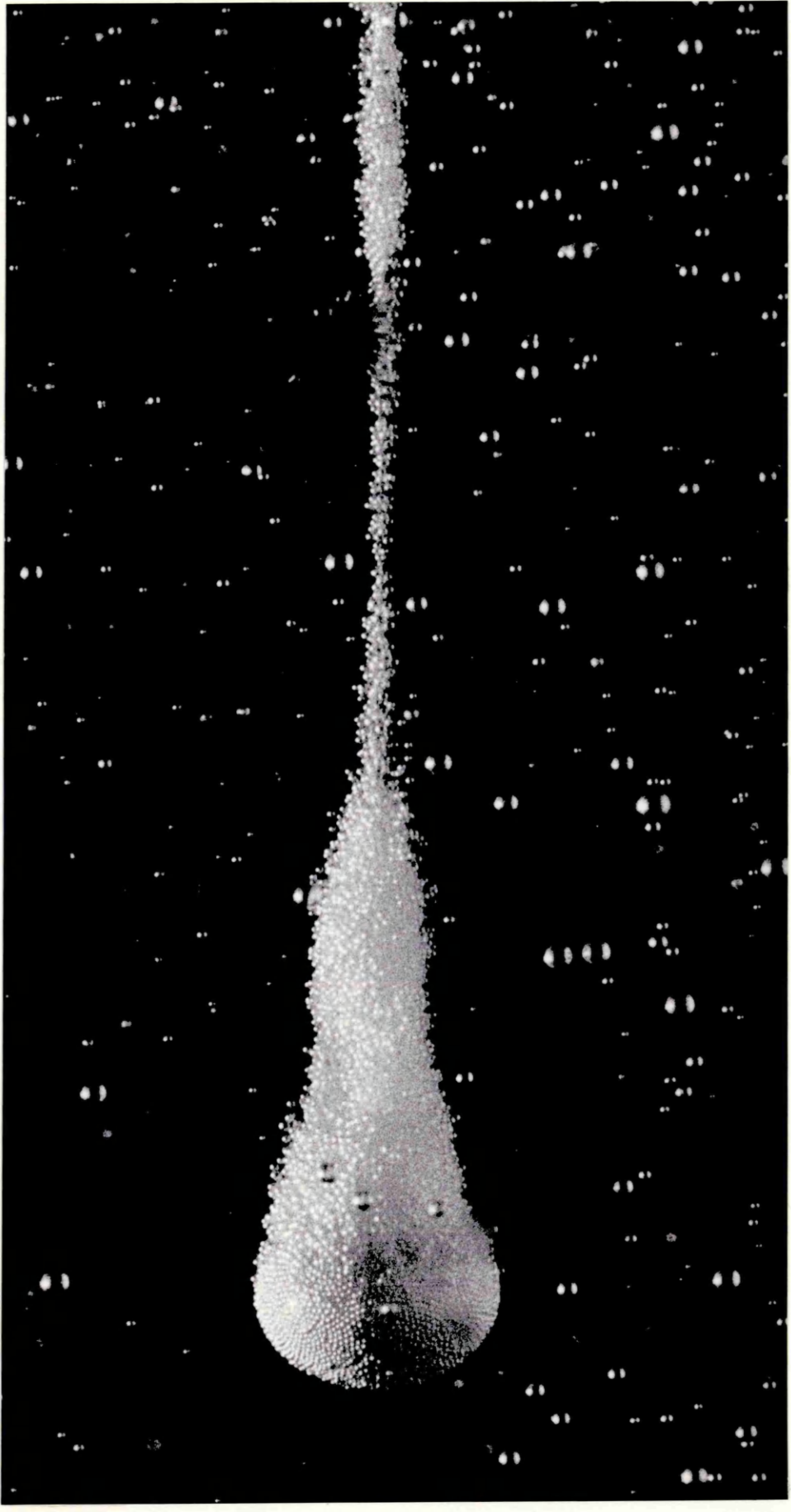


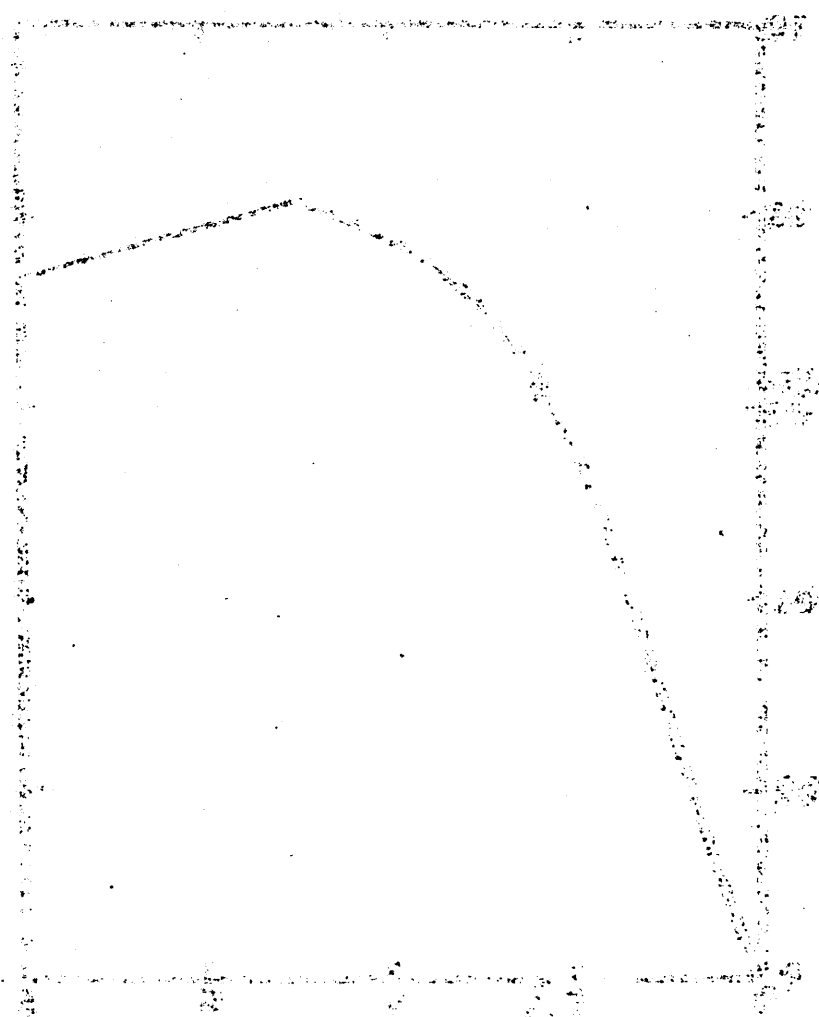
PLATE 13

An amalgam droplet, initially containing
0.18 wt. % Na, during free fall through 2.0 N HCl water
glycerol solution.

15 x actual size



The following table shows the results of the tests conducted on the various specimens of the material under consideration.

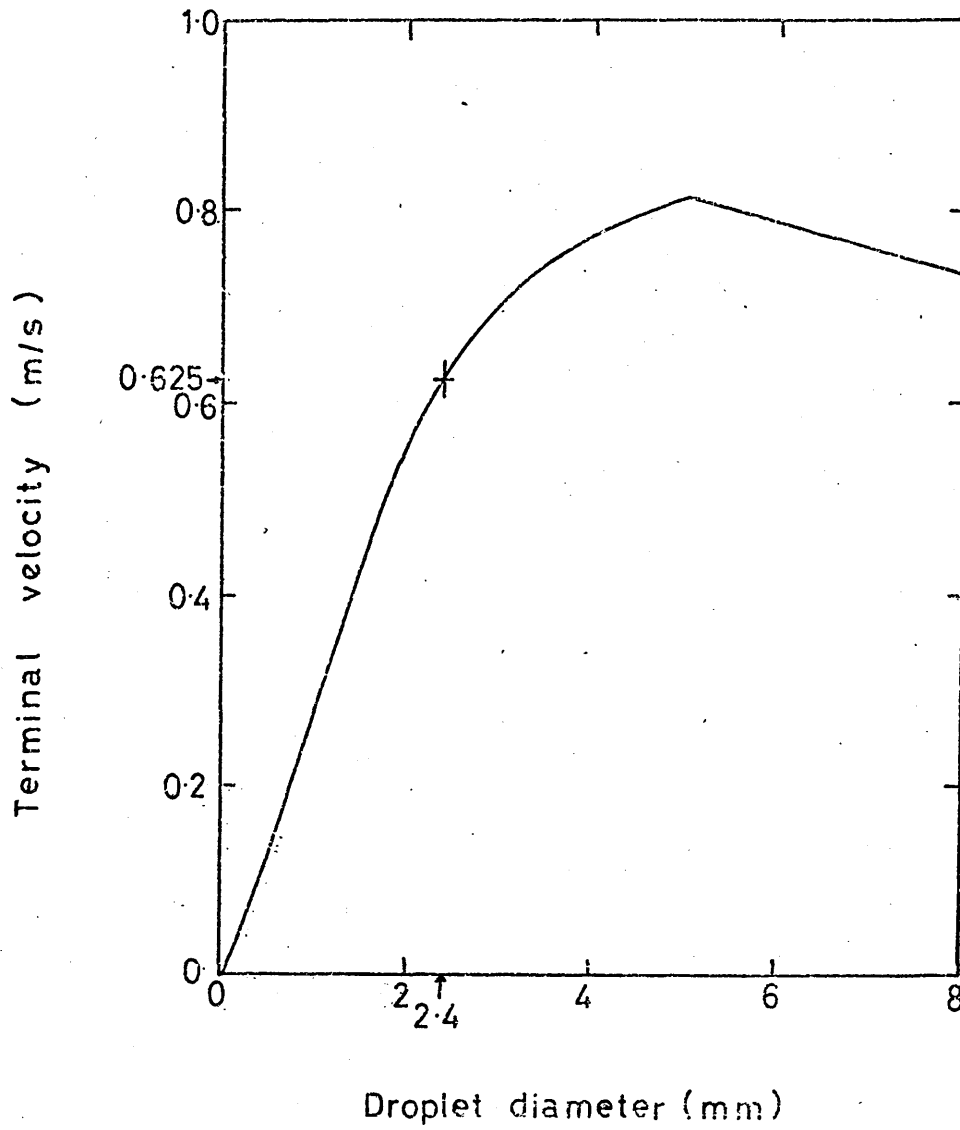


Strength vs. Time

Graph showing the results of the tests.

Figure 16

The terminal velocity of amalgam droplets in 60v% glycerol-water solution, from the Hu Kintner relationship.



Year	Month	Day	Time	Location	Remarks
1941	Jan	1	10:00
1941	Jan	2	10:00
1941	Jan	3	10:00
1941	Jan	4	10:00
1941	Jan	5	10:00
1941	Jan	6	10:00
1941	Jan	7	10:00
1941	Jan	8	10:00
1941	Jan	9	10:00
1941	Jan	10	10:00
1941	Jan	11	10:00
1941	Jan	12	10:00
1941	Jan	13	10:00
1941	Jan	14	10:00
1941	Jan	15	10:00
1941	Jan	16	10:00
1941	Jan	17	10:00
1941	Jan	18	10:00
1941	Jan	19	10:00
1941	Jan	20	10:00
1941	Jan	21	10:00
1941	Jan	22	10:00
1941	Jan	23	10:00
1941	Jan	24	10:00
1941	Jan	25	10:00
1941	Jan	26	10:00
1941	Jan	27	10:00
1941	Jan	28	10:00
1941	Jan	29	10:00
1941	Jan	30	10:00
1941	Jan	31	10:00

Year	Month	Day	Time	Location	Remarks
1941	Jan	1	10:00
1941	Jan	2	10:00
1941	Jan	3	10:00
1941	Jan	4	10:00
1941	Jan	5	10:00
1941	Jan	6	10:00
1941	Jan	7	10:00
1941	Jan	8	10:00
1941	Jan	9	10:00
1941	Jan	10	10:00
1941	Jan	11	10:00
1941	Jan	12	10:00
1941	Jan	13	10:00
1941	Jan	14	10:00
1941	Jan	15	10:00
1941	Jan	16	10:00
1941	Jan	17	10:00
1941	Jan	18	10:00
1941	Jan	19	10:00
1941	Jan	20	10:00
1941	Jan	21	10:00
1941	Jan	22	10:00
1941	Jan	23	10:00
1941	Jan	24	10:00
1941	Jan	25	10:00
1941	Jan	26	10:00
1941	Jan	27	10:00
1941	Jan	28	10:00
1941	Jan	29	10:00
1941	Jan	30	10:00
1941	Jan	31	10:00

Table 3 - The effect of acid concentration on the velocity of 2.4 mm diameter droplets in 60v% glycerol-water solution.

HCl conc.	Mean velocity (m/s)			Incubation period (s)	Initial Na content	No. of droplets
	Top half of column	Lower half of column	Overall			
0.52 N	0.487	0.490	0.489	0.088	0.55wt%	45
1.07 N	0.460	0.468	0.464	0.075	0.56wt%	40
1.47 N	0.454	0.458	0.456	0.057	0.55wt%	45
2.09 N	0.447	0.457	0.452	0.038	0.58wt%	40
2.75 N	0.452	0.457	0.454	-	0.61wt%	15

Table 4 - The effect of sodium concentration on the velocity of 2.4 mm diameter droplets in 60 v % glycerol-water solution.

HCl conc.	NaCl conc. (moles/l)	Initial Na conc	Mean velocity (m/s)			No. of droplets
			Top half of column	Lower half of column	Overall	
2.09 N	0	0.58 wt %	0.447	0.457	0.452	40
2.09 N	0	0.16 wt %	0.316	0.310	0.313	22
2.09 N	0.5	0.16 wt %	0.312	0.307	0.309	13
2.75 N	0	0.61 wt %	0.452	0.457	0.454	15
2.75 N	0	0.16 wt %	0.301	0.309	0.305	14

Figure 17 The effect of acid concentration on the terminal velocity of amalgam droplets.

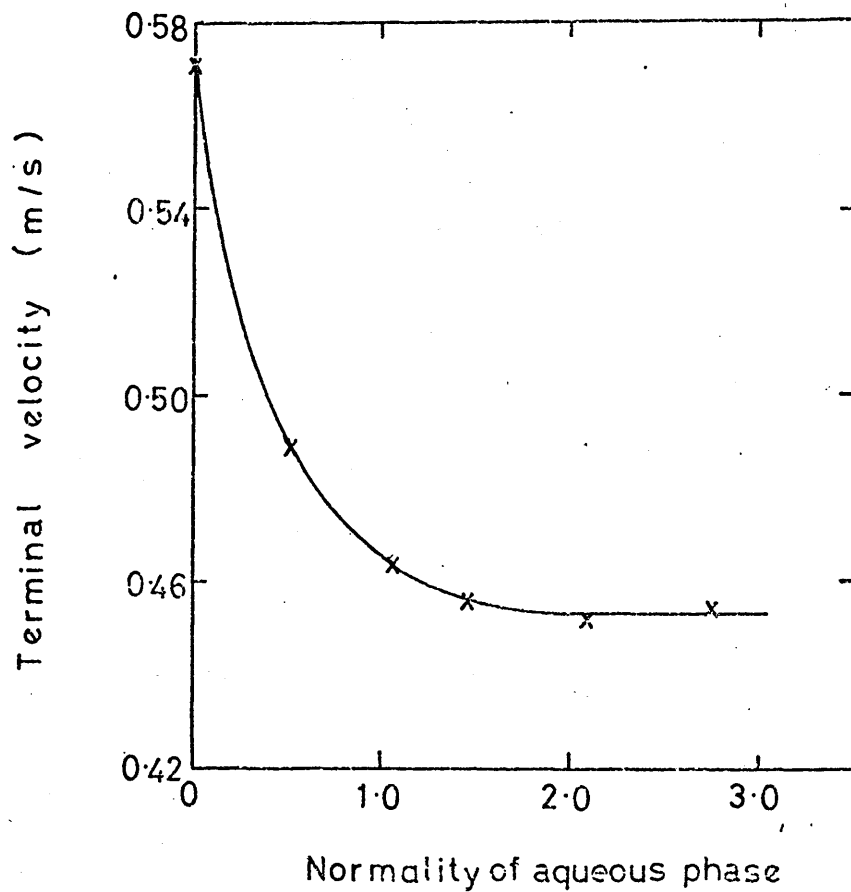


Figure 18 The effect of acid concentration on the incubation period.

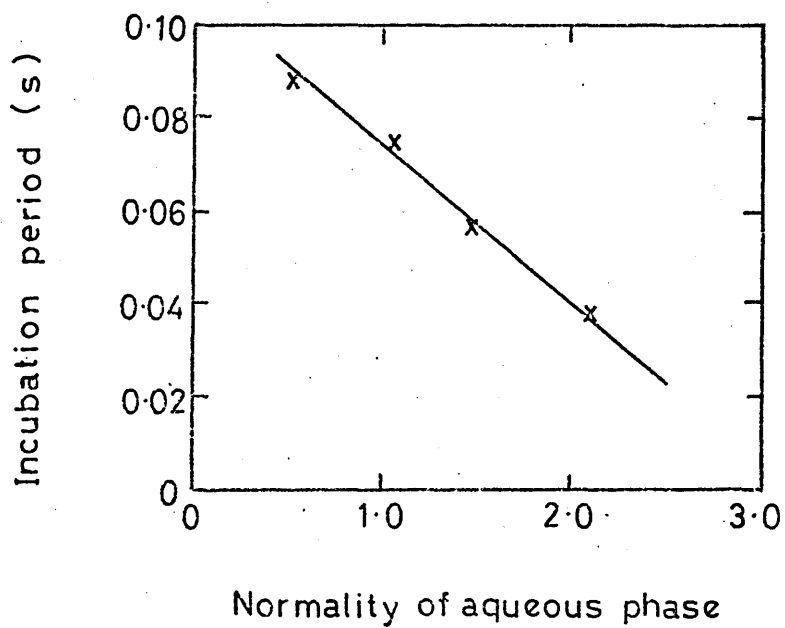


Table 5 - The effect of sodium chloride concentration on the velocity of 2.4 mm diameter droplets in 60 v % glycerol-water solution.

HCl conc	NaCl conc. (moles/l)	Initial Na conc.	Mean Velocity (m/s)			Incubation period (s)	No. of droplets
			Top half of column	Lower half of column	Overall		
1.07 N	0	0.56 wt %	0.460	0.468	0.464	0.075	40
1.00 N	1.0	0.59 wt %	0.445	0.452	0.449	0.089	23
1.0 N	2.0	0.59 wt %	0.413	0.420	0.417	0.108	31
1.47 N	0	0.55 wt %	0.454	0.458	0.456	0.057	45
1.47 N	0.75	-	0.436	0.440	0.438	-	15
1.47 N	1.75	0.52 wt %	0.408	0.412	0.410	-	14
2.09	0	0.58 wt %	0.447	0.457	0.452	0.038	40
2.09	0.5	0.61 wt %	0.430	0.430	0.430	-	17
2.09	1.0	0.61 wt %	0.408	0.400	0.404	-	17

Figure 19 The effect of sodium chloride concentration on the terminal velocity of amalgam droplets.

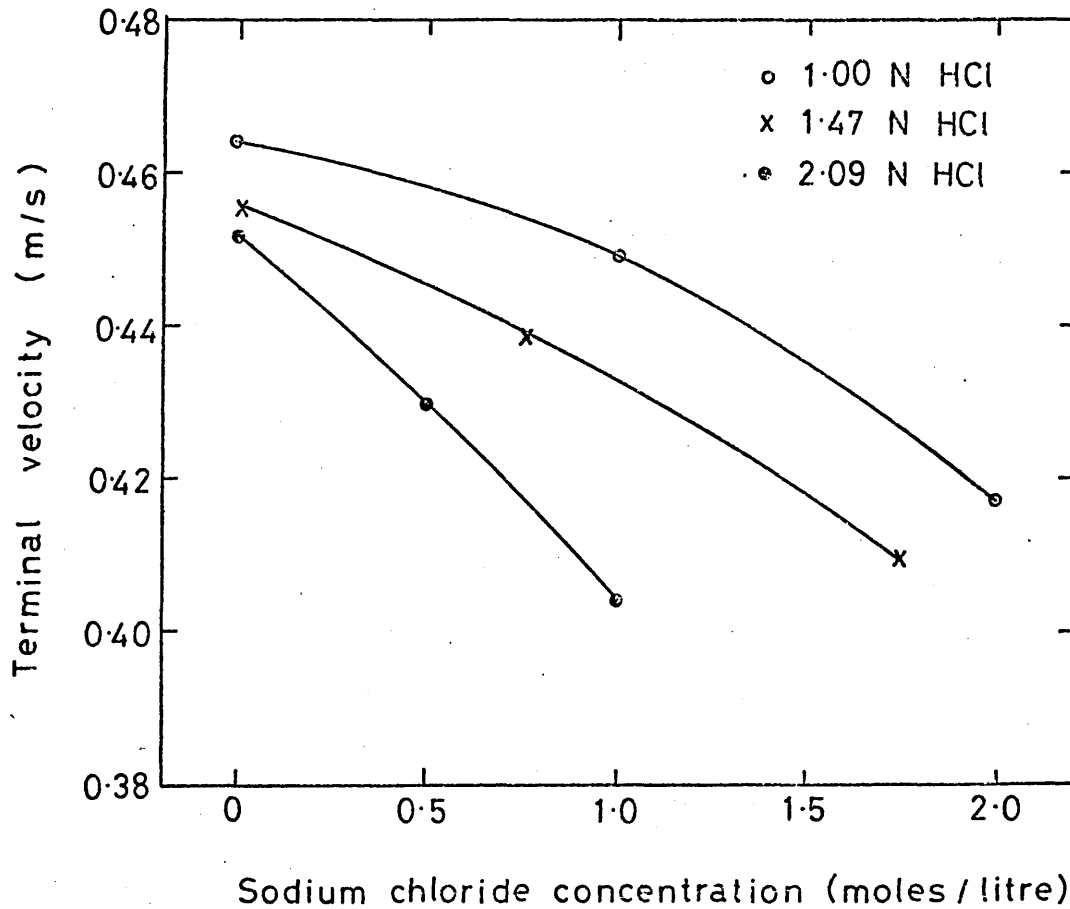


Figure 20 The effect of sodium chloride concentration on the incubation period.

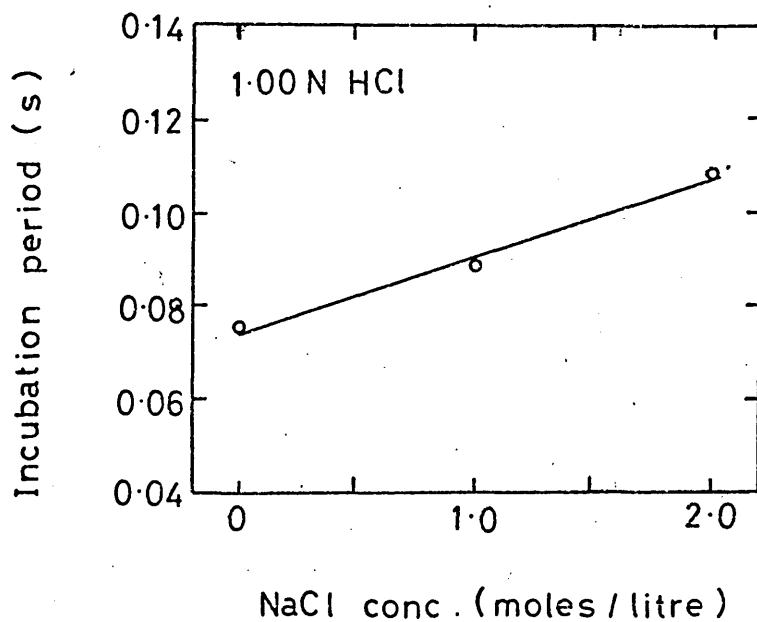
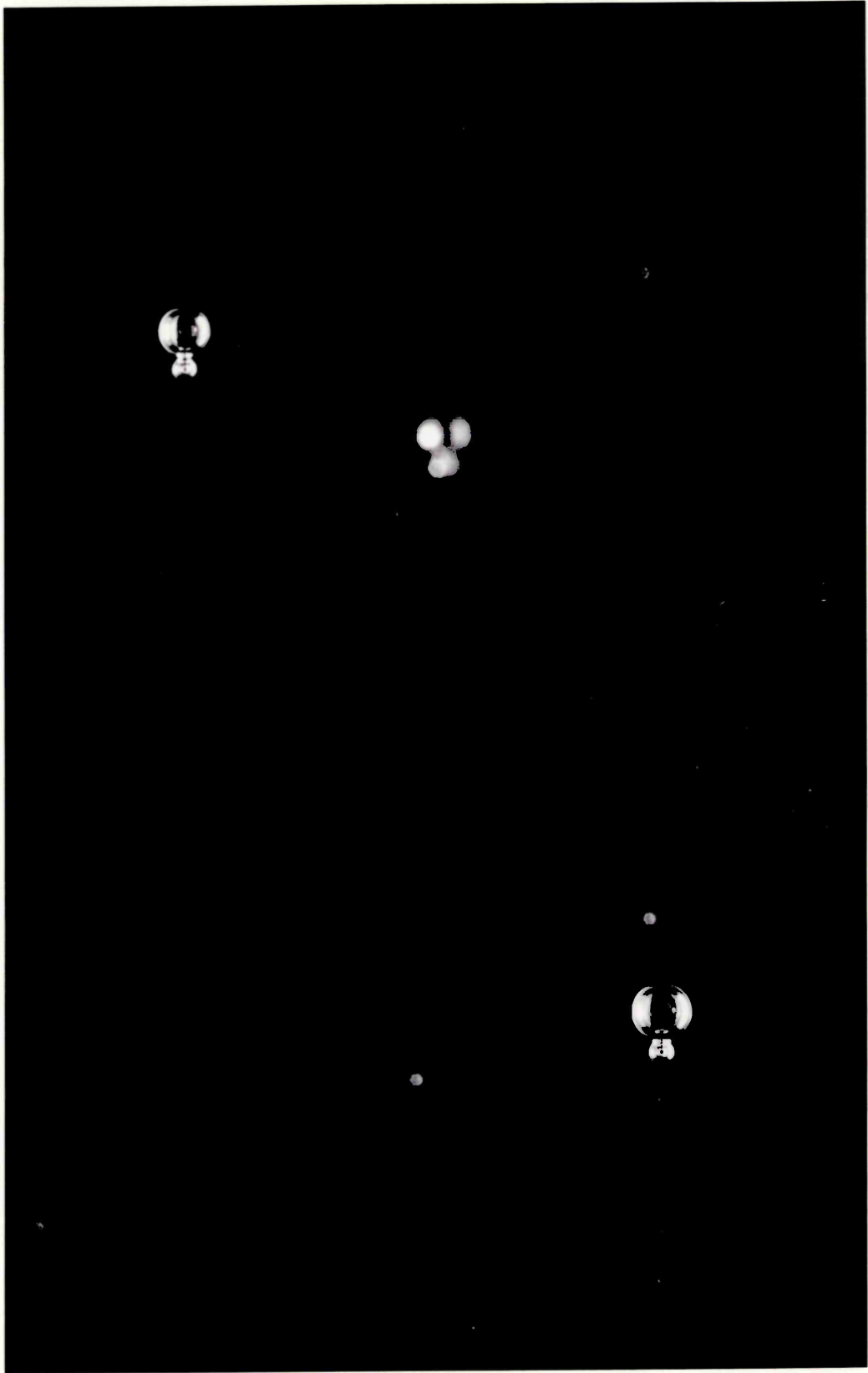


PLATE 14

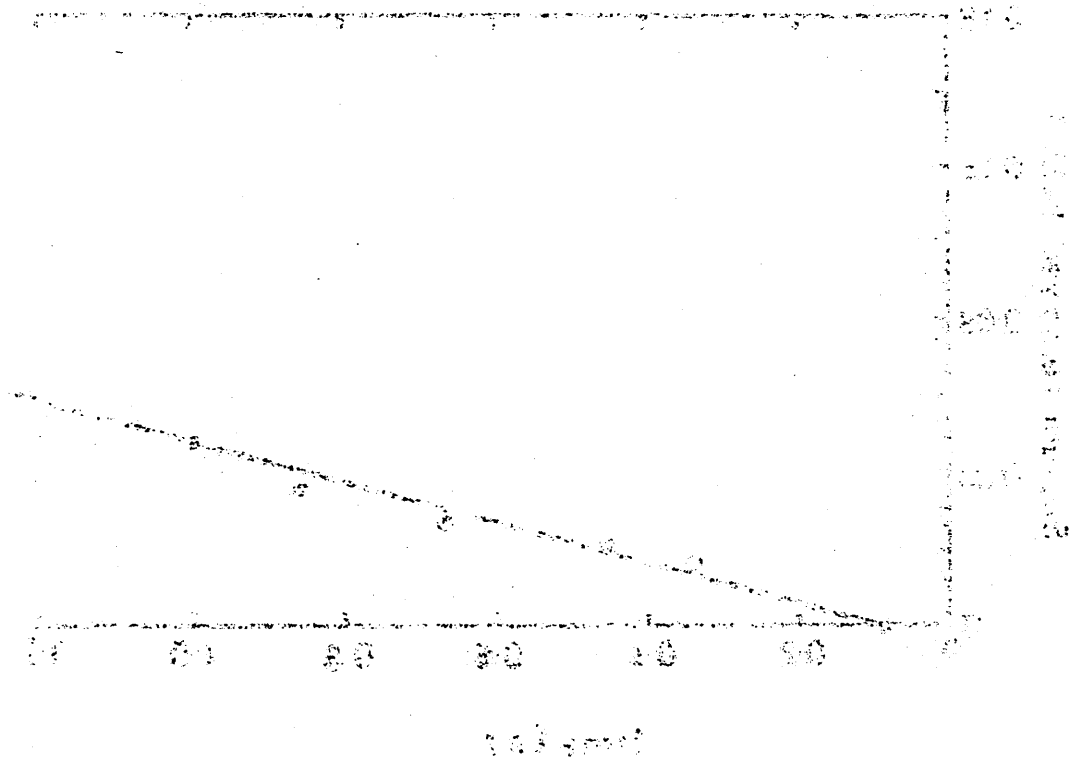
Small amalgam droplets with attached bubbles, rising up
the column of acidified aqueous solution.

12 x actual size



The solution of water-glycol solution

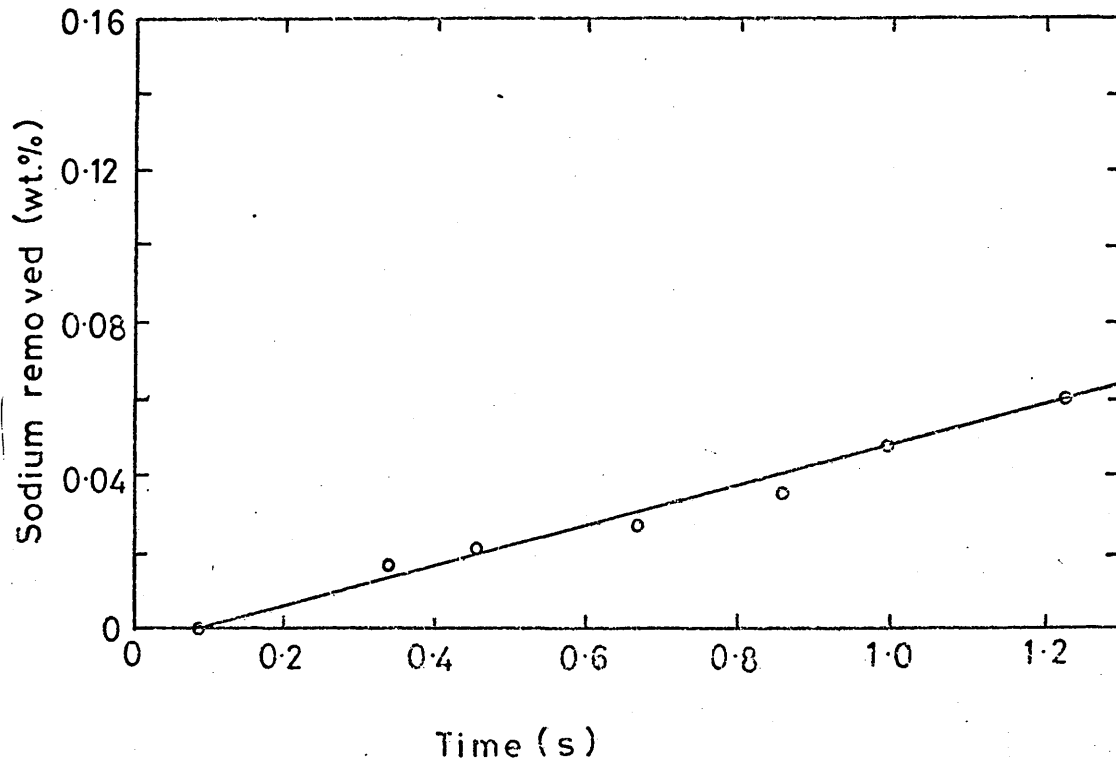
0.50N HCl, water-glycol solution



0.50N HCl - aqueous solution

Figure 21

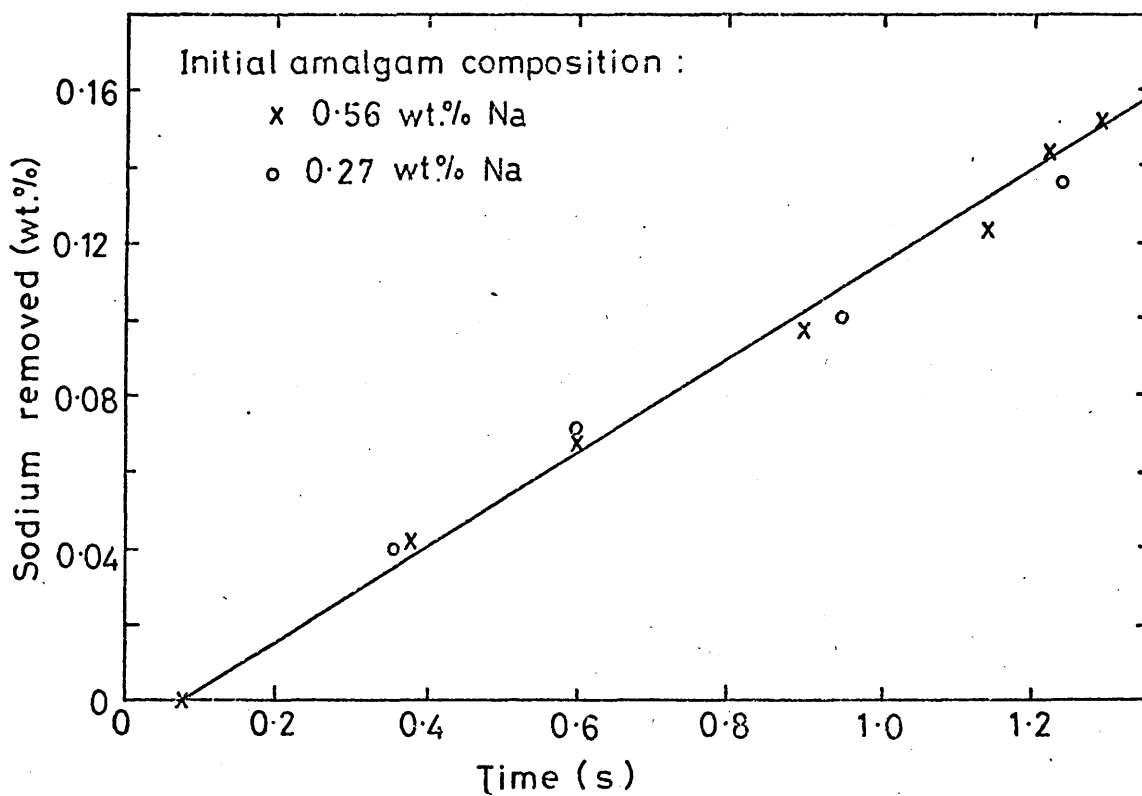
The reaction of single droplets of amalgam with
0.50 N HCl, water-glycerol solution.



Initial composition of amalgam - 0.54 wt.% Na

Figure 22 The reaction of amalgam droplets with approximately 1N HCl water-glycerol solution.

(a) 1.00 N HCl solution



(b) 0.91 N HCl solution containing 0.5 moles of NaCl / litre.

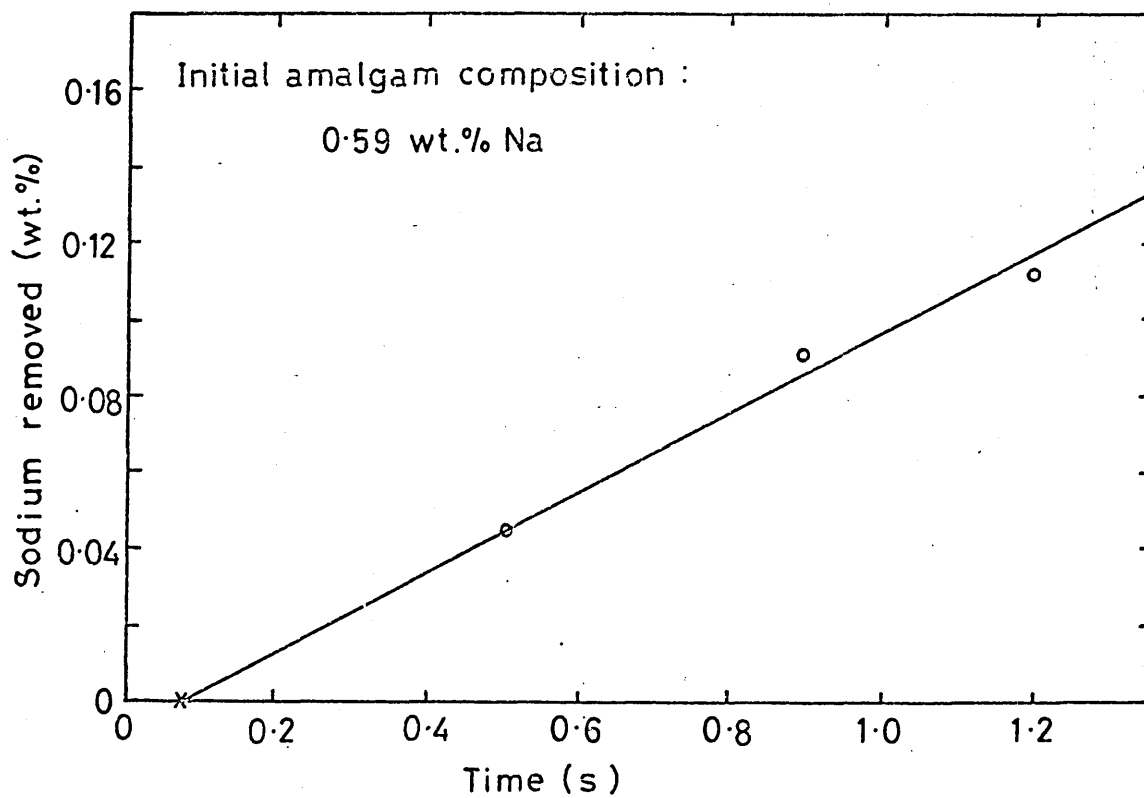
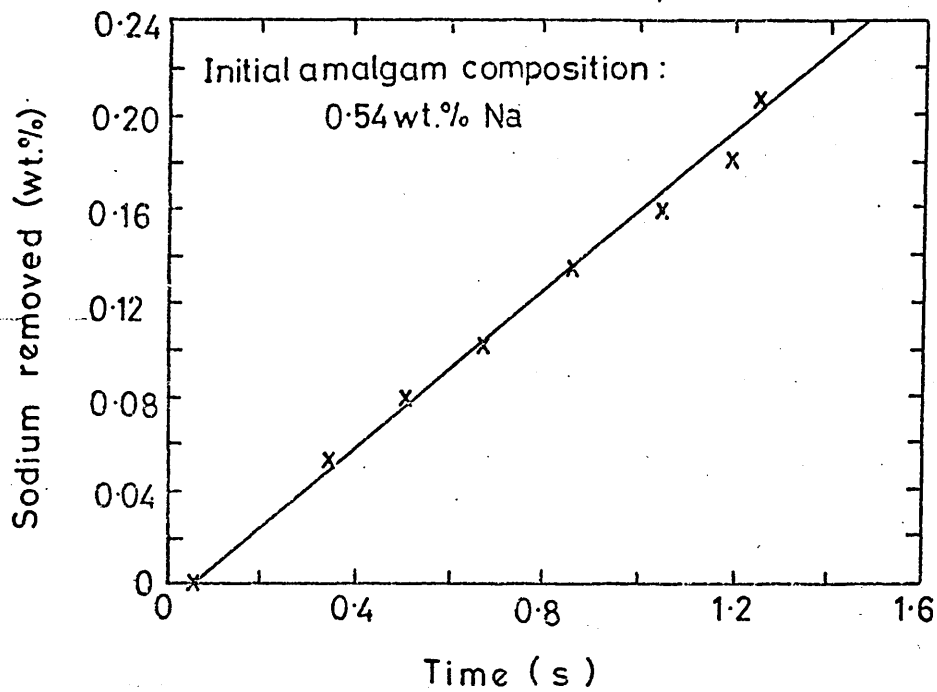


Figure 23 The reaction of amalgam droplets with 1.47 N HCl, water-glycerol solution.

(a) Salt free solution.



(b) Containing 0.5 moles of NaCl / litre.

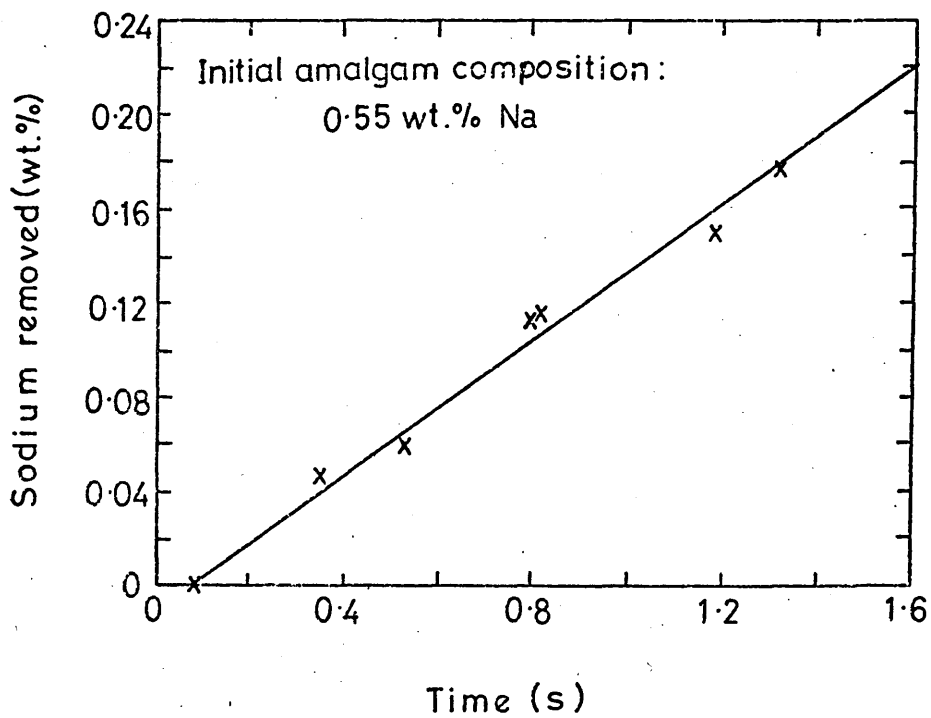
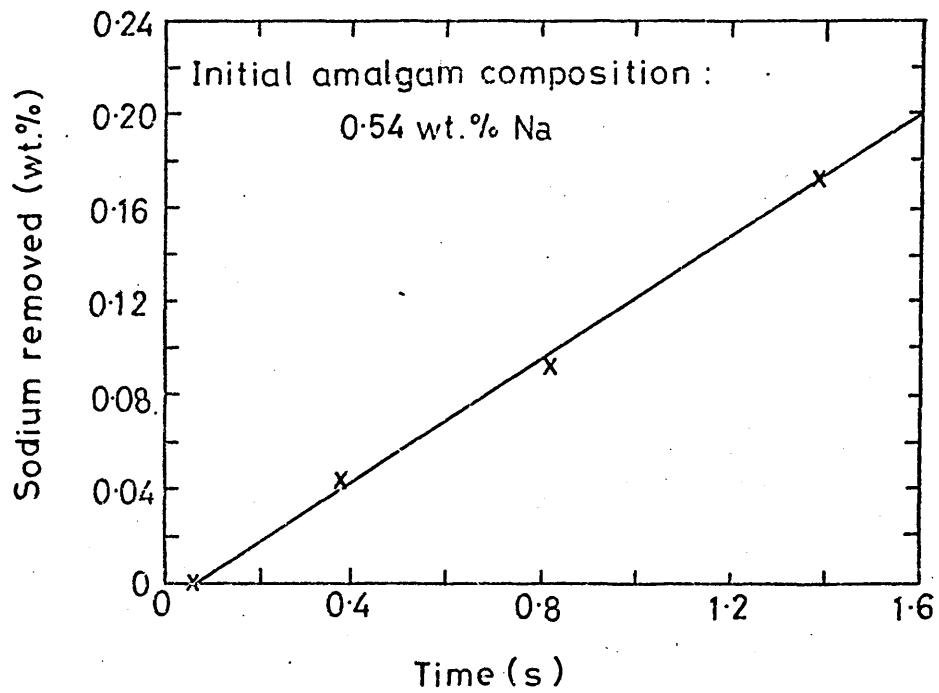


Figure 23 continued

(c) Containing 1.0 moles of NaCl / litre.



(d) Containing 1.75 moles of NaCl / litre.

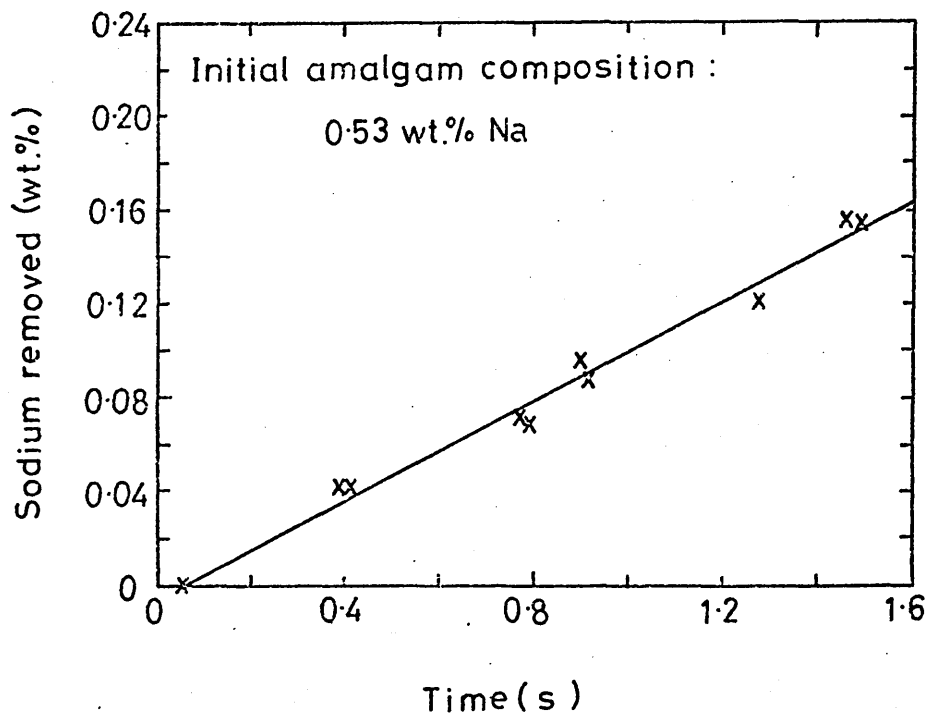
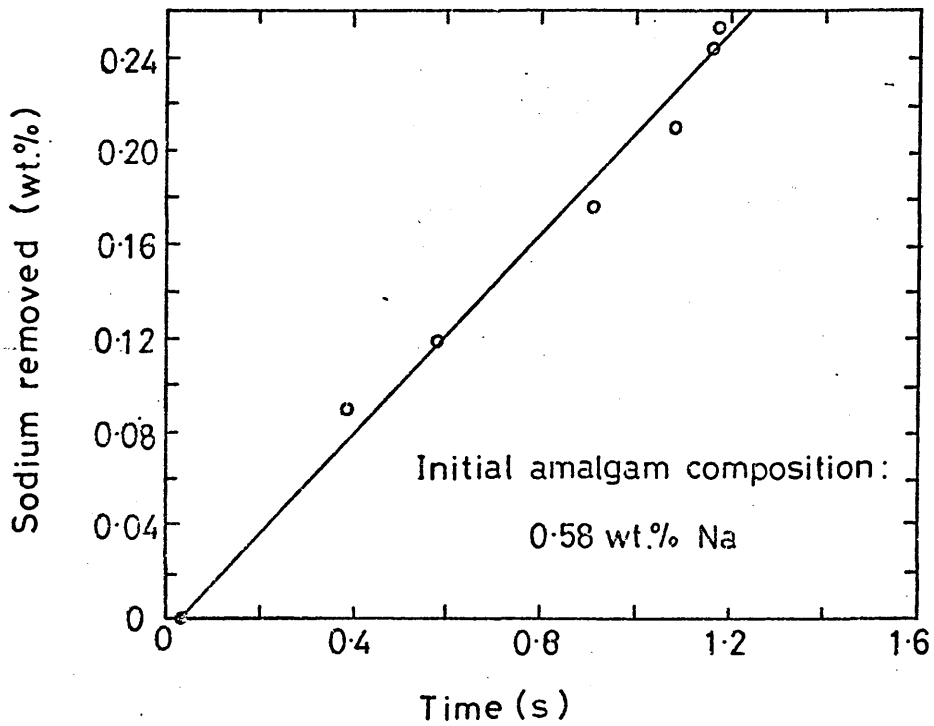


Figure 24 The reaction of amalgam droplets with 2.01 N HCl, water-glycerol solution.

(a) Salt free solution.



(b) Containing 0.5 moles of NaCl / litre .

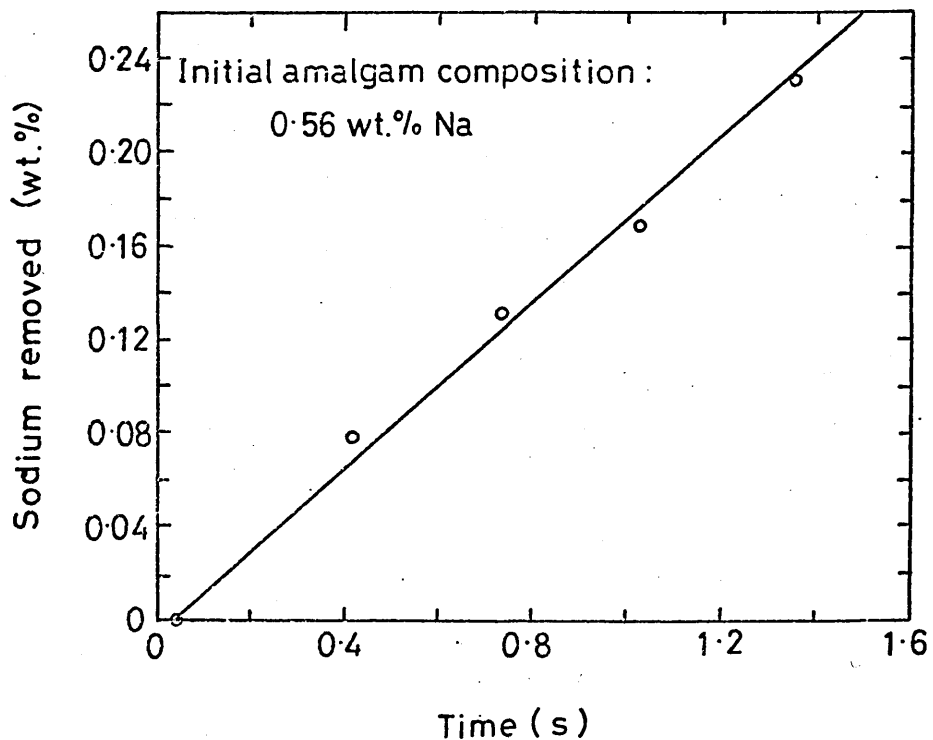


Figure 24 continued.

(c) Containing 1.0 moles of NaCl / litre.

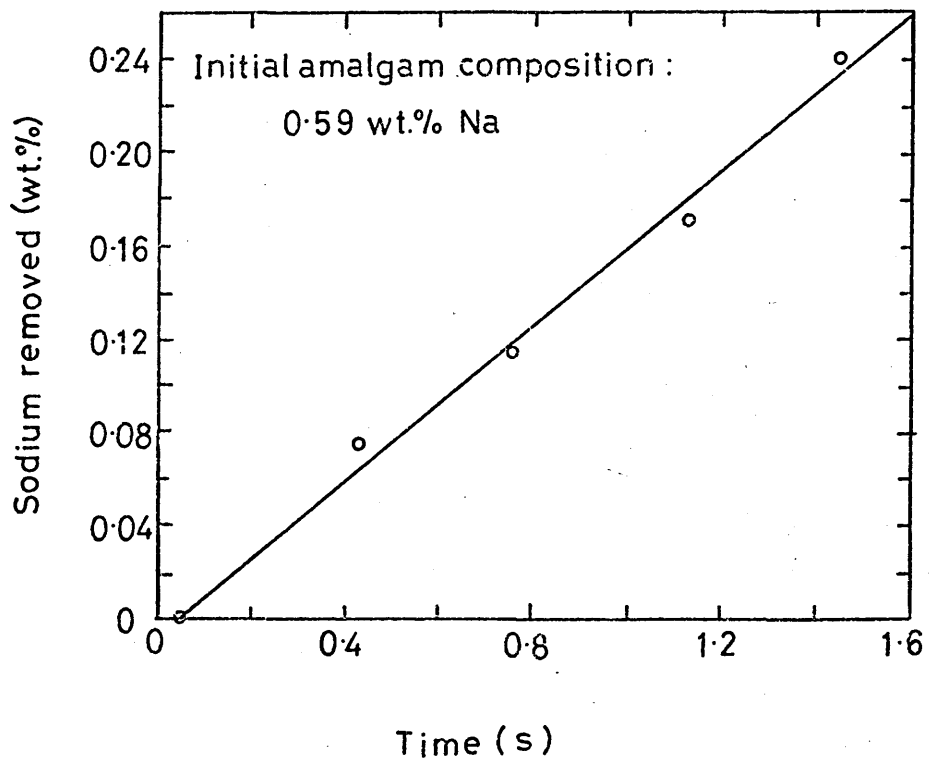
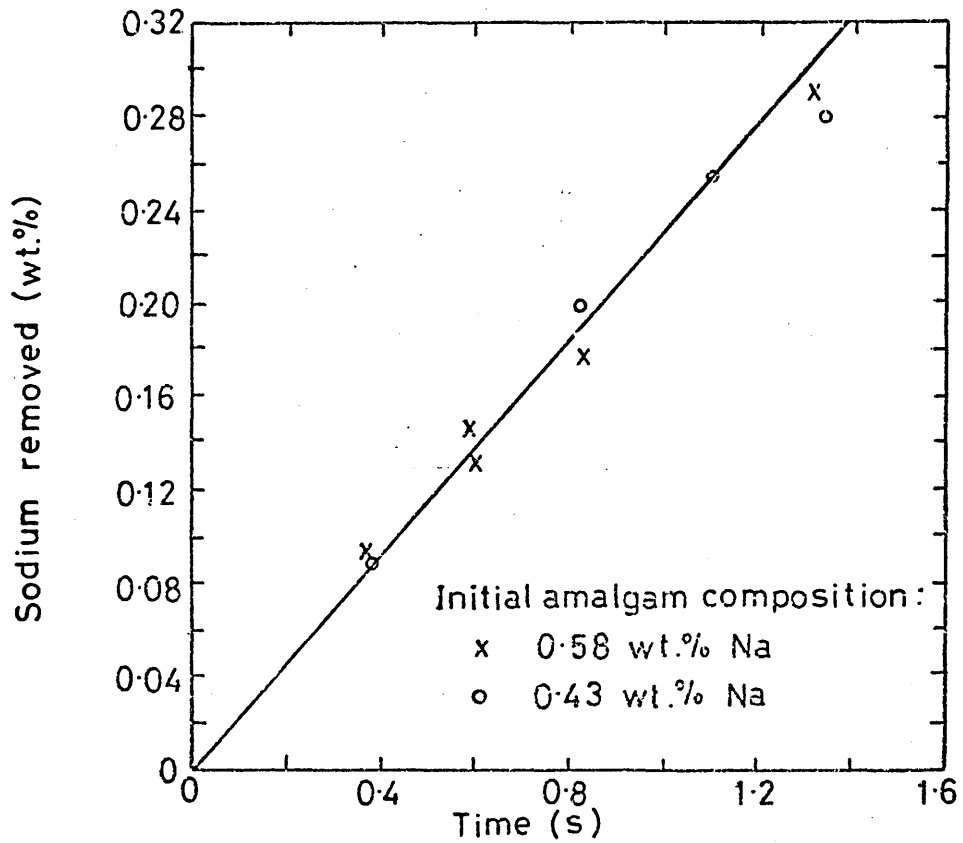


Figure 25 The reaction of amalgam droplets with 2.73 N HCl, water-glycerol solution.

(a) Salt free solution.



(b) Solution containing 0.5 moles of NaCl / litre.

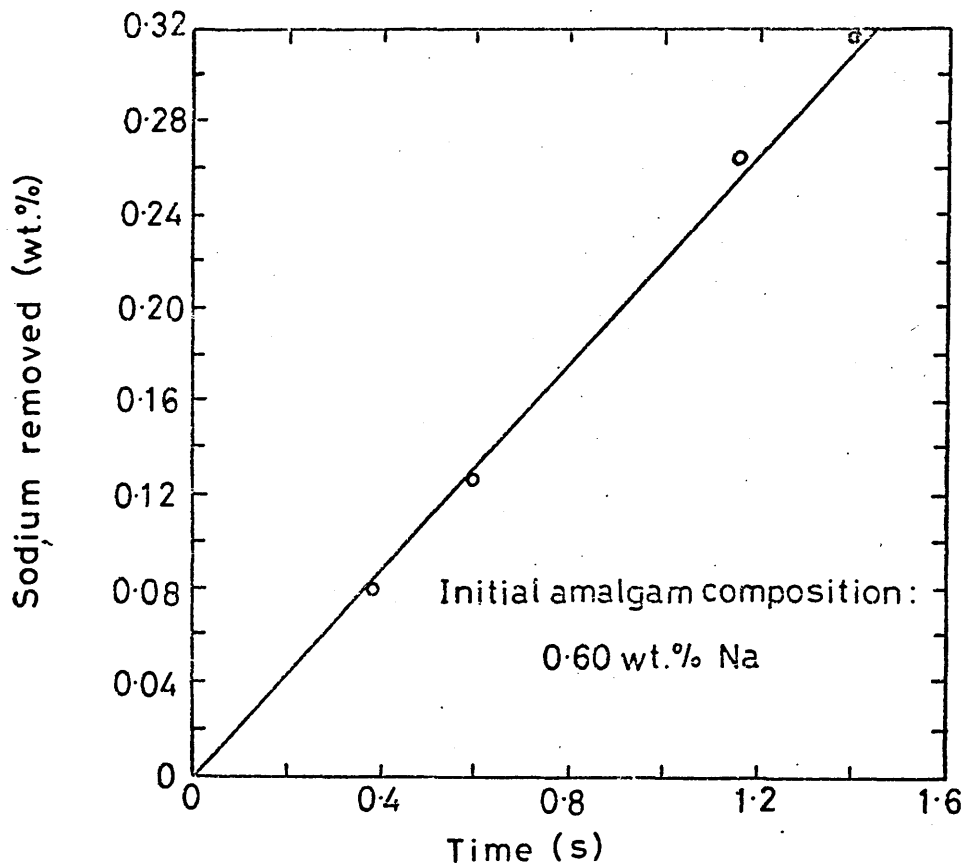
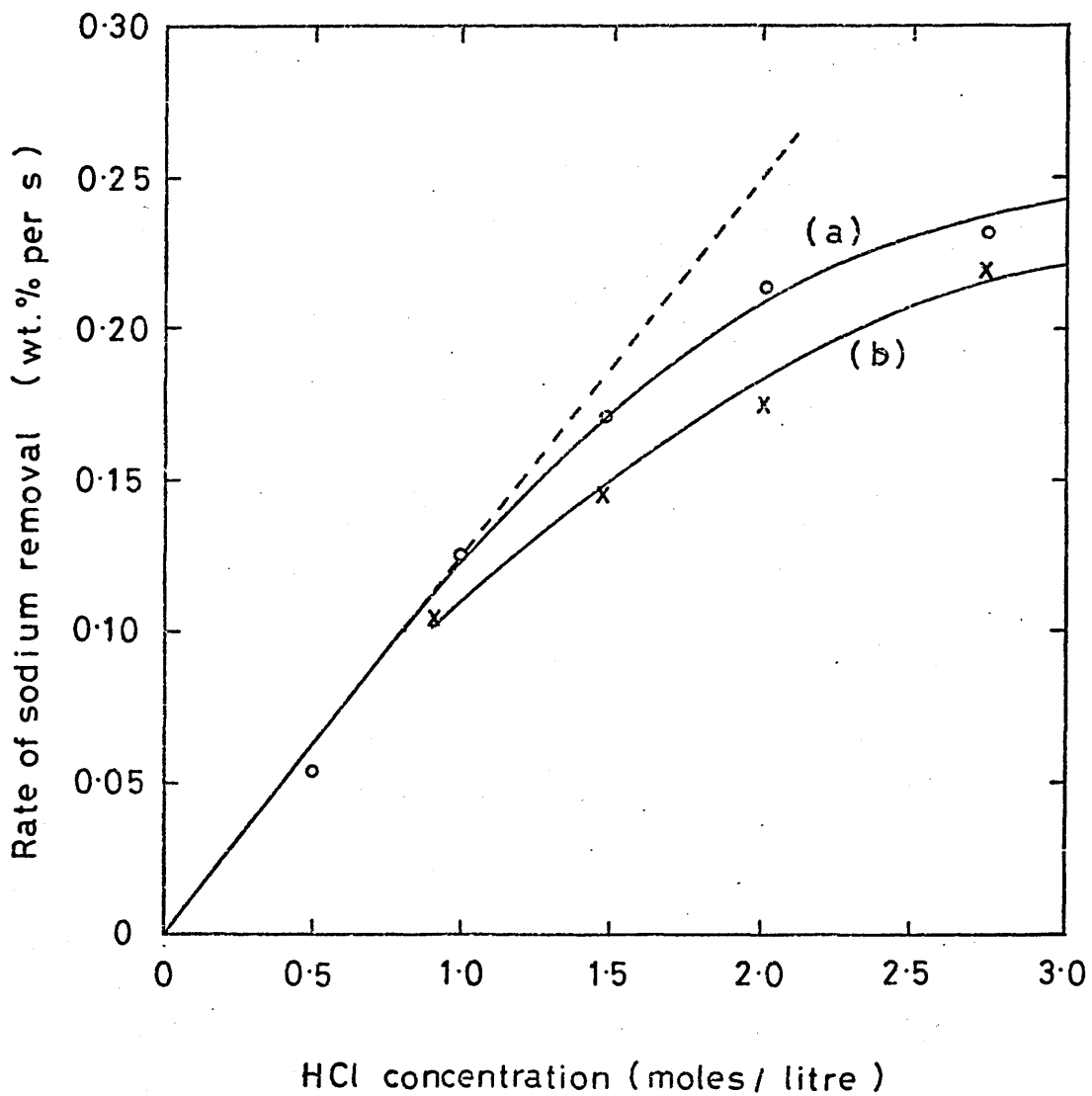


Table 6 - The effect of acid concentration on the rate of sodium removal from 2.4 mm diameter amalgam droplets in 60 v % glycerol-water solution.

HCl conc.	NaCl conc. (moles/l)	Na removal rate (wt %/sec)	Initial amalgam composition (wt % Na)	Temp. °C	Figure No.
0.50 N	0	0.053	0.540 \pm 0.015	20	21
1.00 N	0	0.125	0.562 \pm 0.012	20	22(a)
1.47 N	0	0.172	0.540 \pm 0.015	18	23(a)
2.01 N	0	0.214	0.581 \pm 0.005	19	24(a)
2.73 N	0	0.231	0.578 \pm 0.008	19	25(a)
0.91 N	0.5	0.105	0.550 \pm 0.012	20	22(b)
1.47 N	0.5	0.144	0.548 \pm 0.010	17	23(b)
2.01 N	0.5	0.175	0.555 \pm 0.009	19	24(b)
2.73 N	0.5	0.221	0.602 \pm 0.007	21	25(b)

Figure 26 The effect of HCl concentration on the rate of sodium removal from amalgam droplets .



(a) No sodium chloride in solution .

(b) Aqueous phase containing 0.5 moles of NaCl / litre .

Table 7 - The effect of sodium chloride concentration on the rate of sodium removal from 2.4 mm diameter amalgam droplets in 60 v % glycerol-water solution.

HCl conc.	NaCl conc. (moles/l)	Na removal rate (wt%Na/s)	Initial amalgam composition (wt % Na)	Temp. °C	Figure No.
1.47 N	0	0.172	0.540 \pm 0.015	18	23(a)
1.47 N	0.5	0.144	0.548 \pm 0.010	17	23(b)
1.47 N	1.0	0.132	0.542 \pm 0.004	17	23(c)
1.47 N	1.75	0.108	0.528 \pm 0.020	17	23(d)
2.01 N	0	0.214	0.581 \pm 0.005	19	24(a)
2.01 N	0.5	0.175	0.555 \pm 0.009	19	24(b)
2.01 N	1.0	0.162	0.593 \pm 0.007	19	24(c)

Figure 27 The effect of NaCl concentration on the rate of sodium removal from amalgam droplets.

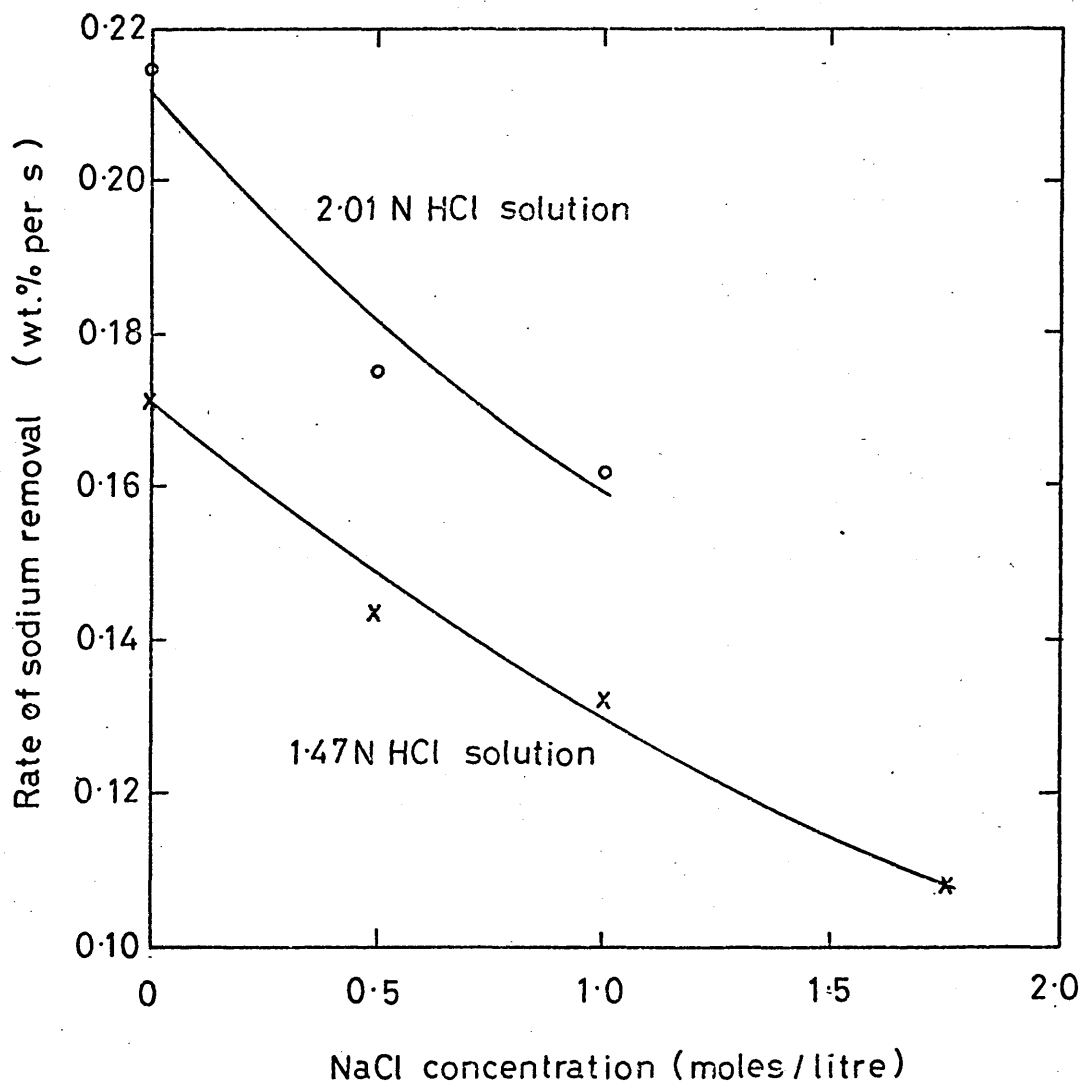
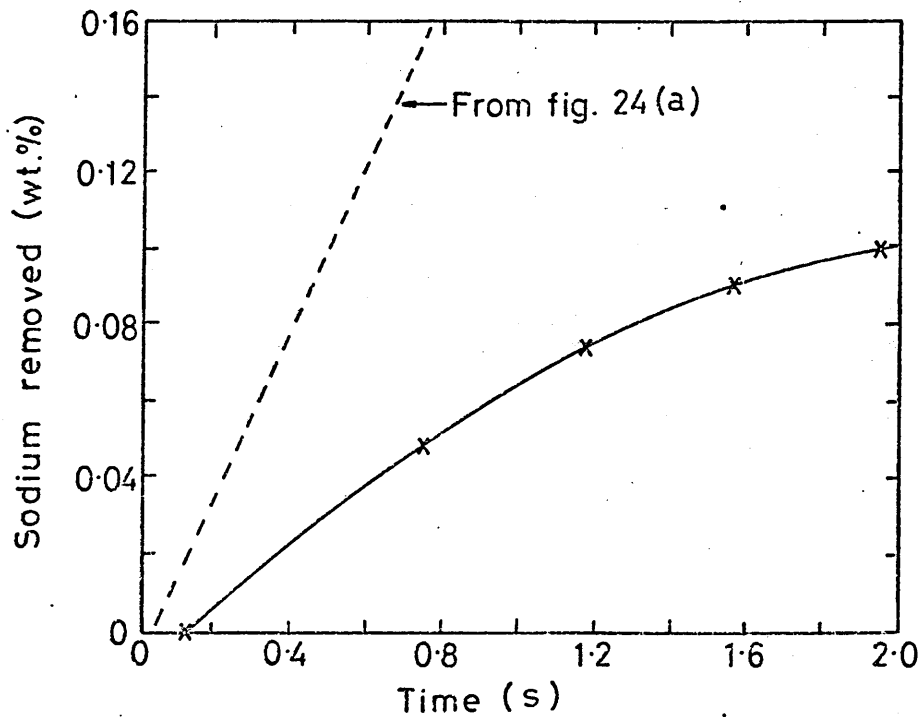
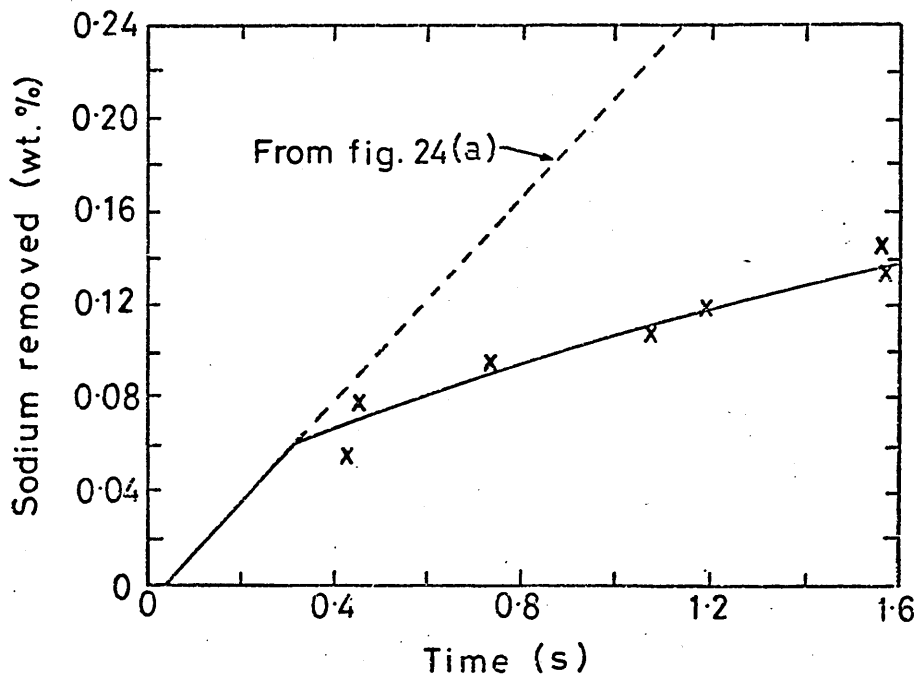


Figure 28 The reaction between 2.01 N HCl water-glycerol solution and amalgam droplets at low sodium concentrations.

(a) Amalgam containing initially 0.19 wt.% Na.



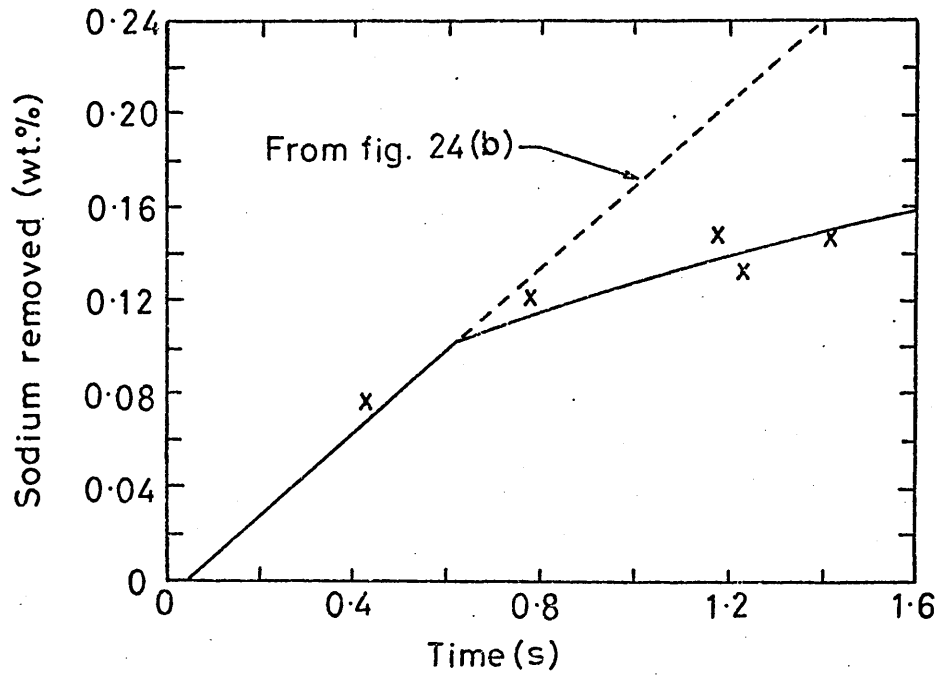
(b) Amalgam containing initially 0.27 wt.% Na.



Mechanism change : 0.21 wt.% Na

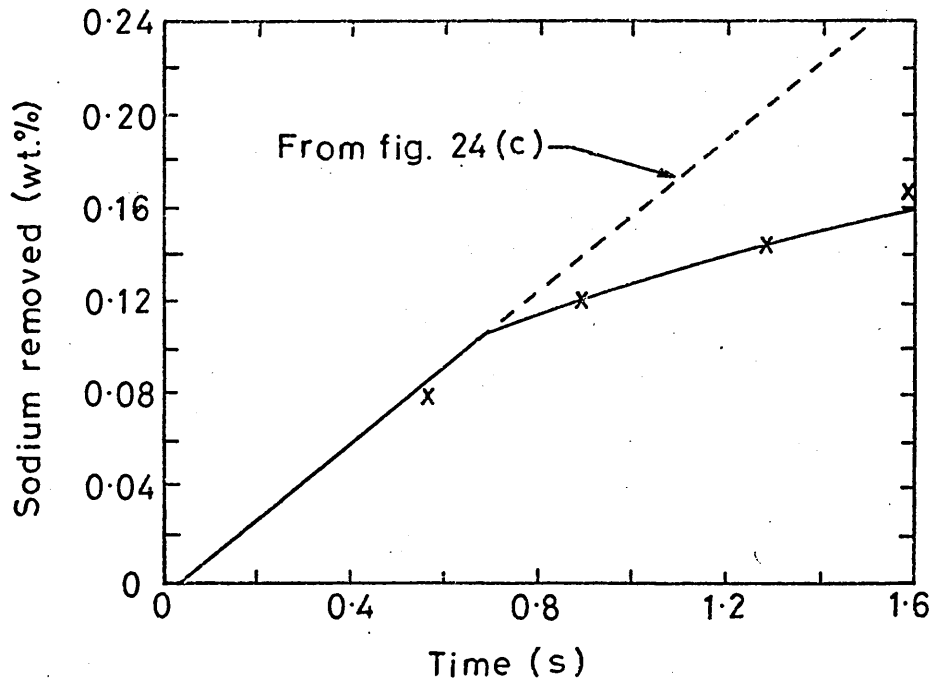
Figure 28 continued.

- (c) Amalgam containing initially 0.28 wt.% Na and aqueous phase containing 0.5 moles of NaCl per litre.



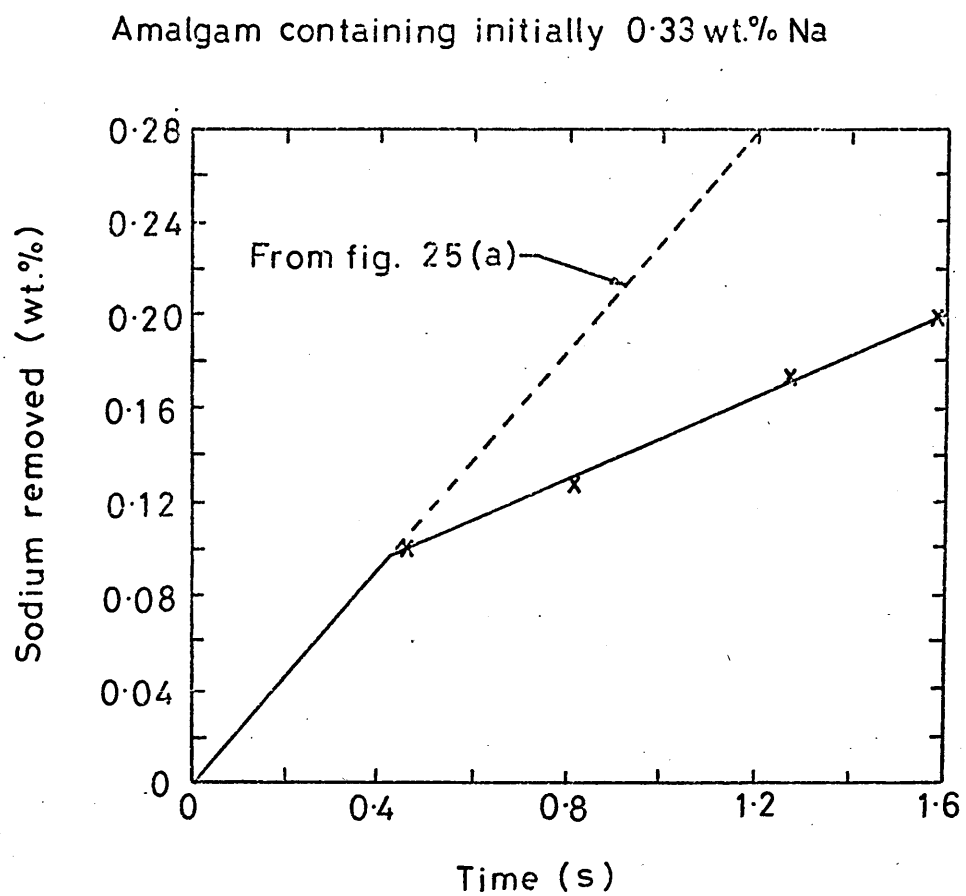
Mechanism change 0.18 wt.% Na

- (d) Amalgam containing initially 0.31 wt.% Na and aqueous phase containing 1.0 mole of NaCl per litre.



Mechanism change 0.20 wt.% Na

Figure 29 The reaction between 2.7N HCl water-glycerol solution and amalgam droplets at low sodium concentrations.



Mechanism change 0.23 wt.% Na

Figure 30 Theoretical rate of sodium removal from amalgam droplets assuming sodium transport control.
($r_d = 1.2$ mm, $\delta_s = 1.0$)

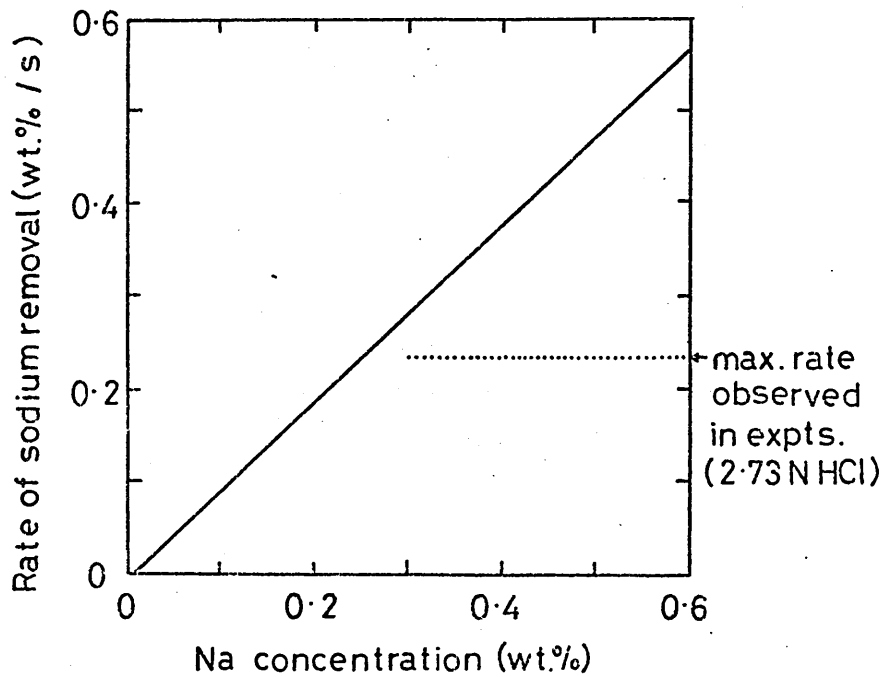


Figure 31 Theoretical rate of sodium removal from amalgam droplets assuming hydrogen ion transport control.
($r_d = 1.2$ mm, $\delta_s = 1.0$)

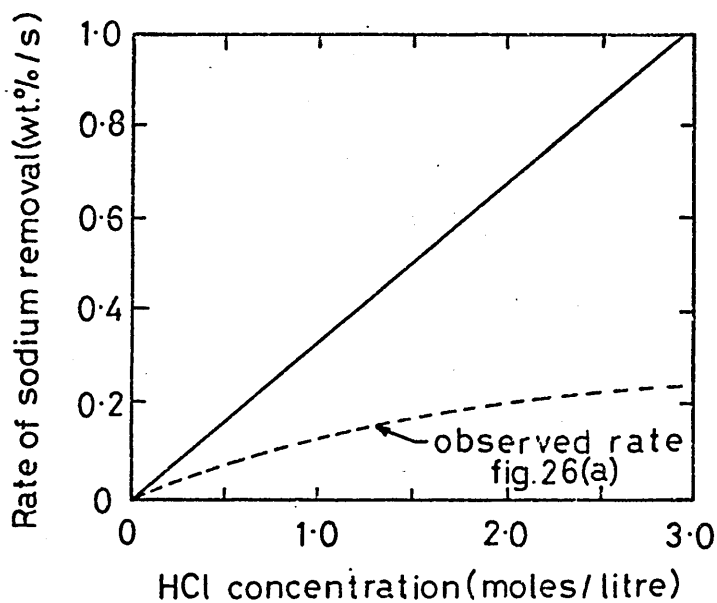


Figure 32 The effect of NaCl and HCl concentration in the aqueous phase on the interfacial concentration of Na^+ ions.

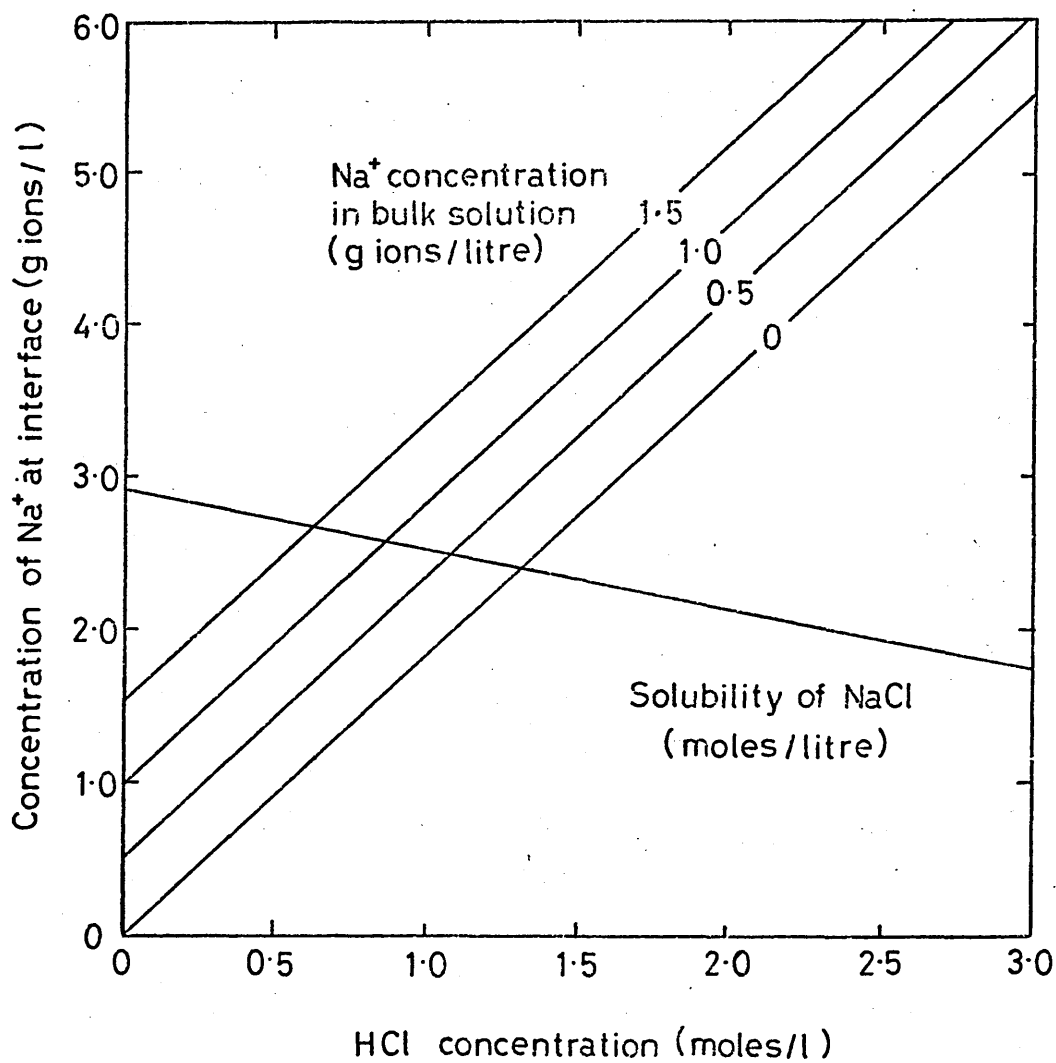


Figure 33 The reaction between 2.01 N HCl water-glycerol solution and amalgam droplets initially containing 0.19 wt.% Na.

Data from figure 28(a) presented in the form of equation 4-23.

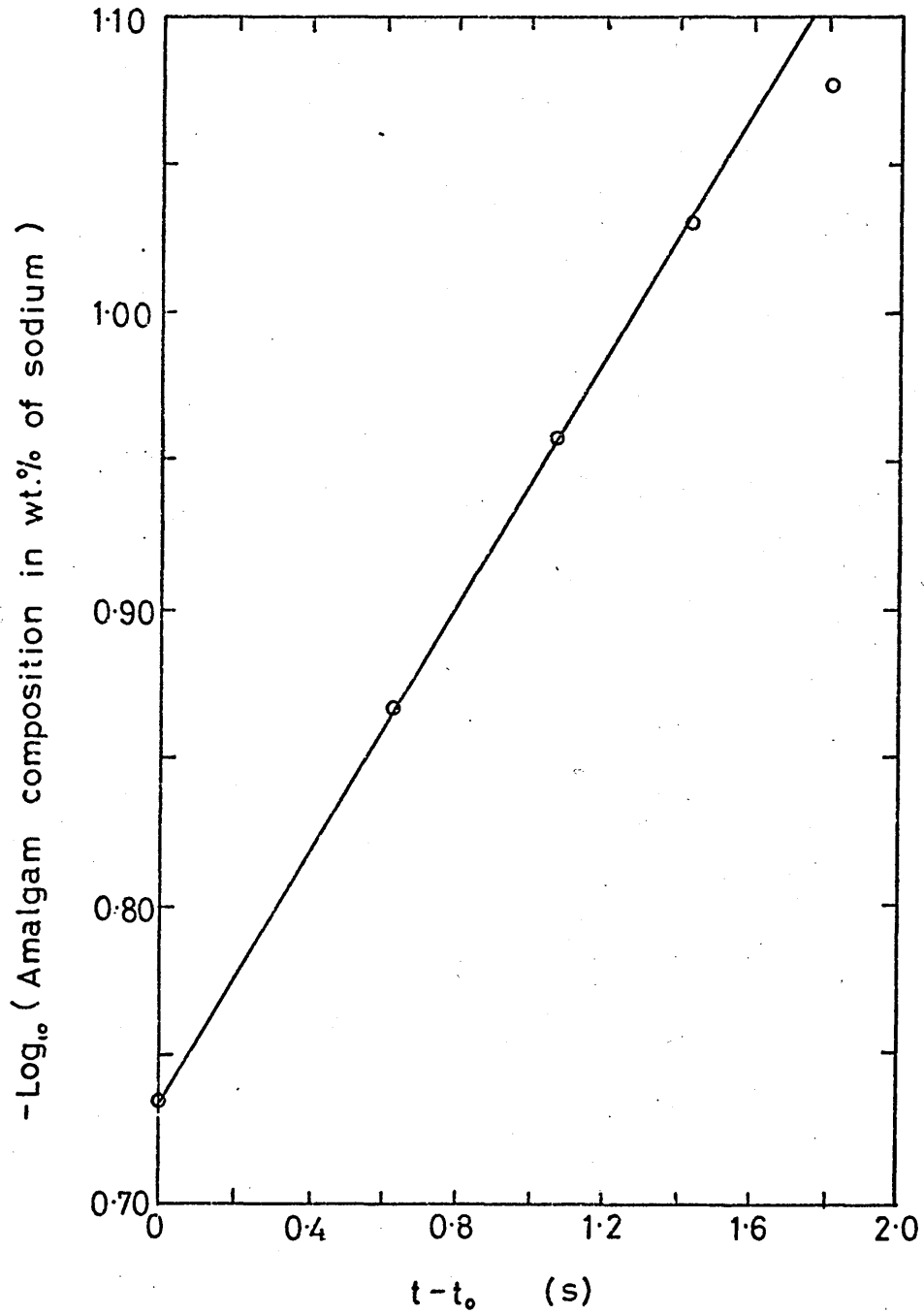
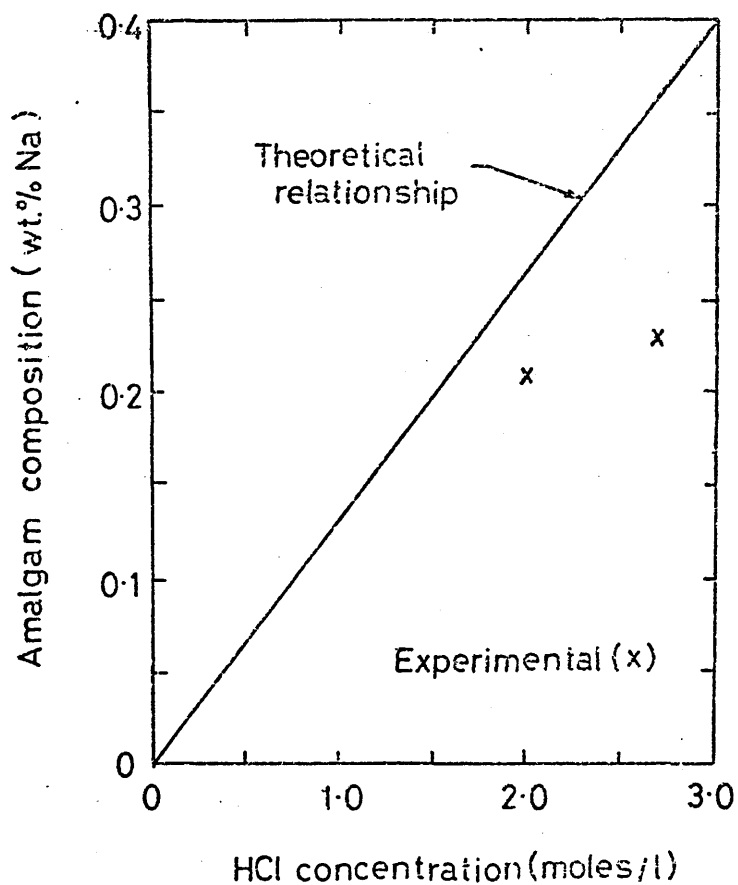


Figure 34 The relationship between the HCl concentration in the aqueous phase and the amalgam composition at which the change from hydrogen ion discharge control to sodium transport control occurs .



Key to Figure 35

- 1 Hydrogen chloride supply via needle valve.
- 2 Nitrogen supply via needle valve.
- 3 7K Rotameter.
- 4 18A Rotameter.
- 5 Mercury manometer.
- 6 Thermometer.
- 7 Mercury manometer
- 8 Thermometer.
- 9 Gas mixing vessel.
- 10 Air bleed valve.
- 11 Thermometer.
- 12 Mercury manometer.
- 13 Lance.
- 14 Model slag.
- 15 Sodium amalgam.
- 16 Model converter vessel.
- 17 Mercury manometer.
- 18 Position of constriction for experiments at elevated vessel pressures.
- 19 Mercury trap.
- 20 Water wash to remove hydrogen chloride.
- 21 Mercury trap.
- 22 Water wash to remove hydrogen chloride.
- 23 Water trap.
- 24 Rotameter.
- 25 Gas sampling system.
- 26 Sample tube.

FIGURE 35 SCHEMATIC DIAGRAM OF MODEL CONVERTER AND ANCILLARY EQUIPMENT .

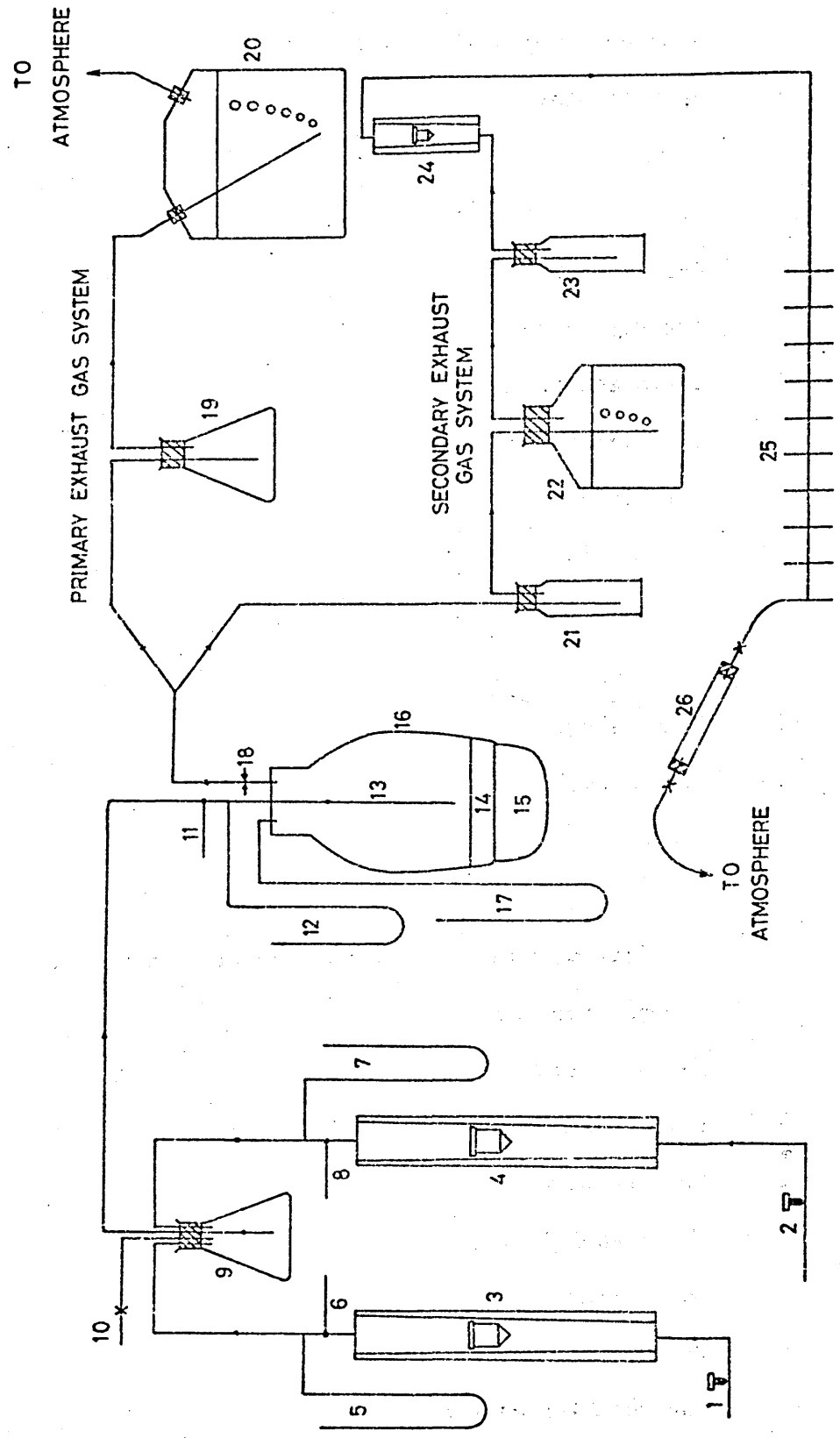
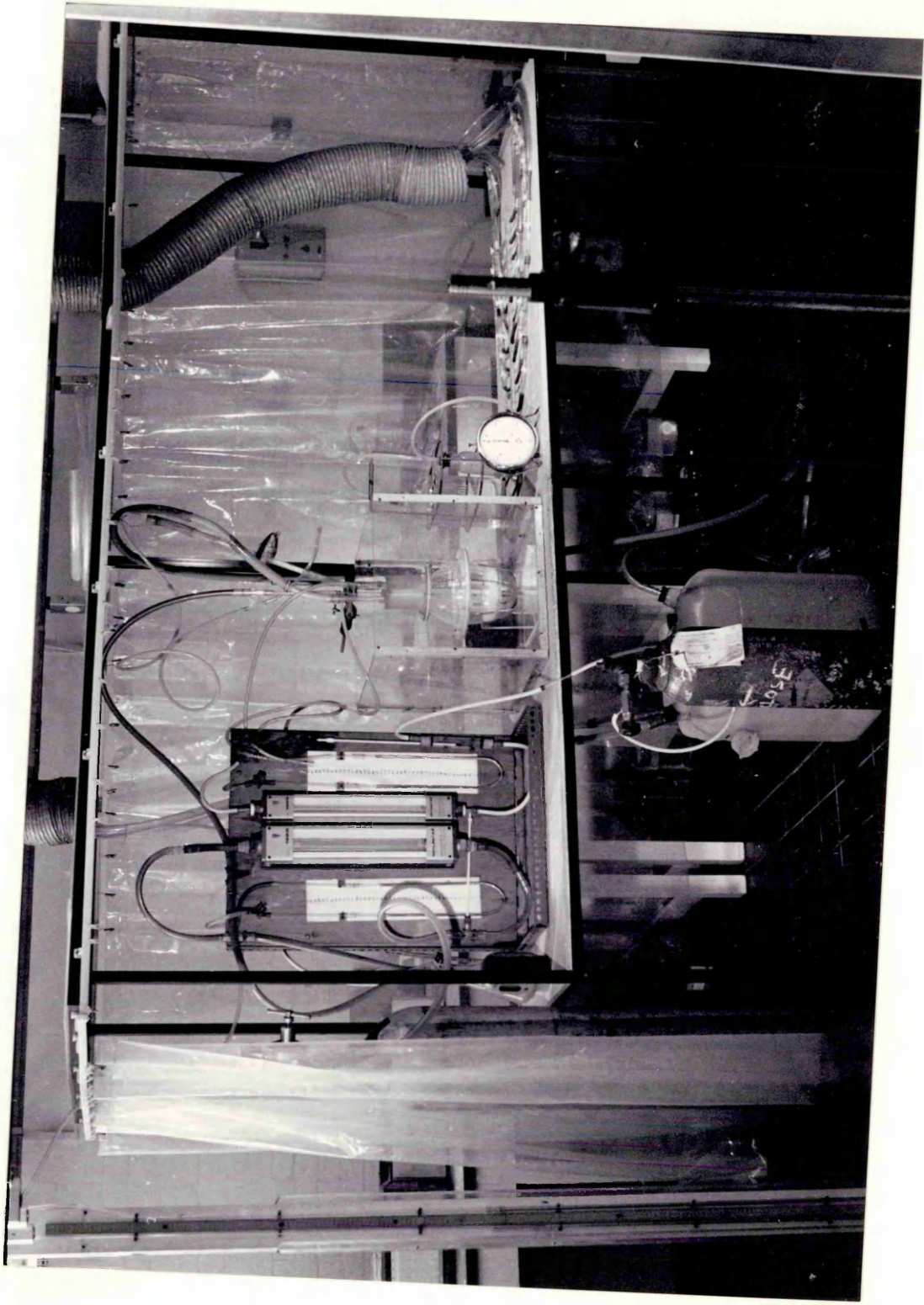
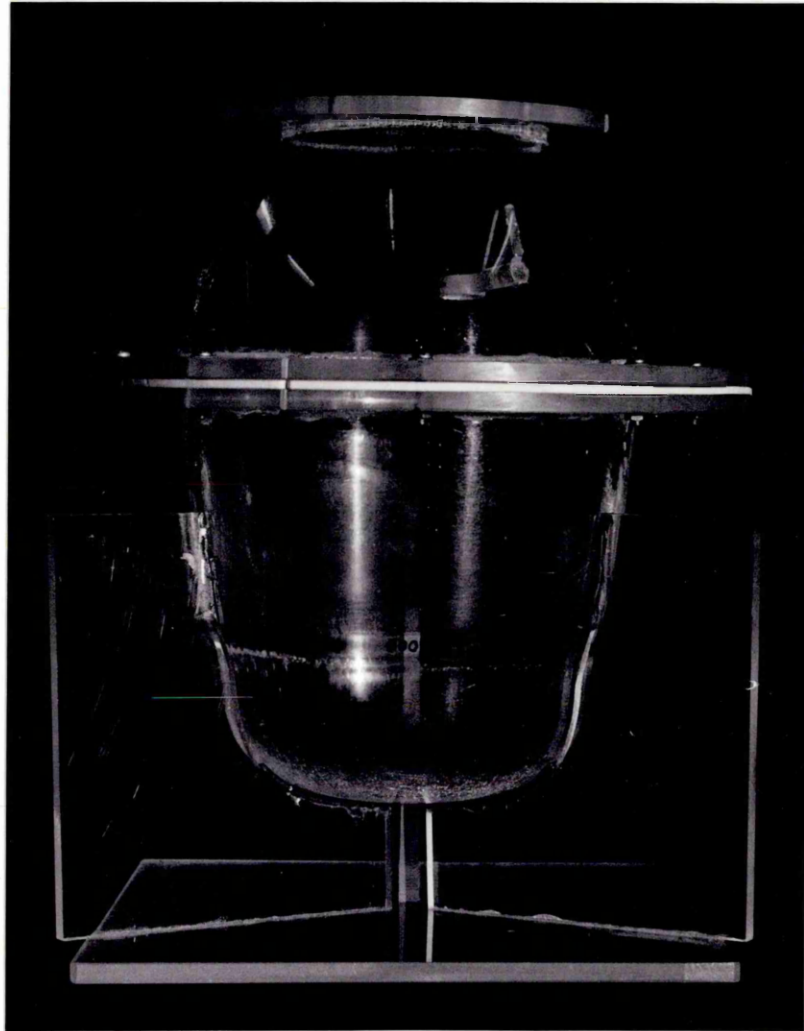
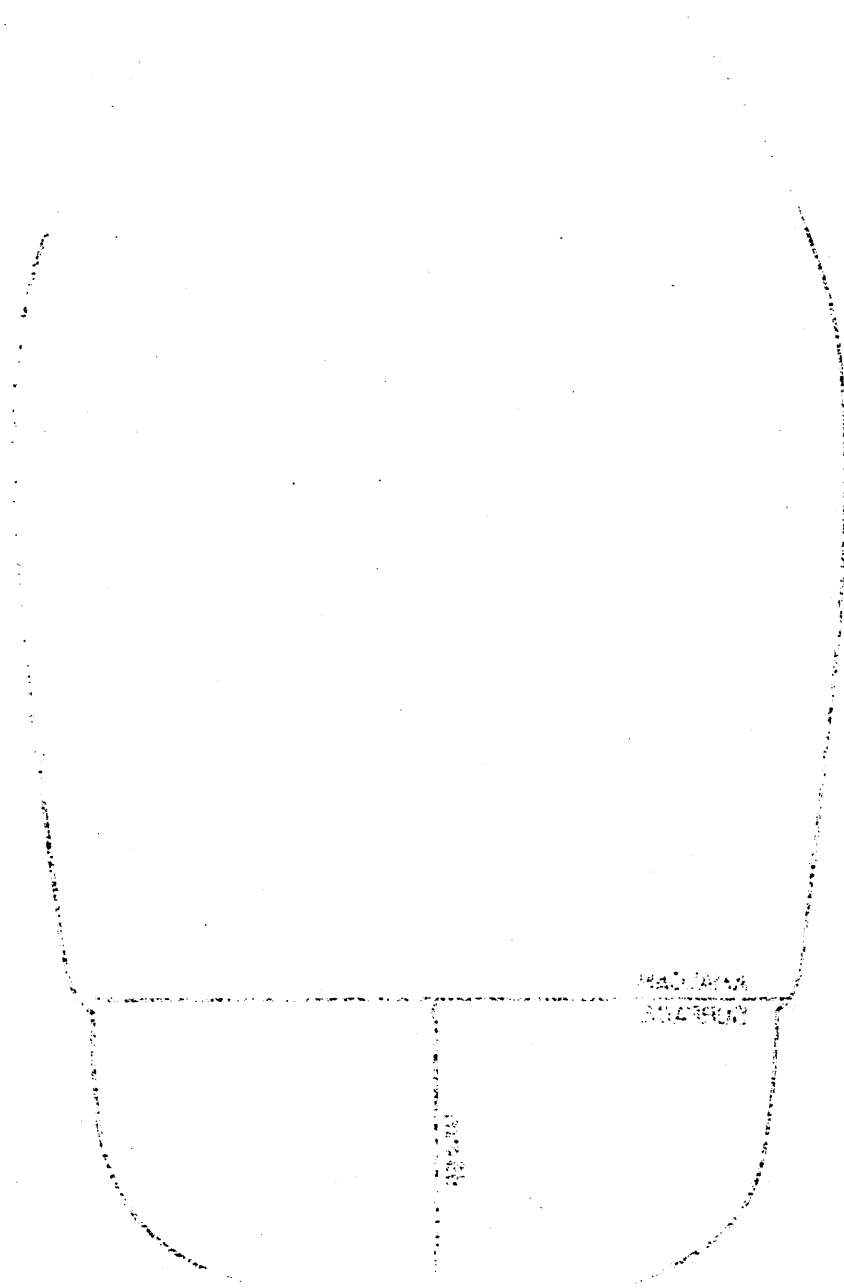


PLATE 15

A general view of the model converter and ancillary equipment.







1917-18-19-20-21-22-23-24-25-26-27-28-29-30-31-32-33-34-35-36-37-38-39-40-41-42-43-44-45-46-47-48-49-50-51-52-53-54-55-56-57-58-59-60-61-62-63-64-65-66-67-68-69-70-71-72-73-74-75-76-77-78-79-80-81-82-83-84-85-86-87-88-89-90-91-92-93-94-95-96-97-98-99-100

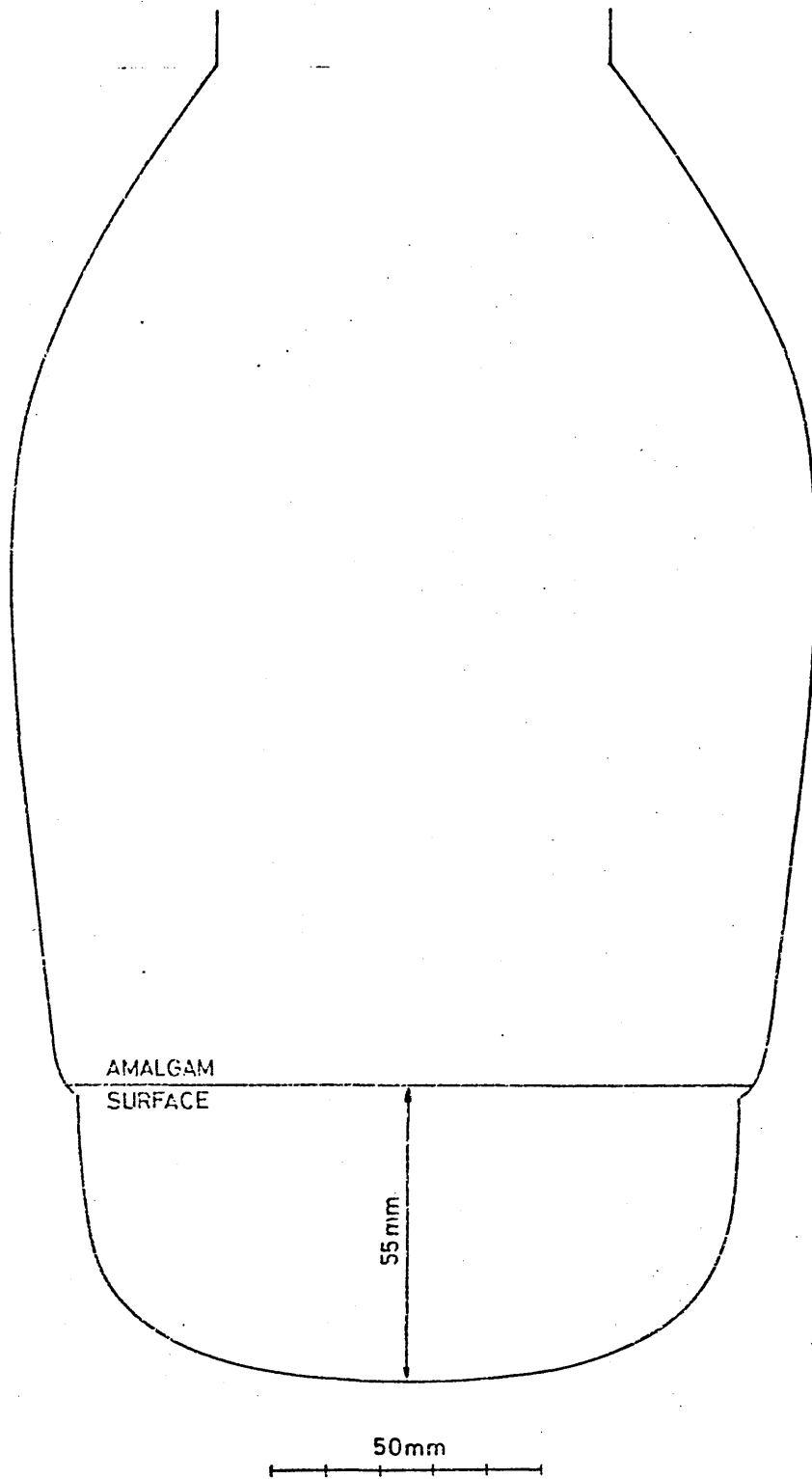


FIGURE 36 INTERNAL PROFILE OF MODEL CONVERTER VESSEL.

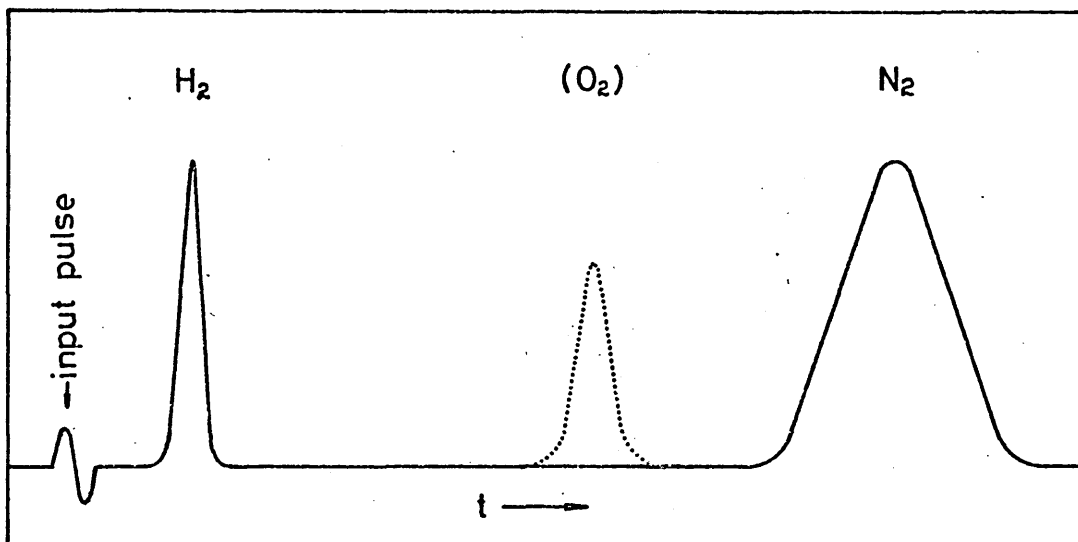
Table 8

Optimum operating conditions for Mini I chromatograph

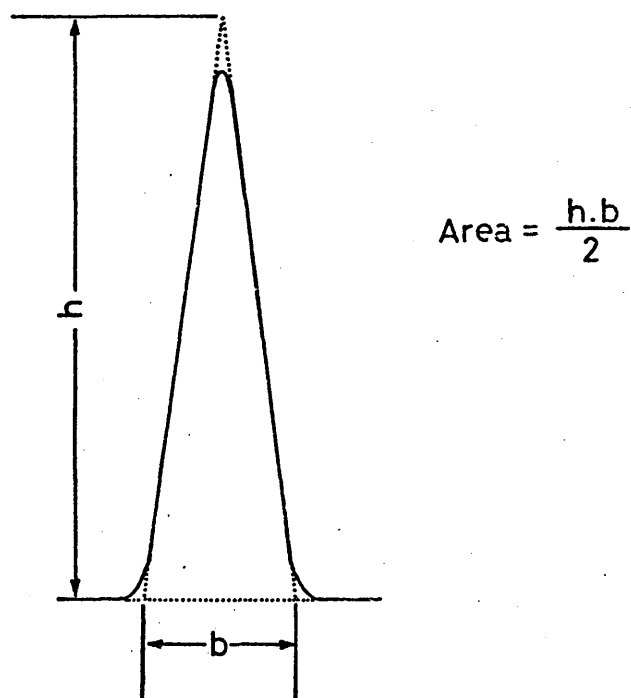
Carrier gas:	Argon
Pressure in carrier gas line:	0.7 kg/cm ² (10 lb f/in ²)
Initial flushing period:	20 minutes
Active column:	5A molecular sieve
Argon flow rate:	47 cm ³ /min
Bridge current:	5 m.a.
Sensitivity:	x 32 or x 64
Output:	0 - 1 mv
Chart recorder:	Honeywell Elektronik 194
Range:	0 - 1 mv
Chart speed:	1 mm/ second

Figure 37

(a) Typical analysis trace from gas chromatograph.



(b) Method of determining area under hydrogen peak .



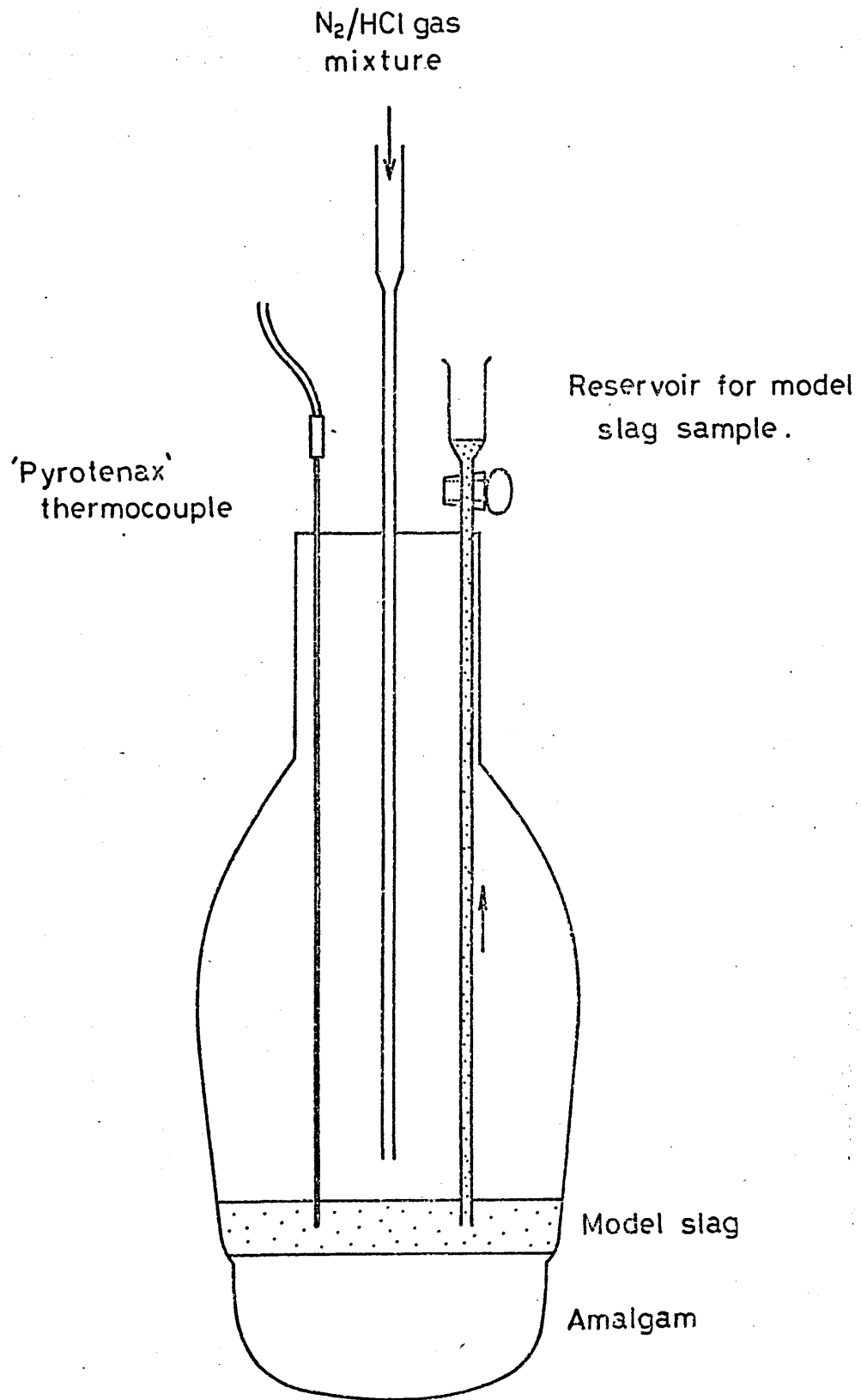
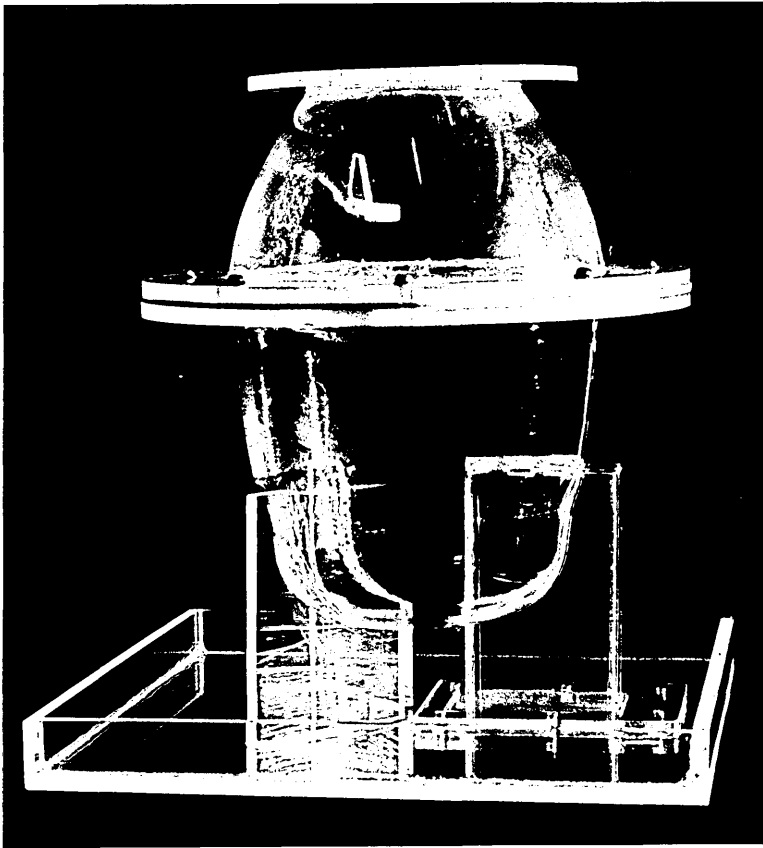


Figure 38 Modified vessel for 'slag' sampling experiments.

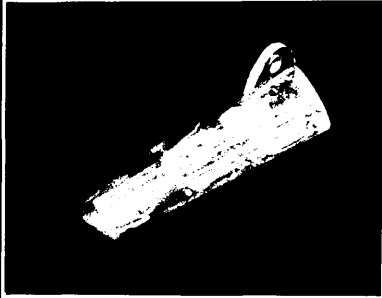
PLATE 17

Various views of the modified converter vessel used to investigate the droplet splashing rate.

- (a) A general view of the assembled vessel.
- (b) A view into the lower section of the vessel showing the droplet trap.
- (c) The lid which covers the droplet trap.



a

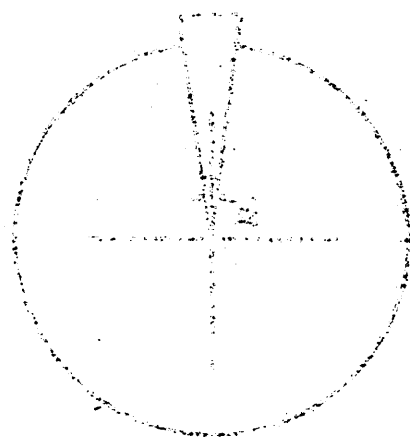


c

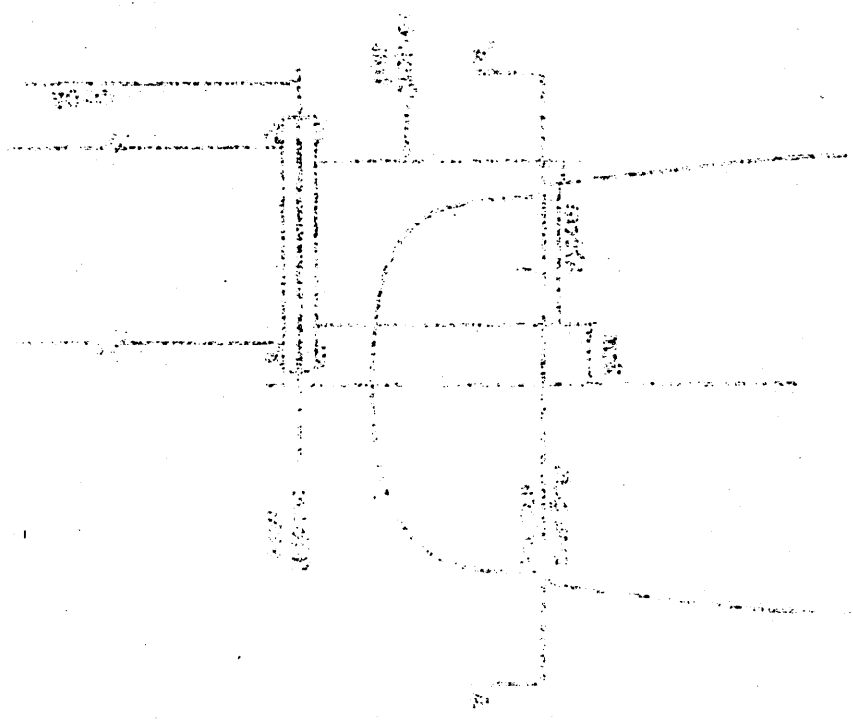


b

PROJEKTIONEN
PROJEKTIONEN



PROJEKTIONEN



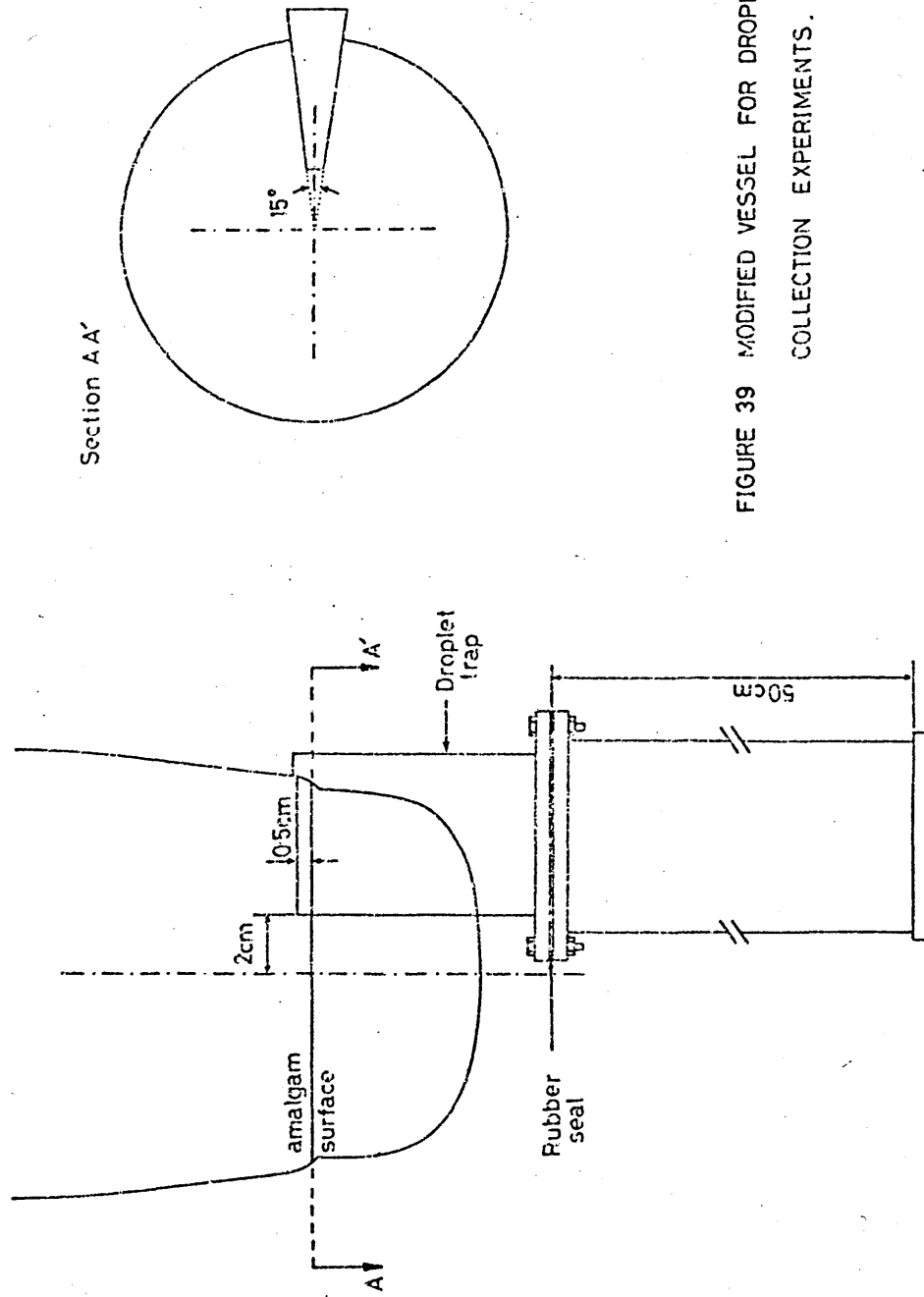


FIGURE 39 MODIFIED VESSEL FOR DROPLET
COLLECTION EXPERIMENTS.

PLATE 18

A general view of the assembled apparatus used to determine the splashing rate within the model converter vessel.

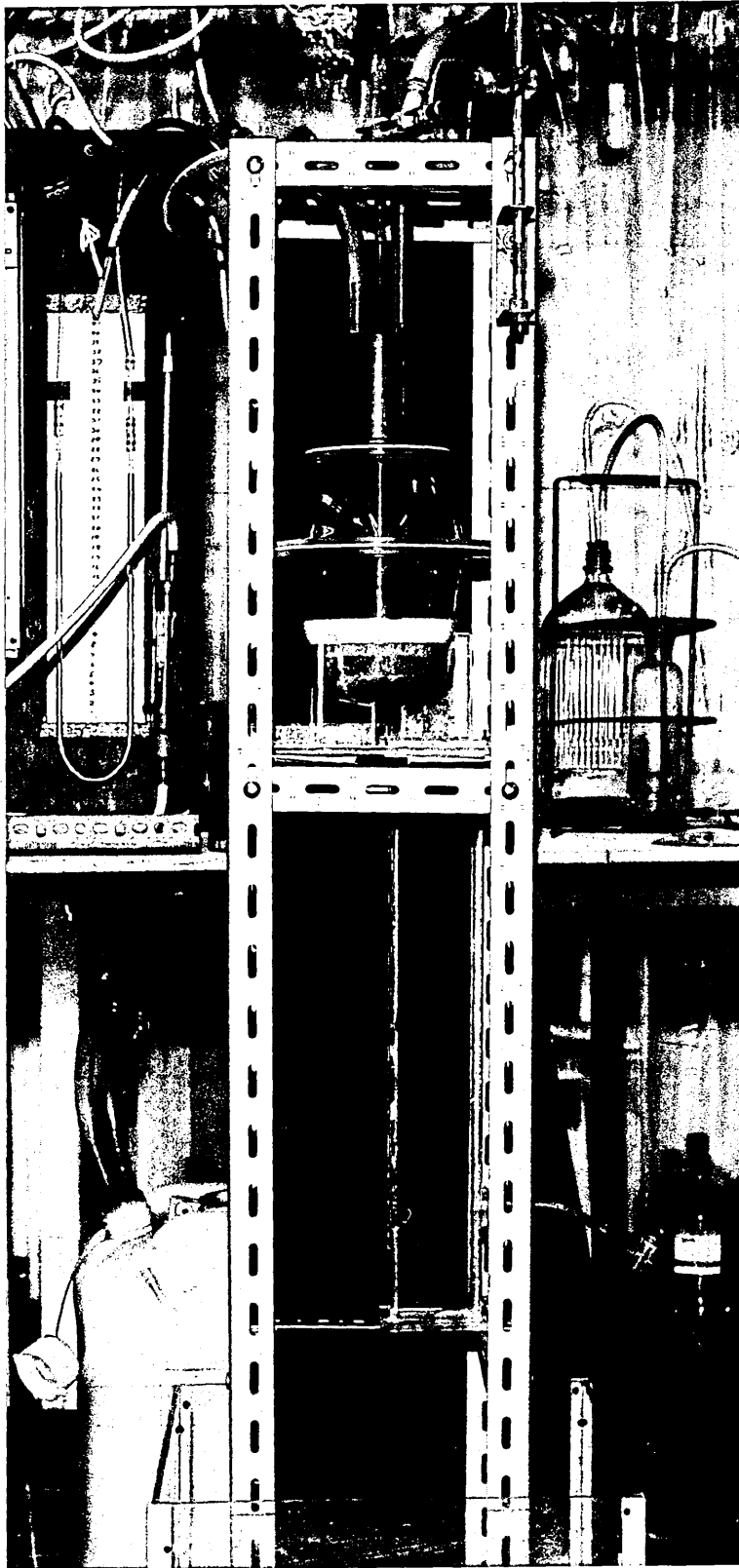


PLATE 19

A series of photographs illustrating the progress of a typical experiment.

(a) The model converter just before the start of the blow.

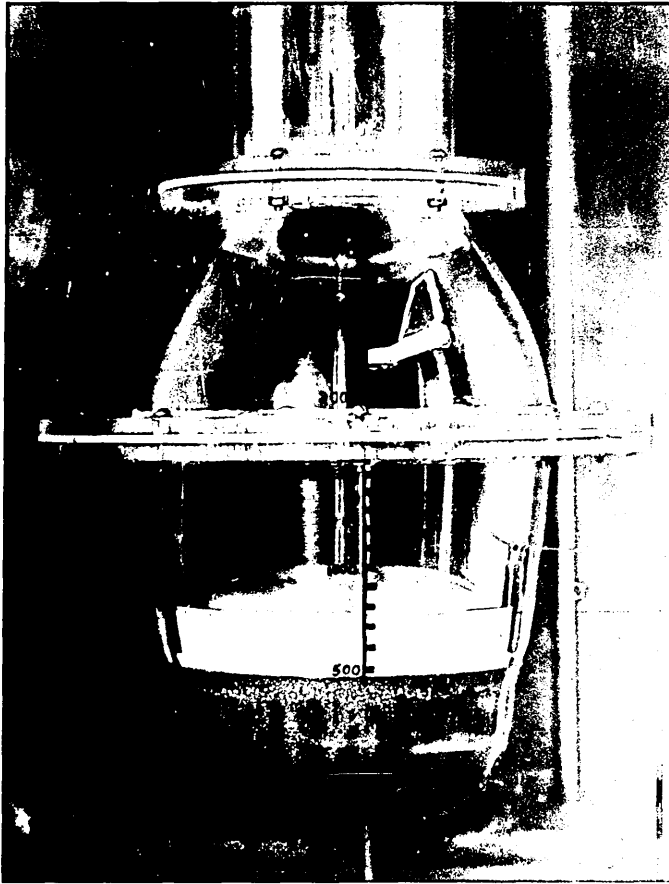
(b) The N_2/HCl gas mixture being introduced through the lance at the start of the experiment.

(c) Showing the extent of foam formation after about $1\frac{1}{2}$ minutes.

(d) The foam reaches a maximum volume after about 3 minutes.

(e) Showing the model converter just prior to terminating the experiment after 6 minutes blowing.

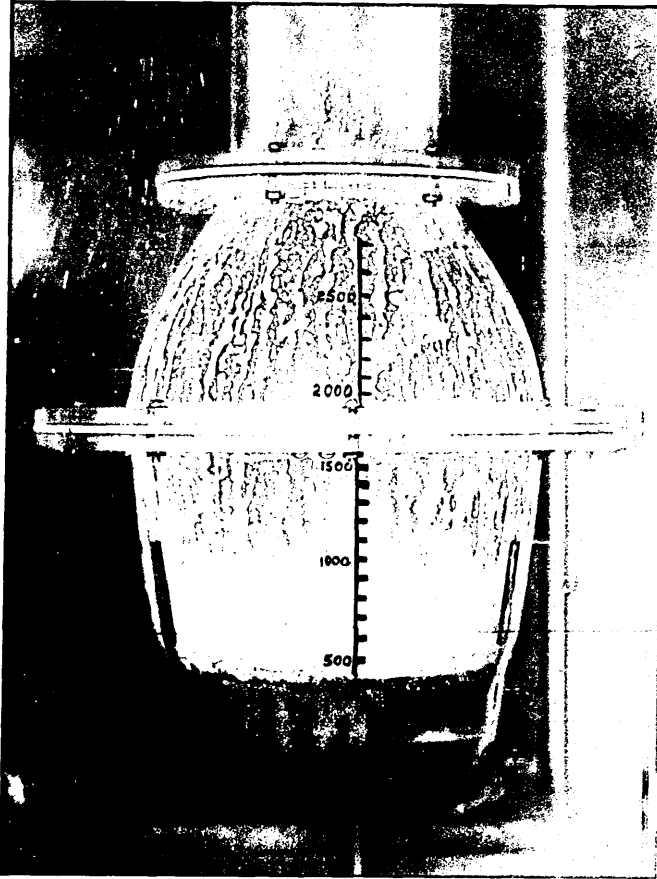
(f) About 20 seconds after terminating the blow.



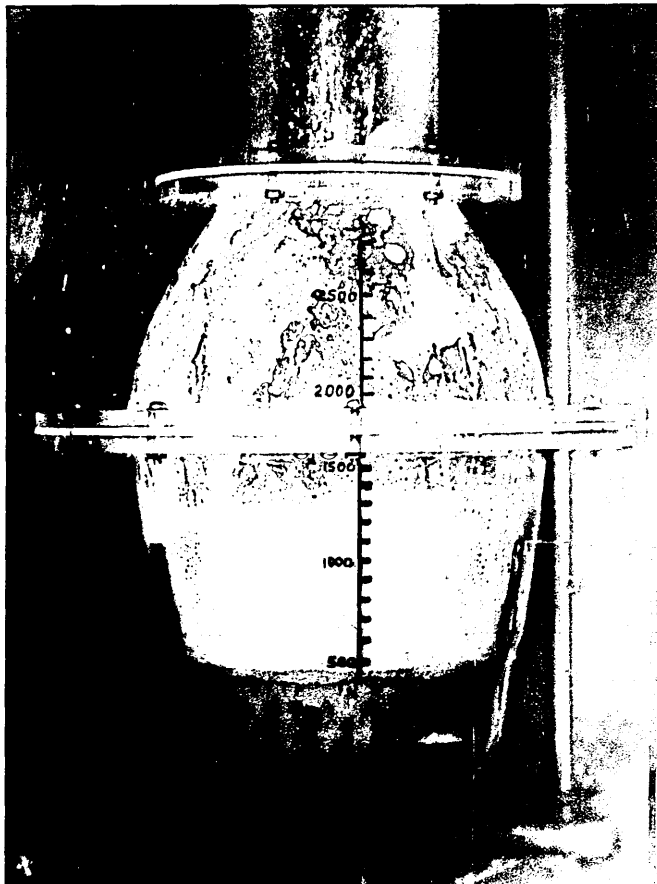
a



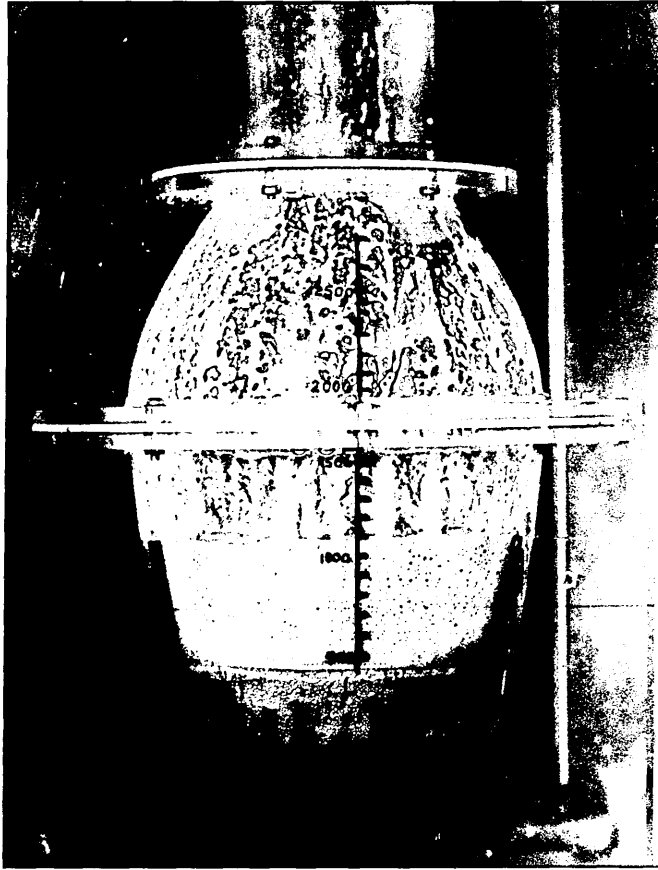
b



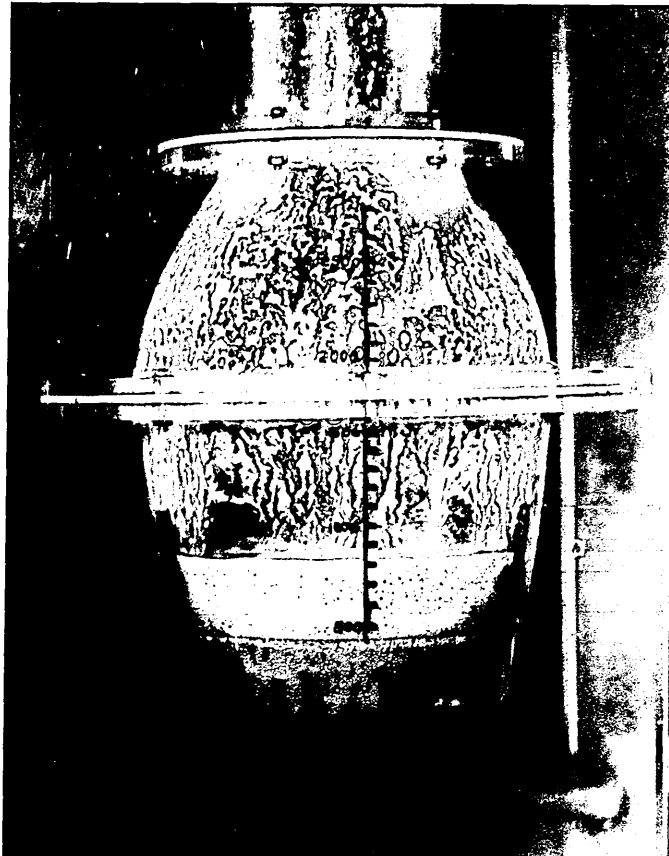
c



d



e



f

PLATE 20

This illustrates the effect of jetting only nitrogen gas onto the amalgam in the model converter.

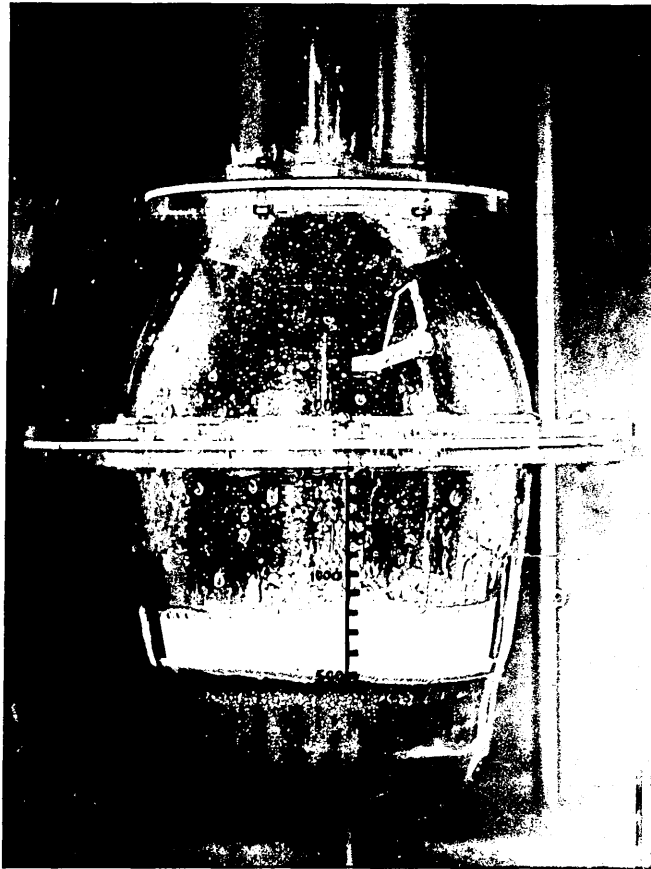
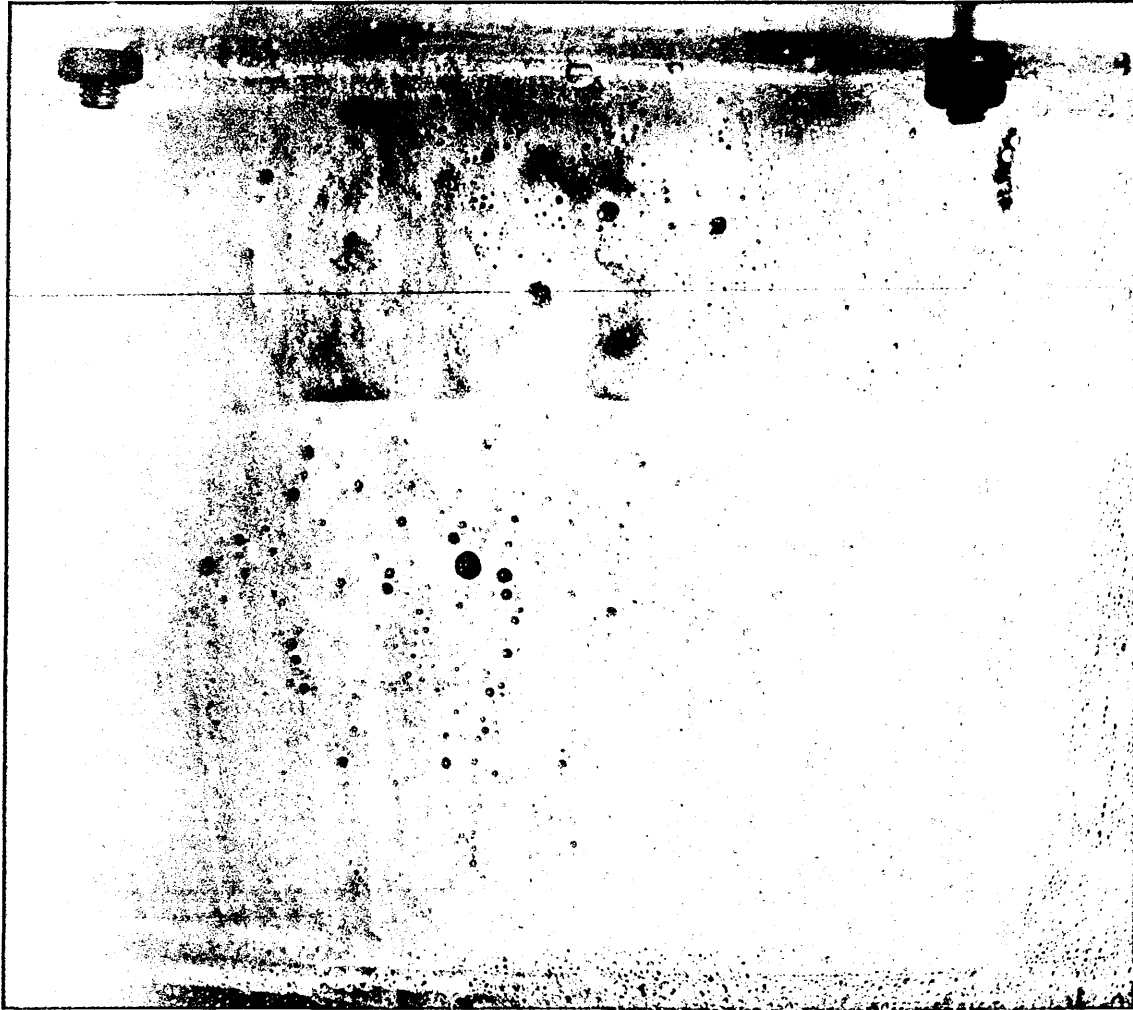


PLATE 21

Reacting amalgam droplets falling through the foam
layer inside the model converter.

1.5 x actual size



Account	Balance	Debit	Credit	Balance	Account
10000	10000			10000	10000
10001	10001			10001	10001
10002	10002			10002	10002
10003	10003			10003	10003
10004	10004			10004	10004
10005	10005			10005	10005
10006	10006			10006	10006
10007	10007			10007	10007
10008	10008			10008	10008
10009	10009			10009	10009
10010	10010			10010	10010
10011	10011			10011	10011
10012	10012			10012	10012
10013	10013			10013	10013
10014	10014			10014	10014
10015	10015			10015	10015
10016	10016			10016	10016
10017	10017			10017	10017
10018	10018			10018	10018
10019	10019			10019	10019
10020	10020			10020	10020

Account Name: [illegible]

[illegible text]

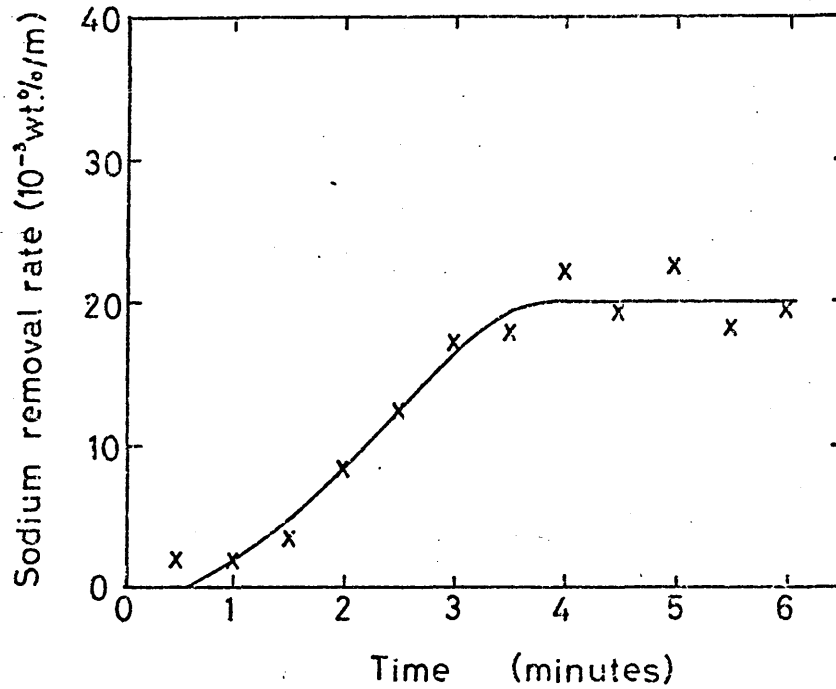
Table 9 - Summary of the experiments carried out to determine the effect of jet composition and jet momentum on the refining rate in the model convecter.

Lance height for all experiments: 2.5 mm

Figure No.	Initial Na in amalgam (wt. %)	Excess vessel pressure (atmospheres)	N ₂ flow rate (l/min. at S.T.P.)	HCl flow rate (l/min. at S.T.P.)	v.%HCl in jet gases	Jet momentum (mN)	Mean stage II refining rate (wt. % Na/min)	Estimated F M, II
40	0.57	0.037	50.2	3.9	7.2	76.8	0.0200	-
41 (72)	0.60	0.037	47.6	6.6	12.2	77.0	0.0311	-
42 (72)	0.61	0.037	47.6	6.6	12.2	77.0	0.0319	0.50
43	0.61	0.034	47.3	6.6	12.3	77.3	0.0344	-
44	0.60	0.037	46.1	7.9	14.6	77.6	0.0403	-
45 (50)	0.54	0.045	59.6	4.1	6.4	100.5	0.0267	0.69
46	0.59	0.040	57.9	6.0	9.4	101.5	0.0373	-
47	0.60	0.040	56.7	7.2	11.3	102.0	0.0405	-
54	0.59	0.040	58.7	8.3	12.4	113.0	0.0465	-
74	0.60	0.038	57.4	8.1	12.4	105.0	0.0465	-
48 (50)	0.58	0.042	55.6	8.4	13.1	102.5	0.0473	0.65

Figure 40 Refining behaviour of model converter using a gas jet containing 7.2 v% HCl with a momentum of 77 mN. (For additional information see table 9.)

(a) Rate of sodium removal from amalgam bath.



(b) Foam volume.

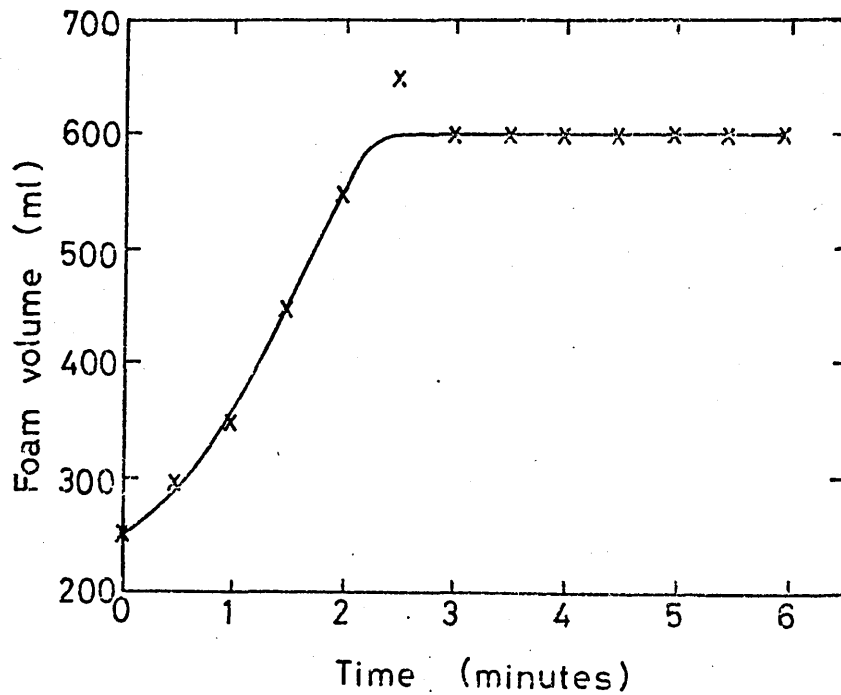
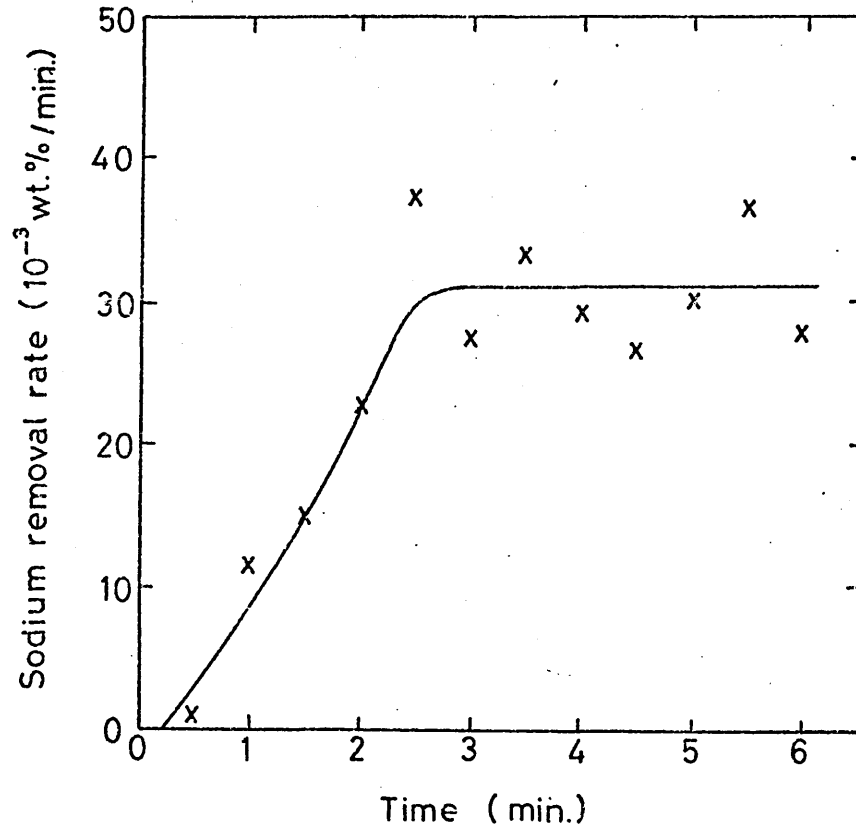


Figure 41 Refining behaviour of model converter using a gas jet containing 12.2 v.% HCl with a momentum of 77 mN. (For additional information see table 9)

(a) Rate of sodium removal from amalgam bath.



(b) Foam volume

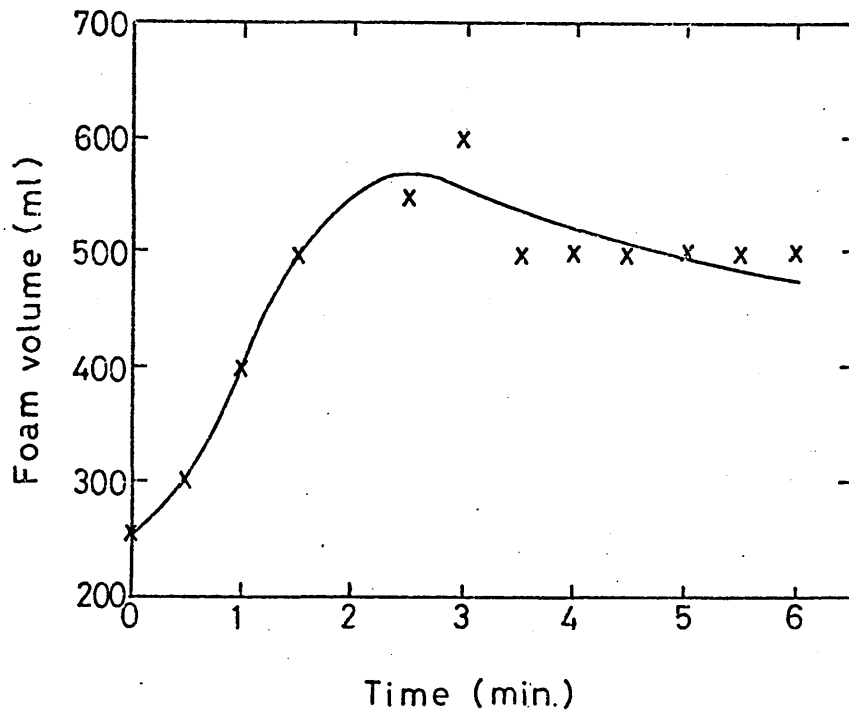
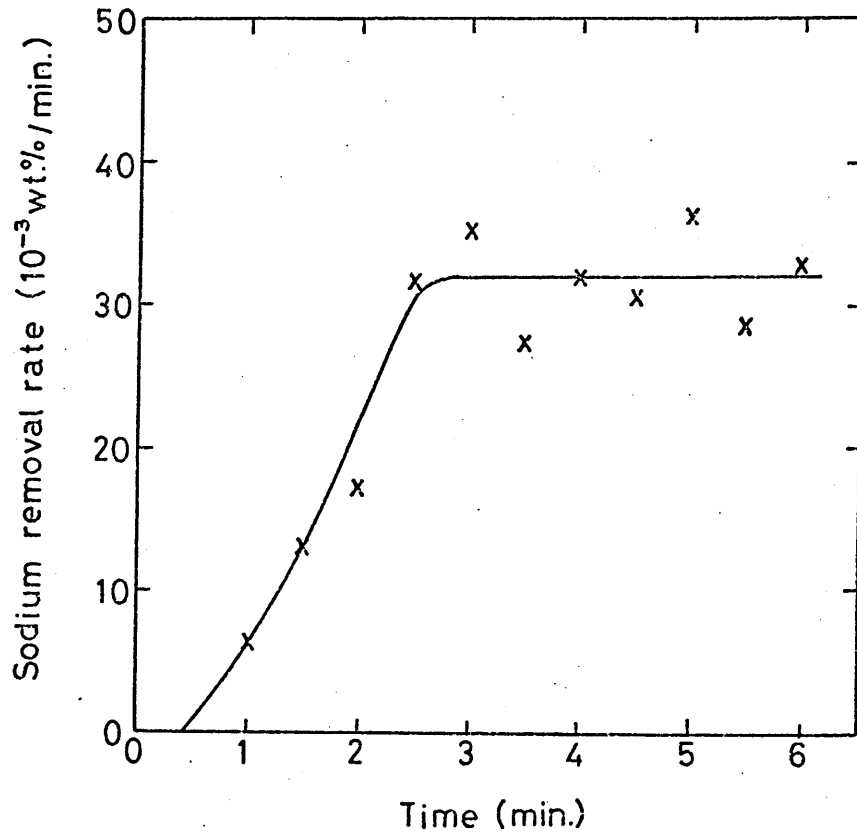


Figure 42 Refining behaviour of model converter using a gas jet containing 12.2v.%HCl with a momentum of 77mN.
(For additional information see table 9)

(a) Rate of sodium removal from amalgam bath.



(b) Foam volume.

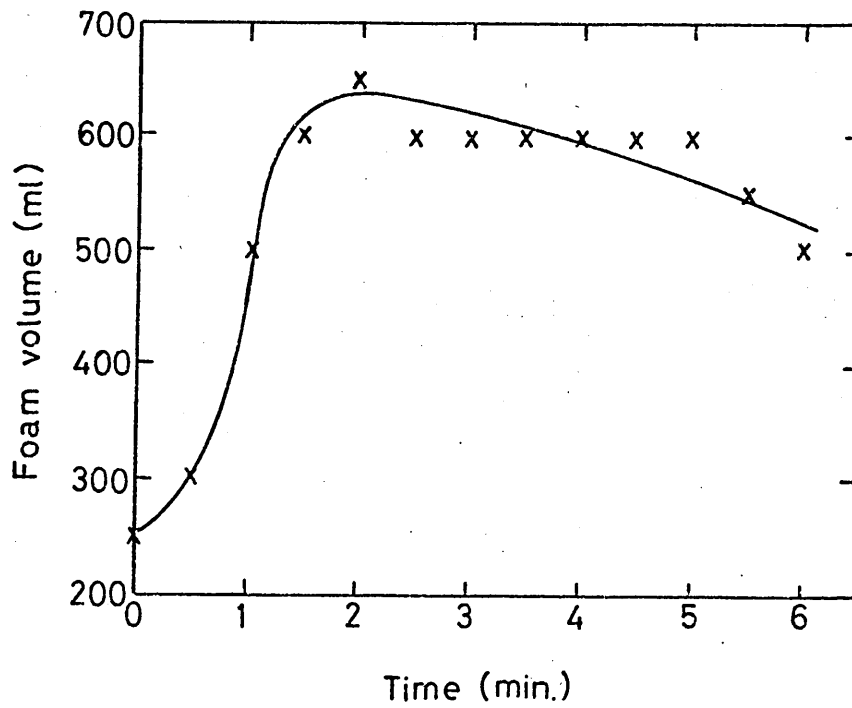
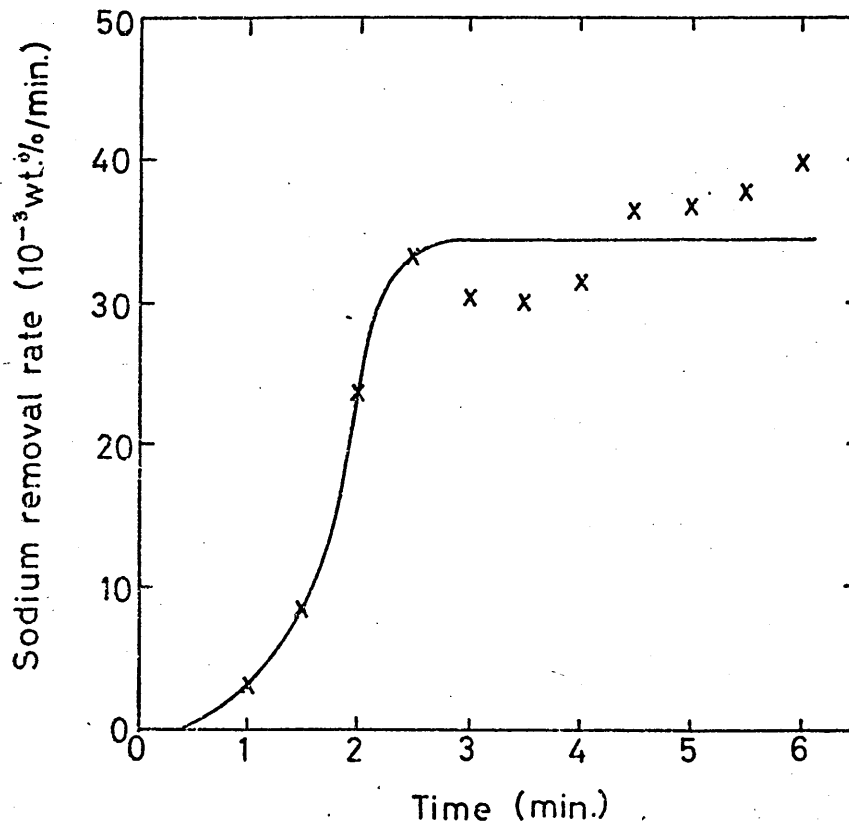


Figure 43 Refining behaviour of model converter using a gas jet containing 12.3 v% HCl with a momentum of 77 mN.
(For additional information see table 9)

(a) Rate of sodium removal from amalgam bath.



(b) Foam volume.

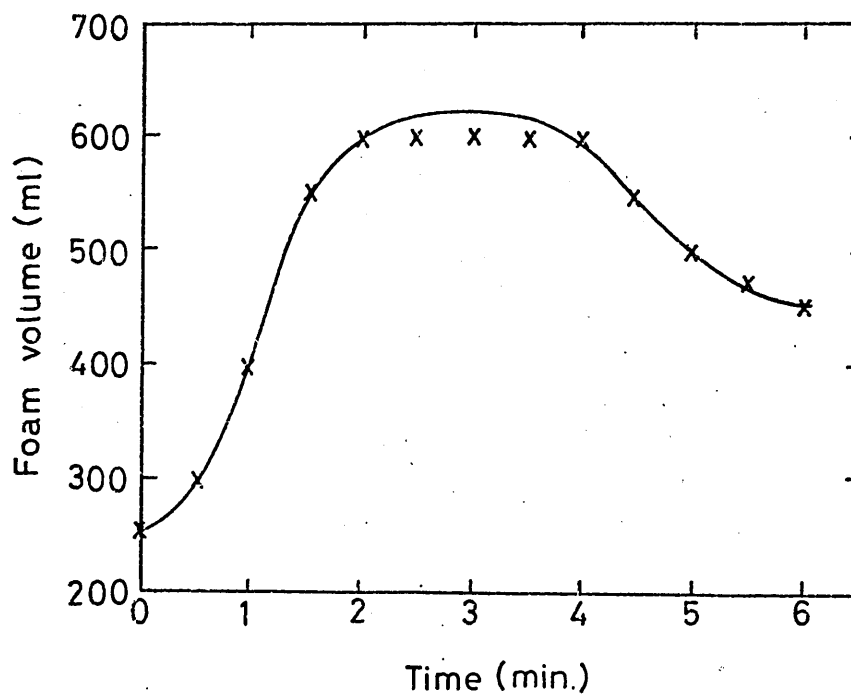
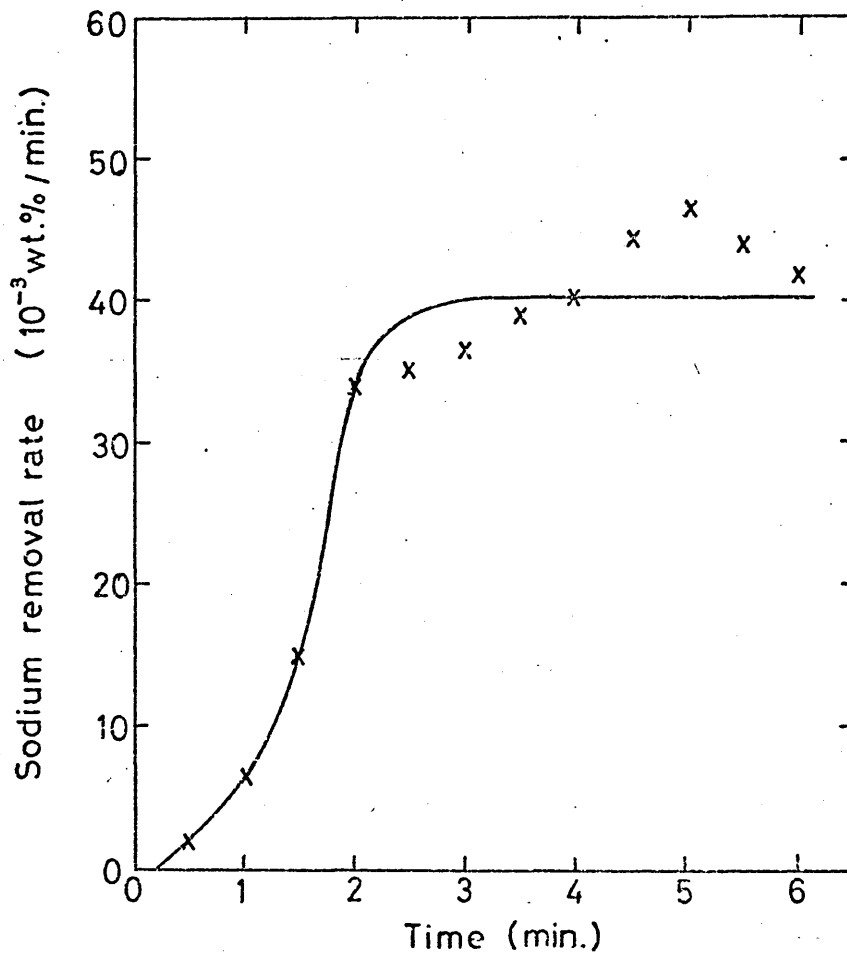


Figure 44 Refining behaviour of model converter using a gas jet containing 14.6v.%HCl with a momentum of 77mN .
(For additional information see table 9)

(a) Rate of sodium removal from amalgam bath.



(b) Foam volume.

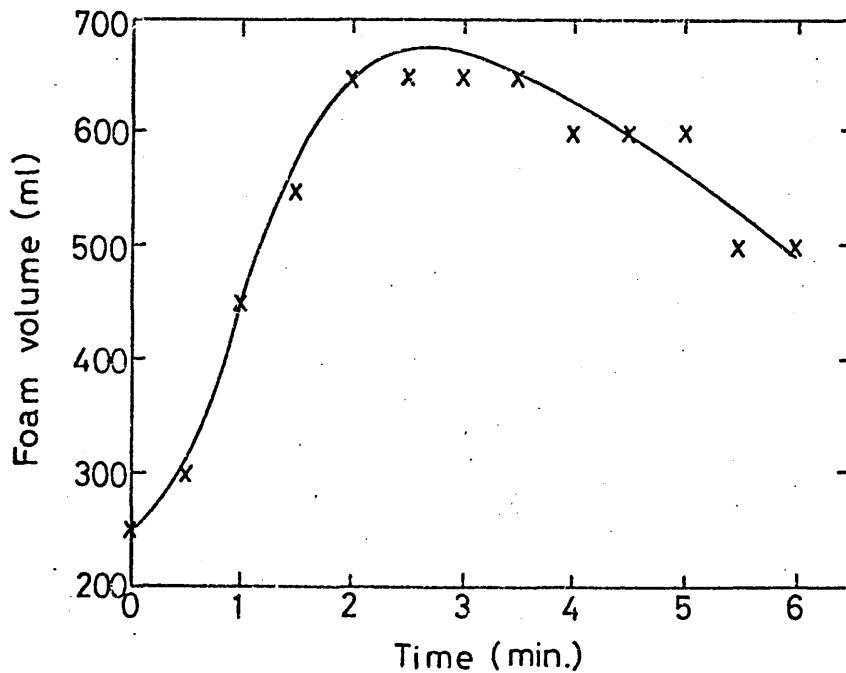
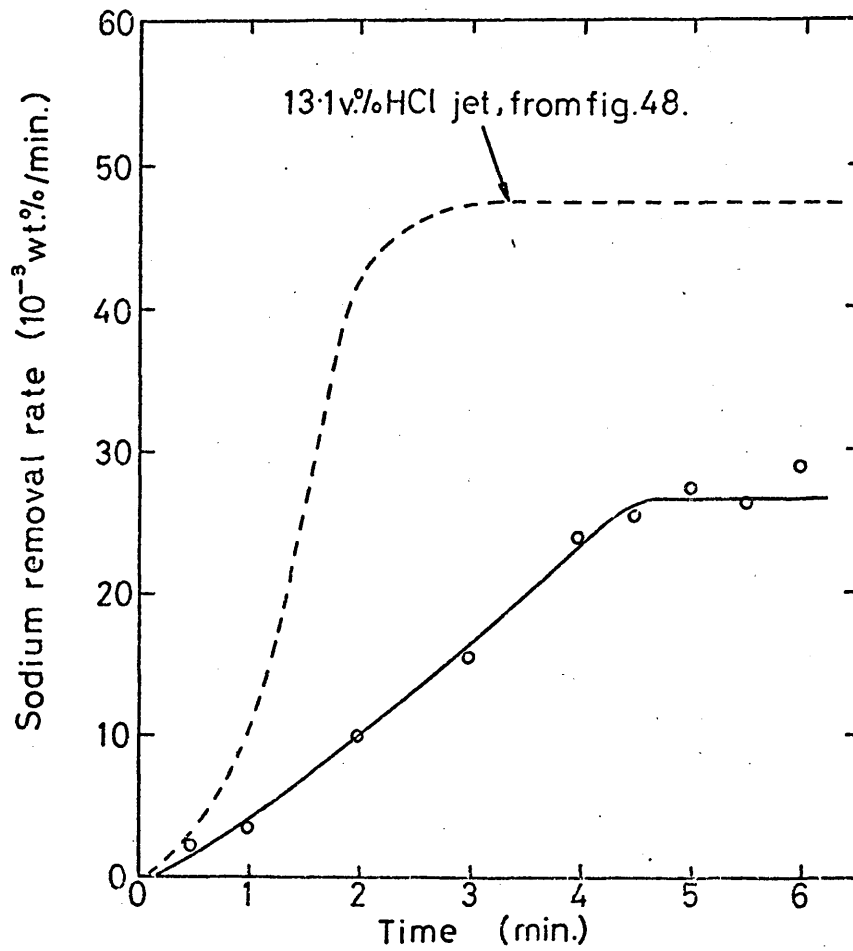


Figure 45 Refining behaviour of model converter using a gas jet containing 6.4v% HCl with a momentum of 102 mN.
(For additional information see table 9)

(a) Rate of sodium removal from amalgam bath.



(b) Foam volume.

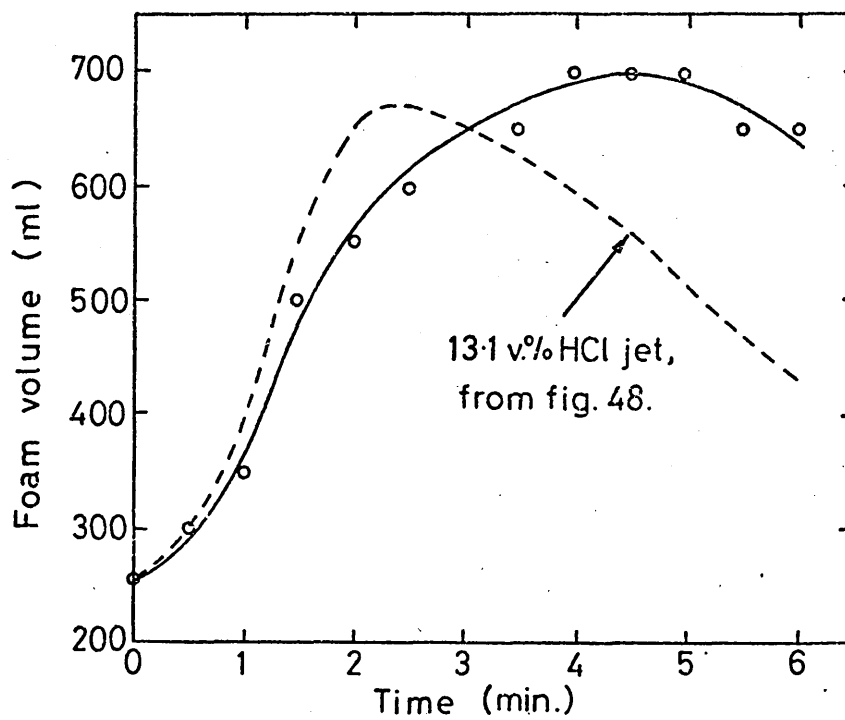
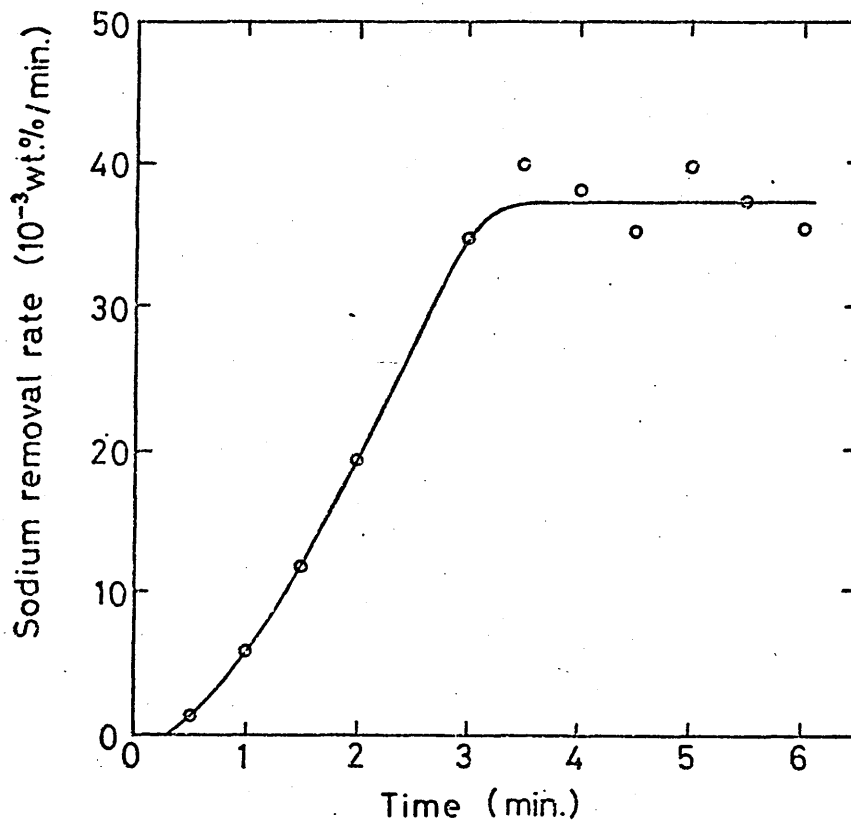


Figure 46 Refining behaviour of model converter using a gas jet containing 9.4v.%HCl with a momentum of 102mN. (For additional information see table 9.)

(a) Rate of sodium removal from amalgam bath.



(b) Foam volume.

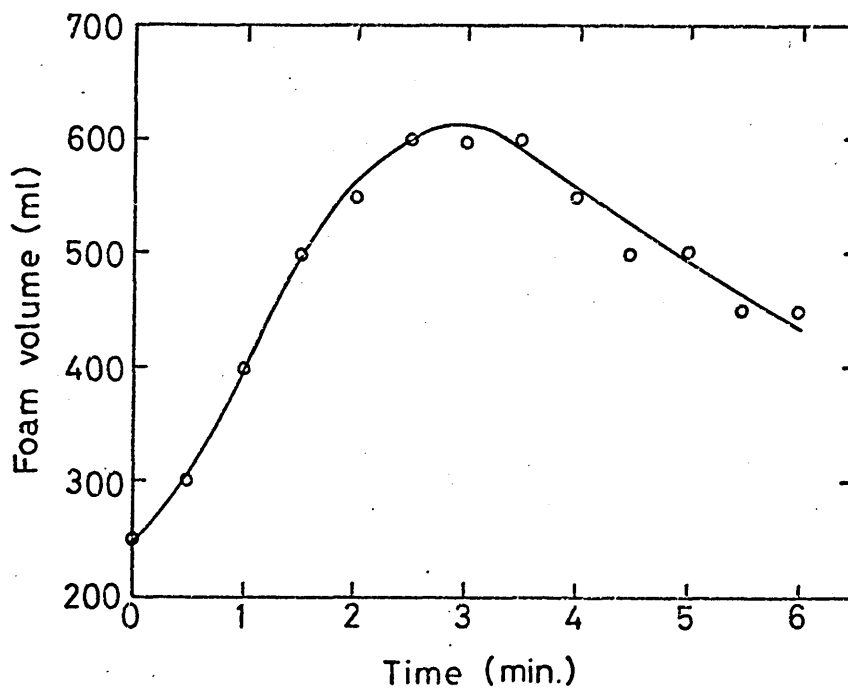
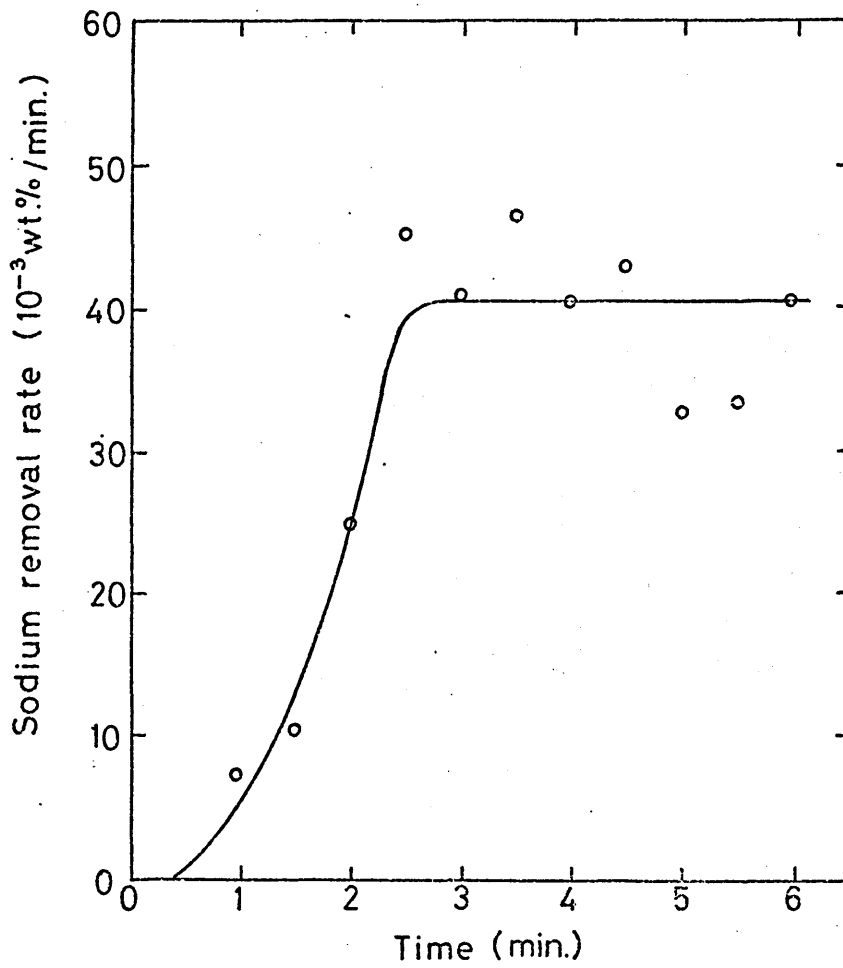


Figure 47 Refining behaviour of model converter using a gas jet containing 11.3 v.% HCl with a momentum of 102 mN. (For additional information see table 9.)

(a) Rate of sodium removal from amalgam bath.



(b) Foam volume.

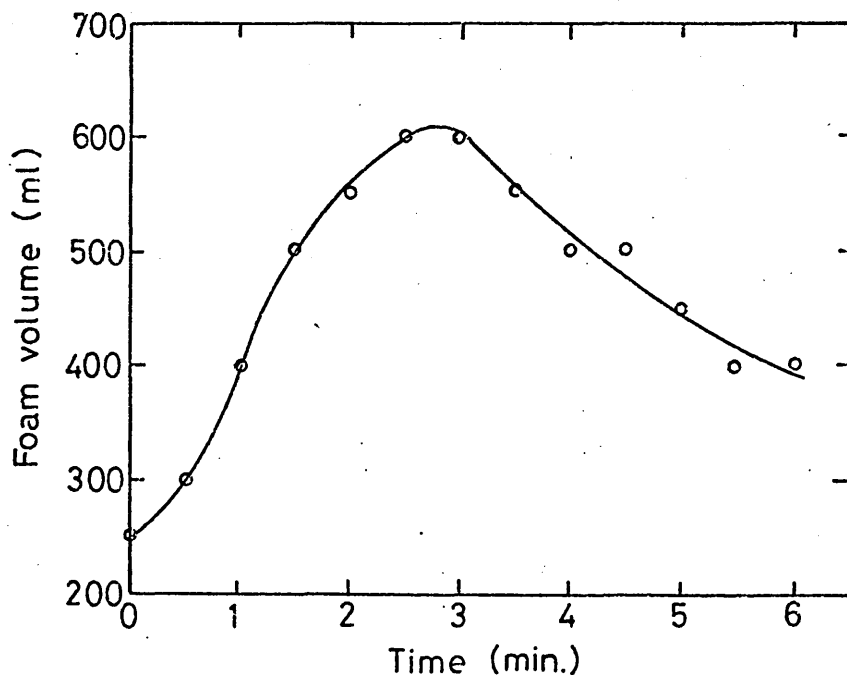
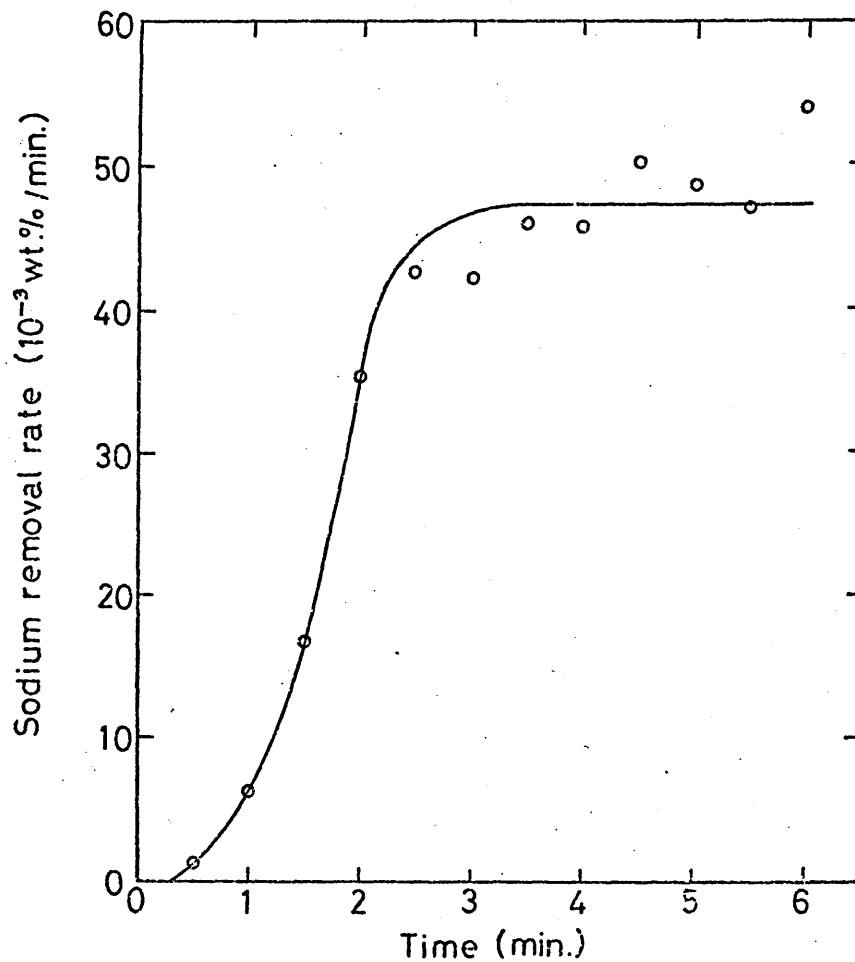


Figure 48 Refining behaviour of model converter using a gas jet containing 13.1v.% HCl with a momentum of 102 mN. (For additional information see table 9.)

(a) Rate of sodium removal from amalgam bath.



(b) Foam volume.

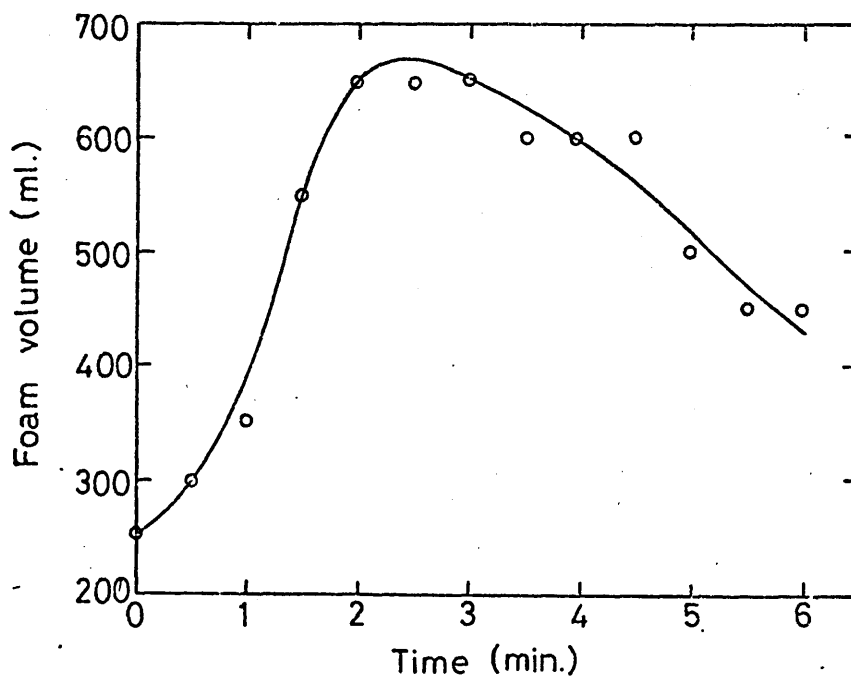
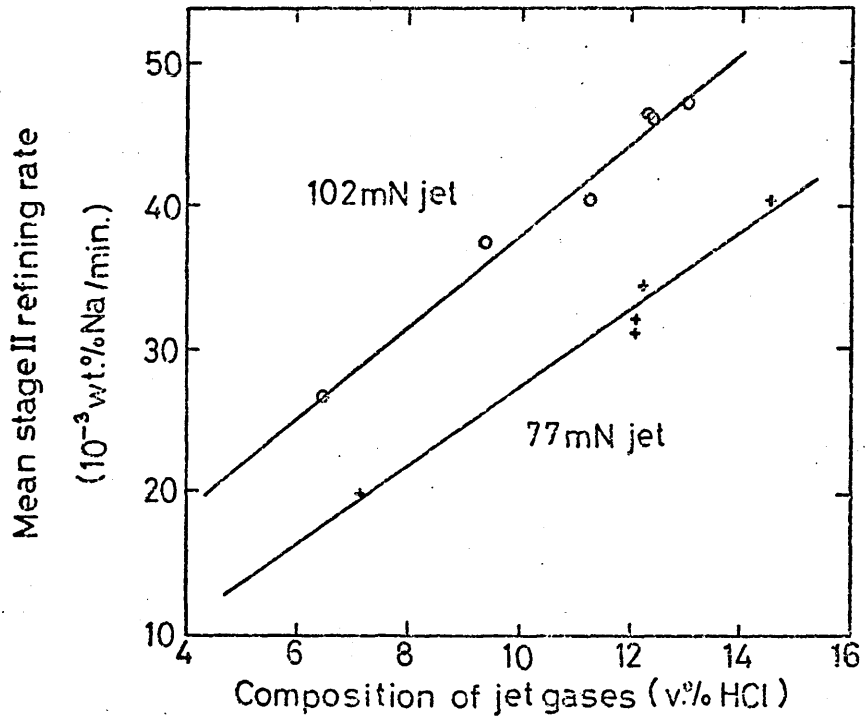


Figure 49 The effect of jet composition and jet momentum on the mean stage II rate of sodium removal from the amalgam bath.

(a) Refining rate versus jet composition.



(b) Refining rate versus the volumetric flow rate of hydrogen chloride into the reaction vessel.

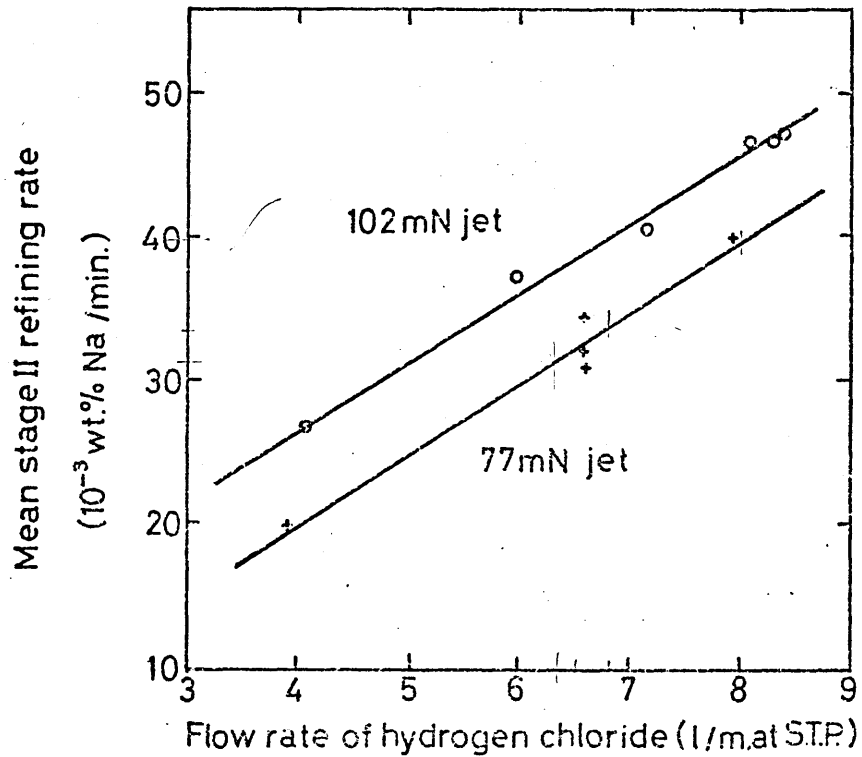
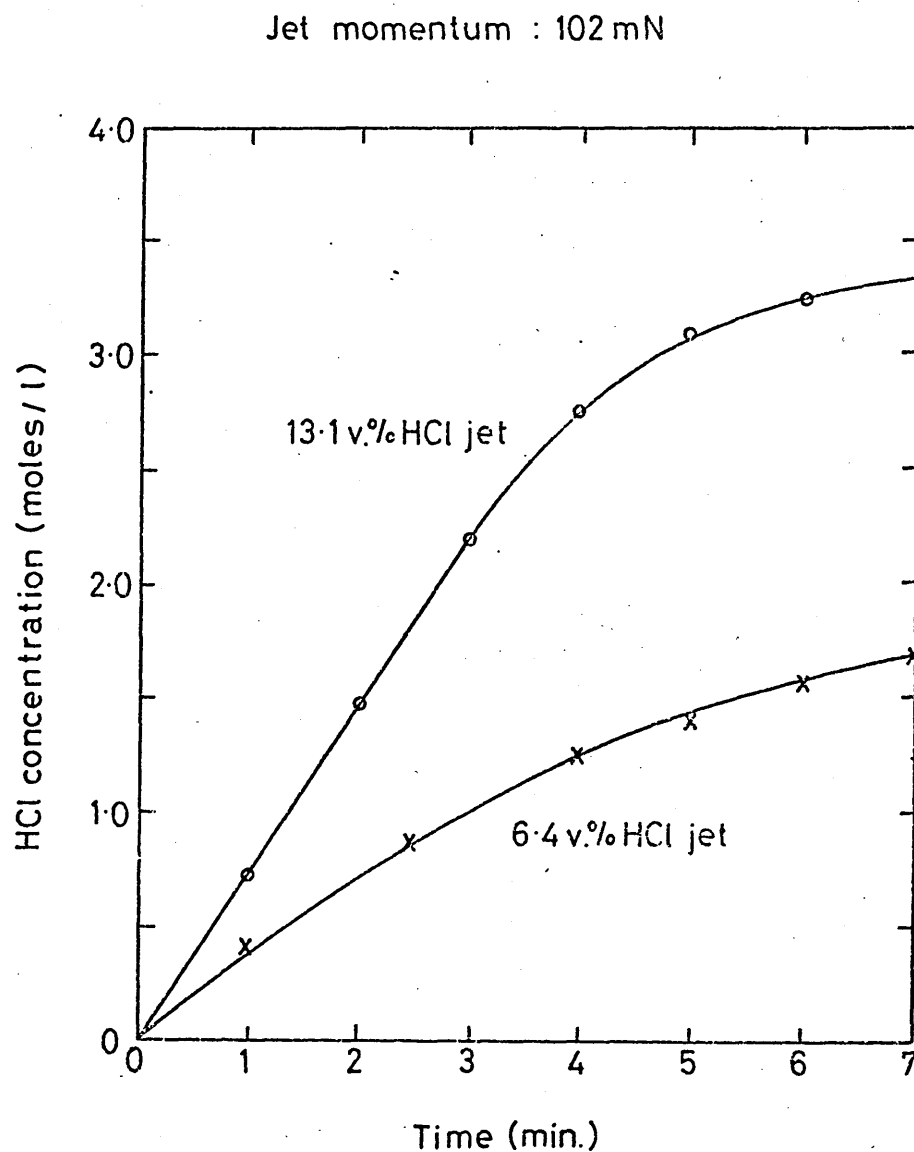


Figure 50 The effect of jet composition on the acid concentration in the model slag during a blow.



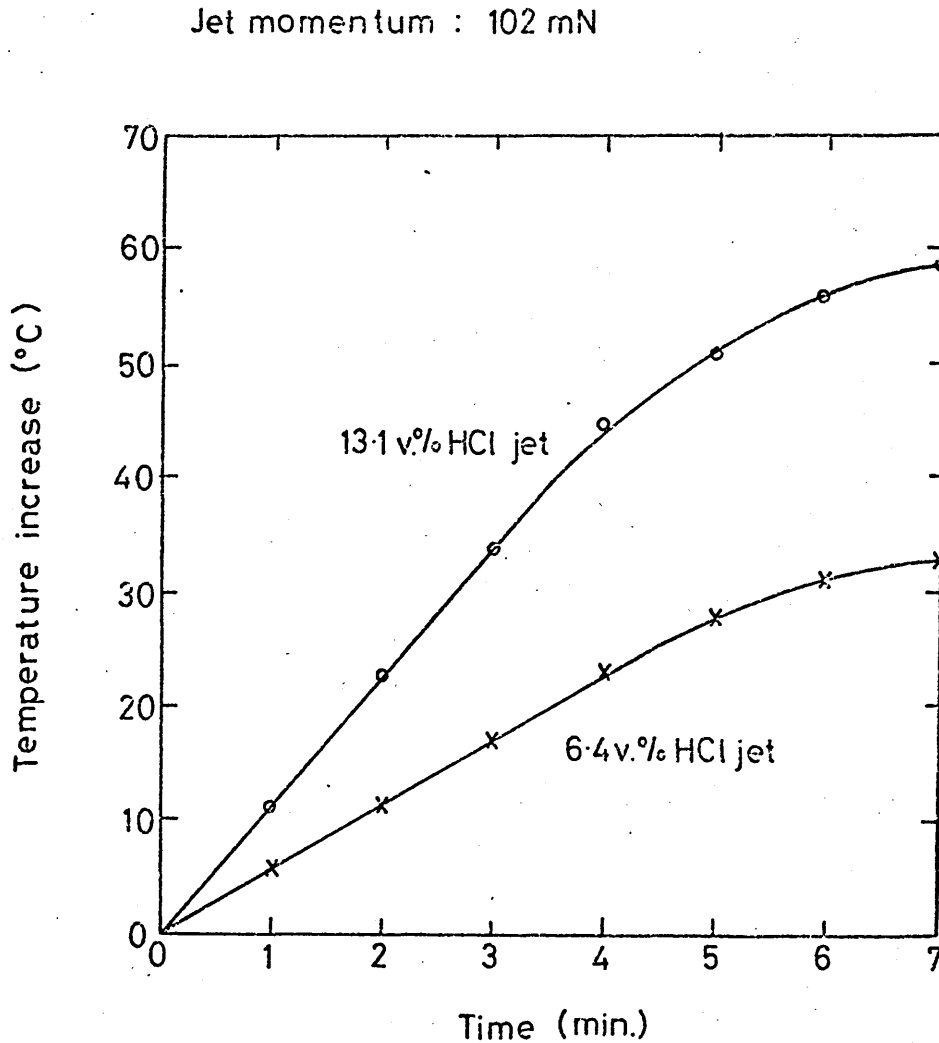
(a) 6.4 v.% HCl jet :- Blowing conditions as for fig. 45 (table 9).

Initial composition of amalgam : 0.57 wt% Na.

(b) 13.1 v.% HCl jet :- Blowing conditions as for fig. 48 (table 9).

Initial composition of amalgam : 0.54 wt% Na.

Figure 51 The effect of jet composition on the temperature of the model slag during a blow.



(a) 6.4 v.% HCl jet :- Blowing conditions as for fig. 45 (table 9).
Initial composition of amalgam : 0.57 wt.% Na.
Initial temperature of model slag : 15° C .

(b) 13.1 v.% HCl jet :- Blowing conditions as for fig. 48 (table 9).
Initial composition of amalgam : 0.54 wt.% Na.
Initial temperature of model slag : 12° C .

Figure 52 The effect of lance height and jet momentum on the rate of splashing from the amalgam bath .

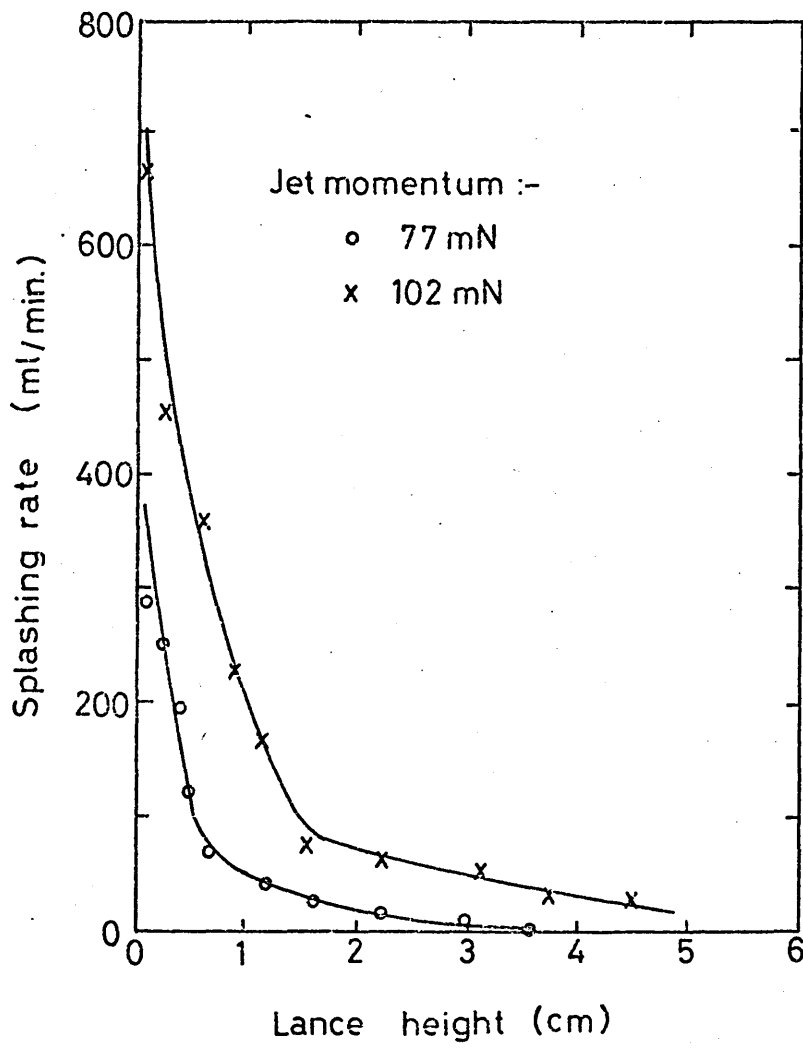


PLATE 22

Amalgam droplets falling down the column below the collection trap, in the modified vessel shown in Plate 18.

2 x actual size

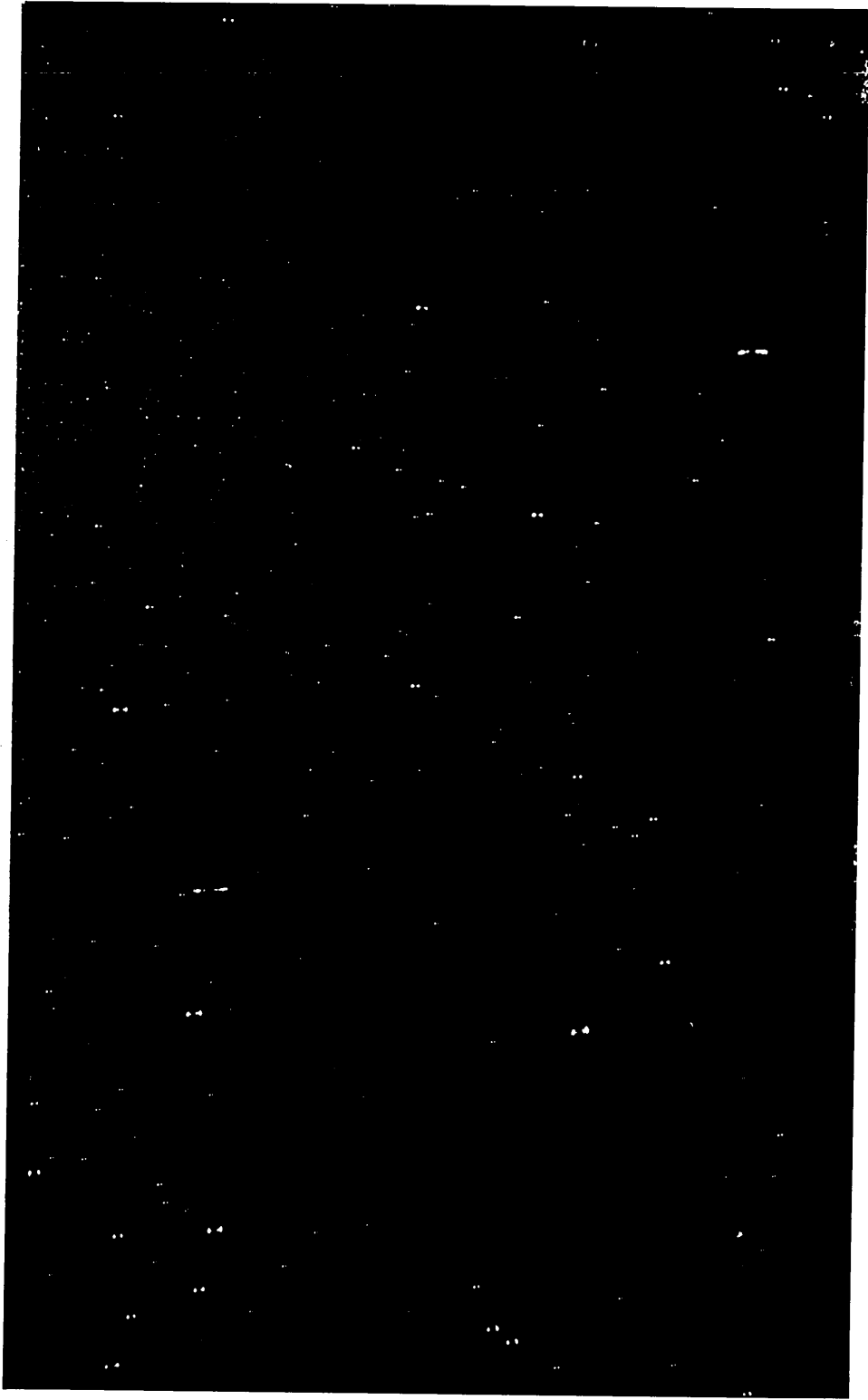
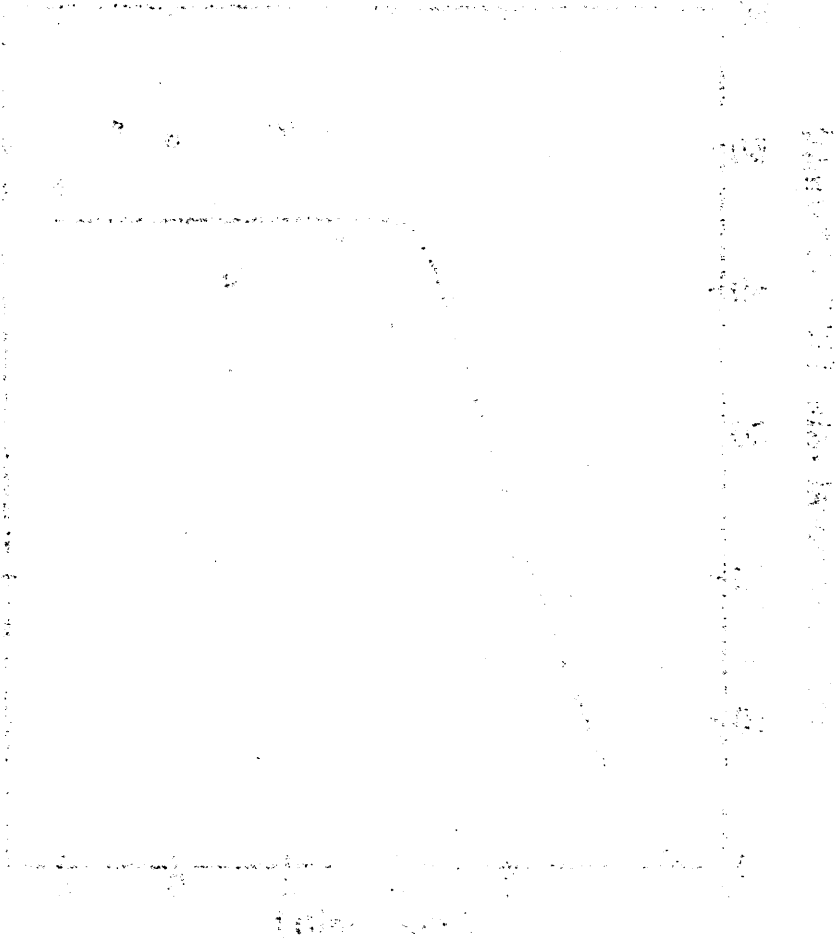


Table 10 - Summary of the experiments carried out to determine the effect of lance height on the refining rate in the model converter.

Nitrogen flow rate: 58.9 l/min. at S.T.P.
 Hydrogen chloride flow rate: 8.1 l/min. at S.T.P.
 Jet composition: 12.1 v. % HCl
 Jet momentum: 110 mN
 Excess vessel pressure: 0.038 atmospheres

Figure No	Initial Na in amalgam (wt.%)	Lance height (mm)	Mean stage II refining rate (wt.% Na/min.)	Estimated F M II
53	0.58	0	0.0454	-
54 (60)	0.59	2.5	0.0465	0.61
55	0.59	12.0	0.0396	-
56 (60)	0.59	21.0	0.0373	0.47
57	0.59	31.0	0.0330	-
58	0.59	44.0	0.0331	-

The temperature dependence of the rate of reaction



The effect of concentration on the rate of reaction

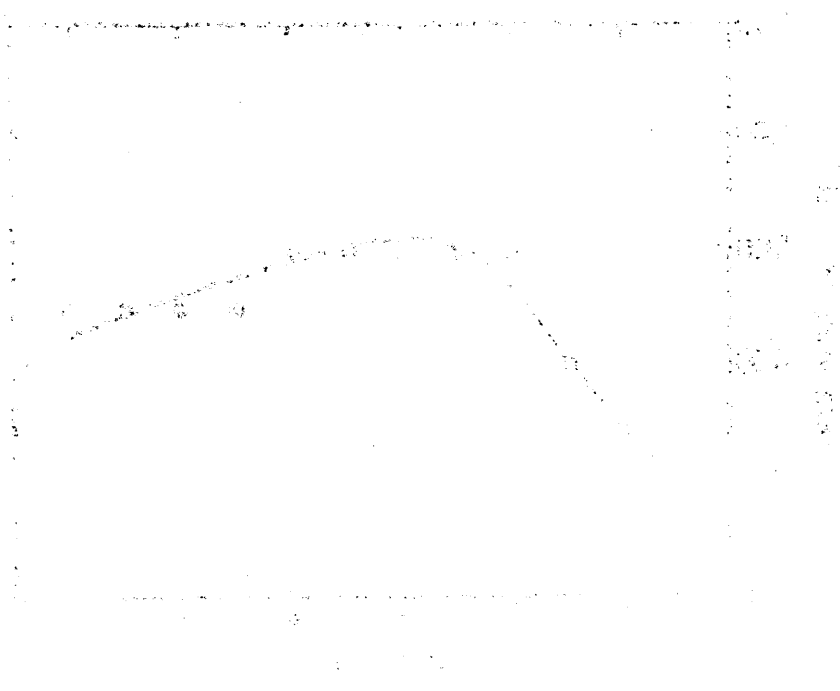
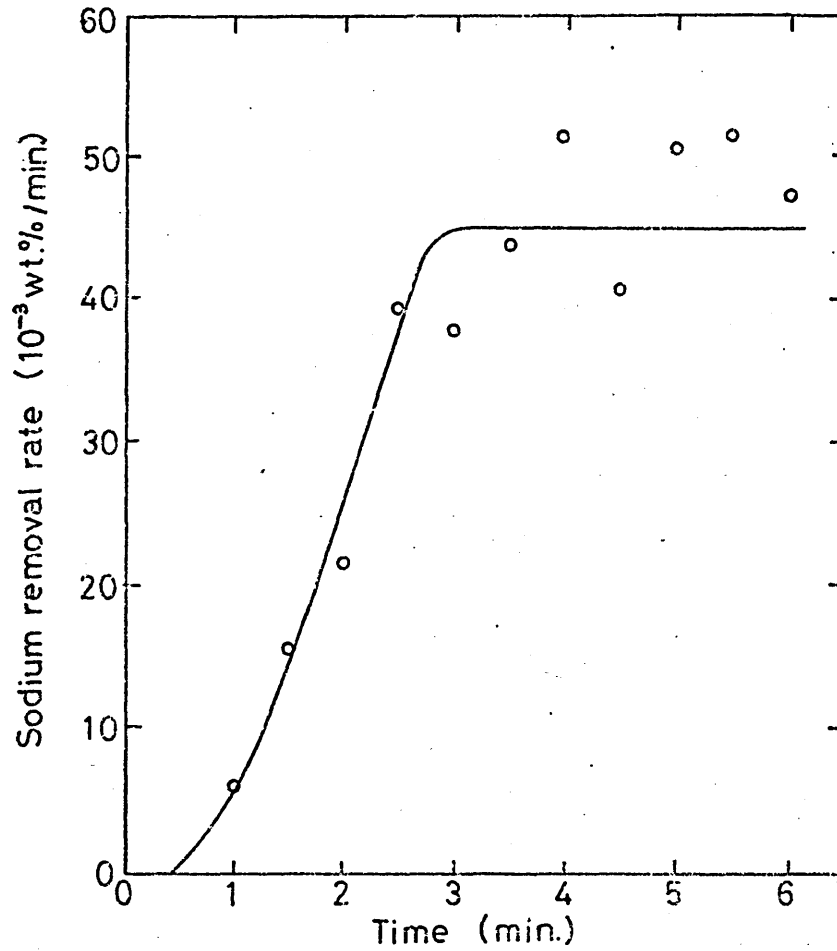


Figure 53 Refining behaviour when the lance tip is at the surface of the amalgam pool.

(For additional information see table 10.)

(a) Rate of sodium removal from amalgam bath.



(b) Foam volume.

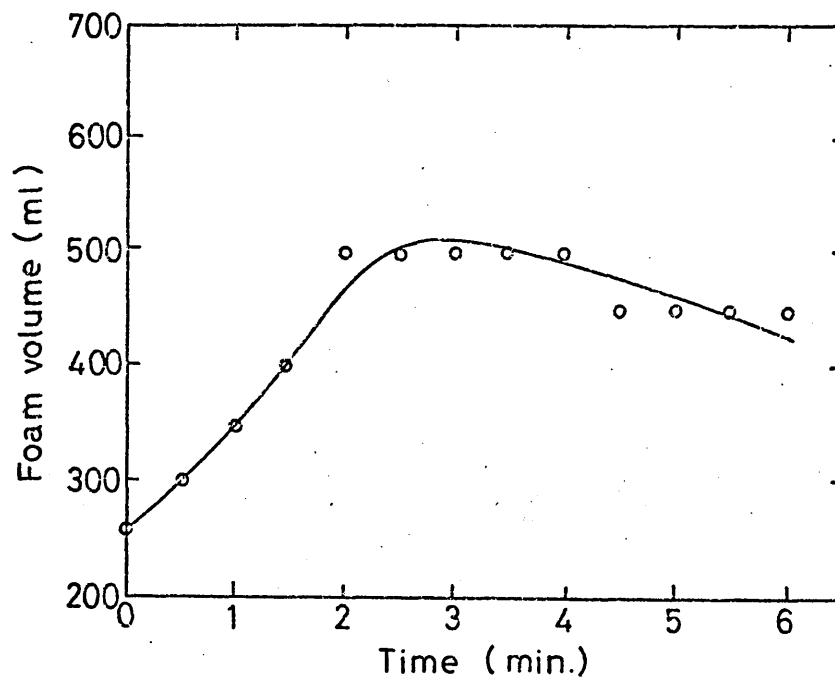
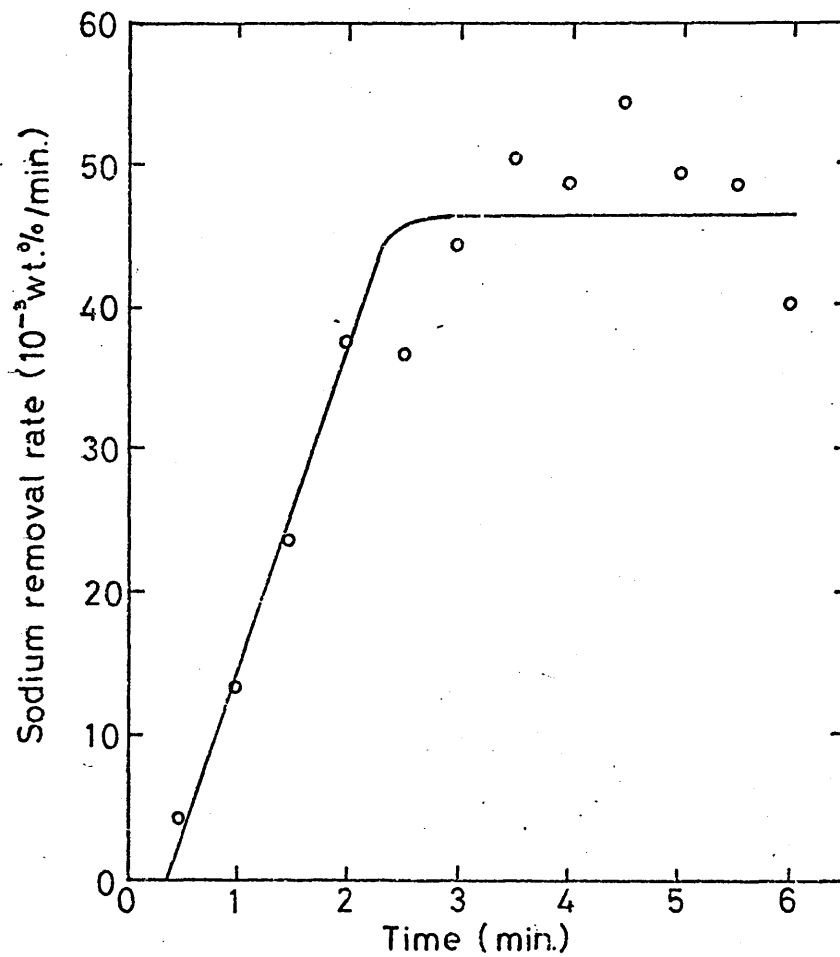


Figure 54 Refining behaviour when lance tip is 2.5 mm above the surface of the amalgam pool.

(For additional information see table 10.)

(a) Rate of sodium removal from amalgam bath.



(b) Foam volume.

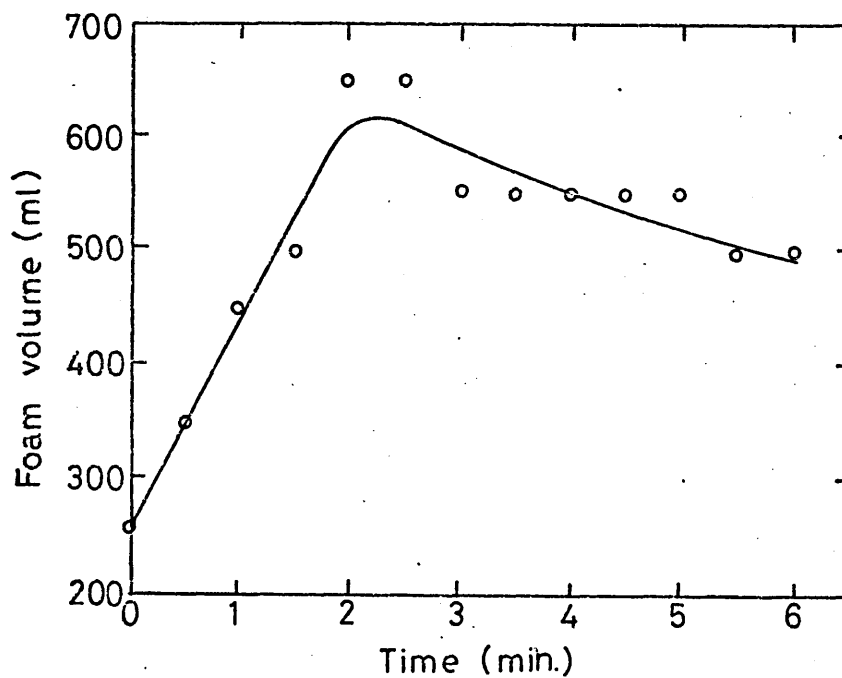
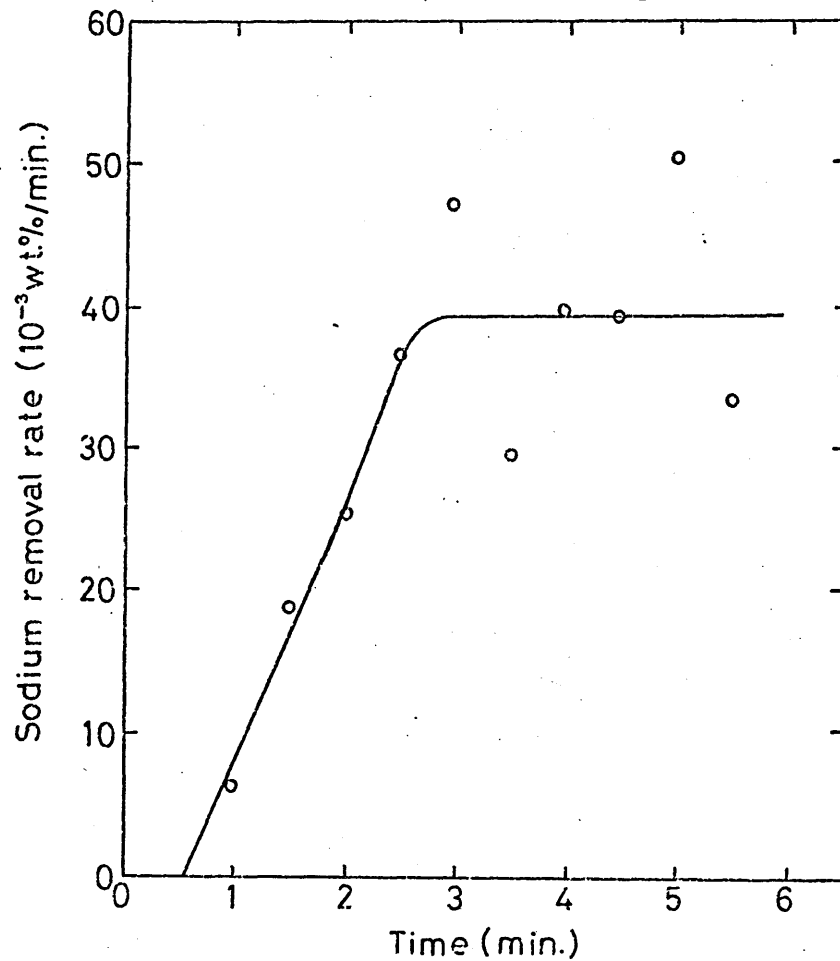


Figure 55 Refining behaviour when lance tip is 12.0 mm above the surface of the amalgam pool.

(For additional information see table 10)

(a) Rate of sodium removal from amalgam bath.



(b) Foam volume.

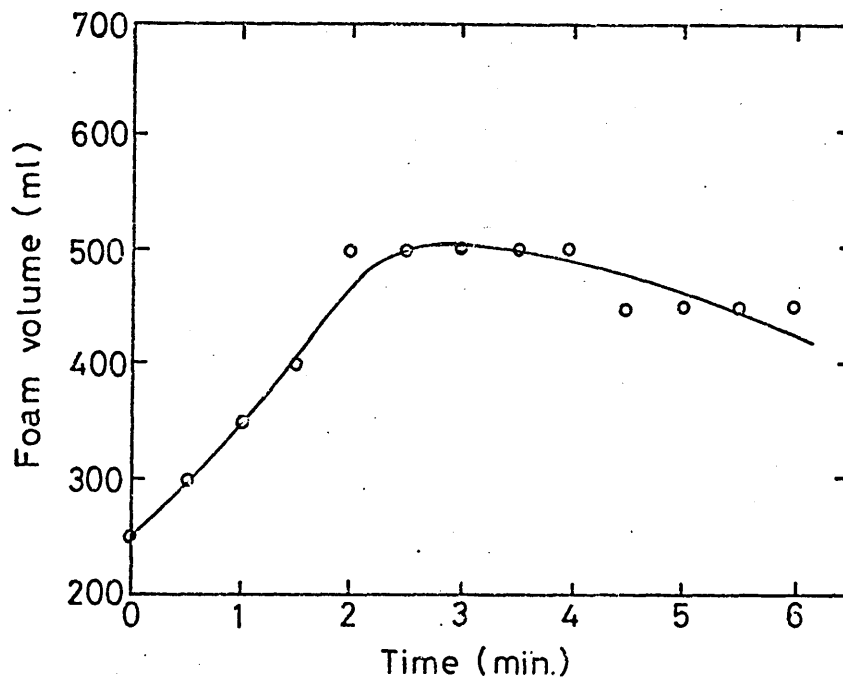
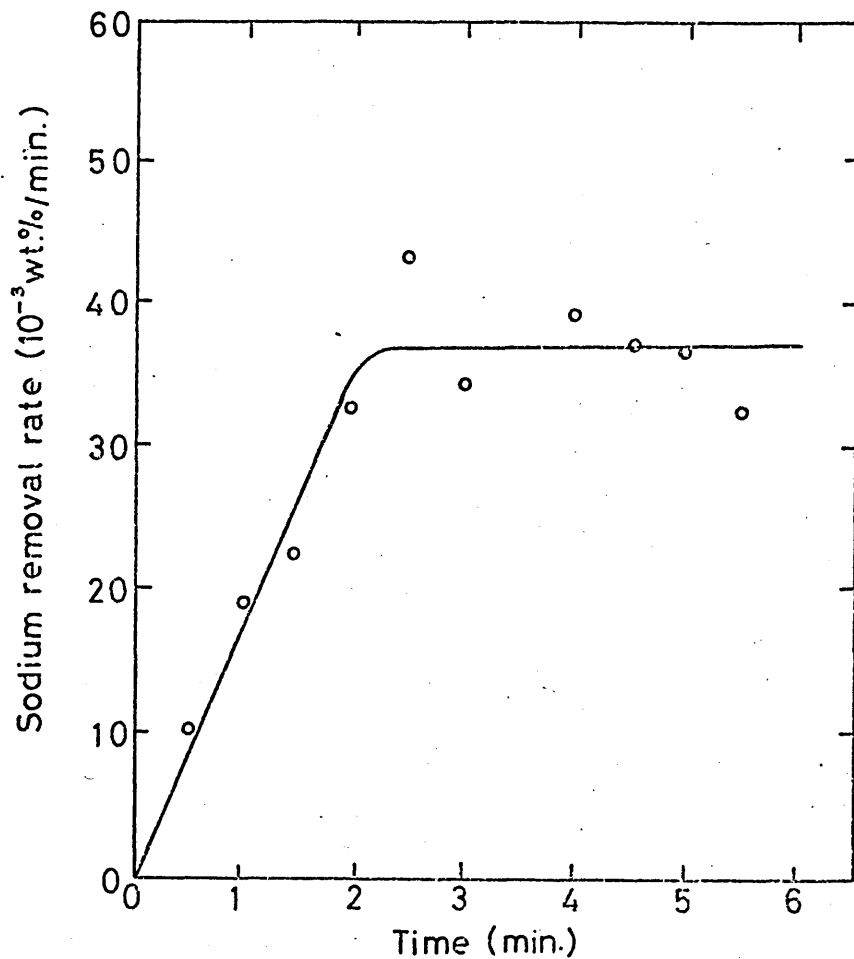


Figure 56 Refining behaviour when lance tip is 21.0 mm above the surface of the amalgam pool.

(For additional information see table 10)

(a) Rate of sodium removal from amalgam bath.



(b) Foam volume.

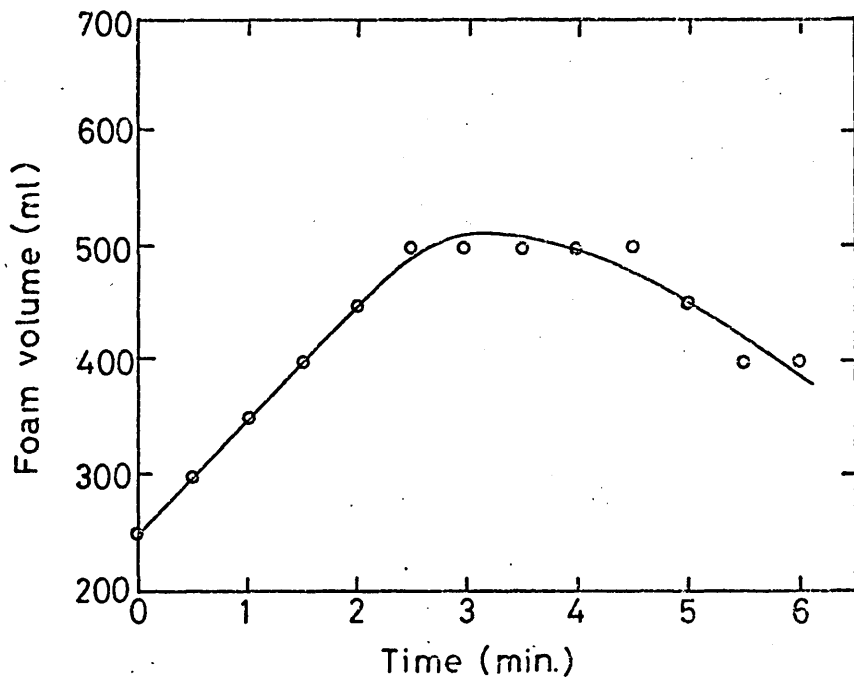
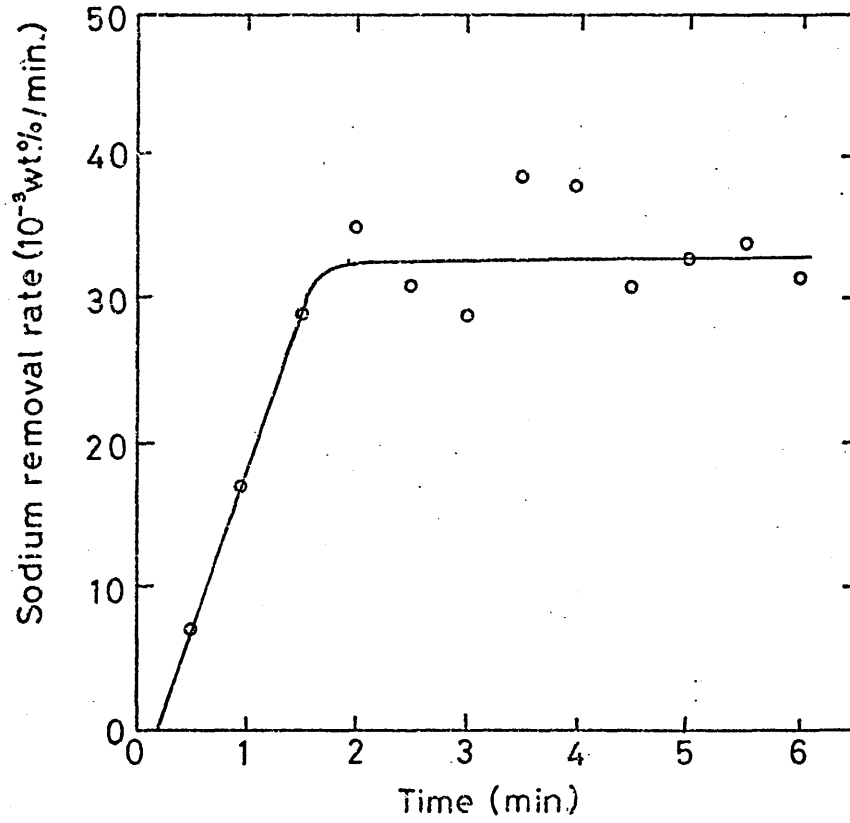


Figure 57 Refining behaviour when lance tip is 31.0 mm above the surface of the amalgam pool.

(For additional information see table 10)

(a) Rate of sodium removal from amalgam bath.



(b) Foam volume.

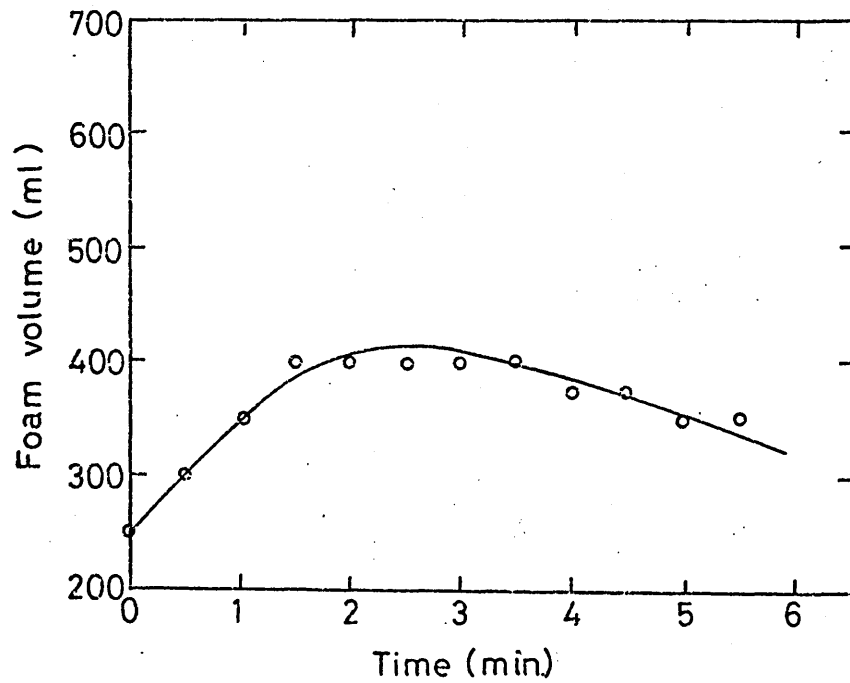
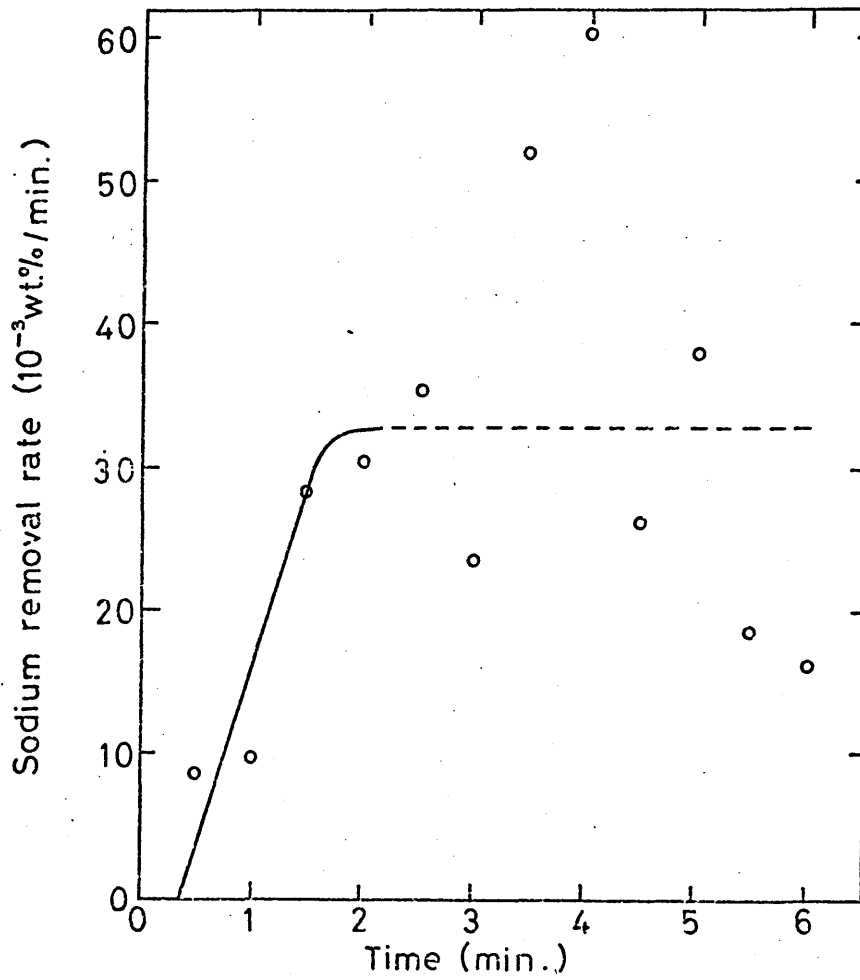


Figure 58 Refining behaviour when lance tip is 44.0 mm above the surface of the amalgam pool.
(For additional information see table 10.)

(a) Rate of sodium removal from amalgam bath.



(b) Foam volume.

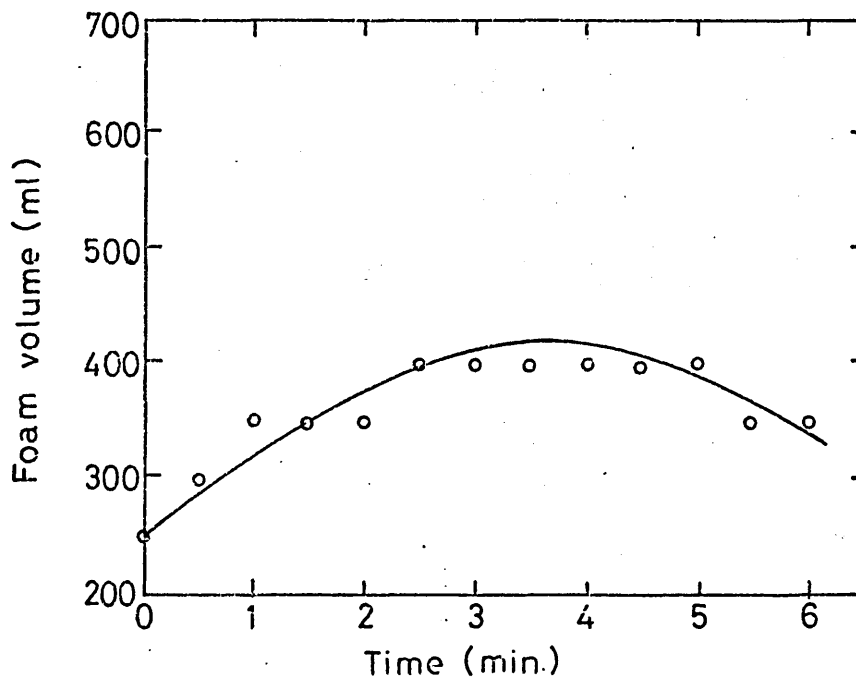


Figure 59 The effect of lance height on the mean stage II rate of sodium removal from the amalgam bath.
(For additional information see table 10.)

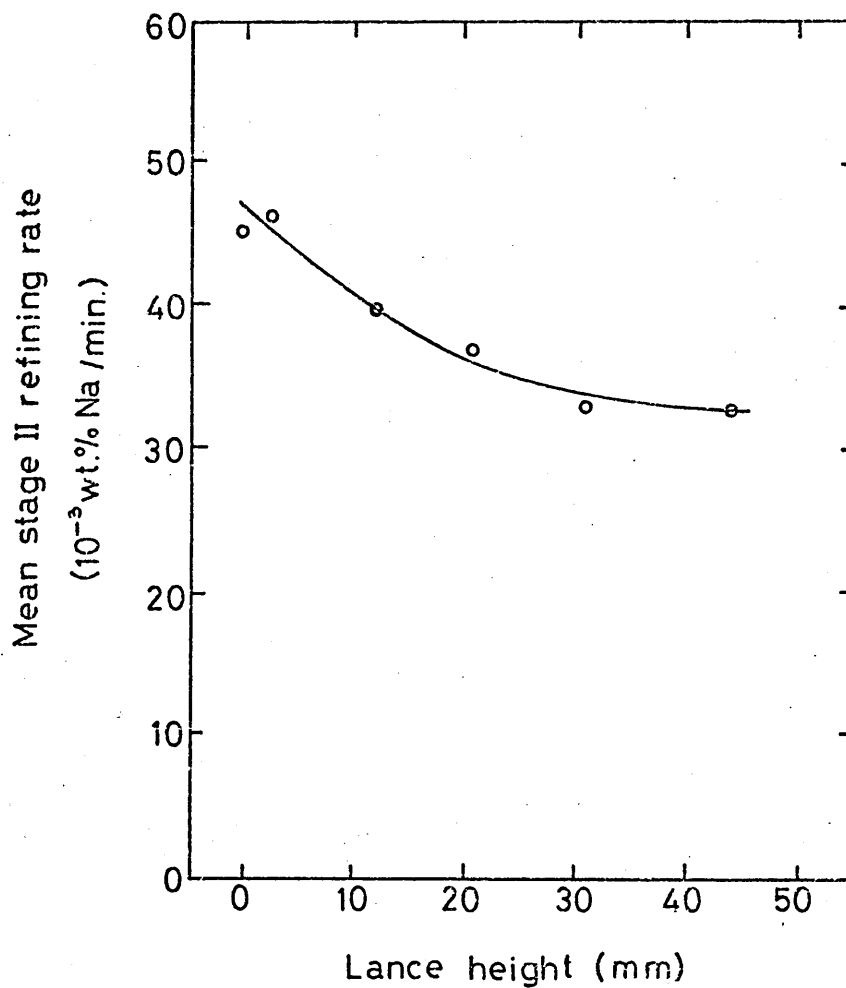
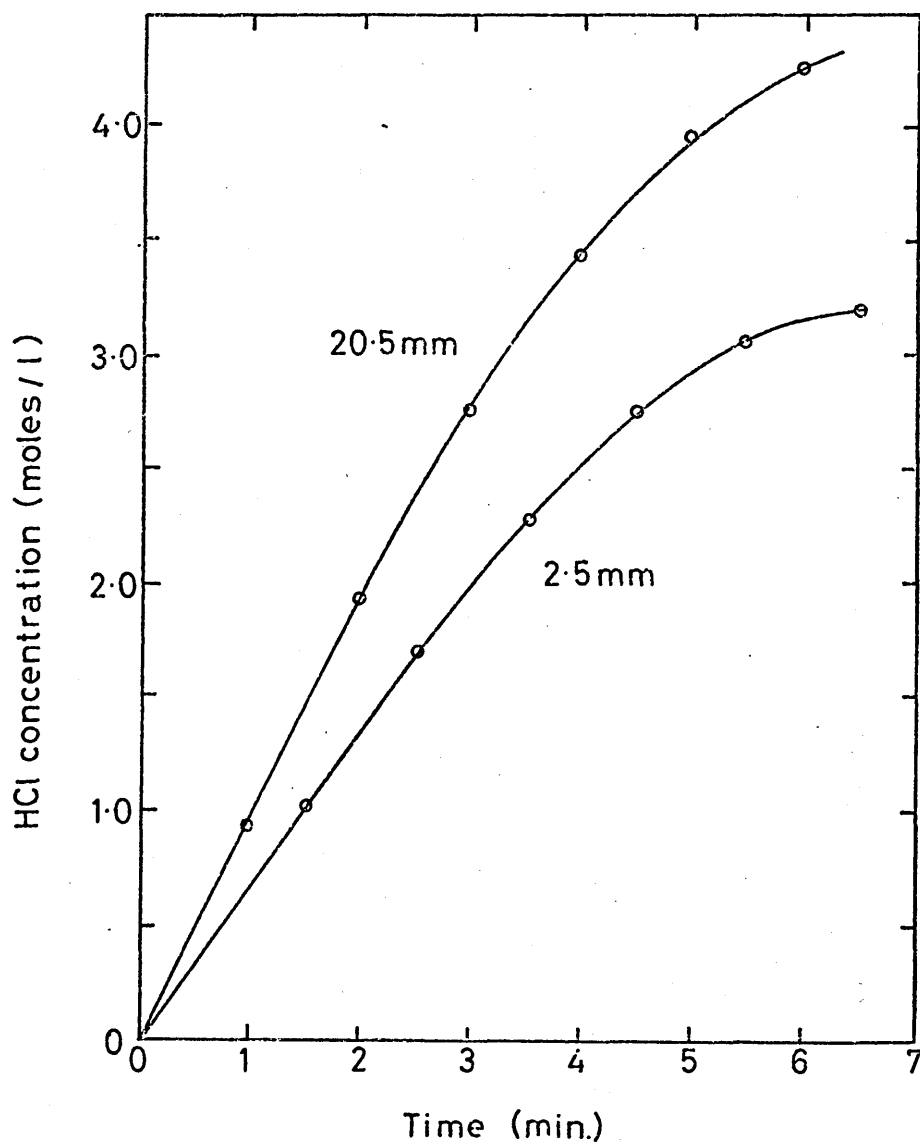


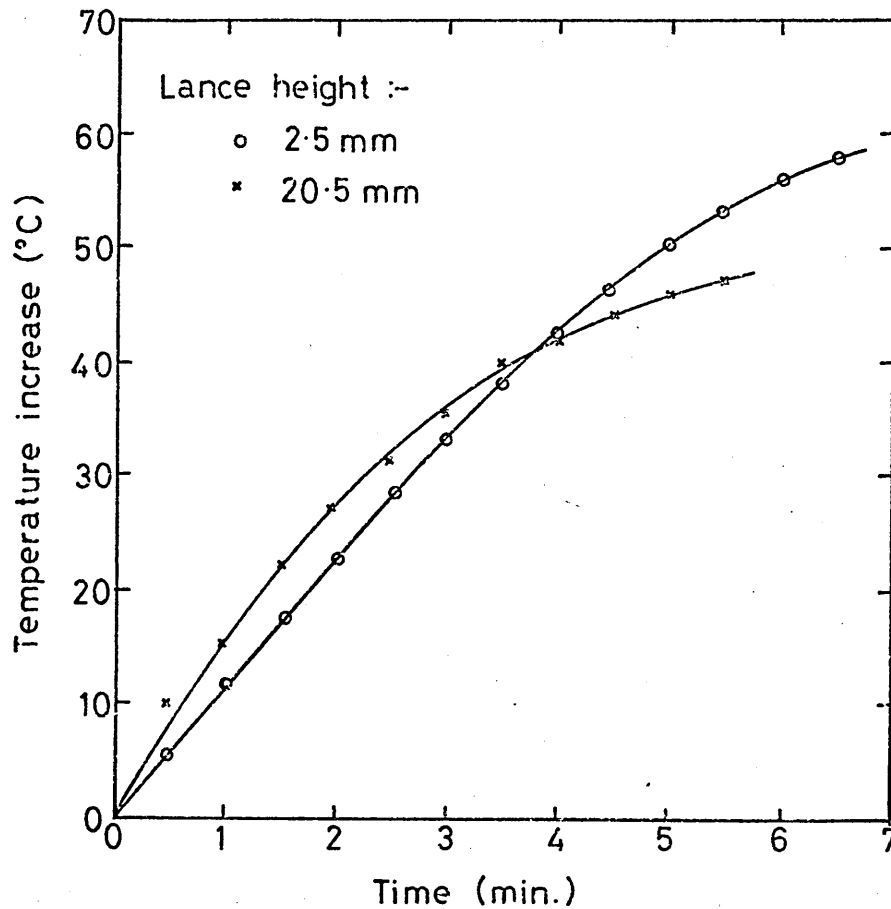
Figure 60 The effect of lance height on the acid concentration in the model slag during a blow.



(a) 2.5mm lance height :- Blowing conditions as for fig. 54 (table 10) .
Initial composition of amalgam : 0.60wt.% Na.

(b) 20.5mm lance height :- Blowing conditions as for fig. 56 (table 10) .
Initial composition of amalgam : 0.58wt.% Na.

Figure 61 The effect of lance height on the temperature of the model slag during a blow.



(a) 2.5 mm lance height :- Blowing conditions as for fig. 54 (table 9).
Initial composition of amalgam: 0.60 wt.% Na.
Initial temperature of model slag : 17°C.

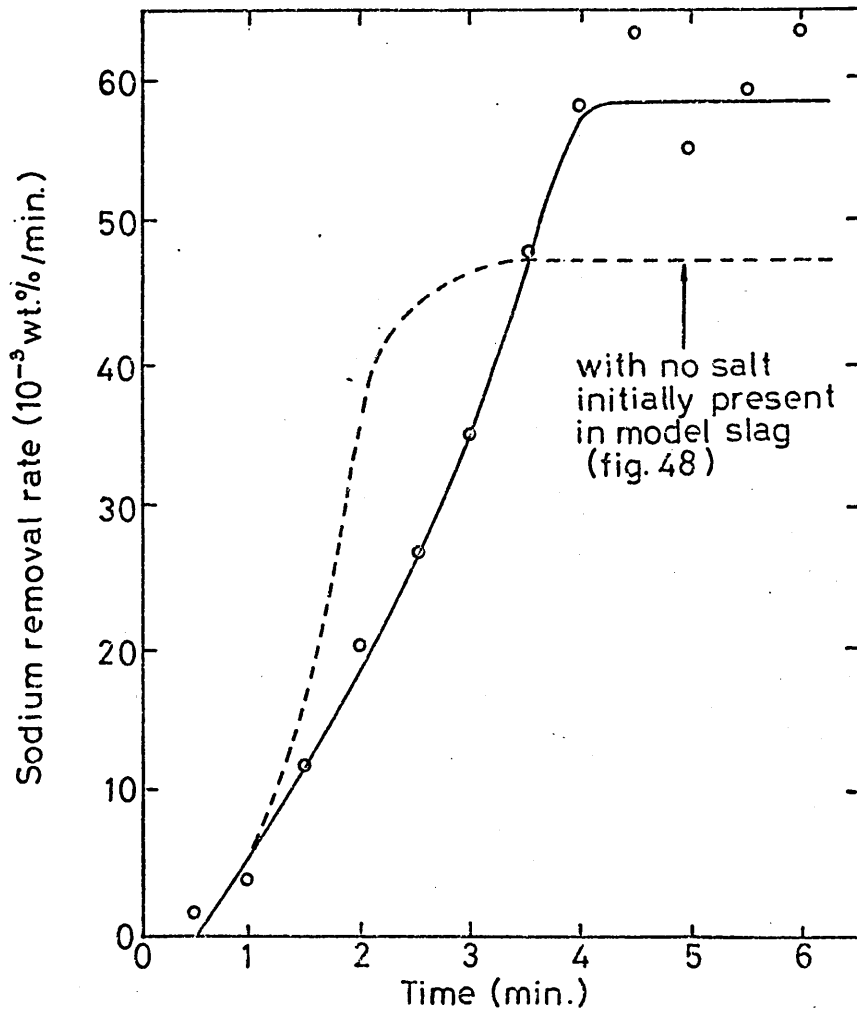
(b) 20.5 mm lance height :- Blowing conditions as for fig. 56 (table 9).
Initial composition of amalgam: 0.58 wt.% Na.
Initial temperature of model slag : 19°C.

Table 11 - Summary of experiments carried out to determine the effect of sodium chloride concentration in the model slag on the rate of sodium removal from the amalgam bath.

Figure number	48 (63)	62 (63)
Initial NaCl concentration in model slag (moles/l)	0	2.0
Initial Na concentration in amalgam (wt. %)	0.58	0.57
Excess vessel pressure (atmos.)	0.042	0.042
N ₂ flow rate (l/min. at S.T.P.)	55.6	55.2
HCl flow rate (l/min at S.T.P.)	8.4	8.3
Jet composition (v.% HCl)	13.1	13.1
Jet momentum (mN)	102.5	102.4
Lance height (mN)	2.5	2.5
Mean stage II refining rate (wt. % Na/min.)	0.0473	0.0581
Estimated mean value of F _m during stage II refining period	0.65	0.71

Figure 62 The effect on the refining behaviour of using a 60v% glycerol-water solution containing initially 0.5 moles of NaCl per litre, as the model slag.
(For additional information see table 11.)

(a) Rate of sodium removal from amalgam bath.



(b) Foam volume.

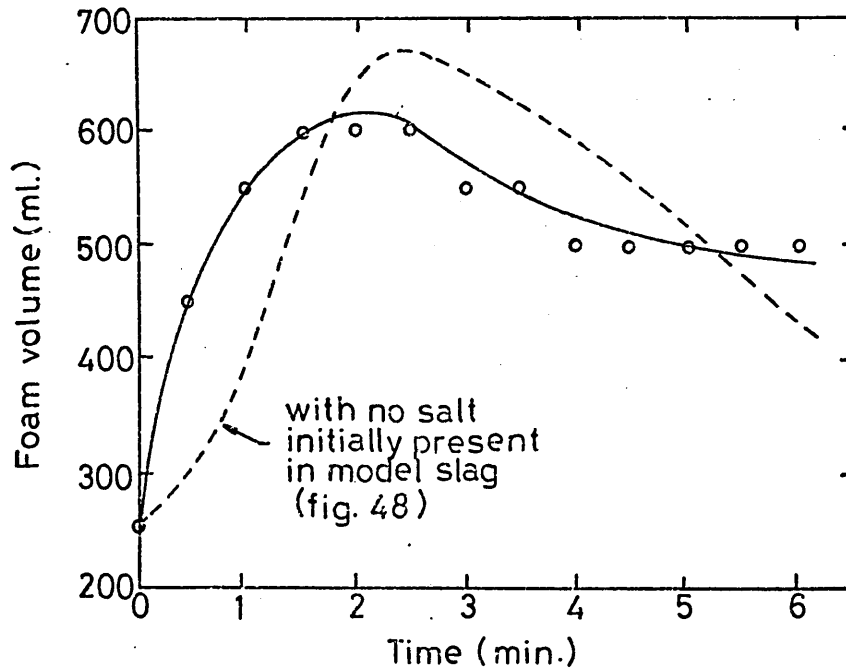
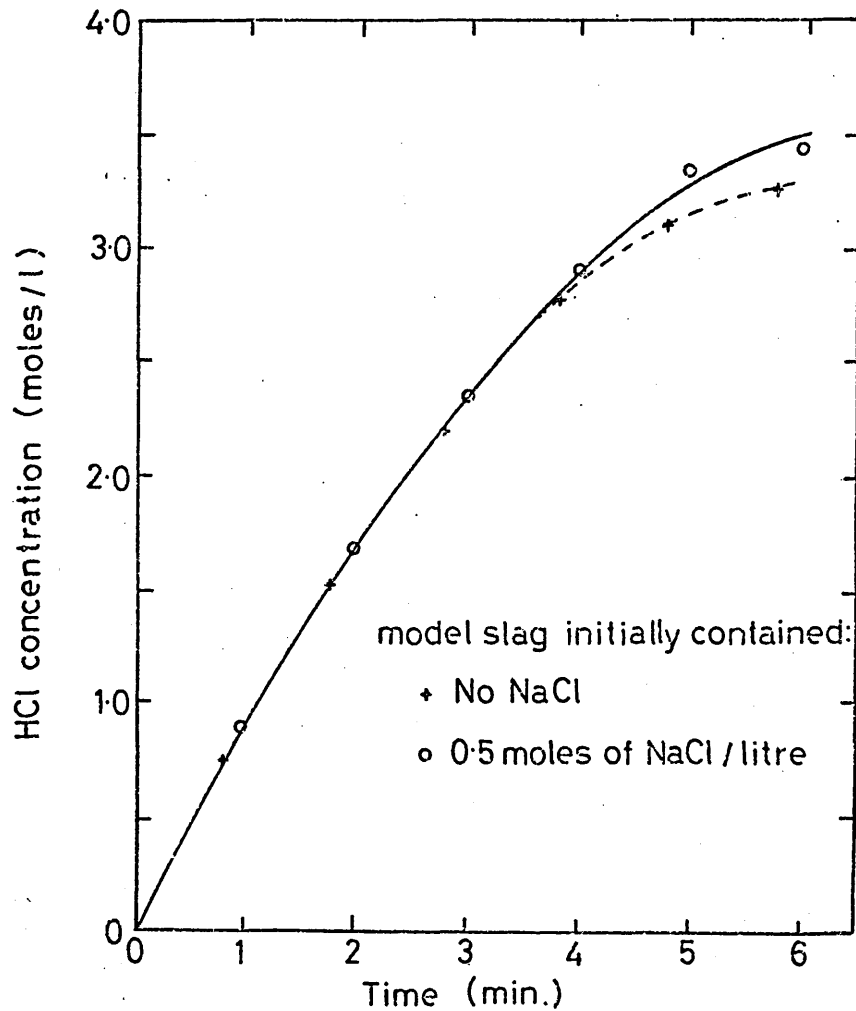


Figure 63 The effect of the initial NaCl concentration on the acid concentration in the model slag during a blow.



(a) No NaCl initially present :-

Blowing conditions as for fig. 48 (table 11).

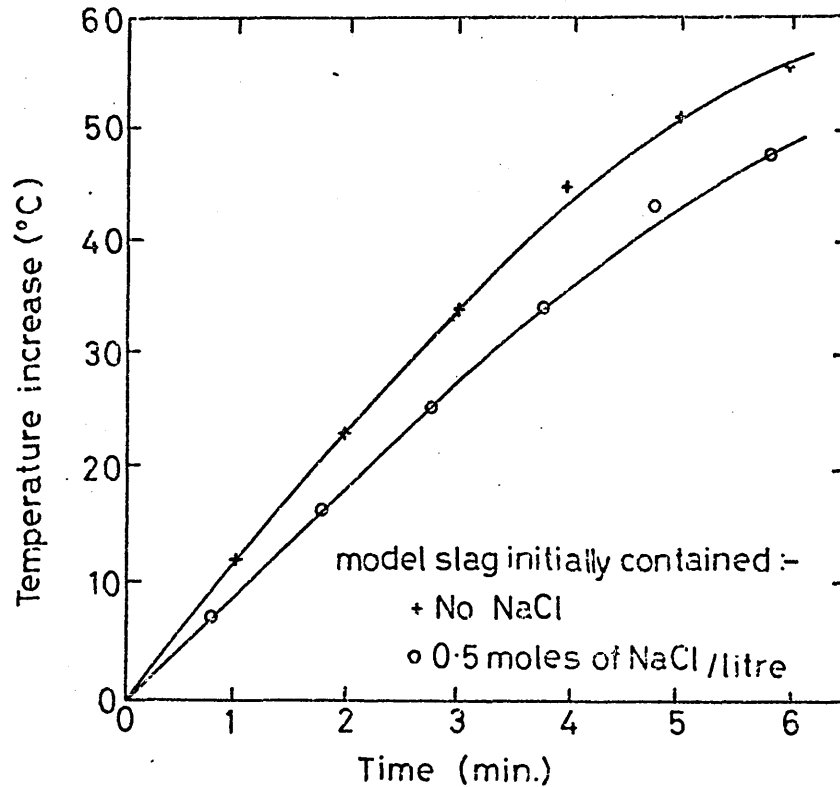
Initial composition of amalgam : 0.54 wt.% Na.

(b) 0.5 moles of NaCl / litre initially present :-

Blowing conditions as for fig. 62 (table 11).

Initial composition of amalgam : 0.55 wt.% Na.

Figure 64 The effect of the initial NaCl concentration on the temperature of the model slag during a blow.



(a) No NaCl initially present :-

Blowing conditions as for fig. 48 (table 11).

Initial composition of amalgam : 0.54 wt.% Na.

Initial temperature of model slag : 12°C.

(b) 0.5 moles of NaCl / litre initially present :-

Blowing conditions as for fig. 62 (table 11).

Initial composition of amalgam : 0.55 wt.% Na

Initial temperature of model slag : 17°C.

Table 12 - Summary of experiments carried out to determine the effect of vessel pressure on the refining rate in the model converter.

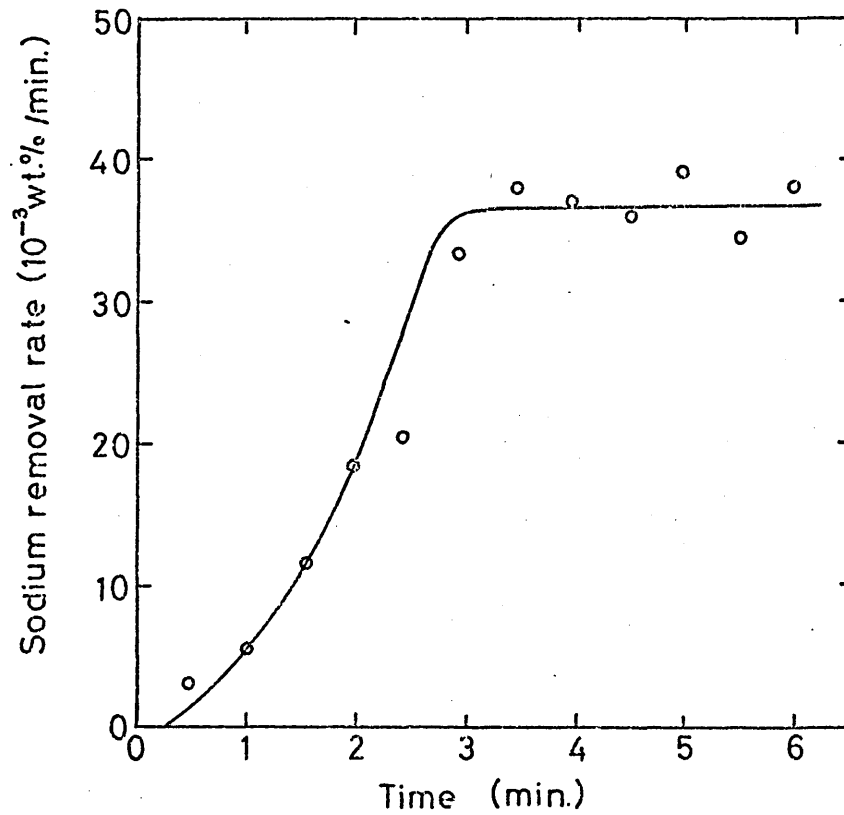
Lance height: 2.5 mm

Jet momentum: 77 mN

Figure No.	Initial Na in amalgam (wt.%)	Excess vessel pressure (atmos.)	N ₂ flow rate (l/min.at S.T.P.)	HCl flow rate (l/min.at S.T.P.)	v.% HCl in jet gases	Mean stage II refining rate (wt.% Na/min.)	Max. foam volume (ml)
41	0.60	0.037	47.6	6.60	12.2	0.0311	600
42	0.61	0.037	47.6	6.60	12.2	0.0319	650
43	0.61	0.034	47.3	6.60	12.3	0.0344	600
65	0.58	0.222	50.8	7.15	12.4	0.0367	600
66	0.58	0.371	53.9	7.55	12.4	0.0406	500
67	0.59	0.545	56.1	7.86	12.3	0.0425	500
68	0.60	0.747	57.4	8.04	12.2	0.0465	375

Figure 65 The refining behaviour of the model converter when operating with an excess vessel pressure of 0.222 atmospheres. (For additional information see table 12.)

(a) Rate of sodium removal from amalgam bath.



(b) Foam volume.

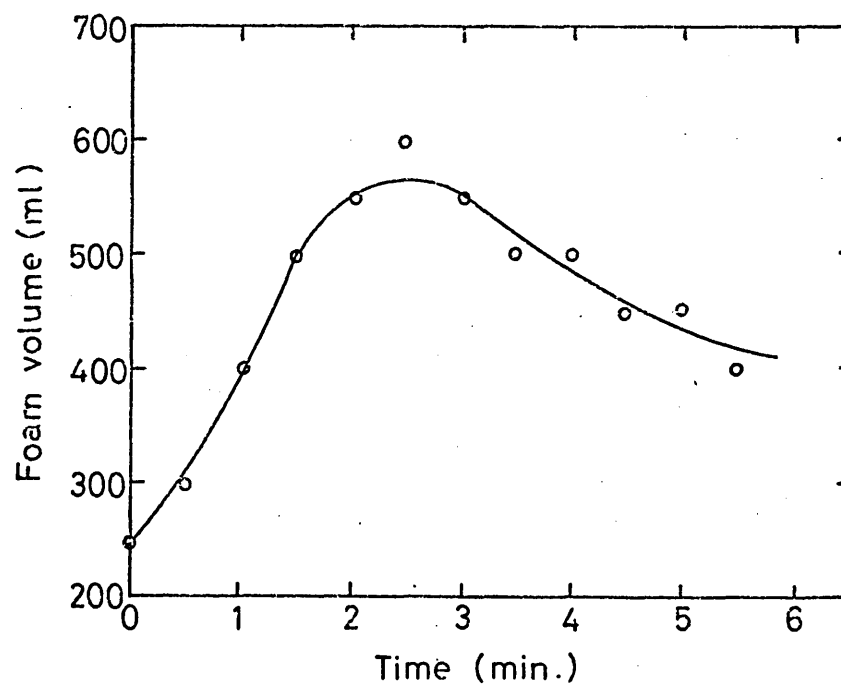
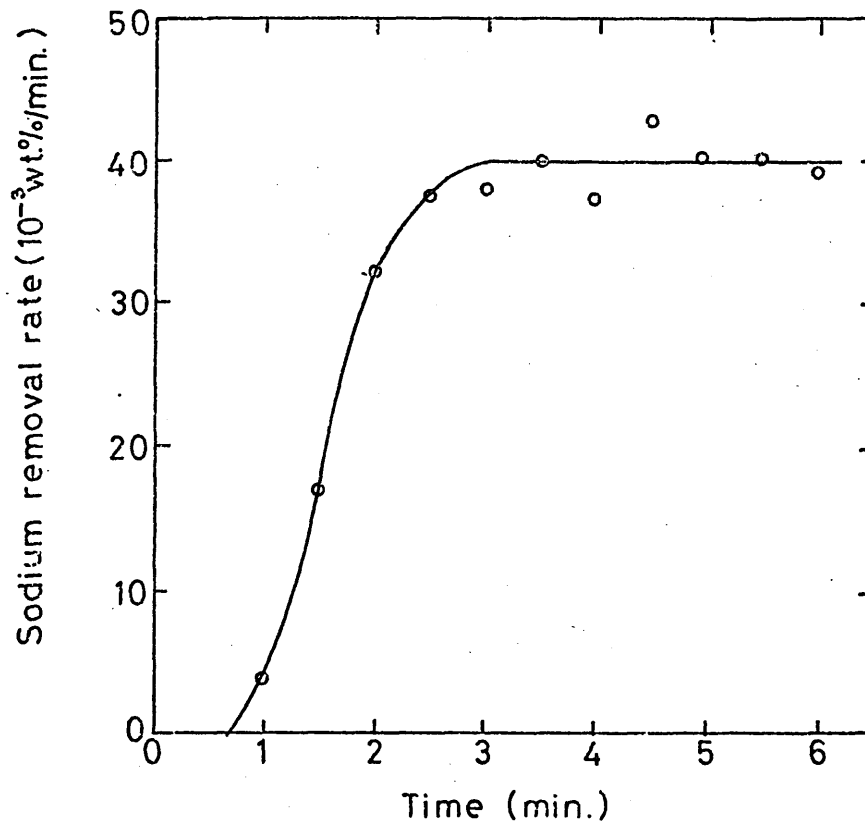


Figure 66 The refining behaviour of the model converter when operating with an excess vessel pressure of 0.371 atmospheres. (For additional information see table 12.)

(a) Rate of sodium removal from amalgam bath.



(b) Foam volume.

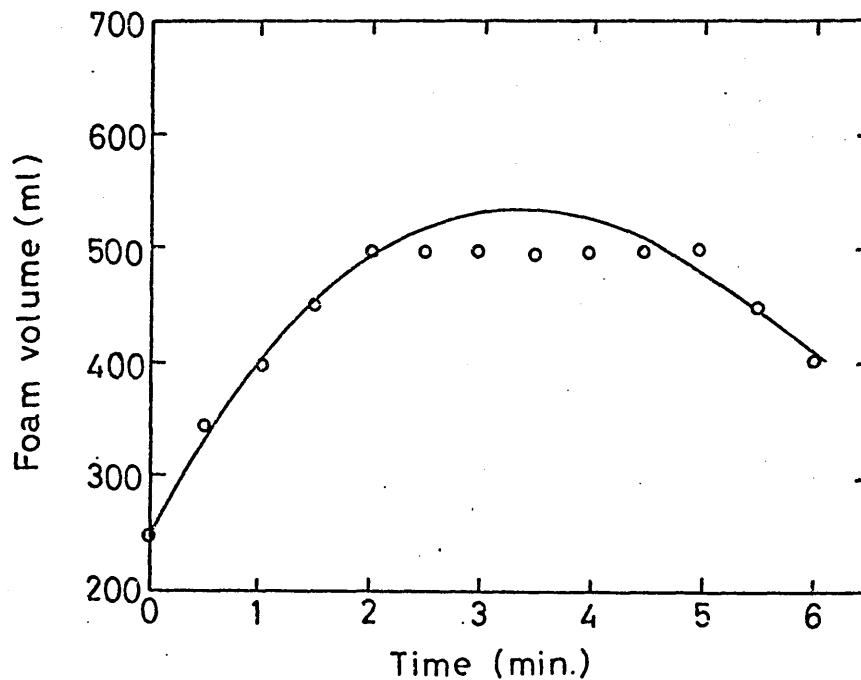
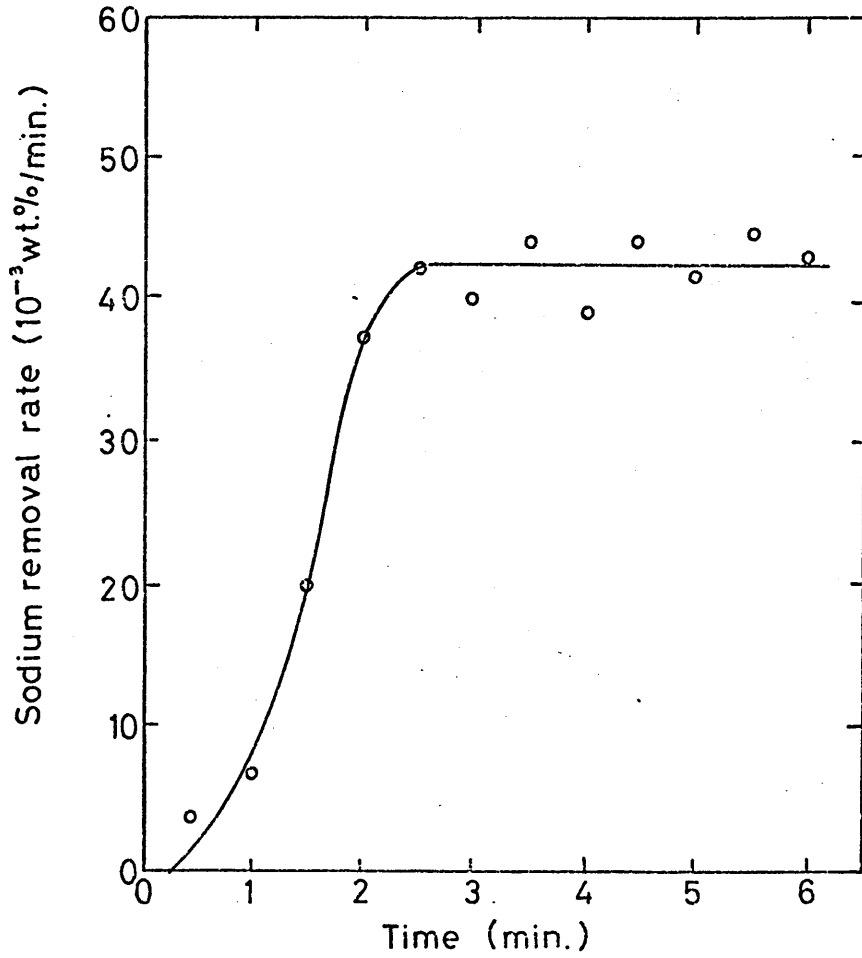


Figure 67 The refining behaviour of the model converter when operating with an excess vessel pressure of 0.545 atmospheres. (For additional information see table 12.)

(a) Rate of sodium removal from the amalgam bath.



(b) Foam volume.

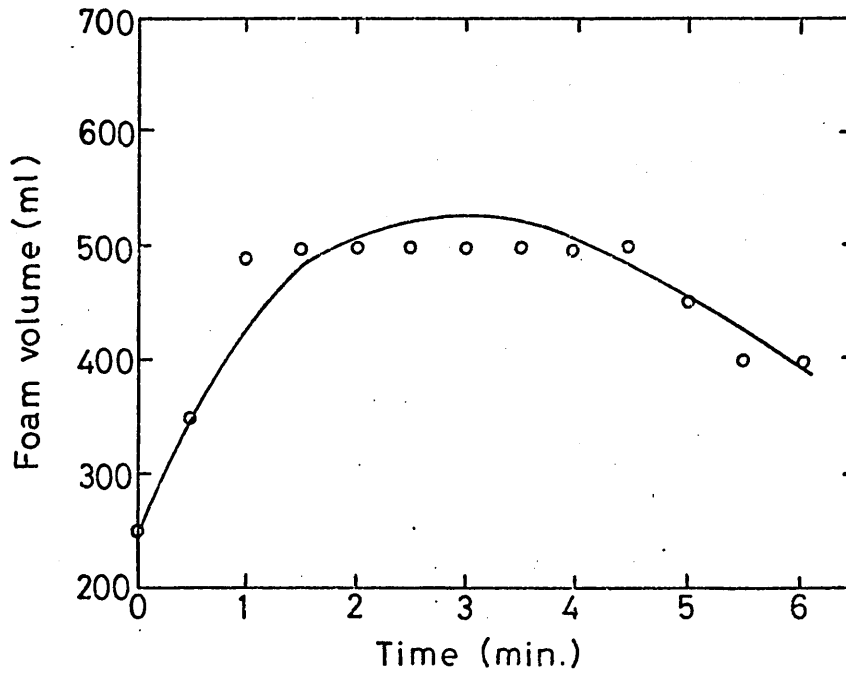
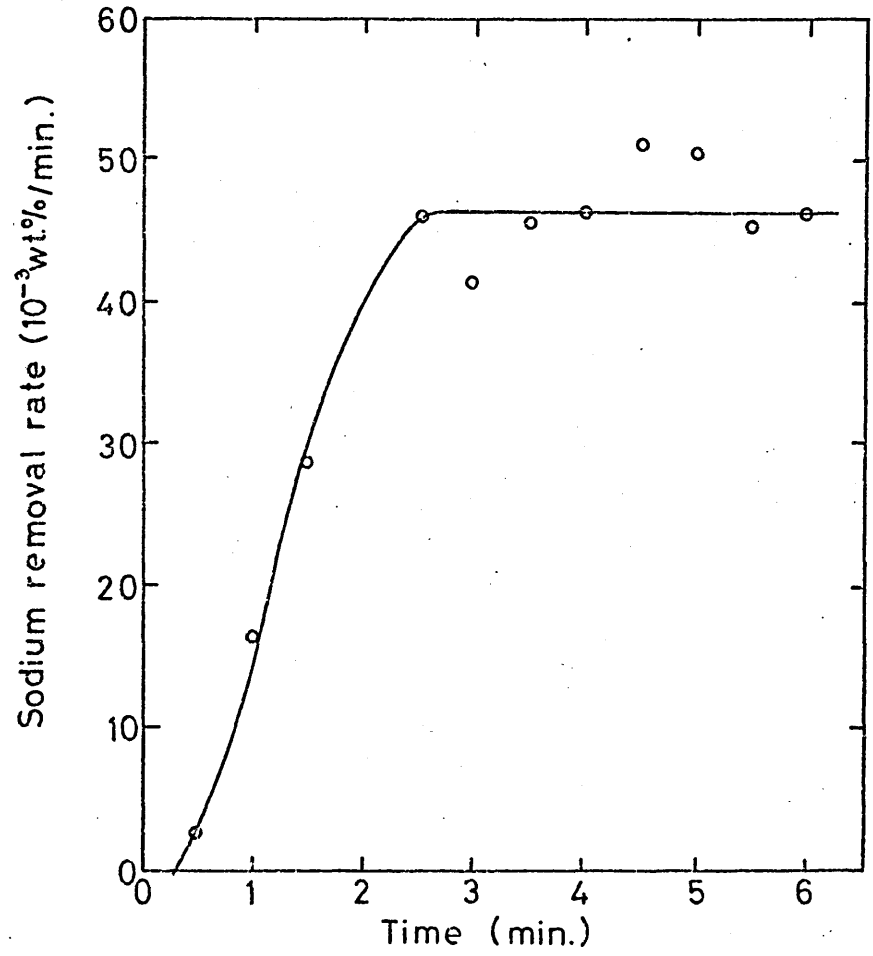


Figure 68 The refining behaviour of the model converter when operating with an excess vessel pressure of 0.747 atmospheres. (For additional information see table 12.)

(a) Rate of sodium removal from the amalgam bath.



(b) Foam volume.

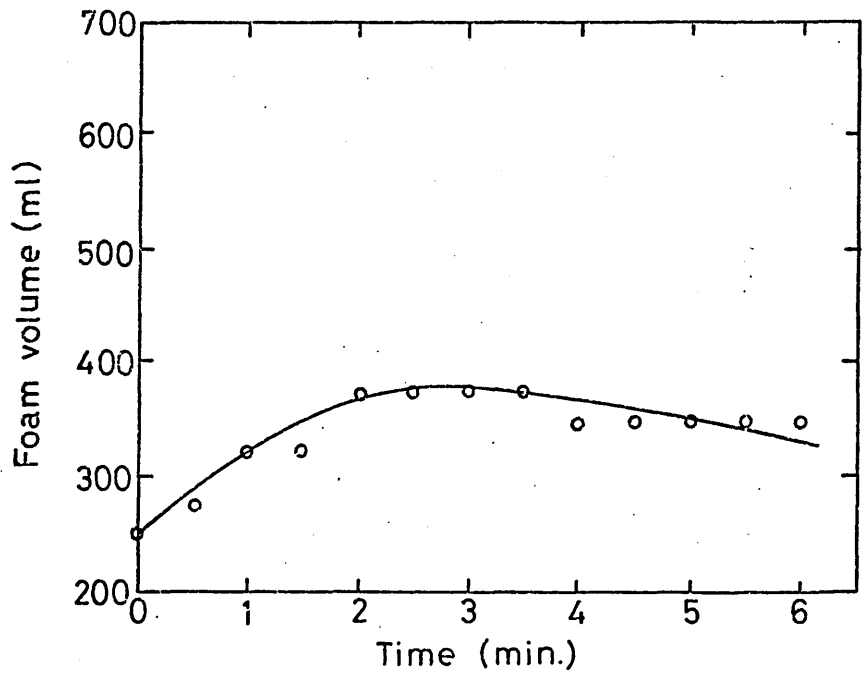


Figure 69 The effect of vessel pressure on the mean stage II rate of sodium removal from the amalgam bath.

Blowing conditions summarised in table 12.

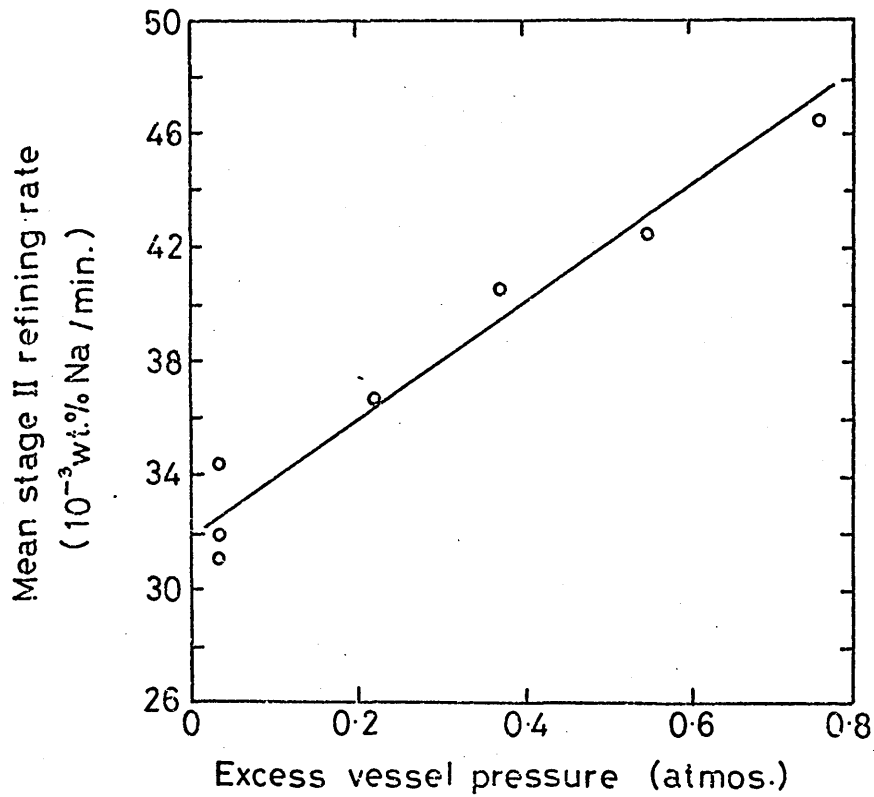


Figure 70 The effect of vessel pressure on the maximum foam volume achieved during a blow.

Blowing conditions summarised in table 12.

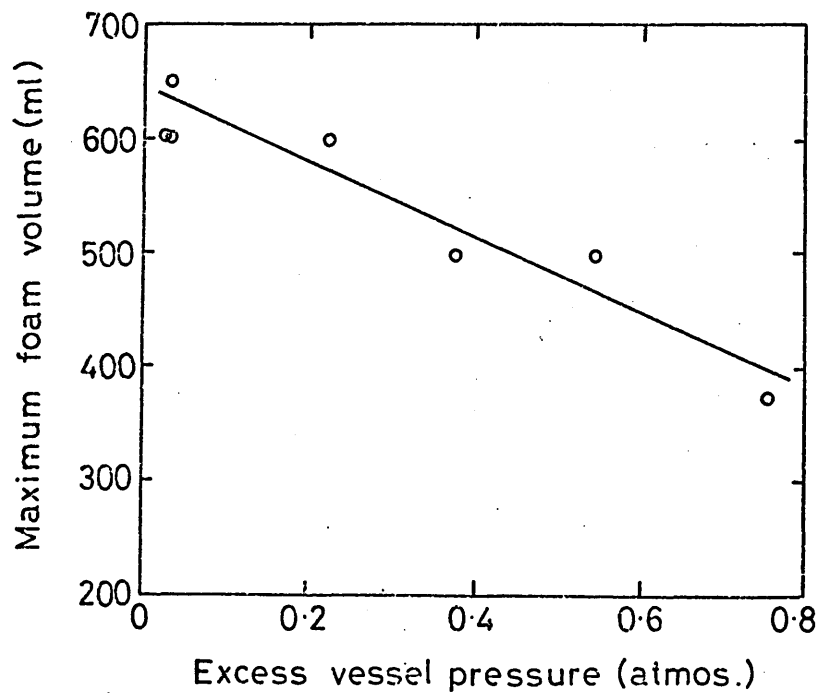
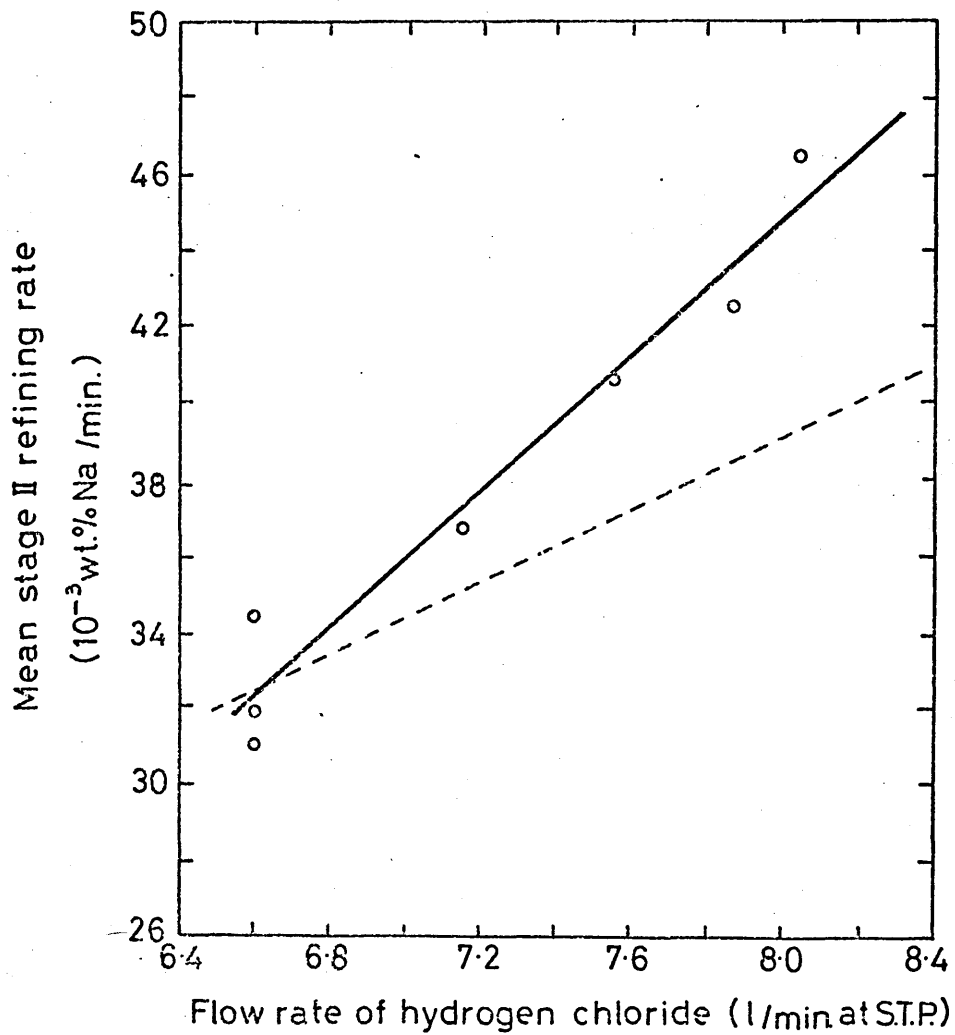
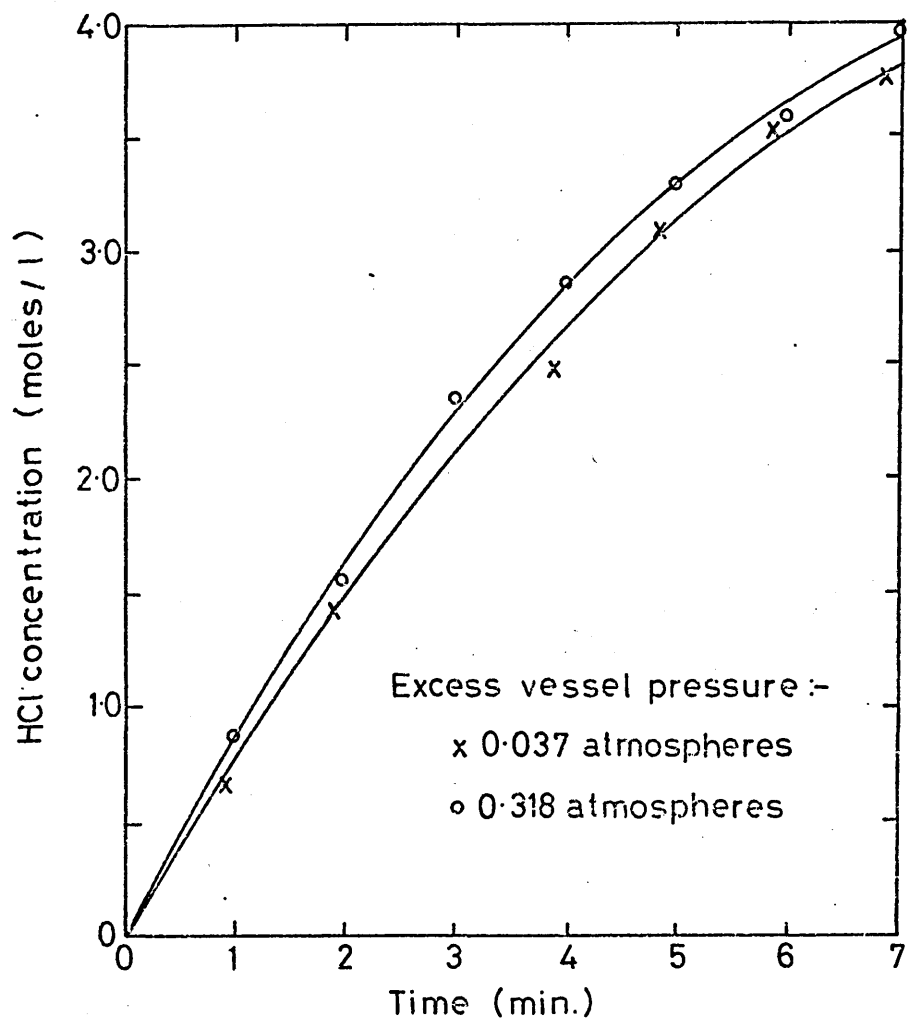


Figure 71 The mean stage II refining rate presented as a function of the volumetric flow rate of hydrogen chloride into the reaction vessel for the experiments conducted with elevated vessel pressures .



The broken line is from figure 49(b) for a series of experiments conducted at atmospheric pressure with a jet momentum of 77mN.

Figure 72 The effect of vessel pressure on the acid concentration in the model slag during a blow.



(a) 0.037 atmospheres :-

Blowing conditions as for figures 41 & 42 (table 12).

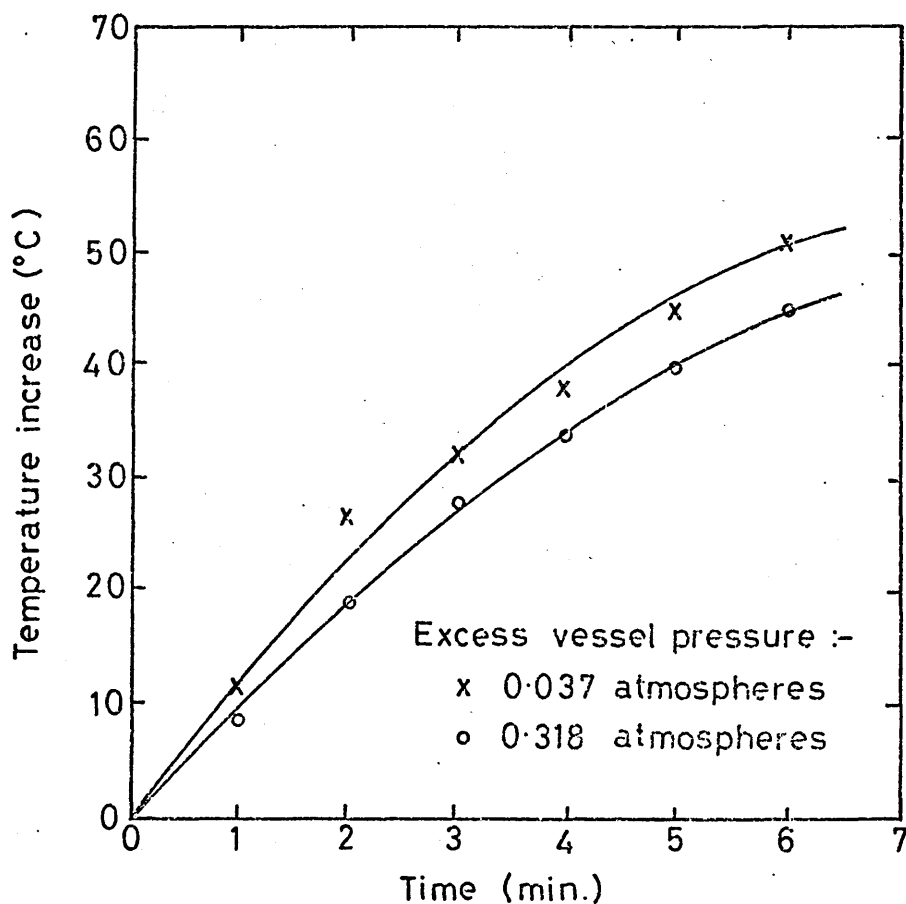
Initial composition of amalgam : 0.62 wt.% Na.

(b) 0.318 atmospheres :-

Blowing conditions similar to fig. 66 (table 12).

Initial composition of amalgam : 0.61 wt.% Na.

Figure 73 The effect of vessel pressure on the temperature of the model slag during a blow.



(a) 0.037 atmospheres :-

Blowing conditions as for figures 41 & 42 (table 12).

Initial composition of amalgam : 0.62 wt.% Na.

Initial temperature of model slag : 21°C .

(b) 0.318 atmospheres :-

Blowing conditions similar to fig. 66 (table 12).

Initial composition of amalgam : 0.61 wt.% Na.

Initial temperature of model slag : 18°C

Table 13 - Summary of those experiments carried out with the same mass flow rate of hydrogen chloride into the reaction vessel but different vessel pressures.

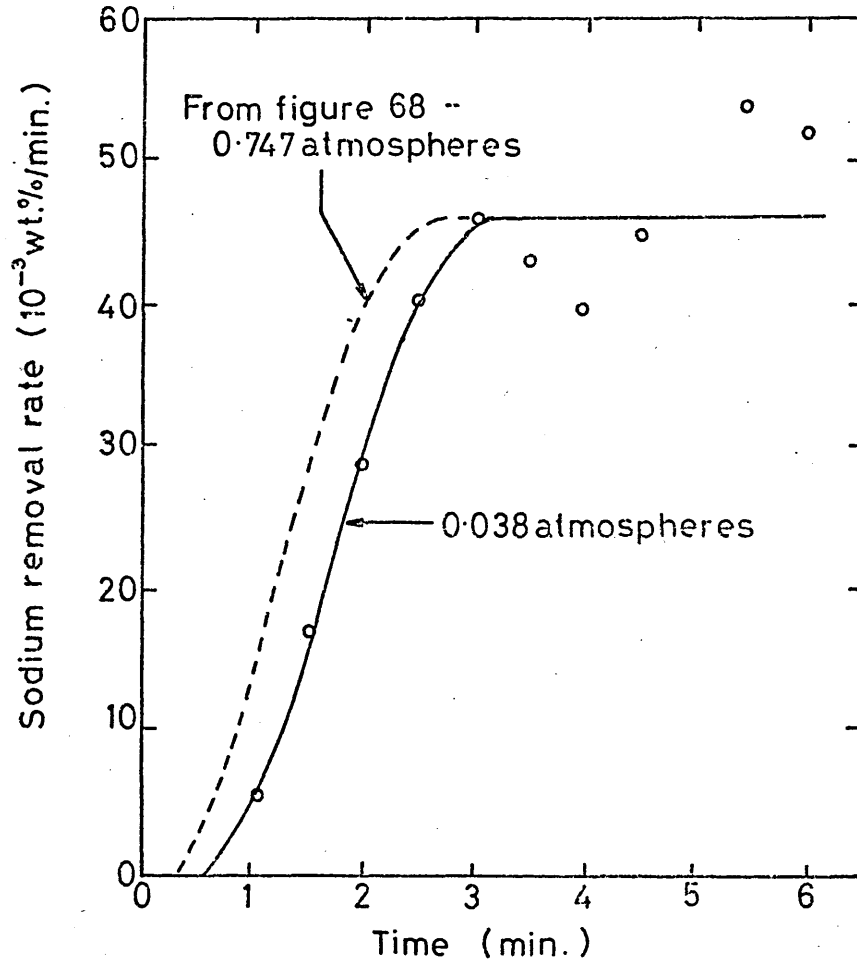
Lance height for all experiments was 2.5 mm

Figure No.	Initial Na in amalgam (wt. %)	Excess vessel pressure (atmos.)	N ₂ flow rate (l/min.at S.T.P.)	HCl flow rate (l/min.at S.T.P.)	v.% HCl in jet gases	Jet momentum (mN)	Mean stage II refining rate (wt.% Na/min.)
68	0.60	0.747	57.4	8.0	12.3	73.0	0.0465
74	0.60	0.038	57.4	8.1	12.4	105.0	0.0465
75	0.63	0.313	55.4	8.3	13.0	84.7	0.0484
48	0.58	0.042	55.6	8.4	13.1	102.5	0.0473

Figure 74 Experiments conducted with a gas jet containing 12.35v% HCl & with a flow rate of 8.05 l/min. of HCl at S.T.P. but different vessel pressures.

(For additional information see table 13.)

(a) Rate of sodium removal from the amalgam bath.



(b) Foam volume.

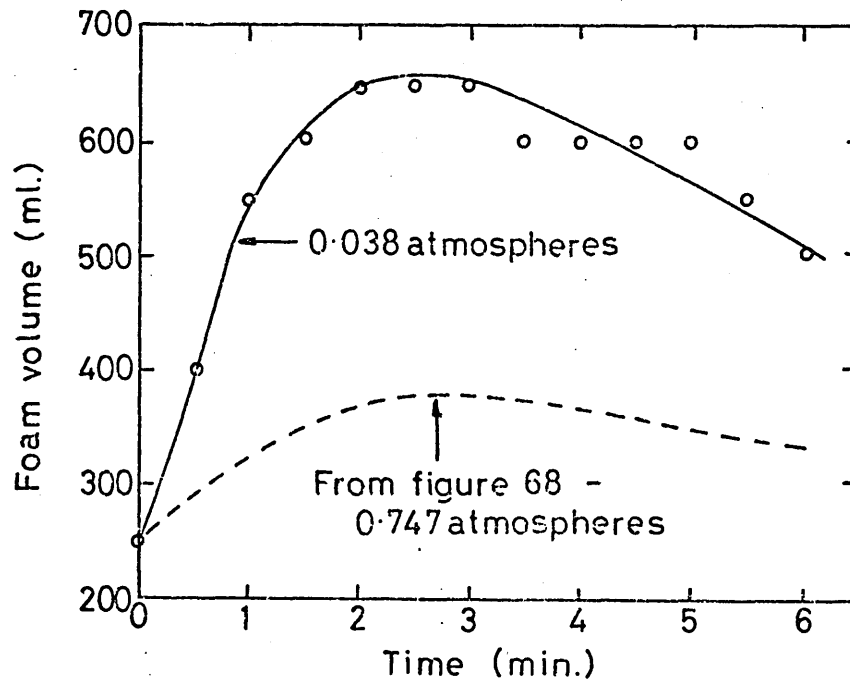
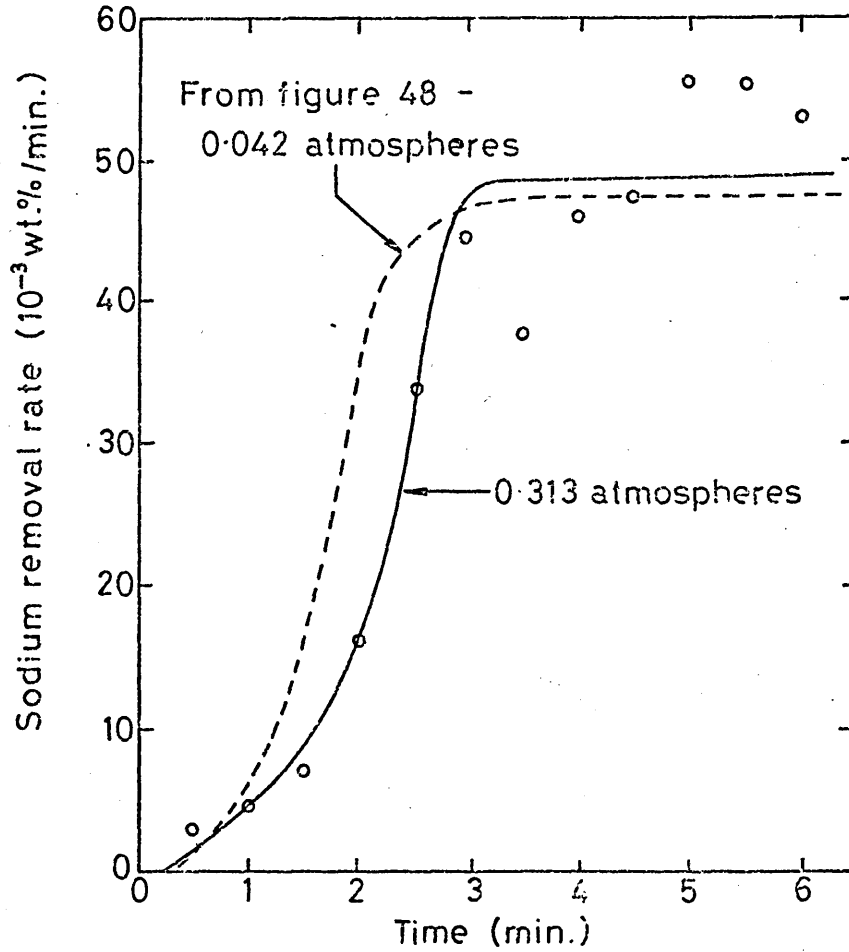


Figure 75 Experiments conducted with a gas jet containing 13.05 v.% HCl & with a flow rate of 8.35 l/min. of HCl at ST.P but different vessel pressures .

(For additional information see table 13.)

(a) Rate of sodium removal from the amalgam bath.



(b) Foam volume.

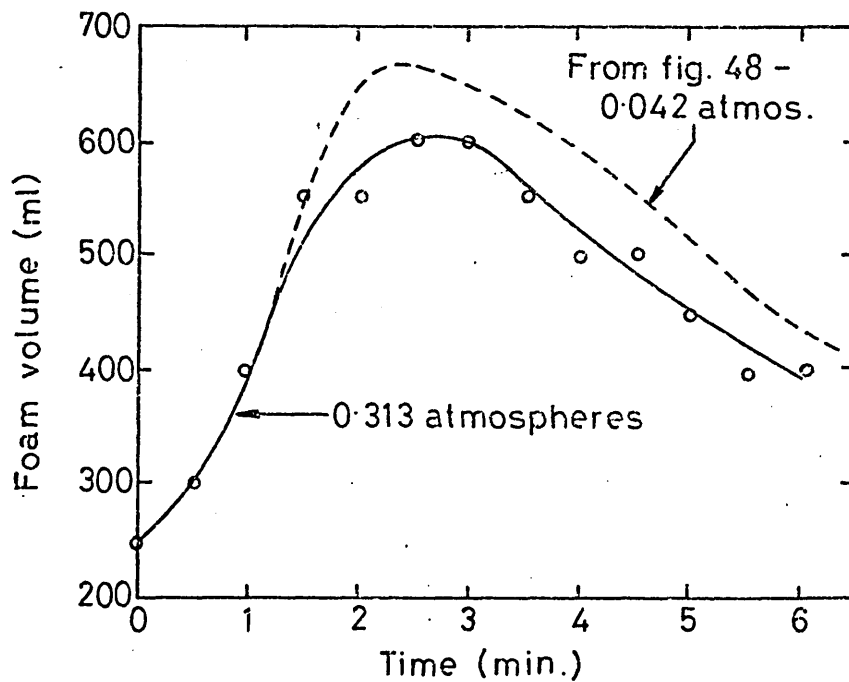
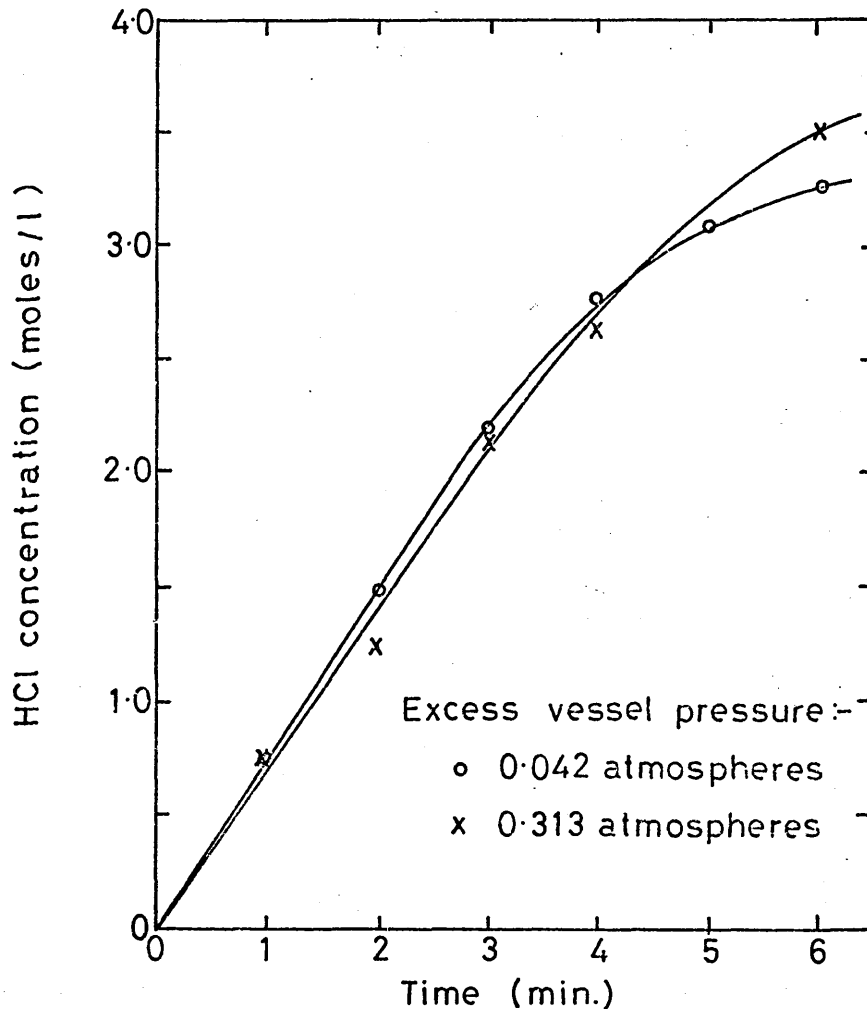


Figure 76 The change in the acid concentration in the model slag for experiments using the same mass flow rate of hydrogen chloride into the reaction vessel but differing vessel pressures.



(a) 0.042 atmospheres :-

Blowing conditions as for figure 48 (table 13)

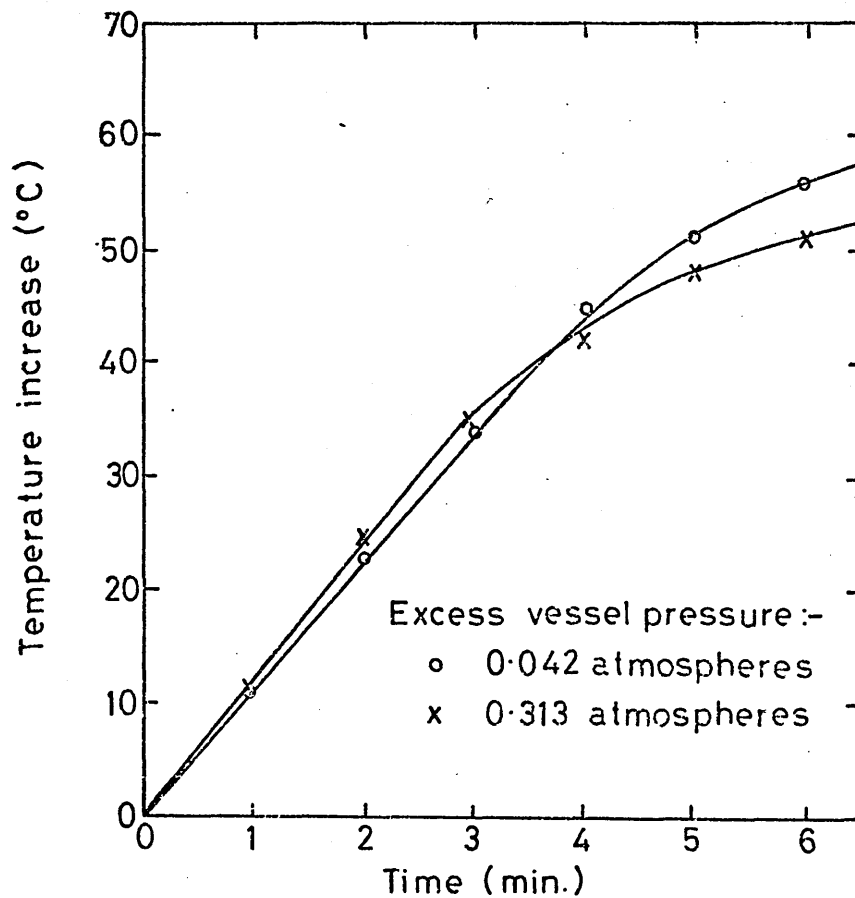
Initial composition of amalgam : 0.54 wt.% Na.

(b) 0.313 atmospheres :-

Blowing conditions as for figure 75 (table 13)

Initial composition of amalgam : 0.60 wt.% Na.

Figure 77 The variation in the temperature of the model slag during experiments using the same mass flow rate of hydrogen chloride into the reaction vessel but different vessel pressures.



(a) 0.042 atmospheres :-

Blowing conditions as for figure 48 (table 13).

Initial composition of amalgam :- 0.54 wt.% Na.

Initial temperature of model slag :- 12°C.

(b) 0.313 atmospheres :-

Blowing conditions as for figure 75 (table 13)

Initial composition of amalgam : 0.60 wt.% Na.

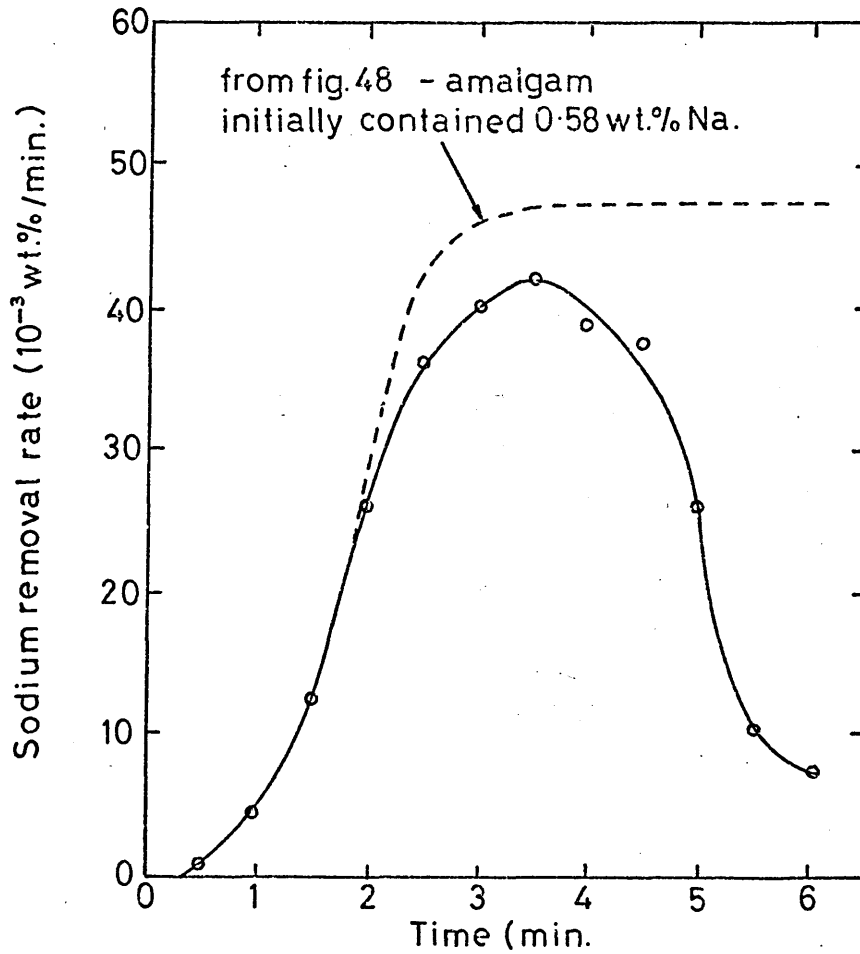
Initial temperature of model slag :- 21°C.

Table 14 - Summary of experiments carried out with a low sodium concentration
in the amalgam bath.

Figure No.	Initial Na in amalgam (wt.%)	Excess vessel pressure (atmos.)	N ₂ flow rate (l/min.at S.T.P.)	HCl flow rate (l/min.at S.T.P.)	v.% HCl in jet gases	Lance height (mm)	Jet momentum (mN)
78	0.32	0.047	55.6	8.4	13.1	2.5	102.5
79	0.30	0.047	55.4	8.4	13.2	2.5	104.6
85	0.29	0.037	55.6	8.3	13.0	20.4	103.8
82	0.30	0.350	62.5	9.4	13.1	2.5	102.5
83	0.32	0.392	62.0	9.4	13.2	2.5	102.6

Figure 78 The refining behaviour at low sodium concentrations.
Initial composition of amalgam :- 0.32 wt.% Na.
(For additional information see table 14.)

(a) Rate of sodium removal from the amalgam bath.



(b) Foam volume.

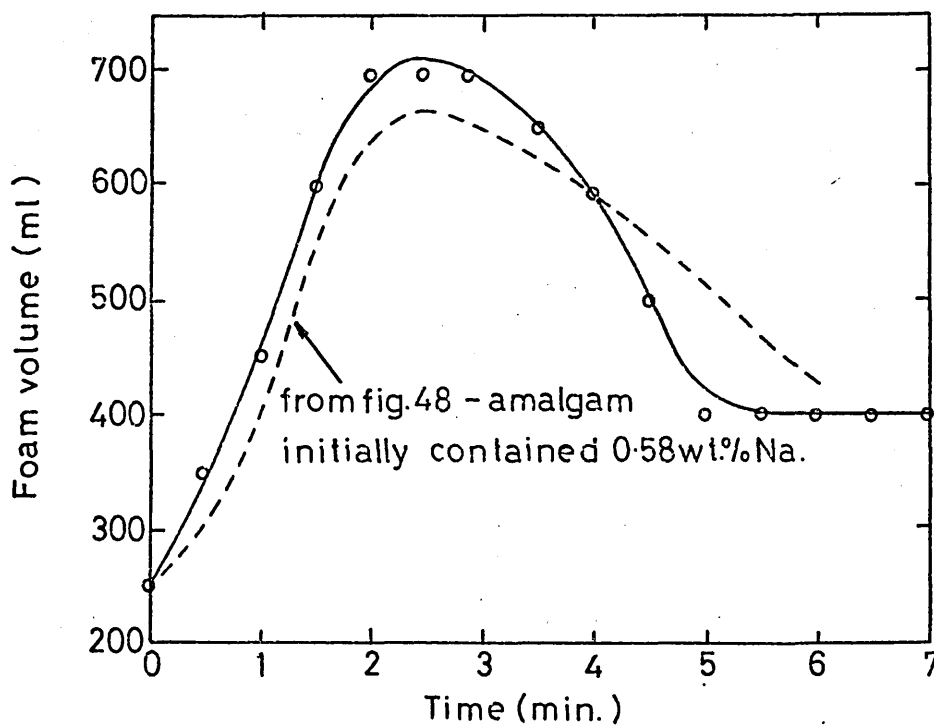
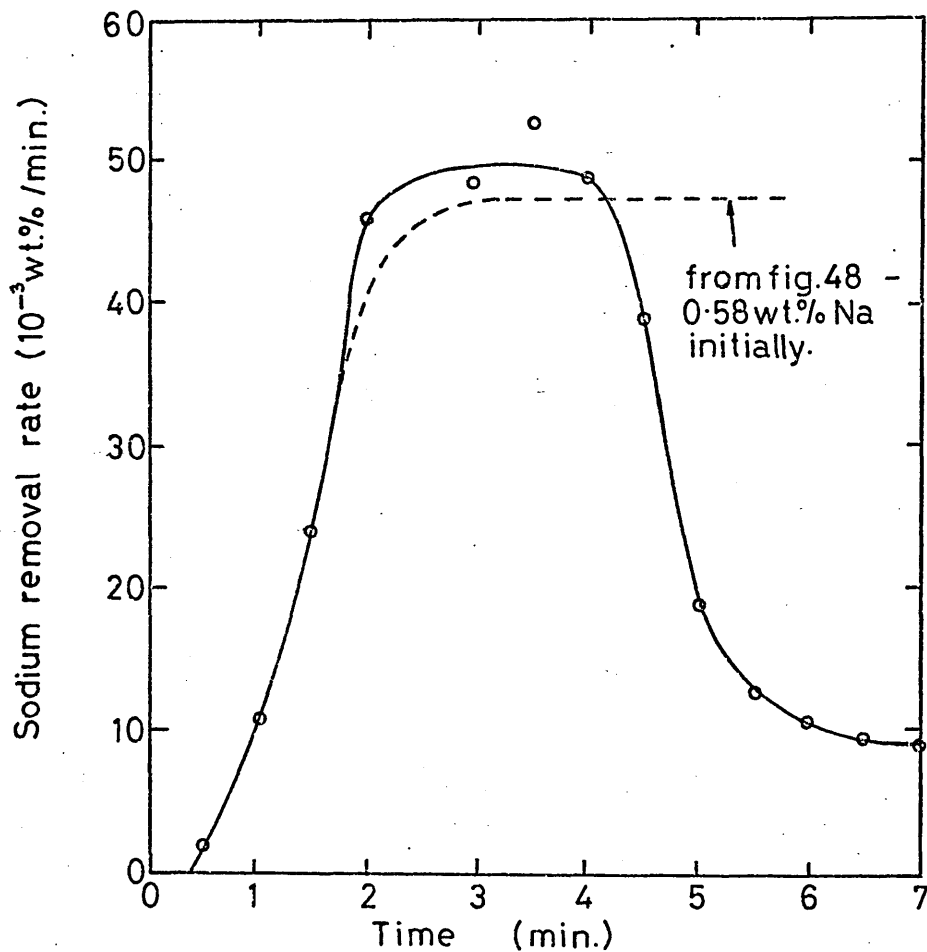


Figure 79 The refining behaviour at low sodium concentrations.
 Initial composition of amalgam :- 0.30 wt.% Na.
 (For additional information see table 14.)

(a) Rate of sodium removal from the amalgam bath.



(b) Foam volume.

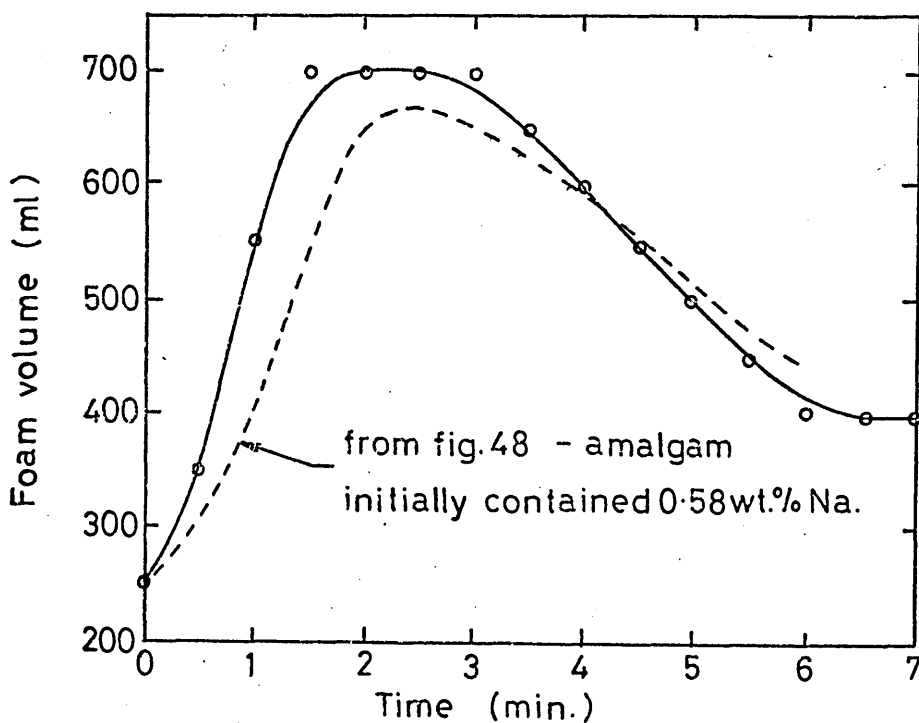
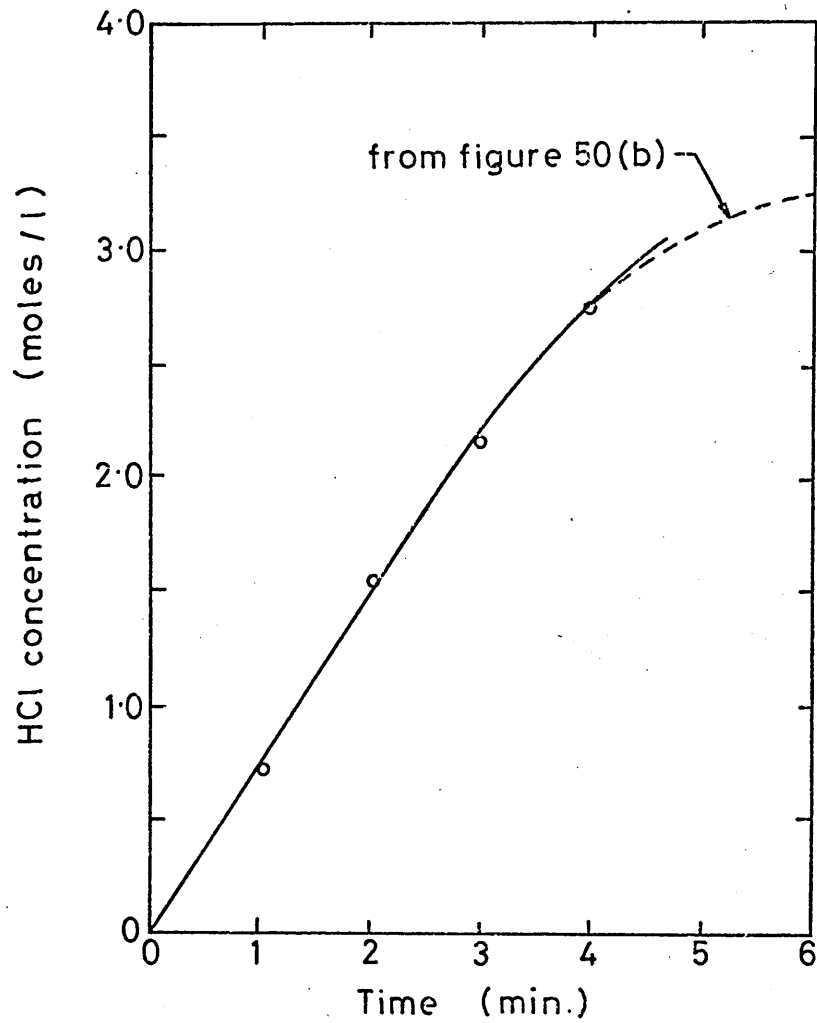


Figure 80 The change in the acid concentration in the model slag for an experiment performed with amalgam initially containing 0.30 wt.% Na.



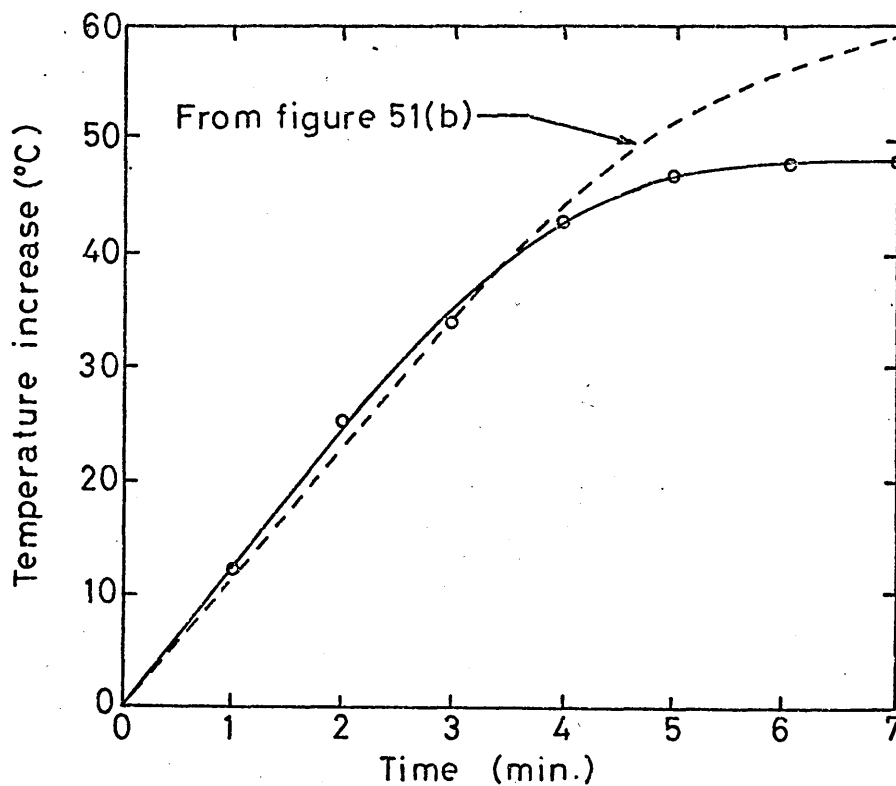
Blowing conditions as for fig.48 (table 9) & fig's 78 & 79 (table 14).

Initial composition of amalgam : 0.30 wt.% Na.

Broken line from fig. 50(b).

Initial composition of amalgam : 0.54 wt.% Na.

Figure 81 The temperature of the model slag during an experiment performed with amalgam initially containing 0.30 wt.% Na.

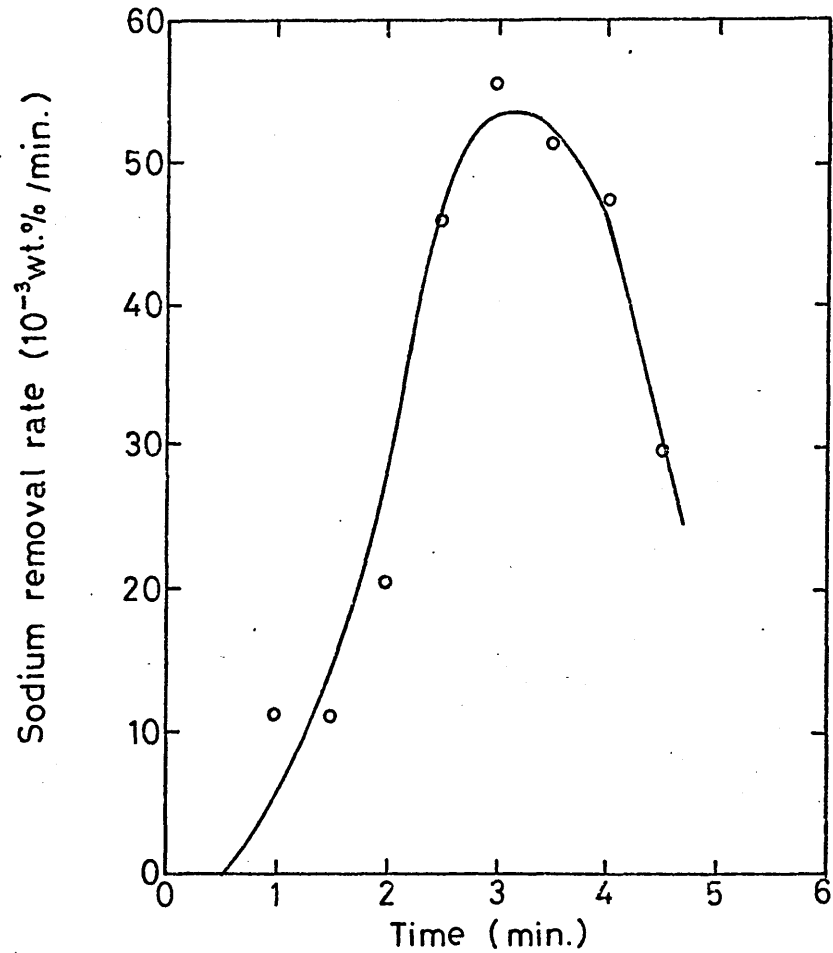


Blowing conditions as for fig. 48 (table 9) & fig's 78 & 79 (table 14).
Initial composition of amalgam : 0.30 wt.% Na.
Initial temperature of model slag : 21°C.

Broken line from fig. 51(b).
Initial composition of amalgam : 0.54 wt.% Na.
Initial temperature of model slag : 12°C.

Figure 82 The refining of an amalgam initially containing 0.30 wt.% Na when the excess vessel pressure was 0.350 atmospheres.
(For additional information see table 14.)

(a) Rate of sodium removal from the amalgam bath.



(b) Foam volume.

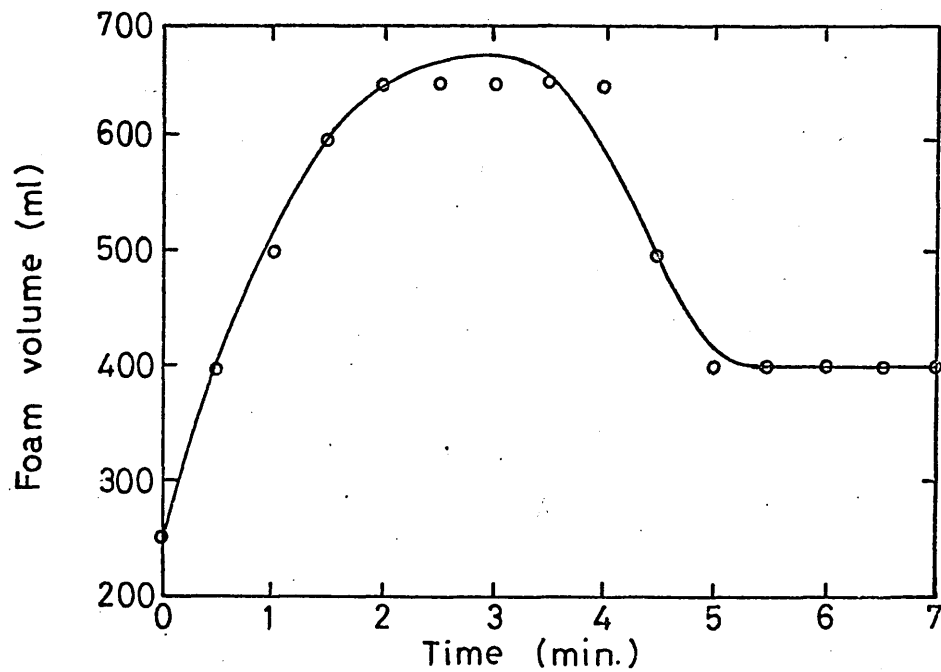
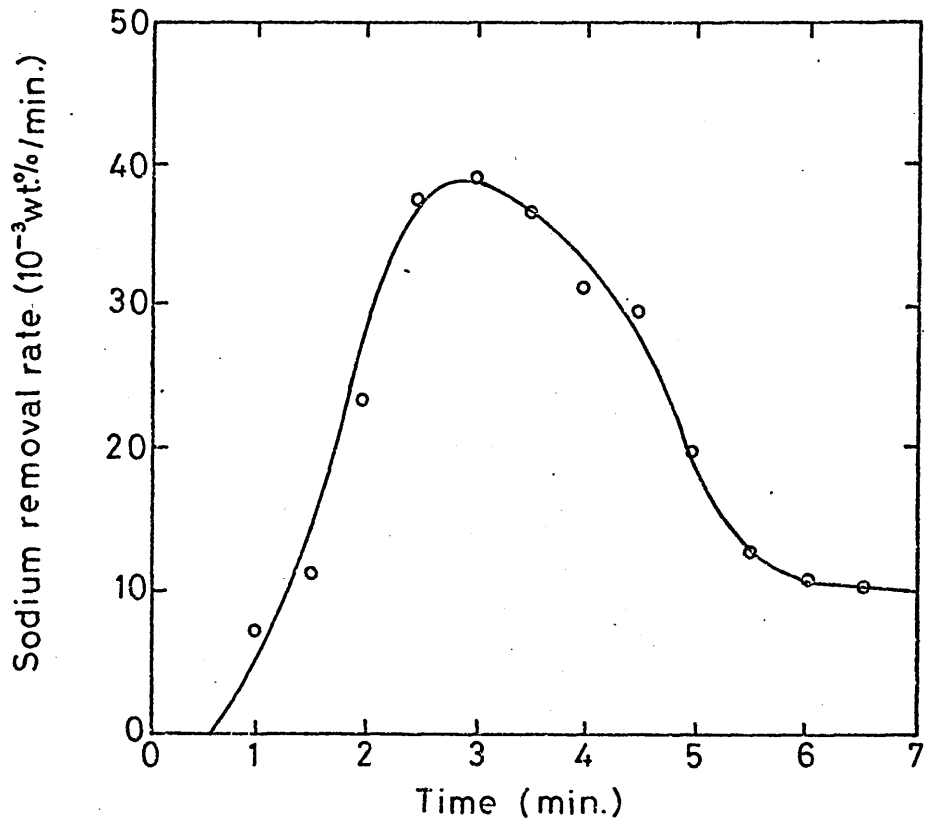


Figure 83 The refining of an amalgam initially containing 0.32 wt.% Na when the excess vessel pressure was 0.392 atmospheres.

(For additional information see table 14.)

(a) Rate of sodium removal from the amalgam bath.



(b) Foam volume.

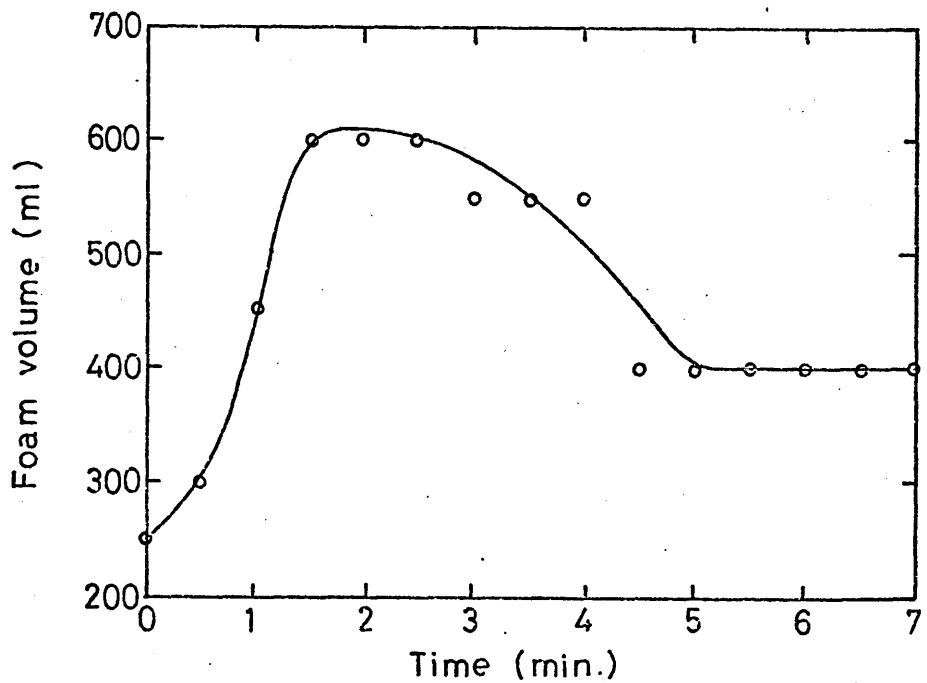
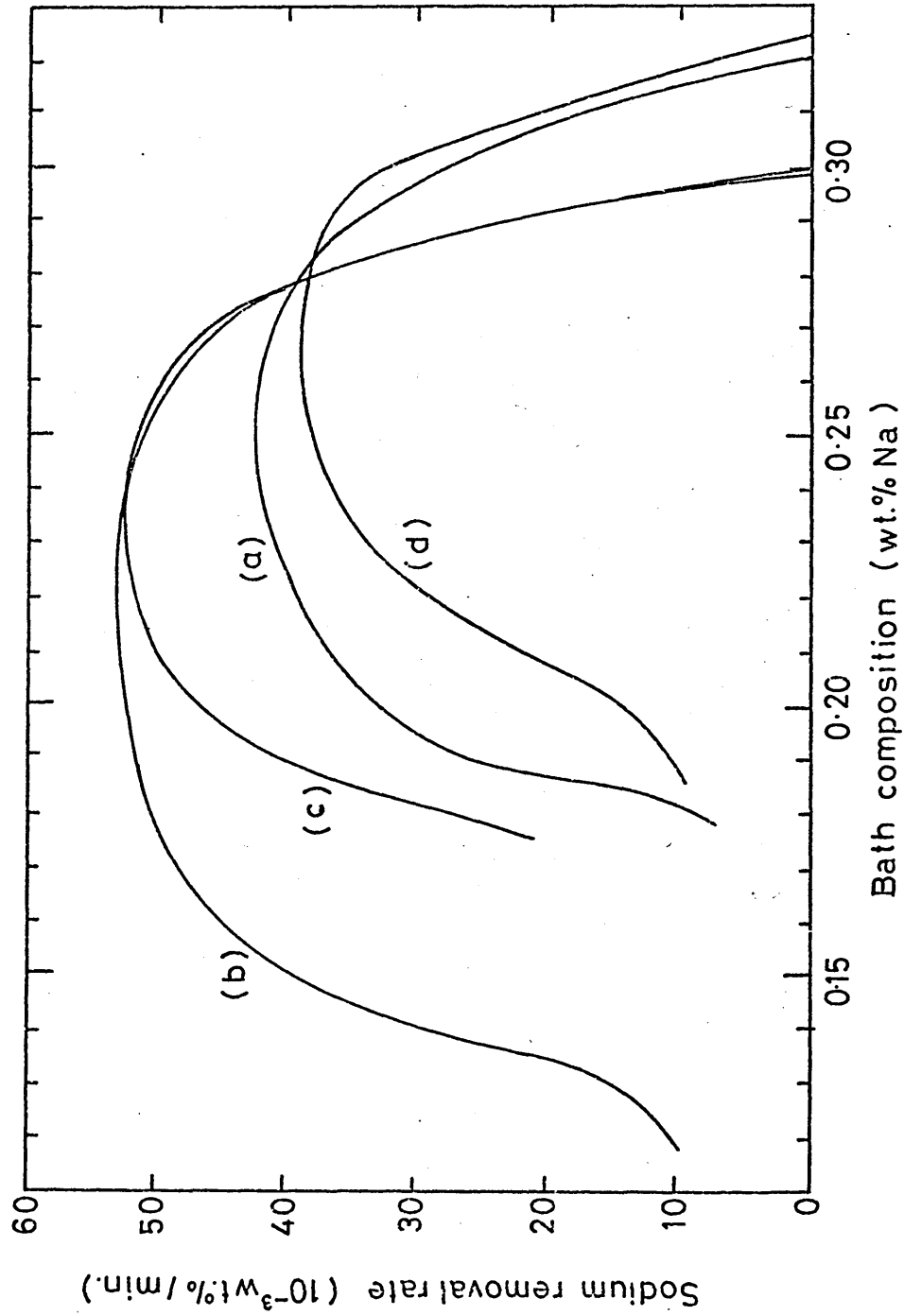


Figure 84 The effect of bath composition on the refining rate in the model converter.



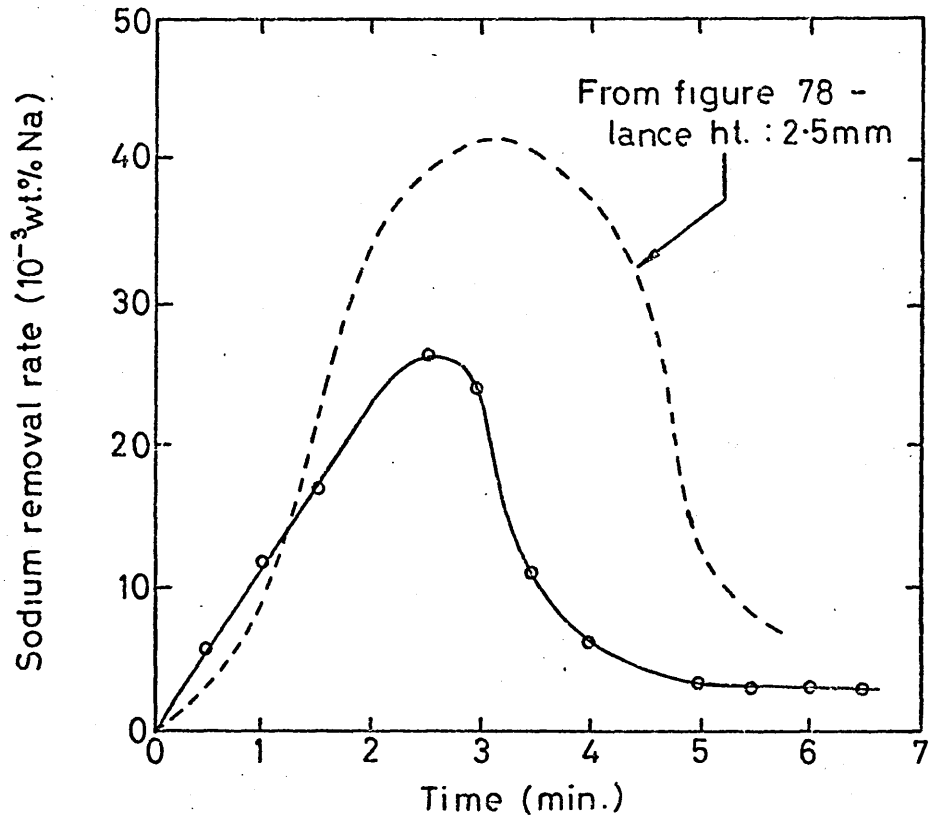
- (a) From fig. 78 (0.047 atmos.)
- (b) From fig. 79 (0.047 atmos.)
- (c) From fig. 82 (0.350 atmos.)
- (d) From fig. 83 (0.392 atmos.)

Blowing conditions summarised in table 14.

Figure 85 The refining of an amalgam initially containing 0.29 wt.% Na using a lance height of 20.4 mm.

(For additional information see table 14.)

(a) Rate of sodium removal from the amalgam bath.



(b) Foam volume.

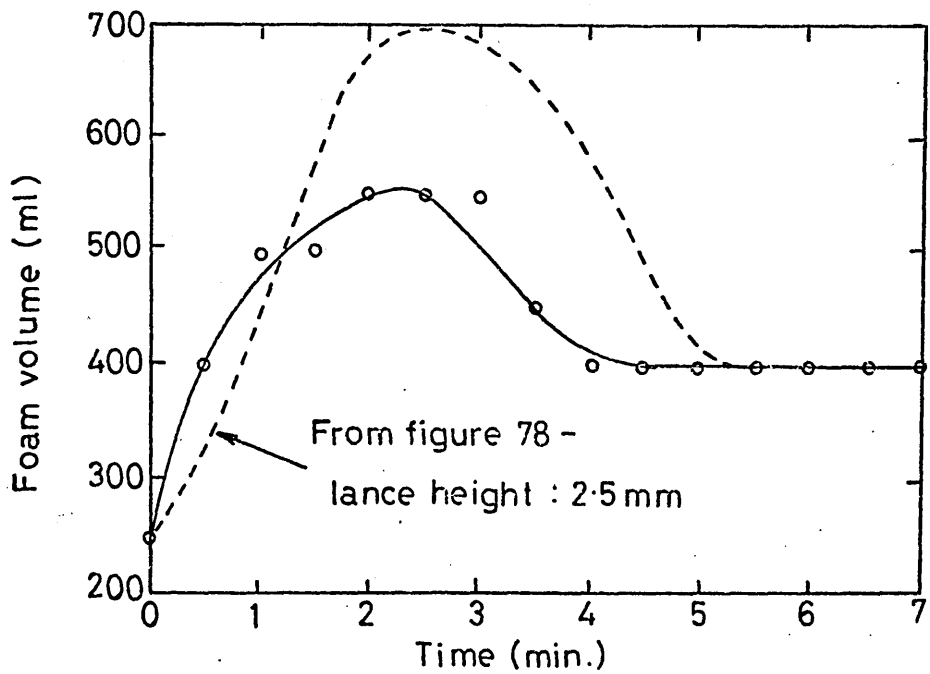


Figure 86 The refining rate from figure 85 presented as a function of bath composition.

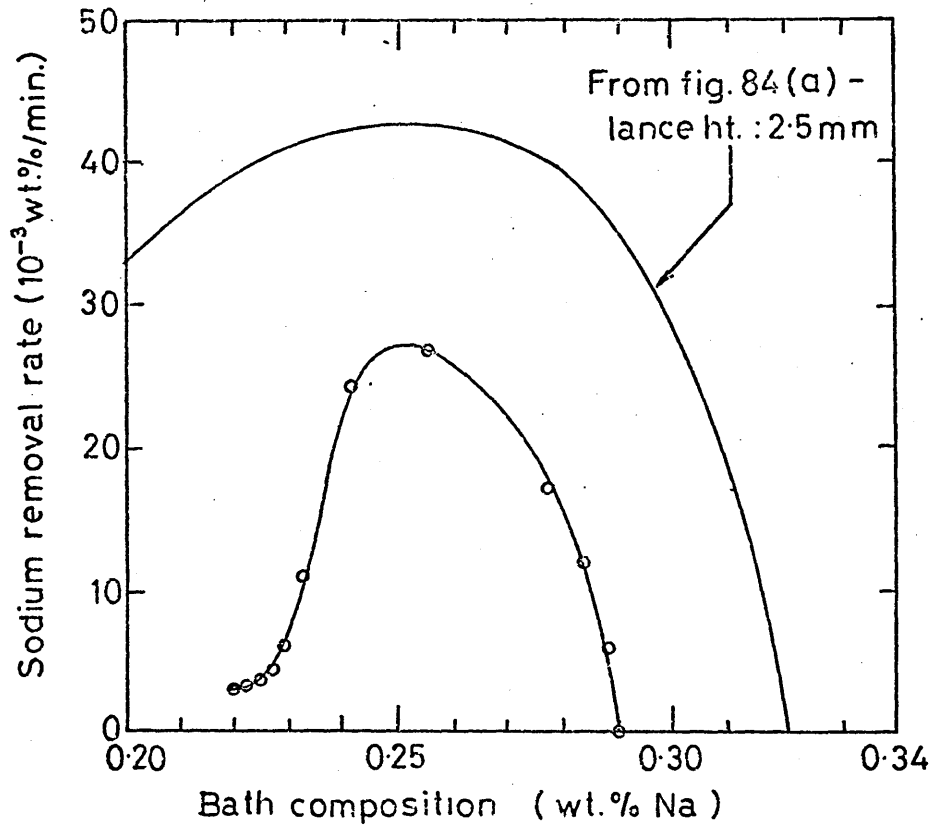


Figure 87 Theoretical refining conditions in the model converter if the sodium removal rate depended only upon the H^+ concentration in the model slag.

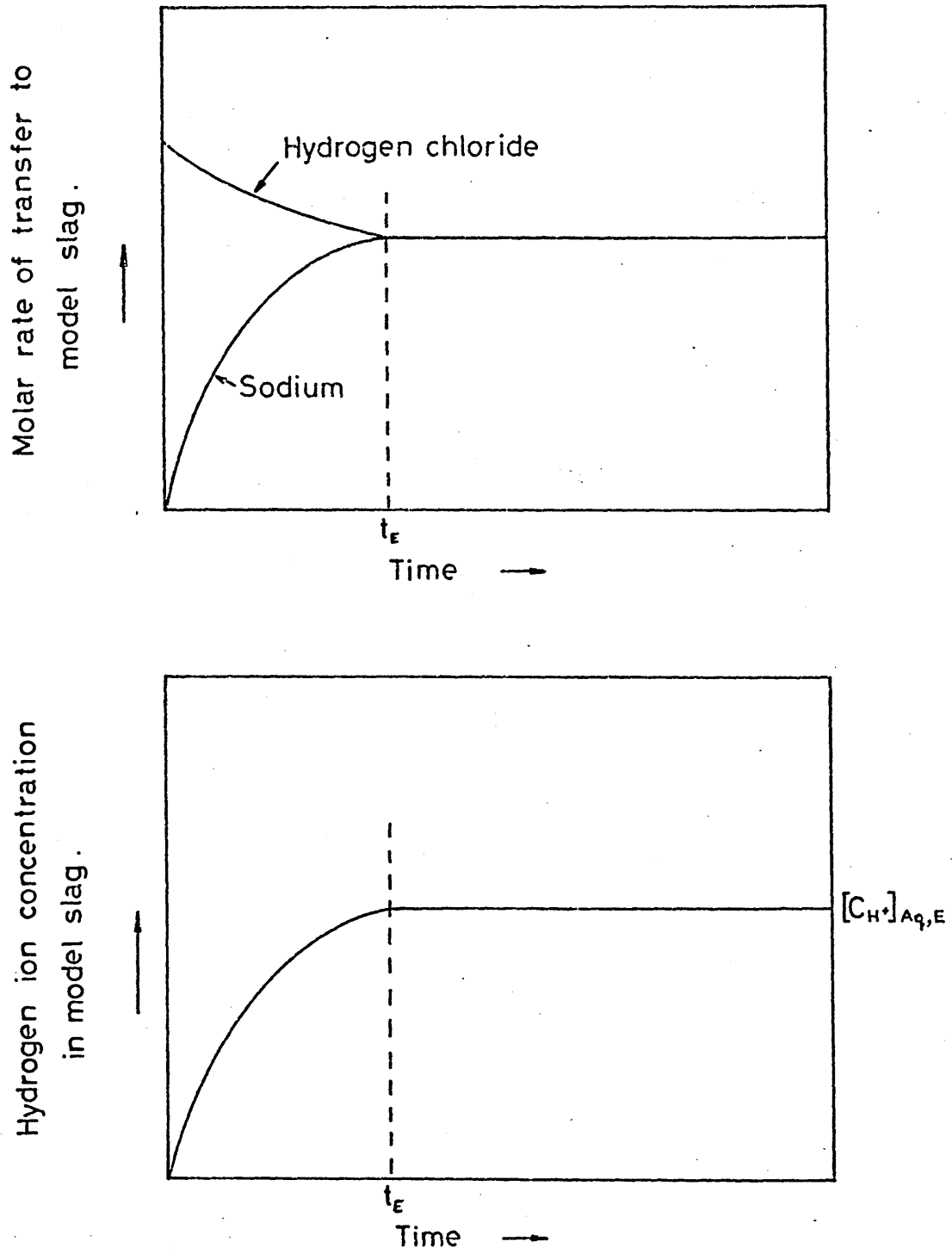
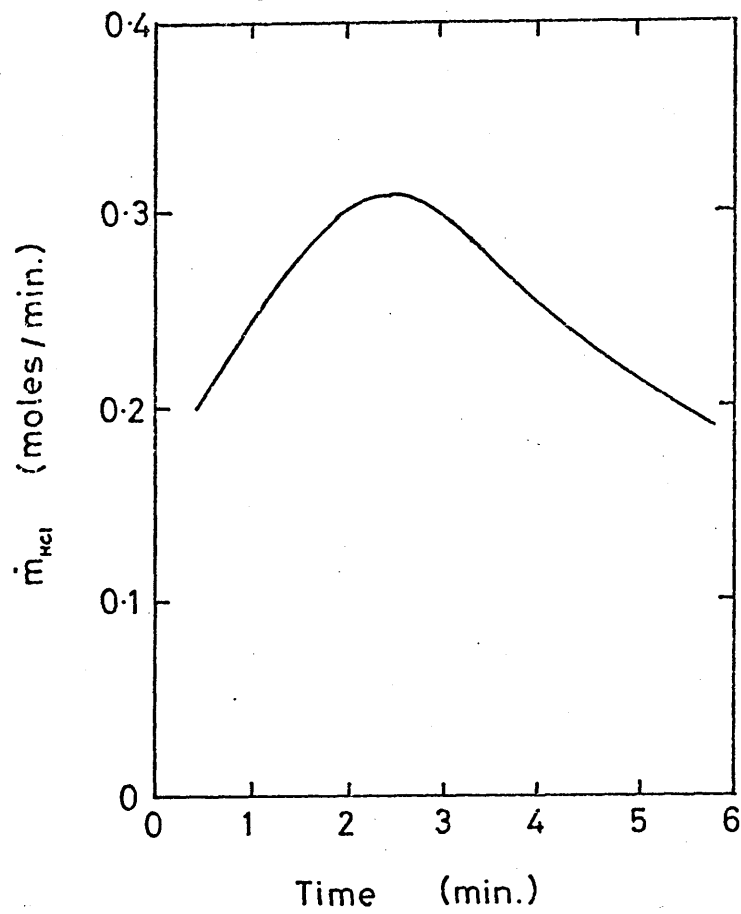


Figure 88 The variation in \dot{m}_{HCl} throughout a blow.



Data from figures 48 and 50(b).

Table 15 - An estimate of the total surface area of amalgam droplets in the foam for various mean droplet sizes and life times in the foam.

(a) For a splashing rate of 250 ml/min.

Life time in foam (seconds)	Total surface area (cm ²)			
	Mean droplet diameter (mm)			
	0.2	1.0	2.0	5.0
0.1	125	25	12	5
0.5	625	125	62	25
1.0	1250	250	125	50
3.0	3750	750	375	150
6.0	7500	1500	750	300
10.0	12500	2500	1250	500

(b) For a splashing rate of 500 ml/min.

Life time in foam (seconds)	Total surface area (cm ²)			
	Mean droplet diameter (mm)			
	0.2	1.0	2.0	5.0
0.1	250	50	25	10
0.5	1250	250	125	50
1.0	2500	500	250	100
3.0	7500	1500	750	300
6.0	15000	3000	1500	600
10.0	25000	5000	2500	1000

Figure 89 The effect of vessel pressure on the refining rate per unit volume of foam.

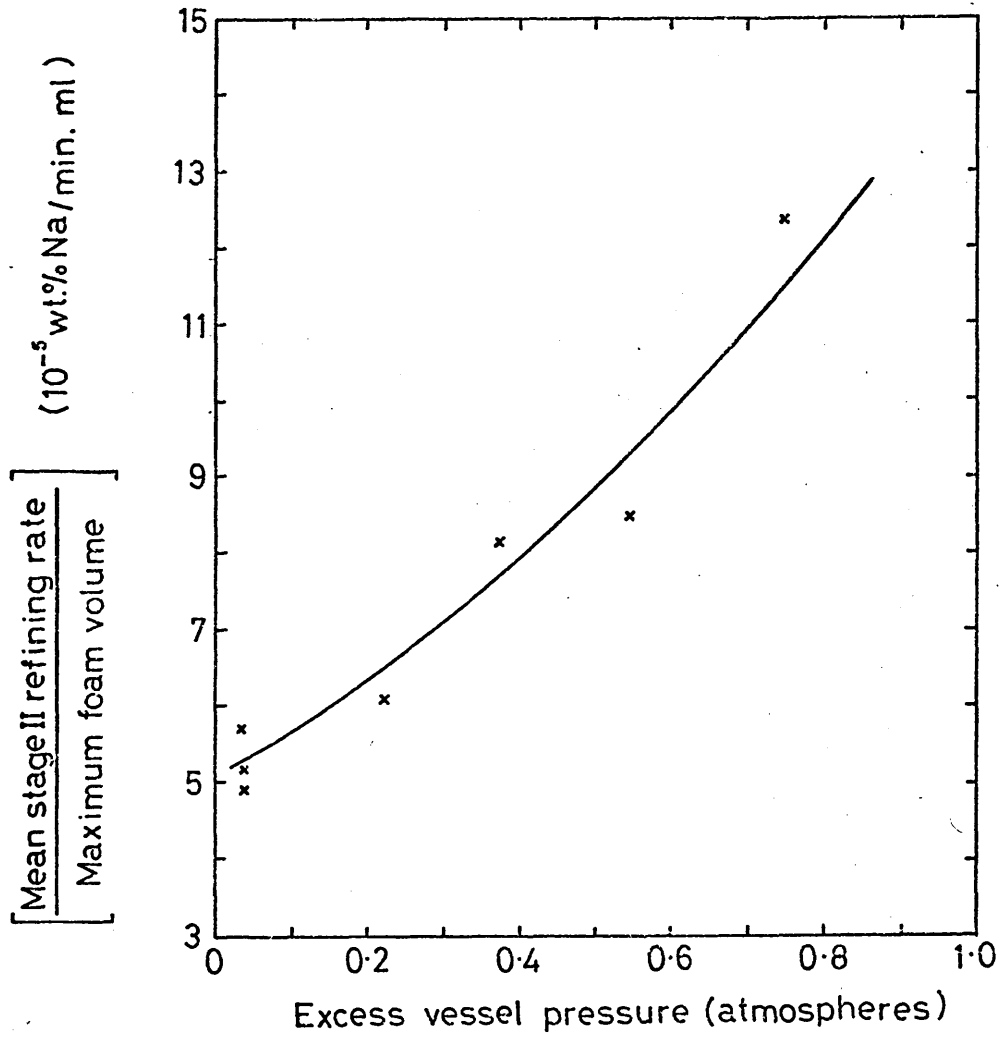


Table 16 - Tabulated results of all mass transfer experiments with single droplets.

Figure No.	HCl conc. (mol/l)	NaCl conc. (mol/l)	Initial Na content (wt%)	Temp. (°C)	Ht. of fall (cm)	Reaction time (s)	H ₂ evolved at S.T.P. (ml/drop)	Na removed (wt %)
21	0.50	0	0.551	20	16.4	0.34	0.0080	0.017
21	0.50	0	0.545	20	22.5	0.46	0.0098	0.021
21	0.50	0	0.551	20	32.6	0.67	0.0126	0.027
21	0.50	0	0.536	20	41.9	0.86	0.0164	0.035
21	0.50	0	0.525	20	48.5	0.99	0.0224	0.048
21	0.50	0	0.533	20	59.7	1.22	0.0276	0.059
22(a)	1.00	0	0.570	19	17.6	0.38	0.0197	0.042
22(a)	1.00	0	0.564	19	27.8	0.60	0.0318	0.068
22(a)	1.00	0	0.561	20	41.8	0.90	0.0458	0.098
22(a)	1.00	0	0.550	20	53.0	1.14	0.0580	0.124
22(a)	1.00	0	0.569	20	56.6	1.22	0.0674	0.144
22(a)	1.00	0	0.558	20	60.2	1.29	0.0711	0.152
22(a)	1.00	0	0.271	17	16.8	0.36	0.0187	0.040
22(a)	1.00	0	0.269	17	28.0	0.60	0.0337	0.072
22(a)	1.00	0	0.276	17	44.0	0.95	0.0473	0.101
22(a)	1.00	0	0.268	17	57.7	1.24	0.0636	0.136
22(b)	0.91	0.5	0.562	20	23.3	0.51	0.0215	0.046
22(b)	0.91	0.5	0.542	20	41.2	0.90	0.0431	0.092
22(b)	0.91	0.5	0.546	20	55.0	1.20	0.0524	0.112
23(a)	1.47	0	0.555	20	15.8	0.35	0.0253	0.054
23(a)	1.47	0	0.527	20	23.1	0.51	0.0379	0.081
23(a)	1.47	0	0.533	20	31.0	0.68	0.0477	0.102
23(a)	1.47	0	0.528	16	39.7	0.87	0.0627	0.134
23(a)	1.47	0	0.550	18	47.8	1.05	0.0748	0.160
23(a)	1.47	0	0.555	18	54.8	1.20	0.0851	0.182
23(a)	1.47	0	0.535	16	57.3	1.26	0.0969	0.207
23(b)	1.47	0.5	0.547	16	15.8	0.35	0.0225	0.048
23(b)	1.47	0.5	0.542	16	23.5	0.53	0.0281	0.060
23(b)	1.47	0.5	0.545	17	35.8	0.80	0.0528	0.113
23(b)	1.47	0.5	0.550	17	37.0	0.83	0.0547	0.117
23(b)	1.47	0.5	0.542	17	53.4	1.19	0.0702	0.150
23(b)	1.47	0.5	0.558	17	58.9	1.32	0.0832	0.178
23(c)	1.47	1.0	0.538	16	16.2	0.38	0.0211	0.045
23(c)	1.47	1.0	0.545	17	35.1	0.82	0.0435	0.093
23(c)	1.47	1.0	0.544	17	59.9	1.39	0.0814	0.174

Table 16 continued

Figure No.	HCl conc. (mol/l)	NaCl conc. (mol/l)	Initial Na content (wt%)	Temp. (°C)	Ht. of fall (cm)	Reaction time (s)	H ₂ evolved at S.T.P. (ml/drop)	Na removed (wt %)
23(d)	1.47	1.75	0.508	17	16.0	0.39	0.0201	0.043
23(d)	1.47	1.75	0.538	15	16.8	0.41	0.0206	0.044
23(d)	1.47	1.75	0.541	17	32.0	0.78	0.0337	0.072
23(d)	1.47	1.75	0.538	17	32.2	0.79	0.0332	0.071
23(d)	1.47	1.75	0.511	17	37.0	0.90	0.0454	0.097
23(d)	1.47	1.75	0.537	17	37.3	0.91	0.0421	0.090
23(d)	1.47	1.75	0.533	17	52.5	1.28	0.0575	0.123
23(d)	1.47	1.75	0.508	17	60.3	1.47	0.0735	0.157
23(d)	1.47	1.75	0.541	17	61.7	1.50	0.0730	0.156
24(a)	2.01	0	0.575	19	17.4	0.39	0.0416	0.089
24(a)	2.01	0	0.577	19	26.3	0.58	0.0552	0.118
24(a)	2.01	0	0.582	20	41.1	0.91	0.0819	0.175
24(a)	2.01	0	0.581	18	48.8	1.08	0.0978	0.209
24(a)	2.01	0	0.586	18	52.5	1.16	0.1132	0.242
24(a)	2.01	0	0.582	20	53.2	1.18	0.1170	0.250
24(b)	2.01	0.5	0.548	19	17.6	0.41	0.0374	0.080
24(b)	2.01	0.5	0.564	19	31.8	0.74	0.0608	0.130
24(b)	2.01	0.5	0.560	19	44.3	1.03	0.0781	0.167
24(b)	2.01	0.5	0.549	19	58.5	1.36	0.1076	0.230
24(c)	2.01	1.0	0.591	19	17.4	0.43	0.0356	0.076
24(c)	2.01	1.0	0.595	19	30.2	0.75	0.0543	0.116
24(c)	2.01	1.0	0.587	19	45.5	1.13	0.0805	0.172
24(c)	2.01	1.0	0.600	19	58.7	1.45	0.1128	0.241
25(a)	2.73	0	0.582	19	16.7	0.37	0.0440	0.094
25(a)	2.73	0	0.581	19	26.7	0.59	0.0683	0.146
25(a)	2.73	0	0.576	19	27.2	0.60	0.0617	0.132
25(a)	2.73	0	0.570	19	37.5	0.83	0.0828	0.177
25(a)	2.73	0	0.578	19	60.2	1.32	0.1357	0.290
25(a)	2.73	0	0.425	20	17.1	0.38	0.0412	0.088
25(a)	2.73	0	0.426	20	37.2	0.82	0.0926	0.198
25(a)	2.73	0	0.431	20	50.1	1.10	0.1193	0.255
25(a)	2.73	0	0.424	20	60.7	1.34	0.1310	0.280
25(b)	2.73	0.5	0.596	21	16.3	0.38	0.0384	0.082
25(b)	2.73	0.5	0.600	21	25.6	0.60	0.0599	0.128
25(b)	2.73	0.5	0.602	21	49.8	1.16	0.1236	0.264

Table 16 continued

Figure No.	HCl conc. (mol/l)	NaCl conc. (mol/l)	Initial Na content (wt%)	Temp. (°C)	Ht. of fall (cm)	Reaction time (s)	H ₂ evolved at S.T.P. (ml/drop)	Na removed (wt %)
25(b)	2.73	0.5	0.609	21	60.7	1.40	0.1480	0.316
28(a)	2.01	0	0.185	17	23.5	0.75	0.0229	0.049
28(a)	2.01	0	0.185	17	37.1	1.19	0.0351	0.075
28(a)	2.01	0	0.187	17	49.1	1.57	0.0430	0.092
28(a)	2.01	0	0.182	17	60.9	1.95	0.0473	0.101
28(b)	2.01	0	0.268	17	16.4	0.43	0.0252	0.054
28(b)	2.01	0	0.276	16	17.0	0.45	0.0365	0.078
28(b)	2.01	0	0.264	19	27.6	0.73	0.0454	0.097
28(b)	2.01	0	0.270	17	40.3	1.07	0.0501	0.107
28(b)	2.01	0	0.264	19	45.3	1.20	0.0557	0.119
28(b)	2.01	0	0.267	19	59.4	1.57	0.0688	0.147
28(b)	2.01	0	0.272	17	59.4	1.57	0.0636	0.136
28(c)	2.01	0.5	0.290	18	16.5	0.43	0.0388	0.083
28(c)	2.01	0.5	0.280	18	29.8	0.78	0.0595	0.127
28(c)	2.01	0.5	0.284	18	44.8	1.18	0.0702	0.150
28(c)	2.01	0.5	0.284	16	46.8	1.23	0.0622	0.133
28(c)	2.01	0.5	0.276	16	53.9	1.42	0.0688	0.147
28(d)	2.01	1.0	0.316	19	21.4	0.57	0.0360	0.077
28(d)	2.01	1.0	0.313	19	33.6	0.89	0.0576	0.123
28(d)	2.01	1.0	0.305	19	48.5	1.28	0.0683	0.146
28(d)	2.01	1.0	0.304	19	60.1	1.59	0.0819	0.175
29	2.70	0	0.335	20	16.8	0.44	0.0468	0.100
29	2.70	0	0.332	20	30.9	0.81	0.0599	0.128
29	2.70	0	0.329	20	48.1	1.27	0.0815	0.174
29	2.70	0	0.333	20	60.3	1.59	0.0941	0.201

Table 17 -

Tabulated results of model converter experiments
- refining rates

Blowing time (mins.)	SODIUM REMOVAL RATE (wt %/minute)					
	Fig. 40	Fig. 41	Fig. 42	Fig. 43	Fig. 44	Fig. 45
0.5	0.0023	0.0009	-	0.0004	0.0022	0.0025
1.0	0.0023	0.0117	0.0068	0.0033	0.0064	0.0035
1.5	0.0037	0.0151	0.0134	0.0088	0.0154	-
2.0	0.0084	0.0226	0.0173	0.0240	0.0341	0.0101
2.5	0.0127	0.0376	0.0319	0.0334	0.0355	-
3.0	0.0173	0.0275	0.0353	0.0304	0.0366	0.0153
3.5	0.0179	0.0332	0.0275	0.0301	0.0392	-
4.0	0.0222	0.0293	0.0319	0.0316	0.0405	0.0239
4.5	0.0195	0.0267	0.0306	0.0362	0.0447	0.0253
5.0	0.0226	0.0301	0.0361	0.0369	0.0464	0.0274
5.5	0.0181	0.0365	0.0287	0.0379	0.0441	0.0267
6.0	0.0175	0.0279	0.0329	0.0390	0.0422	0.0302

Table 17 continued

Blowing time (mins.)	SODIUM REMOVAL RATE (wt %/minute)					
	Fig. 46	Fig. 47	Fig. 48	Fig. 53	Fig. 54	Fig. 55
0.5	0.0015	-	0.0017	-	0.0042	-
1.0	0.0060	0.0075	0.0063	0.0063	0.0134	0.0065
1.5	0.0122	0.0105	0.0167	0.0157	0.0235	0.0188
2.0	0.0194	0.0248	0.0354	0.0215	0.0376	0.0254
2.5	-	0.0454	0.0427	0.0394	0.0367	0.0371
3.0	0.0351	0.0412	0.0423	0.0379	0.0442	0.0473
3.5	0.0400	0.0475	0.0462	0.0438	0.0503	0.0296
4.0	0.0382	0.0404	0.0459	0.0516	0.0487	0.0400
4.5	0.0355	0.0430	0.0504	0.0408	0.0543	0.0397
5.0	0.0400	0.0326	0.0490	0.0505	0.0494	0.0504
5.5	0.0373	0.0332	0.0473	0.0517	0.0487	0.0332
6.0	0.0353	0.0406	0.0549	0.0474	0.0398	-

Table 17 continued

Blowing time (mins.)	SODIUM REMOVAL RATE (wt %/minute)				
	Fig. 56	Fig. 57	Fig. 58	Fig. 62	Fig. 65
0.5	0.0106	0.0071	0.0088	0.0017	0.0036
1.0	0.0193	0.0169	0.0098	0.0038	0.0054
1.5	0.0223	0.0294	0.0286	0.0120	0.0112
2.0	0.0327	0.0348	0.0305	0.0204	0.0186
2.5	0.0436	0.0311	0.0356	0.0269	0.0205
3.0	0.0343	0.0288	0.0237	0.0331	0.0337
3.5	-	0.0384	0.0522	0.0482	0.0381
4.0	0.0395	0.0381	0.0607	0.0582	0.0371
4.5	0.0375	0.0311	0.0264	0.0634	0.0361
5.0	0.0364	0.0324	0.0381	0.0555	0.0395
5.5	0.0327	0.0340	0.0188	0.0593	0.0345
6.0	-	0.0320	0.0163	0.0638	0.0381

Table 17 continued

Blowing time (mins.)	SODIUM REMOVAL RATE (wt %/minute)				
	Fig. 66	Fig.67	Fig. 68	Fig. 74	Fig. 75
0.5	-	0.0036	0.0026	-	0.0031
1.0	0.0040	0.0069	0.0167	0.0057	0.0052
1.5	0.0168	0.0190	0.0285	0.0172	0.0067
2.0	0.0325	0.0376	-	0.0287	0.0160
2.5	0.0379	0.0426	0.0450	0.0403	0.0338
3.0	0.0383	0.0402	0.0414	0.0458	0.0446
3.5	0.0402	0.0440	0.0458	0.0428	0.0373
4.0	0.0376	0.0392	0.0466	0.0394	0.0450
4.5	0.0430	0.0441	0.0514	0.0449	0.0477
5.0	0.0405	0.0420	0.505	-	0.0555
5.5	0.0405	0.0448	0.454	0.0541	0.0555
6.0	0.0390	0.0431	0.462	0.0521	0.0530

Table 17 continued

SODIUM REMOVAL RATE (wt %/minute)					
Blowing time (minutes)	Fig. 78	Fig. 79	Fig. 82	Fig. 83	Fig. 85
0.5	0.0010	0.0022	-	-	0.0057
1.0	0.0045	0.0112	0.0114	0.0077	0.0120
1.5	0.0126	0.0240	0.0110	0.0114	0.0169
2.0	0.0262	0.0460	0.0205	0.0236	-
2.5	0.0363	-	0.0460	0.0376	0.0263
3.0	0.0404	0.0484	0.0555	0.0392	0.0239
3.5	0.0422	0.0529	0.0513	0.0367	0.0110
4.0	0.0384	0.0488	0.0474	0.0311	0.0059
4.5	0.0374	0.0388	0.0300	0.0297	0.0041
5.0	0.0262	0.0189	-	0.0199	0.0033
5.5	0.0101	0.0125	-	0.0126	0.0031
6.0	0.0074	0.0110	-	0.0106	0.0033
6.5	-	0.0094	-	0.0106	0.0026
7.0	-	0.0094	-	0.0077	-

Table 18 - Tabulated results of model converter experiments

- foam volume

Blowing time (minutes)	FOAM VOLUME (ml)					
	Fig. 40	Fig. 41	Fig. 42	Fig. 43	Fig. 44	Fig. 45
0	250	250	250	250	250	250
0.5	300	300	300	300	300	300
1.0	350	400	500	400	450	350
1.5	450	500	600	550	550	500
2.0	550	550	650	600	650	550
2.5	650	550	600	600	650	600
3.0	600	600	600	600	650	650
3.5	600	500	600	600	650	650
4.0	600	500	600	600	600	700
4.5	600	500	600	550	600	700
5.0	600	500	600	500	600	700
5.5	600	500	550	475	500	650
6.0	600	500	500	450	500	650

Table 18 continued

Blowing time (minutes)	FOAM VOLUME (ml)					
	Fig. 46	Fig. 47	Fig. 48	Fig. 53	Fig. 54	Fig. 55
0	250	250	250	250	250	250
0.5	300	300	300	300	350	300
1.0	400	400	350	350	450	350
1.5	500	500	550	400	500	400
2.0	550	550	650	500	650	500
2.5	600	600	650	500	650	500
3.0	600	600	650	500	550	500
3.5	600	550	600	500	550	500
4.0	550	500	600	500	550	500
4.5	500	500	600	450	550	400
5.0	500	450	500	450	550	400
5.5	450	400	450	450	500	400
6.0	450	400	450	450	500	400

Table 18 continued

Blowing time (minutes)	FOAM VOLUME (ml)				
	Fig. 56	Fig. 57	Fig. 58	Fig. 62	Fig. 65
0	250	250	250	250	250
0.5	300	300	300	450	300
1.0	350	350	350	550	400
1.5	400	400	350	600	500
2.0	450	400	350	600	550
2.5	500	400	400	600	600
3.0	500	400	400	550	550
3.5	500	400	400	550	500
4.0	500	375	400	500	500
4.5	500	375	400	500	450
5.0	450	350	400	500	450
5.5	400	350	350	500	400
6.0	400	300	350	500	400

Table 18 continued

Blowing time (minutes)	FOAM VOLUME (ml)				
	Fig. 66	Fig. 67	Fig. 68	Fig. 74	Fig. 75
0	250	250	250	250	250
0.5	350	350	275	400	300
1.0	400	490	325	550	400
1.5	450	500	325	600	550
2.0	500	500	375	650	550
2.5	500	500	375	650	600
3.0	500	500	375	650	600
3.5	500	500	375	600	550
4.0	500	500	350	600	500
4.5	500	500	350	600	500
5.0	500	450	350	600	450
5.5	450	400	350	550	400
6.0	400	400	350	500	400

Table 18 continued

Blowing time (minutes)	FOAM VOLUME (ml)				
	Fig. 78	Fig. 79	Fig. 82	Fig. 83	Fig. 85
0	250	250	250	250	250
0.5	350	350	400	300	400
1.0	450	550	500	450	500
1.5	600	700	600	600	500
2.0	700	700	650	600	550
2.5	700	700	650	600	550
3.0	700	700	650	550	550
3.5	650	650	650	550	450
4.0	600	600	650	550	400
4.5	500	550	500	400	400
5.0	400	500	400	400	400
5.5	400	450	400	400	400
6.0	400	400	400	400	400
6.5	400	400	400	400	400
7.0	400	400	400	400	400

Tabulated results of model converter experiments
 - acid concentration and temperature in model slag.

Blowing time (minutes)	HCl concentration (moles/l)		Temperature increase (°C)	
	Fig. 50(a)	Fig. 50(b)	Fig. 51(a)	Fig. 51(b)
0	0	0	0	0
1.0	0.42	0.74	6	11
2.0	-	1.48	11	23
2.5	0.87	-	-	-
3.0	-	2.20	17	34
4.0	1.25	2.77	23	45
5.0	1.43	3.09	28	51
6.0	1.58	3.26	31	56
7.0	1.69	-	33	59

Table 19 continued

Blowing time (minutes)	HCl concentration (moles/l)		Temperature increase (°C)	
	Fig. 60(a)	Fig. 60 (b)	Fig. 61(a)	Fig. 61(b)
0	0	0	0	0
0.5	-	-	6	10
1.0	-	0.95	12	15
1.5	1.04	-	18	22
2.0	-	1.95	23	27
2.5	1.70	-	29	31
3.0	-	2.76	33	35
3.5	2.28	-	38	38
4.0	-	3.44	42	42
4.5	2.77	-	46	44
5.0	-	3.97	50	46
5.5	3.07	-	53	47
6.0	-	4.25	56	-
6.5	3.18	-	58	-
7.0	-	-	59	-

Table 19 continued

Blowing time (minutes)	HCl concentration (moles/l)		Temperature increase (°C)	
	Fig. 63(a)	Fig. 63(b)	Fig. 64(a)	Fig. 64(b)
0	0	0	0	0
0.75	-	0.73	-	7
1.0	0.88	-	12	-
1.75	-	1.49	-	16
2.0	1.69	-	23	-
2.75	-	2.20	-	25
3.0	2.37	-	34	-
3.75	-	2.77	-	34
4.0	2.93	-	45	-
4.75	-	3.09	-	43
5.0	3.36	-	51	-
5.75	-	3.26	-	48
6.0	3.44	-	56	-

Table 19 continued

Blowing time (minutes)	HCl concentration (moles/l)		Temperature increase (°C)	
	Fig. 72(a)	Fig. 72(b)	Fig. 73(a)	Fig. 73(b)
0	0	0	0	0
1.0	0.63	0.87	12	9
2.0	1.42	1.54	27	19
3.0	-	2.35	32	28
4.0	2.46	2.85	38	34
5.0	3.10	3.29	45	40
6.0	3.55	3.57	51	45
7.0	3.75	4.00	53	49

Table 19 continued

Blowing time (minutes)	HCl concentration (moles/l)		Temperature increase (°C)	
	Fig. 76(a)	Fig. 76(b)	Fig. 77(a)	Fig. 77(b)
0	0	0	0	0
1	0.75	0.75	11	11
2	1.48	1.23	23	25
3	2.20	2.13	34	35
4	2.76	2.63	45	42
5	3.09	-	51	48
6	3.26	3.65	56	51
7	-	3.93	59	53

Table 19 continued

	HCl concentration (mol/l)	Temperature increase (°C)
Blowing time (minutes)	Fig. 80	Fig. 81
0	0	0
1.0	0.70	12
2.0	1.56	25
3.0	2.17	34
4.0	2.75	43
5.0	-	47
6.0	-	48
7.0	-	48